SCK•CEN/30259620
ER-0221

The geochemical perturbation of Boom Clay due to the $NaNO_3$ plume released from Eurobitum bituminised radioactive waste: status 2013

Topical Report

Nele Bleyen, An Mariën and Elie Valcke

Publication date: September 2018

Contract name: Contrat de R&D "Gestion à long terme des déchets radioactifs" (2015-2020)

Contract number: CO-90-14-3690-00 / CCHO 2015-0304/00/00

Contract information: RS 15-SCK-BIT-09: Finalisation of the Topical Report on geochemical perturbation by $NaNO_3$

SCK•CEN
Boeretang 200
BE-2400 Mol
Belgium

© SCK•CEN
Studiecentrum voor Kernenergie
Centre d'Etude de l'énergie Nucléaire
Boeretang 200
BE-2400 Mol
Belgium

Phone +32 14 33 21 11
Fax +32 14 31 50 21

http://www.sckcen.be

Contact:
Knowledge Centre
library@sckcen.be

Configuration Control

Document History

Revision	Status	Author	Date	Changes

Document Approval

	Name	Date	Signature
Author: (Function)	Nele Bleyen (Project leader)	11/9/18	
Reviewed by: (Function)	Elie Valcke (Head of Unit RDW)	12/9/2018	
Approved by: (Function)	Elie Valcke (Head of Unit RDW)	12/9/2018	
Approved for QA: (Function)	Elke Jacops (QA coordinator)	14/9/2018	
Security approval: (Function)			

Distribution List

Name	Affiliation/Expert Group/Unit	Number of copies	Format
Benny De Blochouse	NIRAS/ONDRAF	5 1	Hard copy Electronically on vignette

Table of Content

List of tables

List of figures

Executive summary

In Belgium, Boom Clay is currently studied as the reference host formation for the geological disposal of Eurobitum intermediate level bituminised radioactive waste, because of its favourable physicochemical characteristics. Indeed, the low hydraulic gradient over the clay in combination with the low hydraulic conductivity, typical of sedimentary clay formations, ensures that the water movement in the clay is very slow and hence controlled by diffusion. Furthermore, the slightly alkaline pH and the reducing conditions imply a very low solubility for many radionuclides, while the presence of clay minerals ensures a high sorption potential. Both result in an efficient retardation of the radionuclide migration. However, Eurobitum contains high concentrations of $NaNO_3$ embedded in a hard bitumen matrix. Leaching of high amounts of nitrate (and also small concentrations of nitrite) and organic degradation compounds from Eurobitum into the host rock could lead to geophysicochemical disturbances of the clay and might therefore have a negative impact on the barrier function of the clay. A study of the extent of these disturbances is therefore essential. In this report, the most important results and insights obtained from experiments in which the geochemical perturbations of Boom Clay and some of its components by $NaNO_3$ were studied, are discussed.

First, the effect of a $NaNO_3$ plume on the physicochemical properties of the Boom Clay and its impact on the transport properties of the clay were studied in $NaNO_3$ percolation and pulse injection tests. Furthermore, the potential microbial reduction of nitrate, which could lead to the formation of a pressurised gas phase in the clay and/or to an oxidation of the clay around the disposal gallery, was studied by means of bioreactor tests. In some of these reactors, the effect of adding extra electron donors (*i.e.* bitumen degradation products, H_2) or acceptors (*e.g.* nitrite, sulphate) was also investigated. Finally, the possibility of an abiotic oxidation of redox-active Boom Clay components by nitrate or nitrite was studied in batch tests. Both batch and bioreactor tests were thus performed to study the impact of $NaNO_3$ on the reducing capacity of Boom Clay towards redox-sensitive radionuclides. Exploratory calculations of the $NaNO_3$ leaching rates from Eurobitum and its migration in the Boom Clay confirm *(i)* that for the assumed slightly conservative $NaNO_3$ leach rates, the Boom Clay properties will determine the long-term evolution of the $NaNO_3$ concentration in the host formation, and *(ii)* that realistic $NaNO_3$ concentrations were and are being used in the different experiments.

The results of combined $NaNO_3$ percolation and radionuclide pulse injection tests on consolidated clay cores revealed that the most important perturbation of the Boom Clay by a $NaNO_3$ plume is the transformation to a clay with a high Na^+ occupancy, due to cation exchange between the clay cations and the additional sodium. However, based on the expected $NaNO_3$ concentrations in the Boom Clay around a disposal gallery for Eurobitum (*i.e.* calculated at a relevant scale and under realistic disposal conditions), this perturbation would be limited in distance to about five meters. A study of the hydromechanical behaviour of these nearly homo-ionic sodium clay cores indicated that the transformation towards a clay with a high Na^+ occupancy does not seem to significantly affect the hydromechanical properties of the clay. The other possible effects of a $NaNO_3$ plume in Boom Clay (*i.e.* increase of the ionic strength, change of the hydraulic conductivity, change in concentration of dissolved organic matter or pH, oxidation of Boom Clay components) appear to be

negligible, especially considering that in real disposal conditions the change in $NaNO_3$ concentration will proceed much more slowly than in the laboratory experiments. Finally, the effect of the $NaNO_3$ plume on the diffusion parameters for tritiated water, iodide, and bicarbonate appears to be small. Only for the anionic species a significant yet modest increase (by ~50%) in diffusion accessible porosity was measured when the ionic strength in the percolation solution increased from 0.016 M to 1 M. Since for anionic species the effective dispersion coefficient depends on the diffusion accessible porosity, also this parameter increased when increasing the ionic strength from 0.016 M to 1 M: ~50% increase for iodide, and ~100% for bicarbonate. All of these observations can be explained to a large extent by the effect of the increased ionic strength on the thickness of the electrical double layer. Because of the lack of reliable values for the dispersion length, the effective diffusion coefficient could not be calculated. However, given the low contribution of the kinematic dispersion, the effective dispersion coefficient can be considered as a conservative estimate of the effective diffusion coefficient.

The bioreactor tests demonstrated that nitrate reducing prokaryota can grow and become active in disturbed Boom Clay in the presence of oxidised N-species. These microorganisms can use Boom Clay components, organic degradation compounds from Eurobitum, as well as H_2 as electron donor for the microbial nitrate reduction processes (*e.g.* denitrification). In the absence of additional electron donors, nitrate reactivity is rather slow, in contrast to when H_2 or easily degradable organic compounds are added. Denitrification will lead to the production of gaseous N-species. However, its effect on the total gas pressure is depending on the electron donor that is used (*e.g.* organic compounds or H_2). Too high gas pressures could occur if organic compounds are used as electron donor and could mechanically disturb the clay and potentially influence the radionuclide transport. On the other hand, if H_2 is used as the electron donor, this gas will be consumed as electron donor for nitrate or nitrite reduction, causing an overall gas pressure decrease. It is, however, still uncertain whether Nitrate Reducing Prokaryota can be (very) active under the prevailing harsh conditions for microorganisms in the repository, such as high pH, rather high $NaNO_3$ concentrations, lack of free space and limited bioavailable nutrients. Additional bioreactor tests are therefore required to study the effect of these conditions (*e.g.* high pH, high $NaNO_3$ concentration), in combination with one or more realistic electron donors, on the microbial activity in (disturbed) Boom Clay.

In the batch tests, a purely chemical nitrate reduction by Boom Clay or its components (pyrite, DOM) was not observed, suggesting that the perturbation of the reducing capacity of Boom Clay by a $NaNO_3$ plume in the absence of microbial activity will not be considerable. On the other hand, batch tests with $NaNO_2$ and Boom Clay or pure redox-active Boom Clay components (pyrite, DOM) reveal a slow abiotic oxidation of pyrite, and possibly also of DOM, by nitrite. However, based on the kinetics of these reactions, the expected low concentration of nitrite entering the Boom Clay and the high total reducing capacity of Boom Clay, the perturbation of the reducing capacity of the Boom Clay surrounding the disposal gallery is expected to be limited.

When microbial activity is allowed in Boom Clay slurries or its components, microbial nitrate and nitrite reduction can occur and both DOM and pyrite can be used as electron donors. These reactions are stimulated by addition of easily degradable organic electron donors, similar to what was observed in the bioreactor tests. Based on this, the natural organic matter

and the pyrite in Boom Clay (pore water) seem to be rather poor electron donors for nitrate reducing prokaryotes.

In conclusion, the results that are currently available so far thus do not reveal an important geochemical disturbance of the Boom Clay. However, several processes still have to be studied more in detail to confirm this, in particular (1) abiotic and biotic nitrate and nitrite reactivity with Boom Clay DOM, pyrite and kerogen and/or in Boom Clay slurries; (2) effect of nitrate / nitrite on the speciation and migration of redox-sensitive radionuclides; (3) nitrate reactivity and its effect on Boom Clay properties under more realistic repository conditions and with/without additional electron donors expected to be present in a repository for Eurobitum; (4) the effect of combined perturbations (*e.g.* $NaNO_3$ and alkaline plume) on the Boom Clay properties. Furthermore, the model (and its assumptions) to determine the extent of the $NaNO_3$ plume could be improved further.

Keywords

Eurobitum, geological disposal, Boom Clay, $NaNO_3$, geochemical perturbation

List of abbreviations

A_x	Absorbance at a wavelength of x nm
Anammox	Anaerobic ammonium oxidation
ATP	Adenosine triphosphate
BCPW	Boom Clay pore water
BDT	Below drilling table
BNS	Bacterial nutrient solution
CEC	Cation exchange capacity
DNA	Deoxyribonucleic acid
DOC	Dissolved organic carbon
DOM	Dissolved organic matter
DNRA	Dissimilative nitrate reduction to ammonium
DNRN	Dissimilative nitrate reduction to nitrite
EBS	Engineered barrier system
EC	Electrolytic conductivity
EDL	Electrical double layer
EDX	Energy dispersive X-ray spectroscopy
EDZ	Excavation damaged zone
EG/BS	Extension Gallery Bottom Shaft
E_{SHE}	Redox potential versus the standard hydrogen electrode
FA	Fulvic acids
FeCit	Ferric citrate
GC	Gas chromatography
HA	Humic acids
HTO	Tritiated water
I	Ionic strength
LB medium	Luria Bertani bacterial growth medium

LM	Langmuir isotherm
MPA	Methane producing archaea
MPN	Most probable number
mRNA	Messenger ribonucleic acid
NCBI	National Center for Biotechnology Information
NRP	Nitrate reducing prokaryotes
NR-SOB	Nitrate reducing sulfur oxidising bacteria
NiRP	Nitrite reducing prokaryotes
NiR-SOB	Nitrite reducing sulfur oxidising bacteria
OM	Organic matter
PCR	Polymerase chain reaction
RBCW	Real Boom Clay Water (in this report: Boom Clay Pore Water sampled from the EG/BS piezometer)
rDNA	DNA sequence coding for ribosomal RNA
RNA	ribonucleic acid
RT PCR	Reverse transcriptase PCR
SA	Specific surface area
SICZH	Synthetic Boom Clay Water without humic acids
SEM	Scanning electron microsopy
SRP	Sulphate reducing prokaryotes
TIC	Total inorganic carbon
TOC	Total organic carbon
TRP	Thiosulphate reducing prokaryotes
UMB	ultramicrobacteria
URL	Underground research laboratory
XRD	X-ray diffraction

The definitions of the migration parameters and their abbreviations are described in Annex 4.

1 Introduction

Eurobitum bituminised radioactive waste has been produced during the exploitation period of the EUROCHEMIC/BELGOPROCESS reprocessing facility (Mol-Dessel, Belgium) for the incorporation of precipitation sludges originating from the chemical reprocessing of spent nuclear fuel. With its total volume of ~3000 m^3 (containing ~3000 ton of waste) and its high specific alpha and beta/gamma activities (~0.1 GBq kg^{-1} and ~10 GBq kg^{-1}, respectively), it is a very important intermediate-level waste form in Belgium. Eurobitum consists of a 'blown' (or: 'hard', 'oxidised') bitumen matrix (~60 wt%), in which the salt crystals, radionuclides and residual water (0.5-1 wt%) are homogeneously dispersed. The salt crystals are mainly $NaNO_3$ (20-30 wt%) and $CaSO_4$ (4-6 wt%), although other salts like CaF_2 (4-10 wt%) can also be found. The total radionuclide inventory (U and Pu isotopes, ^{241}Am, ^{244}Cm, ^{60}Co, ^{90}Sr, ^{137}Cs, ...) is ~0.4 wt% for drums with the average radioactivity, but can be as high as 1.15 wt% for drums with the maximum radioactivity [1-4].

The current reference solution pursued by the Belgian Agency for the Management of Radioactive Waste and Fissile Materials (ONDRAF/NIRAS) envisages the direct underground disposal of Eurobitum in a geologically stable clay formation [5]. Several 220 L Eurobitum drums would be grouped in cement-based waste containers (*i.e.* monolith), which in turn are to be placed in concrete-lined disposal galleries that are excavated at mid-depth in the clay layer. Boom Clay is being investigated as a reference formation for methodological studies on nuclear waste disposal, due to its interesting physicochemical properties, which cause a delay and spread in time of the migration of leached radionuclides after failure of the engineered containment [5]. The low hydraulic gradient over the clay in combination with the low hydraulic conductivity, typical of sedimentary clay formations, ensures that water movement in the clay is very slow. Hence, the solute transport through the formation is essentially controlled by diffusion. The slightly alkaline pH and reducing conditions imply a very low solubility for many radionuclides, and the presence of clay minerals ensures a high sorption potential, which results in an efficient retardation of the radionuclide migration [5, 6]. As a result, the projected radiation level in the biosphere is expected to be several orders of magnitude below the natural radiation level [7].

As the disposal of Eurobitum might affect the barrier function of the clay, ONDRAF/NIRAS launched a large research programme to study the compatibility of Eurobitum with the Boom Clay. Basically, two types of perturbations could occur [8]:

(i) a geomechanical disturbance, caused by the swelling of the waste and the increase of the stress in and around the waste, due to (a) the uptake of water by the dehydrated hygroscopic salts embedded in the waste [9] and (b) due to gas generation by anaerobic corrosion of the steel drums, radiolysis and possibly microbial activity [10].

(ii) a geochemical disturbance by the release of (a) large amounts of $NaNO_3$ and other soluble salts, and (b) water-soluble organic and potentially complexing compounds originating from the radiolytic and chemical degradation of the bitumen [11, 12]. Although the disturbance is of a chemical nature, it can also have physical effects such as changes of hydraulic conductivity.

In this topical report we discuss the most important results and insights from experiments in which we have investigated several geochemical perturbations of Boom Clay and some redox-active Boom Clay components by $NaNO_3$. These tests have been performed in the framework of the following research projects at SCK•CEN: 'General Migration Studies' (2001-2003), 'Geochemical Perturbations in Boom Clay' (2004-2008), and 'EUROCOMPAT' (2006-2008 and 2009-2014).

2 Background on Boom Clay and Boom Clay Pore Water

Boom Clay is a poorly indurated marine tertiary clay sediment (~30 million years old), consisting of silty clay and clayey silt layer alternations [13]. The mineralogical composition of undisturbed Boom Clay in Mol (Belgium) consists of 23 to 59 wt% clay minerals (mainly smectite and mixed layer illite-smectite, kaolinite and illite) and non-clay (mineral) constituents: quartz (23 to 55 wt%), feldspars (10 to 13 wt%), carbonates (1 to 3 wt%), pyrite (1 to 2 wt%), and organic carbon (1 to 5 wt%) [6, 13]. Furthermore, it has a slightly alkaline pH (~8.2 to 8.6[1]) and a low vertical hydraulic conductivity (2 to 4×10^{-12} m s^{-1}) [6, 14].

An important fraction of the Boom Clay clay minerals consists of so-called 2:1 clay minerals (*e.g.* smectite, illite, and mixed illite/smectite), which are composed of TOT layers, *i.e.* structural units made of an alumina octahedral (O) sheet sandwiched between two silica tetrahedral (T) sheets (Figure 1). The TOT layers have dimensions in the a and b directions of about 1 µm. Substitution of trivalent Al for the tetravalent Si in the tetrahedral layer, and of divalent cations (*e.g.* Fe, Mg) for the trivalent Al in the octahedral layer, leads to a permanent negative lattice charge, which is compensated by the preferential electrostatic attraction (sorption) of cations on the layer surfaces in combination with the (electrostatic) repulsion of anions. As a result of the negative surface charge, neutralised by the attraction of cations, the TOT layers are combined one above the other to form platelets [15-17]. In addition to the permanent charges on the clay minerals due to isomorphic substitution, terminal hydroxylic groups exist on the edges of the clay platelets. The amphoteric properties of these groups give rise to variable charges on the clay surface [17].

At the outer planes of the clay platelets and/or stacks, and under the condition that sufficient space is available, the negatively charged surface and its effect on the cations and anions in the solution lead to the formation of a diffuse layer or Electrical Double Layer (EDL) close to the mineral surface. This EDL contains both cations and anions, but has a net positive charge compensating the net negative charge on the clay surface, *i.e.* anions are expelled from the diffuse double layer, a process called anion exclusion. The higher the charge of the anion, the larger the exclusion effect. Moreover, the composition of the solution in contact with the surface and the degree of compaction also affect the anion exclusion [16]. In Annex 1, expressions are shown, which allow the estimation of the thickness of the EDL based on the EDL theory.

The adsorbed cations on the clay surface can be exchanged with cations in the pore water in such a way that the electroneutrality of both the solid and the solution is preserved. The cation exchange capacity (CEC) of a clay, expressed in charge equivalents per unit of clay mass, is a measure for the amount of cations that balance the negative charge of the clay surface. Honty [18] reported CEC values of Boom clay ranging from 130 ± 33 to 270 ± 20 meq kg^{-1} bulk rock at the reference site Mol-Dessel. This range of values is consistent with previously reported average CEC values (overview shown by Honty [18]). The CEC variations depend on the smectite content (which contributes for ~90% to the CEC) and thus on the

[1] This range is based on an *in situ* measurement with the ARCHIMEDE piezometer (pH 8.2) and a model fit (speciation calculation) through which the pH was fitted to measured calcium and TIC concentrations in Boom Clay Pore Water (Morpheus piezometer; pH 8.3 to 8.6) [6].

location of the Boom Clay samples throughout the Boom Clay profile in the Mol-1 borehole [18]. For undisturbed Boom Clay, the exchangeable clay cations are mainly Na^+ (47%), Ca^{2+} (20%), Mg^{2+} (20%), and K^+ (12%) [6].

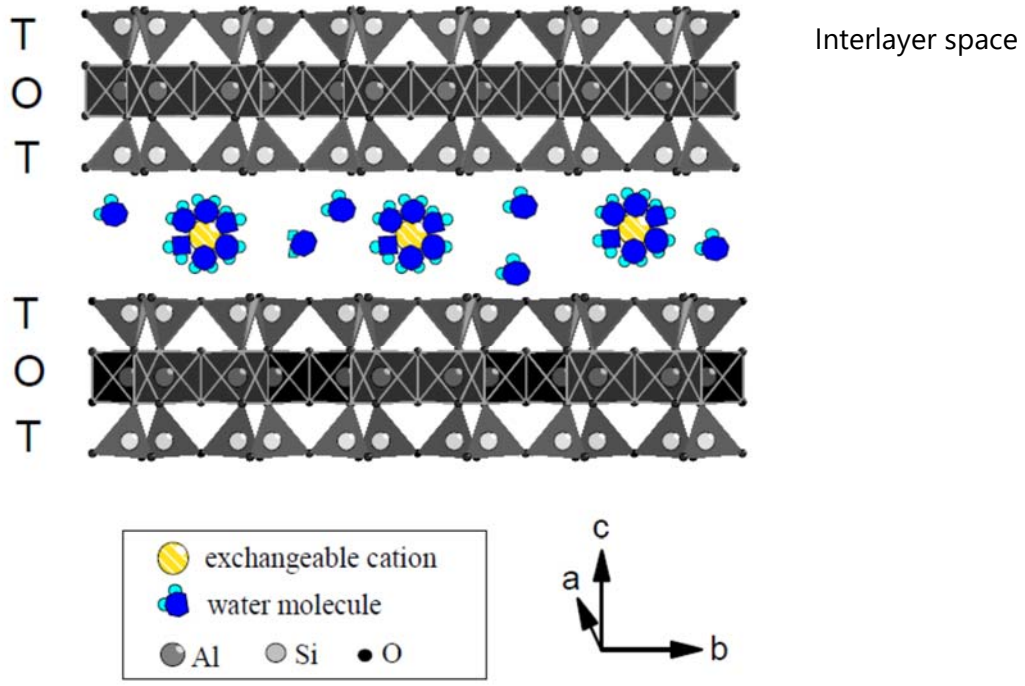

Figure 1: Schematic representation of the montmorillonite structure [15].

Despite their similar unit structure, the clay minerals in Boom Clay can behave differently upon saturation (*i.e.* swelling vs non-swelling behaviour) and consolidation. For instance, smectites (*e.g.* montmorillonite) are swelling clay minerals, while illites are non-swelling [17]. In a swelling clay mineral such as montmorillonite, the thickness of the platelets is only a few individual montmorillonite layers. Larger clay particles are formed from stacks of these platelets, in which the number of platelets in each stack varies from 3-5 in Na-montmorillonite up to 10-20 (and more) for Ca-montmorillonite [15, 16]. In montmorillonite, water and other polar molecules can enter between the unit layers, causing interlayer swelling, *i.e.* expansion in the c direction (Figure 1). The c-axis lattice parameter is ~0.96 nm in the absence of any polar molecules in the interlayer. The interlayers in montmorillonite tend to take up water "layer-wise" and each monolayer of water increases the c-spacing by ~0.25 nm [15, 16].

On the other hand, the isomorphic substitution in illitic clay minerals takes places essentially in the tetrahedral layer. This results in a much higher (negative) surface charge density than in case of the smectite minerals, which in illite is neutralised by dehydrated potassium cations that fit closely in the ditrigonal cavities of the basal oxygen planes. This creates a very stable structure of repeating TOT sheets, which is characterised by a c-spacing of 1 nm. As a result, illite clay minerals do not swell, in contrast to smectite minerals [15-17].

The pore space in a compacted clay such as Boom Clay, can be subdivided as follows (Figure 2) [15, 16, 19]:

(i) The interlayer space, *i.e.* the space between individual TOT layers;
(ii) The interparticle or outerlayer space, *i.e.* the space located beween the clay platelets and/or clay stacks and/or between other grains of minerals present in the clay material.

The water in the interparticle space can further be subdivided into diffuse double layer water, and free water (Figure 2).

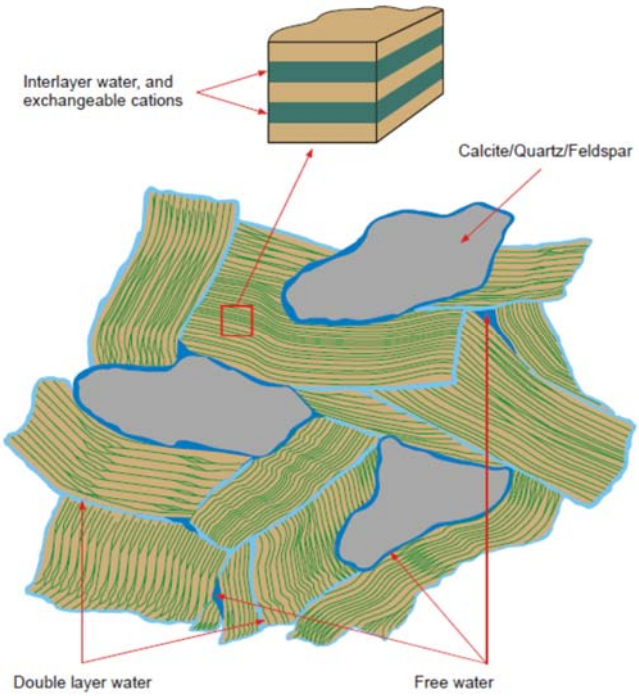

Figure 2: Schematic representation of the interlayer water, the double layer water, and the free water in compacted bentonite [15].

The Boom Clay pore water (BCPW) at the Mol site is basically a 15 mM $NaHCO_3$ solution with Ca^{2+}, Na^{+}, Mg^{2+} and K^{+} as major cations, at concentrations depending on the vertical position in the Boom Clay. Furthermore, this water contains relatively high levels of dissolved organic carbon, *i.e.* 78 – 263 mg C L^{-1}, is rich in humic (HA) and fulvic acids (FA) with a wide molecular size spectrum and has a pCO_2 of $10^{-2.8}$ to $10^{-2.4}$ atm [6, 20]. The reference chemical composition of BCPW, sampled from different piezometers in the HADES Underground Research Laboratory (URL), is reported by De Craen *et al.* [6].

The Boom Clay pore water used in the experiments discussed in this report was sampled from the EG/BS (Extension Gallery Bottom Shaft) piezometer in the HADES underground research laboratory at SCK•CEN (Mol, Belgium). The EG/BS piezometer contains one stainless steel cylindrical filter screen of 60 mm length, with pores ranging from 7 to 16 µm. This filter is centralised in a 13 m long coarse sand column, which enhances the water-draining capabilities of the piezometer and encompasses the silty Double Band of the Boom Clay. Due

to its higher hydraulic conductivity, this Double Band influences to some extent the chemical properties of BCPW [6]. This pore water will later be referred to as Real Boom Clay Water (RBCW) and its composition is described in Annex 2. In anaerobic conditions, nitrate, nitrite or ammonium concentrations are normally below the detection limit of the instrumental techniques used [6]. Furthermore, care was taken to avoid any oxygen contamination during sampling by repeatedly placing the sampling equipment under vacuum and flushing it with N_2 prior to connection to the piezometer.

The presence of pyrite, organic carbon (kerogen), and dissolved organic matter (DOM) in the Boom Clay result in the reducing environment in the Boom Clay ($E_{SHE} \leq$ -270 mV) [6, 14]. The Boom Clay therefore has a certain reducing capacity towards added oxidants [*e.g.* nitrate, redox sensitive (radioactive) species, …].

In the Boom Clay, pyrite is predominantly present as framboids (size ranging from 5 to 100 µm) and as aggregates of small framboids, although discrete octahedral pyrite crystals (0.5 to 8 µm, possibly associated with framboids) also frequently occur. On the other hand, some of the pyrite in Boom Clay is present as concretionary bodies, *i.e.* cylindrical concretionary worm tubes, spherical pyrite nodules, and layered pyrite. These bodies are mostly composed of amorphous pyrite and octahedral crystals [21].

The natural organic matter contains typically functional groups like hydroxylic, carbonylic, carboxylic, phenolic, benzene carboxylic and aromatic carbon groups [22, 23]. The dissolved organic fraction consists of highly aromatic humic acids (42%) and a larger fraction of fulvic acids (58%), which are less aromatic and are rich in carboxylic acids, phenolic and ketonic groups. In general, DOM is composed of more or less equal amounts of linear (n-alkanes, alcanoic acids) and aromatic compounds. The latter fraction is mostly monocyclic and their functional groups are mainly oxygenated and of the acidic and/or methoxy type. Size fractionation of DOM in RBCW showed the presence of very small (< 10 kDa) molecules and larger (30-300 kDa) colloids. Within the > 50 kDa fraction, equal amounts of aromatic and aliphatic organic compounds can be found. The humic acids in RBCW display a wider size range compared to the fulvic acids, which are mostly below 30 kDa [20, 23, 24].

The reducing capacity of DOM is defined as the amount of moles of electron charges per gram of carbon, which is transferred by DOM to an added oxidant (over a given timescale) [25, 26]. The reducing capacity of dissolved natural OM in RBCW using ferricyanide as oxidant is reported to be 4.8 to 9.3 meq gC^{-1} (Section 6.3.2; [26, 27]). The reducing capacity of pyrite and kerogen from Boom Clay has not yet been reported up to now, although the theoretical reducing capacity of pyrite in Boom Clay was estimated to be ~2 meq g^{-1} pyrite (assuming only surface oxidation) to even 10^3 meq g^{-1} pyrite (assuming bulk volume oxidation) [28]. Furthermore, preliminary tests have been performed to estimate the reducing capacity of kerogen extracted from Boom Clay, using ferricyanide (at pH 7; using the initial procedure in Table 8 with 0.1 wt% NaN_3). These tests suggested a reducing capacity of ~2 meq g^{-1} kerogen. However, note that the extracted kerogen also contained a considerable amount of pyrite (up to 50%) that could also have reacted with ferricyanide.

3 Background on the $NaNO_3$ plume

To have an idea to which extent the Boom Clay around a disposal gallery for Eurobitum could be disturbed and to design the experiments in which the impact of these perturbations could be assessed properly, it is important to know the magnitude of the $NaNO_3$ plume in the clay. Modelling calculations were therefore performed to estimate the $NaNO_3$ concentration profiles in a repository for Eurobitum [29].

These modelling calculations aim

(i) to select realistic $NaNO_3$ concentrations to be used in experiments in which the effect of a $NaNO_3$ plume is investigated, *i.e.* percolation tests (see Sections 5.2 and 6.1), bioreactor tests (see Sections 5.3 and 6.2), batch tests (see Sections 5.4 and 6.4), and compressibility tests (see Section 5.2 and 6.1.3);

(ii) to support the calculations to assess the safety of a geological repository for Eurobitum, *i.e.* general safety calculations that possibly include the effect of a $NaNO_3$ plume on the migration parameters of radionuclides.

In the following sections we briefly discuss the modelled $NaNO_3$ concentration profiles around a disposal gallery for Eurobitum. For a more detailed discussion, the reader is referred to the report of Weetjens *et al.* [29].

3.1 Model description

The $NaNO_3$ concentration profiles were estimated (1) by calculating a realistic source term for the release of $NaNO_3$ from Eurobitum bituminised waste into the engineered barrier system (EBS) first and (2) by performing diffusive transport calculations[2] for the migration of Na^+ and NO_3^- in the EBS and Boom Clay in a second step. The concentration profiles were determined under the following boundary conditions and assumptions:

(i) The current design for disposal of Eurobitum with 5 drums per gallery cross section is taken into account [30].

(ii) Cation exchange between Na^+ and Boom Clay cations and linear reversible sorption of Na^+ on cement-based materials (disposal waste container, liner, backfill) is included in the calculations.

(iii) Unreactive transport is considered for nitrate, which provides an upper limit of the concentration profiles. Indeed, it is possible that nitrate will be converted into other compounds, due to radiolysis (near field), abiotic redox reactions (near field and far field), and microbially mediated reactions.

The model was built in a 1D axisymmetric geometry, neglecting solute transport in the axial direction. This results in a slight overestimation of the local $NaNO_3$ concentrations. A Na^+ concentration in the young concrete water of 1490 mg L^{-1} (65 mM) [31] and in BCPW of 359 mg L^{-1} (15.6 mM) [6] are assumed as the initial conditions. No background concentrations were considered for NO_3^-.

[2] A diffusive solute transport model was set up in COMSOL Multiphysics 3.5a (COMSOL AB, 2008).

The source term for the release of $NaNO_3$ from Eurobitum bituminised waste into the EBS is based on the $NaNO_3$ leaching rates observed during hydration of small non-radioactive Eurobitum samples under conditions representative for the different phases after closure of a disposal gallery (free swelling phase and restricted swelling phase) [32, 33]. The $NaNO_3$ release rates obtained for small scale samples have been upscaled to estimate the release rates from real scale Eurobitum waste packages.

Two different source terms were determined to take into account the barrier function of the steel drum to prevent water infiltration through other surfaces of the waste than the upper surface. In the first case it is assumed that the steel drum is only intact during the free swelling phase, which is estimated to last for about 150 years based on results obtained by Sneyers and Van Iseghem [32]. In the other case the drum is assumed to fulfill its barrier function during the whole leaching period. The two different source terms are summarised in Table 1.

Table 1: Overview of the two source terms for the release of $NaNO_3$ from Eurobitum bituminised waste into the engineered barrier system, as determined by upscaling $NaNO_3$ leaching results of water uptake tests with small inactive Eurobitum samples [32, 33].

	Steel drum prevents water infiltration	***Na^+ release rate [a] ($g\ y^{-1}\ drum^{-1}$)/ ($mol\ y^{-1}\ drum^{-1}$)***	***NO_3^- release rate [a] ($g\ y^{-1}\ drum^{-1}$)/ ($mol\ y^{-1}\ drum^{-1}$)***	***Drum depletion time [b] (years)***
Case 1	No	50/ 2.2	136/ 2.2	~290
Case 2	Yes	10.5/ 0.46	29/ 0.46	~1400

[a] The $NaNO_3$ leaching results of the small scale water uptake tests clearly demonstrate a congruent release of Na^+ and NO_3^-.

[b] Time during which the total $NaNO_3$ inventory is released from a Eurobitum drum.

It can be remarked that the release rates (Table 1), are probably overestimated, since constant leaching rates are assumed in the model, while it is expected that the leaching rates will eventually decrease in time due to the compression of leached Eurobitum layers (formation of low-porosity layers; [9]). On the other hand, as higher leaching rates are expected for radioactive Eurobitum that is hydrated in the repository at a water pressure of 22 bar, the overestimation of the source term [based on water uptake tests with inactive samples that are hydrated at low water pressure (~2 bar)] will be slightly[3] mitigated.

Migration properties of Na^+ in Boom Clay are not available at the moment of writing this report. In the transport calculations, the pore diffusion coefficient and porosity values for Na^+ in Boom Clay are therefore assumed to be similar to those of Rb^+ for which migration data exist, *i.e.* a pore diffusion coefficient (D_{pore}) of 1.5×10^{-9} $m^2\ s^{-1}$ and a diffusion accessible porosity (η) of 0.37 [34]. Diffusion through the concrete monolith is assumed to be ten times

[3] As discussed by Mariën *et al.* [9], the effect of water pressure on the $NaNO_3$ release rate from inactive Eurobitum appears to be rather low. However, a significant though small effect of ageing degree (due to radiolysis) on the leaching rate is visible.

slower than in the host formation, due to the lower diffusion accessible porosity. For the backfill, the same D_{pore} as for Boom Clay is used. Sorption of Na^+ on concrete and backfill is considered to be linearly reversible in the calculations, although the value for the retardation factor (R) indicates that Na^+ sorption on concrete is almost neglibible (Table 2). In Boom Clay, this cation will considerably sorb on the clay minerals by cation exchange processes. Exchange of sodium with Boom Clay cations was accounted for by including either a Langmuir isotherm or a linear isotherm (K_d approach, see Annex 4) in the model. These isotherms were obtained by fitting the sorbed Na^+ fraction as a function of the liquid Na^+ concentration for undisturbed Boom Clay conditions[4], as determined with a cation exchange model (in PHREEQC; [35]). The values of the migration parameters for Na^+, which are used in the calculations are shown in Table 2.

The applied migration parameters of NO_3^- in Boom Clay were equal to those of I^- [36], taking anion exclusion into account through the utilisation of the diffusion accessible porosity. The migration parameters in concrete and backfill are based on material properties (porosity) and a conservative estimation of the value of D_{pore} based on the value in Boom Clay (Table 2). Sorption of nitrate was not assumed in the transport calculations.

Table 2: Applied Na^+ and NO_3^- migration parameters through the EBS and Boom Clay [29]. A general description of the transport parameters used in this model is given in Annex 4.

	Concrete		***Backfill***		***Boom Clay***	
	Na^+	NO_3^-	Na^+	NO_3^-	Na^+	NO_3^-
η	0.11	0.11	0.30	0.30	0.37	0.16
ρ (kg L^{-1})	2.360		1.855		1.700	
K_d (L kg^{-1})	0.04		0.02		3.32[a] | LM[b]	
R	1.86		1.12		16.25 | -	
D_{pore} (m^2 s^{-1})	1.50×10^{-10}	1.40×10^{-10}	1.50×10^{-9}	1.40×10^{-10}	1.50×10^{-9}	1.40×10^{-10}

[a-b] Sorption of Na^+ on the Boom Clay minerals accounted for by including a linear isotherm ([a]) or a Langmuir (LM) isotherm ([b]) in the model.

3.2 Discussion on modelled $NaNO_3$ concentration profiles

Figures 3 and 4 show the synthesis plots containing the concentration envelopes[5] for Na^+ and NO_3^- in the Boom Clay for the different studied cases, *i.e.* two different source terms (see Table 2) and two different approaches to describe cation exchange between sodium and Boom Clay cations (linear or Langmuir isotherm; Table 2). First, it can be observed that the differences between the two assumed leaching rates, 2.2 mol y^{-1} $drum^{-1}$ vs 0.46 mol y^{-1} $drum^{-1}$ (Table 1), only affect the Na^+ and NO_3^- concentrations in the first two meters in the host formation, and even here the effect is small. This result shows that both leaching rates are too high, relative to the transport through Boom Clay, to have a drastic effect on the maximum $NaNO_3$ concentration in the Boom Clay. On the other hand, the $NaNO_3$ concentration in the

[4] The total amount (sorbed fraction + fraction in solution) of the competing cations Ca^{2+}, Mg^{2+}, and K^+ was kept constant, and only the total amount of Na^+ was increased.

[5] The concentration envelopes show the maximum concentrations of Na^+ and NO_3^- that will be reached at a given distance from the waste. Note that the COMSOL Multiphysics code cannot check for charge equilibrium.

disposal gallery is mainly affected by the difference in both leaching rates. A second observation is that the maximum Na^+ and NO_3^- concentrations are rather low at the interface between the gallery and the Boom Clay. The Na^+ concentration increases by a factor 4 to 5 at most at the gallery interface compared to the initial background concentration (Figure 3). The NO_3^- concentrations at the gallery interface do not exceed 0.5 M (source term = 0.46 mol y^{-1} $drum^{-1}$) or 1 M (source term = 2.2 mol y^{-1} $drum^{-1}$). These concentrations decrease rapidly within the first meters of the host rock. For instance, at a distance of 5 m in the Boom Clay, the nitrate concentration has decreased to a value of about 0.1 M (Figure 4). Note that the maximum concentrations are conservative values due to the assumptions in the model (see Section 3.1).

Figure 5 shows the time evolution of the sodium occupancy of Boom Clay at different distances from the waste, for case 1 (source term = 2.2 mol y^{-1} $drum^{-1}$) and case 2 (source term = 0.46 mol y^{-1} $drum^{-1}$), based on the Langmuir isotherm approach. It can be observed that for the (more realistic) case 2 at the gallery interface the Na^+ occupancy increases from ~50% to ~80% at most. Since the $NaNO_3$ plume will also contain Ca^{2+}, Mg^{2+}, K^+, and possibly NH_4^+, the real Na^+ occupancy is expected to be smaller. At five metres in the Boom Clay, no significant increase in Na^+ occupancy can be seen. These results demonstrate that the extent of the Boom Clay layer that could be transformed into a clay with a high Na^+ occupancy is limited.

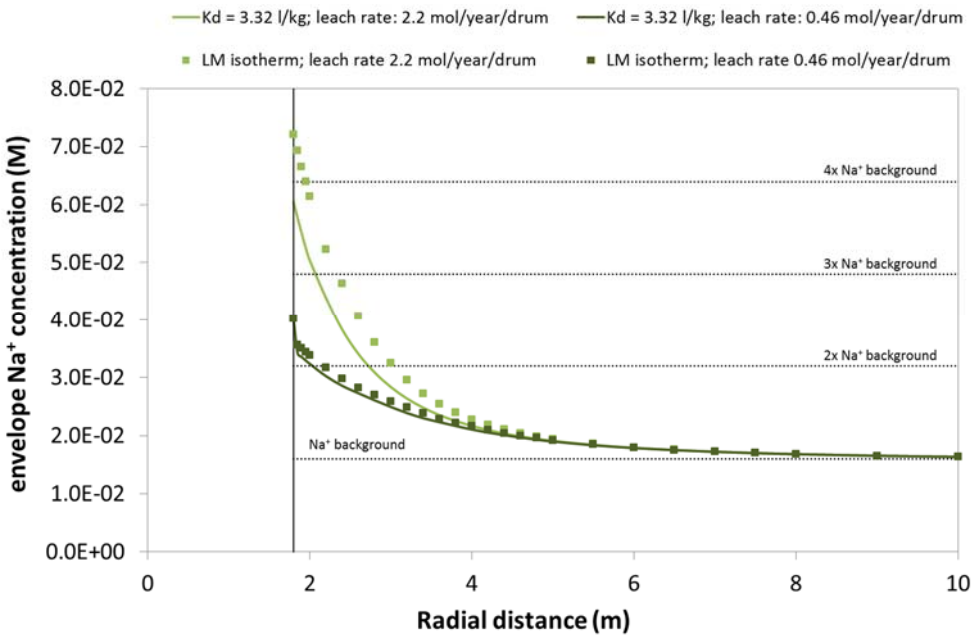

Figure 3: Synthesis plot of the Na^+ concentration envelopes in function of the radial distance from the gallery centre and for the different studied cases, *i.e.* two different source terms (see Table 1) and two different approaches to describe cation exchange between sodium and Boom Clay cations (linear isotherm (K_d approach) or a Langmuir isotherm). The Na^+ concentration of (undisturbed) reference BCPW is 0.016 M [6]; the gallery has an outer diameter of 3.6 m (gallery-Boom Clay interface at 1.8 m, indicated by the vertical line).

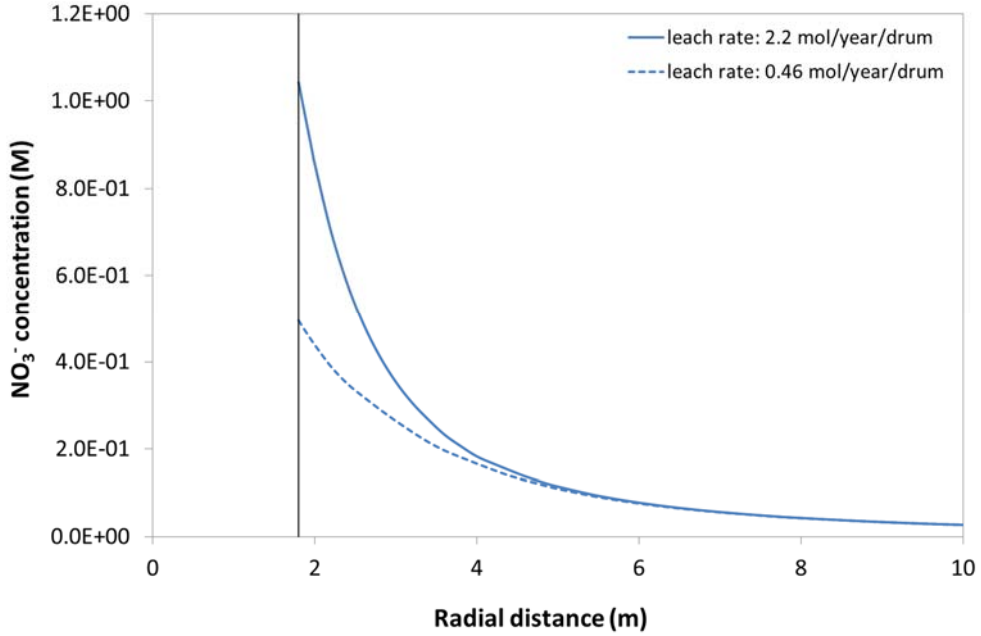

Figure 4: Synthesis plot of the NO_3^- concentration envelopes for the studied cases, *i.e.* two different source terms (see Table 1), in function of the radial distance from the gallery centre. The background nitrate concentration in the Boom Clay is extremely low (usually < 1 – 2 mg L^{-1} according to De Craen *et al.* [6]); the gallery has an outer diameter of 3.6 m (gallery-Boom Clay interface at 1.8 m, indicated by the vertical line).

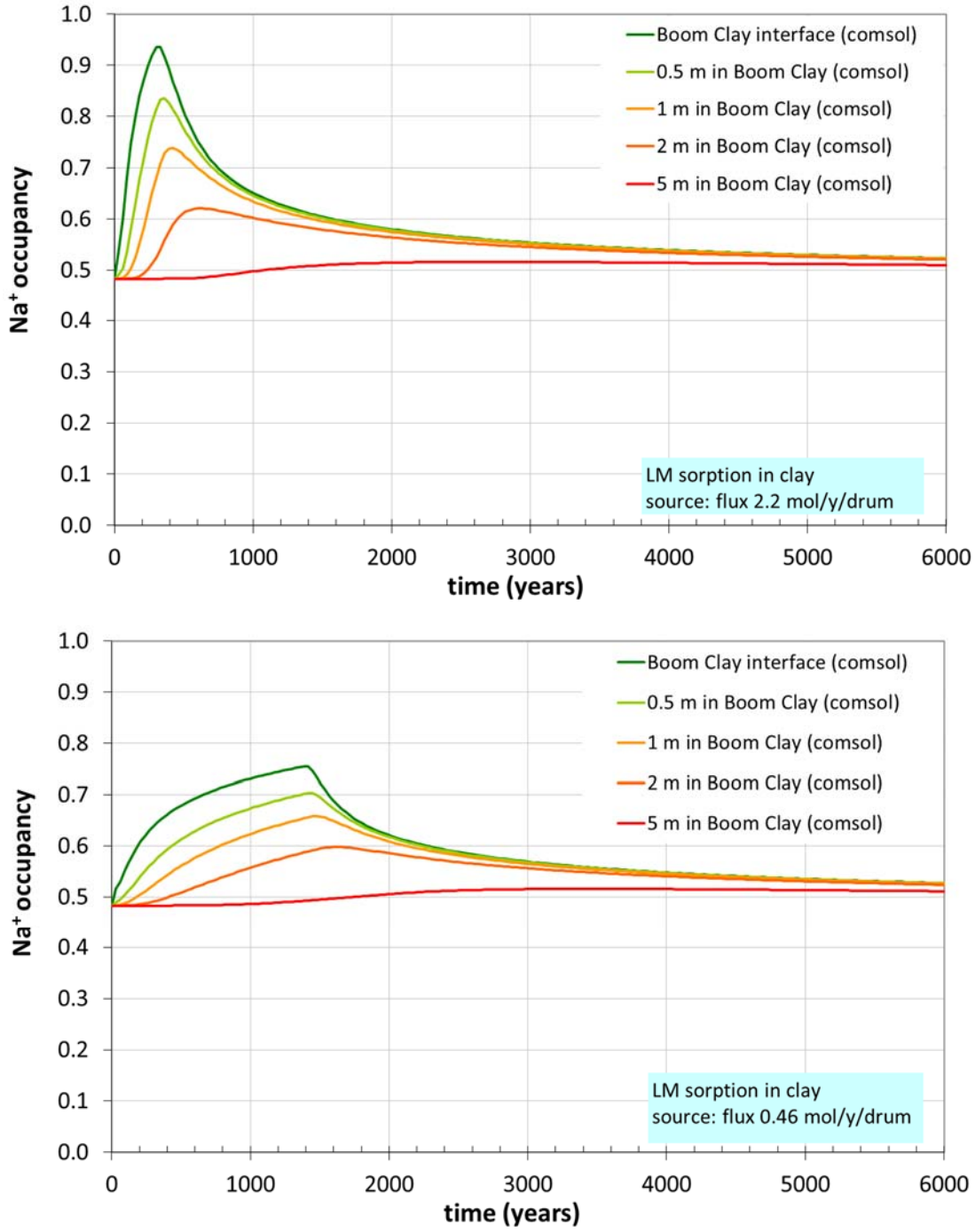

Figure 5: Sorbed Na^+ concentration in Boom Clay in case of non-linear sorption (Langmuir isotherm) for a Na^+ release rate of 2.2 (top; case 1 in Table 1) and 0.46 (bottom; case 2 in Table 1) mol/y/drum (case 1 in Table 1).

4 Geochemical perturbations caused by a $NaNO_3$ plume

In preparation of an assessment basis for SFC-1 with respect to radionuclide migration and retention processes, topical reports have been written by the research unit R&D Disposal at SCK•CEN, to present the most up-to-date understanding and data of the migration of anionic, cationic and neutral radionuclides in Boom Clay. The reader is referred to these reports for an overview of the effect of several parameters (Boom Clay anisotropy, consolidation pressure, temperature and pore water chemistry[6]) on the migration parameters of radionuclides in clay formations [36-42].

The presence of large amounts of $NaNO_3$ in the Boom Clay could however disturb, over a long period of time, the favourable chemical properties of the Boom Clay in its role as a geological barrier. $NaNO_3$ could affect the performance of the clay in several ways: (1) by increasing the ionic strength, (2) by causing a cation exchange between sodium and exchangeable clay cations, (3) by oxidising the redox-active Boom Clay components, (4) by stimulating the microbial activity, and (5) by altering the speciation of redox-sensitive radionuclides. Below, we will discuss each perturbation and the related expected effect on the clay properties more in detail.

4.1 Increase of the ionic strength

An increase of the ionic strength[7] in the Boom Clay has several consequences:

(i) At higher ionic strengths, the charges on the surface of the clay minerals are better shielded and the EDL becomes thinner [43, 44], resulting in a weaker repulsion of the anions, as explained in Annex 1. A variation in EDL thickness could affect the hydraulic conductivity, the clay compaction degree, the filtration (or retention) capacity of the clay towards large mobile organic molecules, and the migration parameters of radionuclides (diffusion accessible porosity, effective diffusion coefficient).

(ii) The stability of the dissolved organic matter and organic colloids in the pore water depends on a combination of van der Waals attraction between the organic molecules that promotes aggregation, and – due to deprotonation of acidic groups – electrostatic repulsive forces that drive the particles apart [45]. Cations will be attracted towards the negatively charged functional groups of the colloids, producing an electrostatic double layer (*i.e.* humic double layer) close to the surface of the organic compounds and stabilising the colloidal suspension [45, 46]. An increase in ionic strength results in a slight increase of the charge density of the dissolved organic matter (and colloids), but also in a higher degree of shielding of these negatively charged functional groups (at pH ~8.2 to 8.6; [47]). This leads to a net decrease in the electrostatic repulsion between the organic compounds (*i.e.* thinner

[6] Note that the effect of $NaNO_3$ on certain transport properties of Boom Clay has been studied in the experiments that are described in this report.

[7] The ionic strength I (M) of an electrolyte is defined as $I = \frac{1}{2}\sum_i z_i^2 . c_i$ with z_i (-) the valence of the ions in the electrolyte and c_i (M) the molar concentration of these ions.

humic double layer) and thus to flocculation [44, 46, 48, 49]. The extent of this process is significantly affected by the valence of the shielding counterions. Polyvalent cations are able to cause 'bridges' between multiple functional groups, and thus cause a higher degree of flocculation [44, 50].

(iii) The solubility of radionuclides could be affected by the presence of other electrolytes in the solution (higher ionic strength). The change in solubility can be derived from the expression of the equilibrium constant of the dissolution reaction. This equilibrium constant is equal to the product of the (solution) activities[8] of the ions in which the radioactive salt dissolves. As the ionic strength of the solution increases, the activity coefficient of these ions changes: at low ionic strength the activity coefficient decreases with increasing ionic strength, while at high ionic strength the activity coefficient re-increases with increasing ionic strength. The turning point depends on the valency and the size of the ion [51]. Therefore, when the ionic strength increases below this turning point, the decrease in activity coefficient will result in an increase in concentration of the dissolved species (increase in solubility). On the other hand, at higher ionic strengths, the re-increasing activity coefficient will lead to a decrease of its concentration (decrease in solubility).

(iv) An increase in ionic strength could lead to an osmotically-induced, local (but relatively small) increase in pore water pressure, with the Boom Clay behaving as a low-efficient semi-permeable membrane [52]. The effect of an increased ionic strength on the osmotically-induced pore water pressure increase in Boom Clay around a disposal gallery has been assessed in a separate project.

4.2 Cation exchange between Na^+ and exchangeable Boom Clay cations

As the waste form degrades, (mainly) sodium cations will be released into the Boom Clay surrounding the disposal gallery for Eurobitum, although sorption of Na^+ on cement and related displacement of K^+ and Ca^{2+}, as well as the leaching of KOH, NaOH and $Ca(OH)_2$ from the cement, will result in K^+ and Ca^{2+} entering the Boom Clay as well. The sodium cations that enter in the clay formation will exchange with the cations on cation exchange sites, transforming the clay minerals (smectite, illite, illite/smectite mixed layers, …) gradually into their sodium form.

At the outerlayer surfaces, exchange of K^+, Mg^{2+} and Ca^{2+}, which initially make up about 50% of the exchangeable alkaline and alkaline earth cations on the clay minerals (see Section 2), by Na^+ results in an increase of the thickness of the EDL. Indeed, the radius of the hydrated Na^+ ion ('the hydrated radius') is about 10% higher than that of K^+, and only about 15% lower than that of Mg^{2+} and Ca^{2+} (Table 3). In combination with the fact that two monovalent Na^+ cations will exchange with one bivalent Mg^{2+} or Ca^{2+} cation, cation exchange with Na^+ results in an expansion of the EDL [17, 44]. The same process will also cause an expansion of the humic double layer [45, 48]. Note that the effect of cation exchange on the double layer thickness with Na^+ is opposite to the effect of the increase in ionic strength. The overall

[8] The activity of ion C in a solution, a_C, is defined as $a_c = \gamma \frac{[C]}{[C^{\ominus}]}$, with γ the activity coefficient (dimensionless), $[C]$ the molar concentration of the ion and $[C^{\ominus}]$ the concentration of the chosen standard state.

change in double layer thickness by a $NaNO_3$ plume will depend on the relative importance of these two counteracting processes, and is expected to be limited.

The consequences of the exchange of K^+, Mg^{2+}, and Ca^{2+}, by Na^+ in the interlayer space is discussed in the next section.

Table 3: Ionic crystal radius and hydrated radius of cations [53, 54].

Cation	*Ionic crystal radius (nm) [53]*	*Hydrated radius (nm) [54][a]*	*Ratio hydrated / crystal [b]*
Li^+	0.068	0.382	5.6
Na^+	0.097	0.358	3.7
K^+	0.133	0.331	2.5
Mg^{2+}	0.066	0.428	6.5
Ca^{2+}	0.099	0.412	4.2
Ba^{2+}	0.112	0.404	3.6

[a] At 25 °C and 1 bar.

[b] Note that for the alkaline and the alkaline earth metals, the ratio of the hydrated radius and the ionic crystal radius decreases with increasing ionic crystal radius. This is related to the lower surface charge density for a higher ionic crystal radius.

The migration of a $NaNO_3$ plume in the Boom Clay can also result in a decreased sorption, and hence in a decreased retardation, of cationic radionuclides, due to a competition with the large amount of Na^+ cations in the pore water. This effect would only be important for cationic (mainly monovalent and bivalent, unhydrolysed) radionuclides, for which the retardation is dominated by cation exchange processes, and not for strongly hydrolysed (multivalent) radionuclides, for which the retardation is dominated by surface complexation (C. Bruggeman, L. Wang, SCK•CEN, personal communication, 2010). Note, however, that a higher Na^+ occupancy of the clay will facilitate the sorption of cationic radionuclides, because of less competition with Na^+ compared to bivalent cations adsorbed on the clay [44]. On the other hand, the higher concentration of competitive cations (*e.g.* K^+, Mg^{2+}, Ca^{2+}) in the pore water solution, will increase the competition between radionuclides and these cations for the sorption sites. The overall effect will probably be a decreased radionuclide sorption.

4.3 Changes in microstructure of Boom Clay

Besides the effect of Na^+ on the cation occupancy of the clay, an increase in sodium in the pore water could also lead to (probably partially irreversible) damage of the clay as Na^+ ions are trapped between the clay particles. For the same reasons as outlined in the previous section, high concentrations of exchangeable sodium could cause swelling, dispersion, and slaking of the clay. Through slaking, the large clay aggregates will be broken down into smaller sized microaggregates. The combination of slaking and dispersion results in a decrease in interparticle space (consisting of diffuse double layer water and free water) and therefore – due to more overlapping EDLs – might result in more immobile pore water and

thus in a lower hydraulic conductivity [55, 56]. These changes in the microstructure of the clay might affect the Boom Clay hydromechanical properties and thus also the Boom Clay characteristic[9]. This in turn might negatively affect the maximum allowable number of Eurobitum drums that can be disposed off in the clay per gallery cross-section without causing an unacceptable geomechanical perturbation [9].

4.4 Oxidation of redox-active Boom Clay components

One of the favourable properties of Boom Clay is its reducing capacity towards redox-sensitive radionuclides. Generally, the Boom Clay has a lower sorption capacity towards the oxidised form of many radionuclides (*e.g.* Tc, Se). Furthermore, redox-sensitive radionuclides (*e.g.*, Tc, Se, and U) are less soluble in their reduced form. Hence, the mobility of radionuclides is expected to be higher when they are present in their oxidised form [37, 42].

The release of nitrate and nitrite in the clay might result in an oxidation of the redox-active Boom Clay components, thereby decreasing the reducing capacity of Boom Clay. On the whole, one has to distinguish between purely chemical and microbial redox processes, in which Boom Clay components are used as electron donors to reduce nitrate or nitrite. Both processes have been studied previously in soil and other sediments [57-61].

Little information is available on an abiotic reaction between nitrate and sediments containing pyrite and organic carbon. Jorgensen *et al.* [60] and Hartog [61] investigated the reduction of nitrate in sediments from Denmark and The Netherlands, respectively. In these studies, microbial nitrate reduction by pyrite and by OM was demonstrated, while no purely chemical reduction of nitrate by pyrite could be observed after up to 6 months. This was confirmed by Schippers and Jorgensen [62, 63], who could not detect a chemical oxidation of pyrite by nitrate after 3 months, although an abiotic MnO_2 reduction by pyrite was observed.

On the other hand, Van Cleemput and Samater [64] showed that in soils under aerobic as well as anaerobic conditions, nitrite can be reduced abiotically by metallic cations (especially ferrous iron) or by soil organic matter, resulting in the formation of several gaseous N-species like NO, NO_2^-, N_2O, and CH_3ONO. Furthermore, reduction of nitrite by phenolic organic soil compounds could lead to the formation of nitro- and nitroso organic compounds, building up organic N in the soil. All the above mentioned non-enzymatic degradation reactions of OM are strongly dependent on the pH and the concentration of the electron donor. At low pH (pH < 5.5), the purely chemical processes tend to dominate over the biological pathways involving nitrite in soils. However, with increasing pH, microbial nitrite reduction appears to become progressively important, rendering the abiotic processes – although still occuring at a very low rate – less significant [64].

Note that an important air oxidation of pyrite in Boom Clay could occur during excavation, causing a decrease in pH, which in turn could affect the surface charge of the clay minerals, and the solubility and speciation of (redox-sensitive) radionuclides ([65]; L. Wang, SCK•CEN, personal communication, 2010). Furthermore, the excavation could also cause oxidation of

[9] The Boom Clay characteristic is the relation between applied stress and resulting volumetric deformation.

the kerogen fraction of Boom Clay, resulting in a higher concentration of DOM and a significant shift in DOM and NOM extractable with solvents towards low molecular weight oxidised organic molecules [23], which might be more easily degraded by microorganisms compared to kerogen.

4.5 Stimulation of bacterial activity

There is some concern that microbial activity in the geological disposal environment could affect the integrity of the repository for Eurobitum. The most important microbial species that could be present in (disturbed) Boom Clay are Nitrate and/or Nitrite Reducing Prokaryotes (respectively NRP and NiRP), Sulphate Reducing Prokaryotes (SRP), and Methane-producing Archaea (MPA). A more detailed description of their metabolism is given in Annex 3.

The release of nitrate and nitrite from Eurobitum into the Boom Clay could stimulate the activity of nitrate or nitrite reducing prokaryotes, leading to the generation of nitrite (by dissimilative nitrate reduction to nitrite (DNRN)), nitrogenous gases (by denitrification) or ammonium (by dissimilative nitrate reduction to ammonium (DNRA)) (Annex 1). The DNRN pathway usually occurs as an intermediate step in the denitrification process, but can also occur without subsequent denitrification, resulting in the accumulation of nitrite [66, 67]. In turn, the produced nitrite might oxidise the clay both biotically and abiotically (see Section 4.4), resulting in a decrease of the reducing capacity of the clay formation. Continuous denitrification could lead to the formation of a separate gas phase if the concentration of produced N gases would exceed the solubility limit of the gases. As the clay is very gas tight, gas evacuation is slow and an excessive gas pressure increase might cause fissuring of the host rock. This might thus result in the formation of preferential pathways for radionuclide migration [68, 69]. Furthermore, ammonium production through DNRA could result in a competition between NH_4^+ and some radionuclides (*e.g.* Cs) for the sorption sites on the clay [70].

Leached radionuclides could also be reduced by the mediation of metal-reducing bacteria (see Annex 3), possibly resulting in an increased sorption and a decreased solubility of these radionuclides [71, 72].

Note that the conditions in the repository for Eurobitum will be rather harsh for microorganisms to grow and be active: limited space and nutrient availability, alkaline conditions and high $NaNO_3$ concentrations in the disturbed clay at the boundary with the concrete liner. These conditions and their effect on the microbial growth and activity are described in detail in Annex 3. This should be taken into account when evaluating the possible perturbations caused by microbial activity in the presence of a $NaNO_3$ plume.

4.6 Direct effect of nitrate on redox-sensitive radionuclides

Nitrate might hinder the reduction of redox-sensitive radionuclides (U, Np, Se, …) that are released from the waste in their oxidised form, and might oxidise radionuclides that occur in their reduced form [71]. For most radionuclides, but not all, the sorption of their oxidised forms on the Boom Clay is lower (*e.g.* Tc, Se) and their solubility is higher, leading to an enhanced mobility (see Section 4.4). Furthermore, nitrate might influence the solubility of radionuclides by complexation.

To study this, preliminary geochemical modelling calculations (L. Wang, SCK•CEN, personal communication, 2010) were performed using the state-of-the-art NEA database [81]. Here, the effect of an increasing redox potential on the speciation of the radionuclides is studied for a range of redox potentials between -400 and +290 mV. The following assumptions were made:

(i) For undisturbed Boom Clay conditions, a 15 mM $NaHCO_3$ solution with pH 8.5 and a fixed redox potential at -275 mV was used to represent Boom Clay pore water. On the other hand, for highly alkaline conditions, the pore water was represented by Young Cement Water (141 mM Na^+, 367 mM K^+, and 0.7 mM Ca^{2+}, pH 13.5). The redox potential of Boom Clay under highly alkaline conditions is expected to be as or even more reducing than in the undisturbed Boom Clay [31], and is therefore assumed to be -400 mV in the calculations.
(ii) $Na_2U_2O_7$, NpO_2 (am, hyd), and NpO_2OH (am, fresh) were considered as the solubility controlling phases in a cement system for U(VI), Np(IV), and Np(V), respectively.
(iii) Only complexation reactions between neptunium or uranium and 'stable' nitrate were considered in the model, *i.e.* redox reactions with nitrate were not taken into account.

These preliminary calculations indicate that

(i) In undisturbed Boom Clay conditions (pH ~8.5, redox ~-275 mV E_{SHE}), strong radionuclide-nitrate complexes are not expected: Np and U will predominantly occur as carbonate and hydroxyl species, even in the presence of up to 1 M nitrate.
(ii) In the highly alkaline and reducing (-400 mV E_{SHE}) conditions expected in and around the disposal gallery, multivalent radionuclides are strongly hydrolysed (*i.e.* formation of stable hydroxyl-complexes), even in the presence of 0.5 M nitrate, *i.e.* no significant complexation reactions between the actinides and nitrate are expected to occur in these conditions.
(iii) Under the reducing conditions expected for Boom Clay (-400 to -275 mV), the solubility of Np is controlled by $Np(IV)(OH)_4$, which is the least soluble oxidation state of Np. However, the solubility of neptunium increases as the redox potential becomes more oxidising (E_{SHE} from -100 to +290 mV), because of the change in oxidation state of Np [from Np(IV) to Np(V)]. Under a highly oxidising redox potential (E_{SHE} +290 mV), the solubility of Np would be controlled by the solubility limit of $Np(V)O_2(OH)_2^-$ instead of the less soluble $Np(IV)(OH)_4$, which prevails in reducing conditions. These oxidising conditions are not expected for the repository, and can only occur when nitrate would be reactive enough to dominate the redox conditions in Boom Clay.

(iv) The solubility of uranium does not change with increasing redox potential, because the oxidation state of U remains as U(VI) for the redox potential range considered in the calculations.

The results of these preliminary geochemical modelling calculations suggest that the effect of nitrate on the solubility of U(IV/VI) and Np(IV/V) is negligible under the expected reducing conditions in the Boom Clay surrounding the disposal gallery of Eurobitum. Only when nitrate would be sufficiently reactive to affect the redox conditions of the Boom Clay significantly, an effect on the solubility of some of the redox-sensitive radionuclides could occur.

In addition, it should be noted that for these preliminary calculations a simple model (the Debye-Hückel model) was used to calculate the activity coefficients. At relatively high ionic strengths (corresponding with nitrate concentrations > ~0.3 M), the uncertainty on the results increases.

4.7 Conclusions

From the discussion above, it is clear that a $NaNO_3$ plume might affect the barrier function of the Boom Clay negatively in different ways:

(1) Impact on the EDL thickness and thereby on the hydraulic conductivity, the anion exclusion and the filtration capacity and migration parameters of radionuclides;
(2) Possible changes of the sorption potential of the clay;
(3) Effect on the microstructure of the clay, caused by the high sodicity and affecting the hydromechanical properties of the clay

Other processes are expected to be of less importance (*e.g.* on the solubility of radionuclides) or could even be positive (*e.g.* cation exchange processes resulting in a lower hydraulic conducitivity). As most of the processes are counteracting, a study of the extent of these disturbances is essential. To this end, several experiments were performed, in which the geochemical perturbations of Boom Clay by $NaNO_3$ or $NaNO_2$ were studied. The setup and results of these experiments are described in the next chapters.

5 Experimental details

This chapter describes the development of several analysis techniques (Section 5.1) and the procedures applied for the experiments to investigate the geochemical perturbations of Boom Clay by $NaNO_3$ (Sections 5.2 to 5.4).

5.1 Development of analysis techniques

To investigate the effect of nitrate on the Boom Clay in the different experiments discussed in this report, some additional analysis techniques were optimised such as microbiological analyses and a method to determine the reducing capacity of RBCW using ferricyanide.

5.1.1 Microbiological analyses

Microbiological analyses of Boom Clay (components) in the experiments described in this report were performed to assess to what extent the influence of the microbial activity should be taken into account when interpreting the results. These analyses were performed both by a conventional microbiological technique (culturing or Most Probable Number method) and by a molecular technique (polymerase chain reaction or PCR).

5.1.1.1 Most probable number (MPN) analysis

Specific culture media were used to quantify certain microbial species present in Boom Clay (slurries) by MPN analysis. For each of these microbiological analyses, 1 mL of slurry or 0.5 mL clay water was serially diluted (10×) in a specific medium. Subsequently, the cultures were incubated until microbial growth and/or activity was observed in a control culture. The microbial concentration was calculated based on the growth and/or activity in the dilution series [82].

As contaminations of the specific media can occur when working in a non-sterile environment (*e.g.* glove box), precautions have to be taken before and when the MPN is performed. For this, the hungate tubes were autoclaved (for 15 min at 121°C) before (re-)use and the septa were properly decontaminated before inoculation of the media in the tubes. These precautions have proven to lower the contamination to a minimum (below detection limit or 3 cells mL^{-1}), thereby making the interpretation of the MPN test reliable. Moreover, a negative control (inoculation with sterile medium itself) was included in each MPN analysis, thereby validating the technique itself.

5.1.1.1.1 Detection of heterotrophic Nitrate or Nitrite Reducing Prokaryotes (NRP and NiRP)

The presence of heterotrophic[10] Nitrate Reducing Prokaryotes (NRP) in the slurries from the first series of bioreactor tests (Section 5.3.3) was analysed after anaerobic incubation in a specific rich medium containing nitrate and glucose as additional electron donor [83] for five weeks at room temperature. The nitrate and nitrite concentration in the medium was measured with Quantofix Test Strips (Machey-Nagel GmbH and Co. KG, Germany). To detect denitrification, a reversed Durham tube was added to the medium. Any generated gas bubbles would remain in the Durham tube.

In the slurries of the 2nd bioreactor tests (Section 5.3.4), the samples were cultured in NRP medium, containing 20 g L^{-1} Luria-Bertani (LB) medium (5 g L^{-1} yeast extract; 5 g L^{-1} NaCl and 10 g L^{-1} tryptone, pH 7.8), 110 mg L^{-1} thioglycolate, 1.0 mg L^{-1} rezazurine and 0.01 M $NaNO_3$ [84]. Denitrification was detected based on the generated gas bubbles in a reversed Durham tube after 2 weeks incubation at room temperature.

In the batch tests (Section 5.4), NRP medium was used for the detection of nitrate reducing prokaryotes. To detect heterotrophic Nitrite Reducing Prokaryotes (NiRP) in the samples of the batch tests with RBCW (Section 5.4.3), MPN tests were performed in NiRP medium, containing 20 g L^{-1} LB medium (pH 7.8), 110 mg L^{-1} thioglycolate, 1.0 mg L^{-1} rezazurine and 0.0072 M $NaNO_2$ (adapted from Drysdale *et al.* [85]). For detection of both NRP and NiRP, the cultures were incubated for four weeks at room temperature. Similar as for NRP, denitrification by NiRP was detected by gas production in reversed Durham tubes. When no gas was produced but bacterial growth did occur (indicated by turbidity of the solutions), the cultures were tested for nitrate or nitrite reduction (or ammonium production) with Merckoquant test strips (Merck KgaA, Germany) according to the manufacturer's instructions.

5.1.1.1.2 Detection of Nitrate or Nitrite-reducing sulfur oxidising bacteria (NR-SOB or NiR-SOB)

The presence of autotrophic[11] NR-SOB and NiR-SOB were detected by using MPN tests with LZ_NO3 and LZ_NO2 medium, respectively. In general, the medium contains 6 g L^{-1} $Na_2S_2O_3.5H_2O$, 1.5 g L^{-1} $NaHCO_3$, 1.5 g L^{-1} Na_2HPO_4, 0.3 g L^{-1} KH_2PO_4, 0.4 g L^{-1} $MgSO_4.7H_2O$, 5.625 mg L^{-1} K_2HPO_4, 5.74 mg L^{-1} NH_4Cl, 1 mg L^{-1} $MgCl_2.6H_2O$, 1 mg L^{-1} $MnSO_4.H_2O$, 1 mg L^{-1} $CaCl_2$ and 1 mg L^{-1} $FeCl_2.6H_2O$ [86]. Furthermore, 3 g L^{-1} KNO_3 or 0.483 g L^{-1} $NaNO_2$ is added to the growth medium as electron acceptor (respectively medium LZ_NO3 and LZ_NO2). Growth and activity were detected in the growth media, incubated at 30°C, after 4 weeks for LZ_NO3 and 6-8 weeks for LZ_NO2, based on turbidity, gas production, and/or ammonium production.

[10] Heterotrophic microorganisms use organic carbon as C source for growth, while autotrophic microorganisms use inorganic carbon.

5.1.1.1.3 Detection of Sulphate and Thiosulphate Reducing Prokaryotes

For the specific culturing of Sulphate Reducing Prokaryotes (SRP) and Thiosulphate Reducing Prokaryotes (TRP) from the slurries of the first series of bioreactor tests (Section 5.3.3), the test kits 'Labège' (commercialised by CFG[11]) were applied according to the manufacturer's instructions. The slurries were diluted serially in the supplied specific liquid growth medium. The inoculated media were then incubated at room temperature for 3 weeks in an anaerobic chamber. For the 2nd series of bioreactor tests (Section 5.3.4), the samples were cultured in Postgate medium (0.5 g L^{-1} K_2HPO_4, 1.0 g L^{-1} NH_4Cl, 1.0 g L^{-1} Na_2SO_4, 0.1 g L^{-1} $CaCl_2.2H_2O$, 2.0 g L^{-1} $MgSO_4.7H_2O$, 2.0 g L^{-1} DL-Na-lactate, 1.0 g L^{-1} yeast extract, 1.0 mg L^{-1} rezazurine, 0.1 g L^{-1} Na-thioglycolate, 0.1 g L^{-1} ascorbic acid, pH 7.8) or RBCW medium [RBCW (filtered with a sterile 0.22 µm filter) with 2 g L^{-1} Na_2SO_4, 0.1 g L^{-1} thioglycolate and 0.1 g L^{-1} ascorbic acid] to detect the presence of SRP [87]. Sulphate and thiosulphate reduction by SRP and TRP was detected by visually checking the blackening of the specific medium due to the formation of FeS.

5.1.1.1.4 Detection of Methane-producing Archaea

The specific media for the detection of Methane-producing Archaea (MPA) were prepared according to Labat and Garcia [88]. The presence of MPA was assessed after five weeks of anaerobic incubation at room temperature by measuring the CH_4 concentration in the head space of the culture tubes using gas chromatography with a flame ionisation detector.

5.1.1.2 Polymerase chain reaction (PCR)

5.1.1.2.1 Background information

PCR is a well known technique to enzymatically amplify a single DNA (deoxyribonucleic acid) fragment or gene using two DNA primers that flank the DNA fragment and copying the DNA in between through repeated cycles of synthesis. This method allows the detection of specific DNA fragments in a wide range of environments, which can provide substantial information about the microbial population that is present. For instance, amplification of the gene encoding nitrate reductase demonstrates the presence of NRP in the sample.

However, the detection of DNA only indicates the presence of bacteria but does not necessarily imply activity of these bacteria, as the DNA could also orginate from dead or dormant cells. To demonstrate the bacterial activity, a reverse transcriptase (RT) PCR should be performed. This technique allows the detection of specific mRNA (messenger ribonucleic acid or transcribed DNA sequence), which would give an indication of the gene expression. However, since RNA is quite unstable after its isolation from the cell, the extraction procedure is complex. Therefore, until now, only PCR (and not RT PCR) has been performed as a diagnostic molecular tool in the experiments described in this report.

[11] Compagnie Française de Géothermie, 3, avenue Claude Guillemin - BP 6429 - 45064 Orléans cedex 2 – France.

5.1.1.2.2 Procedure used in the second series of bioreactor tests

During DNA extraction from soil samples difficulties due to the presence of numerous organic impurities (*e.g.* humic acids) can occur, which can result in a bias of the microbial diversity and/or PCR inhibition. First of all, microbial diversity can be biased due to a difference in adherence of the bacterial groups to soil particles. When the bacteria and soil particles are separated prior to the destruction of the cells, the composition of the microbial community in the separated sample might differ from the original one. However, usually, the cells are lysed inside the soil sample and the DNA is subsequently extracted from the soil sample [89]. DNA from the lysed microorganisms can however become adsorbed to the soil colloids and these DNA-soil complexes cannot be separated easily. Subsequent DNA purification is therefore difficult and even more so in the presence of a high amount of humic acids. Such DNA-organic matter complexes can severely inhibit the PCR as the binding of the DNA polymerase enzyme is hindered, thus preventing the DNA amplification. Therefore, the extraction and purification procedure has to be carefully optimised to the soil type, to avoid the formation of DNA-organic matter complexes as much as possible [90].

Several commercial kits designed for DNA extraction from soil samples were tested for Boom Clay samples and adjusted (including more washing steps of the DNA) to examine their efficiency, *i.e.* the degree in DNA purification and in DNA concentration. Comparison of the test kits showed that the ZR Soil Microbe DNA kit delivered the best results of the commercially available kits [87]. Nevertheless, later tests indicated that even this commercial kit could not guarantee an extracted DNA sample with a high purity. Using these samples in PCR reactions frequently resulted in inhibition of the reaction.

To solve this problem, a new DNA extraction technique has been developed at SCK•CEN (H. Moors, SCK•CEN, personal communication, 2011). Briefly, microbial cells in clay slurries or clay water were lysed overnight in a PEX-lysis buffer (1% potassium ethyl xanthogenate, 0.2 M disodium-EDTA, 2% SDS, 0.8 M ammonium acetate, Tris buffered at pH 8) at 70°C. The DNA fraction was then separated from the cellular debris and impurities from the clay by several consecutive steps: (1) centrifugation; (2) extraction with a mixture of phenol, chloroform, and isoamylacohol (25:24:1); (3) precipitation of DNA in 2-propanol; (4) washing of the DNA by ultrafiltration over a 30 kDa membrane. The pure DNA was then used in the PCR tests for detection of specific microbial populations in the clay slurries. More details on the procedure are given by Wouters *et al.* [91].

PCR amplification of DNA extracted from the clay slurries was carried out in a GeneAmp® PCR System 2700 thermocycler (Applied Biosystems™). Four different PCR reactions were performed to detect the general presence of bacteria (detection of the bacterial 16S rDNA[12]) or to specifically detect SRP (detection of the *apsA* gene), NRP (detection of the *nirS* gene), or MPA (detection of the *mcrA* gene) in the clay slurries. All PCR reactions were performed according to the DreamTaq™ Green PCR Master Mix system (Fermentas, Thermo Scientific). The PCR mixtures (50 µl final volume) contain 0.2 mM of each dNTP, 1 × PCR buffer, 2 mM MgCl2, 0.4 µM of each primer, and ~200 ng DNA template. The primers, which were applied for each of the PCR reactions, are indicated in Table 4 along with the PCR conditions. The PCR products were visualised on 1% agarose gels, which were stained with GelRed™ (Biotium

[12] rDNA is the DNA sequence coding for the ribosomal RNA, which is present in prokaryotic ribosomes.

Inc.). The FastRuler DNA ladder High range (Fermentas, Germany) was used as a molecular weight marker.

Table 4: Overview of the PCR tests, the applied primer and PCR conditions, to detect the presence of microorganisms in the clay water fraction of the second series of bioreactor tests.

PCR	*Primer name*	*Amplified gene*	*Reference to primers*	*PCR conditions*
16S rDNA PCR (all common bacteria)	8f and 926r	16S rDNA	[92]	94°C for 3 min, 30 cycles (94°C for 60s, 56°C for 60s, 72°C for 90s), 72°C for 7 min
SRP PCR	APS7-F and APS8-R	*apsA*	[93]	94°C for 3 min, 35 cycles (94°C for 60s, 49°C for 60s, 72°C for 90s), 72°C for 7 min
NRP PCR	nirS1F and nirS3R	*nirS*	[94]	94°C for 3 min, 30 cycles (94°C for 60s, 47°C for 60s, 72°C for 90s), 72°C for 7 min
MPA PCR	MCRf and MCRr	*mcrA*	[95]	94°C for 3 min, 40 cycles (95°C for 30s, 55°C for 40s, 72°C for 40s), 72°C for 7 min

5.1.2 Selection of an appropriate bacterial inhibitor to create abiotic conditions

Inhibition of bacterial growth and activity can be accomplished via a wide variety of methods. First, physical treatments can be applied, which cause a complete sterilisation, like heat sterilisation (autoclaving), radiation sterilisation (γ-irradiation, X-rays, UV irradiation), and sterile filtration (micro- or ultrafiltration). Alternatively, a chemical treatment with a bacteriocidal or a bacteriostatic (bacterial inhibitor) agent can respectively kill or inhibit the growth/activity of (certain) microorganisms [76].

The mode of action of a bacterial inhibitor varies widely and determines the degree of specificity. Inhibitors that interact with major cellular components (*e.g.* DNA, proteins, lipid membranes, major membrane components) will most likely be broad spectrum inhibitors. These broad spectrum inhibitors include heavy metals, cyanides, azides, aldehydes, antibiotics, and halogenated compounds [76].

Several gradations in microbial inhibition are possible [96]:

(i) Total inhibition of the growth of the target microorganisms.
(ii) Partial inhibition of microbial growth: this could be due to an underdosage of the inhibitor.

(iii) Delayed inhibition: after a certain incubation period, the growth of the target microorganisms will be inhibited. This occurs when the compound needs time to be converted in its active form.

(iv) Transient inhibition: inhibition occurs during a certain period of time, but after this, microbial growth can re-occur (with a growth rate similar to that of a non-inhibited population).

(v) Transient suppressed inhibition: transient inhibition except for a lower final growth rate compared to that of a non-inhibited population.

(vi) Transient enhanced inhibition: transient inhibition except for a higher final growth rate compared to that of a non-inhibited population.

To select an appropriate method for inhibition of the bacterial activity in the abiotic batch tests with Boom Clay components (see Section 5.4), several preliminary experiments using different chemical inhibitors and one physical sterilisation method were performed. The ideal treatment should prevent microbial activity whilst having no or a minimal effect on the geochemistry of Boom Clay (components). As this method should inhibit NRP activity and growth, the presence of nitrate and nitrite should not influence its efficiency. Furthermore, as the batch tests would be running for several years, total inhibition should be achieved (see higher).

In a first series of experiments, Boom Clay slurries with a solid to liquid weight ratio[13] of 1/3, 1/10, and 1/100 were prepared in an anaerobic glove box with deoxygenated RBCW, filtered over a 0.22 µm sterile filter. The outer (possibly oxidised) surface of the Boom Clay cores was removed with a sterile knife to avoid microbial contamination. Glass flasks were filled with 20 to 30 mL of the clay slurries to which the inhibitors and $NaNO_3$ or $NaNO_2$ were added (Table 5). Several inhibitors for NRP were tested: formaldehyde (CH_2O, universal inhibitor), sodium azide (NaN_3, universal inhibitor), mercury chloride ($HgCl_2$, universal inhibitor), Triclosan (universal operating antibiotic), and Chloramphenicol (universal operating antibiotic).

The slurries were incubated for several weeks (Table 5) at room temperature with intermittent sampling of the clay slurries solution to follow up possible changes in the chemical composition. A chemical analysis was performed on the supernatant of the centrifuged Boom Clay slurries. The supernatant of the slurries with a solid to liquid weight ratio of 1/3 was analysed for the major cations in Boom Clay water (Ca, Fe, K, Mg, Na, Si and Mo, analysis with ICP-AES) and for several anions (Cl^-, Br^-, NO_3^-, SO_4^{2-}, $S_2O_3^{2-}$, F^-; analysis with IC and ISEC301F electrode for F^-). The supernatant of the slurries with a solid to liquid weight ratio of 1/10 and 1/100 was analysed for NO_3^-, NO_2^-, SO_4^{2-}, N_3^-, and Hg^{2+}. In addition, the efficiency of the inhibitors was evaluated by assessing the evolution of the NRP concentration (by an MPN test, see Section 5.1.1.1.1) present in the slurries (only determined after 7 weeks of incubation) [84, 97].

[13] Solid/liquid weight ratio = mass Boom Clay/mass Boom Clay pore water.

Table 5: Composition of Boom Clay slurries with $NaNO_3$, $NaNO_2$, and different inhibitors (NaN_3, $HgCl_2$, CH_2O, Triclosan, and Chloramphenicol) to select an appropriate inhibitor for nitrate reducing and denitrifying prokaryotes [84, 97].

Inhibitor	*Concentration inhibitor*	*solid to liquid weight ratio[a] (g Boom Clay/ g RBCW)*	*[$NaNO_3$] (M)*	*[$NaNO_2$] (M)*	*Incubation period (weeks)*	*MPN test[c]*
No		1/3	0, 1	0	52	/
		1/10	0.1, 1	0	3, 7 and 17	+
		1/100	0.1	0	3, 7 and 17	+
		1/100	0	0.1	3, 7 and 17	+
CH_2O	1%	1/3	1	0	52	/
	0.1 and 1%	1/10	0.1	0	3, 7 and 17	+
		1/100	0.1	0	3, 7 and 17	+
		1/100	0	0.1	3, 7 and 17	+
NaN_3	0.1 and 1%	1/10	0.1	0	3, 7 and 17	+
		1/100	0.1	0	3, 7 and 17	+
		1/100	0	0.1	3, 7 and 17	+
$HgCl_2$	0.1 and 0.5%	1/10	0.1, 1[b]	0	3, 7 and 17	+
		1/100	0.1	0	3, 7 and 17	+
		1/100	0	0.1	3, 7 and 17	+
Triclosan	10, 100 and 1000 µM	1/10	0.1	0	3, 7 and 17	+
		1/100	0.1	0	3, 7 and 17	+
Chloram-phenicol	20, 200 and 1000 mg L^{-1}	1/10	0.1	0	3, 7 and 17	+
		1/100	0.1	0	3, 7 and 17	+

[a] Solid to liquid weight ratio = mass Boom Clay/mass RBCW

[b] 0.5% $HgCl_2$ was not tested in the 1 M $NaNO_3$ solutions

[c] + indicates that MPN tests were performed after 7 weeks of incubation in an aerobic box.

In a second series of preliminary tests, the influence of the different inhibitors on the Boom Clay and/or pore water chemistry was examined. For this, different concentrations of some of the inhibitors (formaldehyde, sodium azide, and mercury chloride, all universal inhibitors) were added to Boom Clay slurries (Table 6), which were prepared as described above. The clay water fraction was analysed chemically after 1 week of incubation for the major cations and anions of Boom Clay water, TOC (total organic carbon), TIC (total inorganic carbon) and alkalinity. The effect of Triclosan and Chloramphenicol was not investigated in detail as the first series of tests revealed that these inhibitors were not efficient [84, 97] (Section 6.3.1).

Table 6: Composition of Boom Clay slurries with different inhibitors (NaN_3, $HgCl_2$, and CH_2O), prepared in an anaerobic glove box to investigate the influence of the inhibitors on the chemical composition of the clay water [84, 97].

Inhibitor	*Concentration inhibitor*	*solid to liquid weight ratio (g Boom Clay/g RBCW)*
CH_2O	0.01 wt%	1/3
	0.1 wt%	1/3, 1/10
NaN_3	0.01 wt%	1/3
	0.1 wt%	1/3, 1/10
	1 wt%	1/3
$HgCl_2$	0.001 wt%	1/3
	0.01 wt%	1/3, 1/10
	0.1 wt%	1/3, 1/10

Finally, the use of a physical treatment, *i.e.* filter sterilisation with a sterile 0.22 µm filter (cellulose acetate syringe filters, Whatman), to inhibit bacterial activity in RBCW solutions was investigated. For this, four RBCW solutions were prepared: two RBCW solutions without $NaNO_3$ and two containing 0.05 M $NaNO_3$. Two of these (N_RBCW and N_RBCW + 0.05 M $NaNO_3$) were not filter sterilised, nor was a bacterial inhibitor added, while the other two (F_RBCW and F_RBCW + 0.05 M $NaNO_3$) were filter sterilised into an autoclaved septum bottle immediately after preparation. All solutions were prepared in the glove box (N_2 atmosphere) at a location cleaned with 70 vol% ethanol prior to the beginning of the experiment. The growth and activity of NRP in these solutions was followed up regularly until 6 months after the start by chemical (NO_3^-, NO_2^- and TOC) and MPN analysis (see Section 5.1.1.1.1).

5.1.3 Determination of the reducing capacity of organic matter

5.1.3.1 Background information

To study the extent of a possible redox reaction between dissolved organic matter in Boom Clay pore water and nitrate or nitrite, the reducing capacity of the dissolved organic matter is determined.

Investigating the chemical reducing capacity of humic (HA) and fulvic (FA) acid fractions is commonly done by redox titrations with a suitable electron acceptor, which is frequently an Fe(III) compound [27, 98-101]. For the batch tests with RBCW (Sections 5.4.3 and 6.4.2), both ferricyanide and ferric citrate were used to assess the reducing capacity of DOM in RBCW.

Ferricyanide, $[Fe(CN)_6]^{3-}$, is often used to determine the reducing capacity of dissolved organic matter (HA or FA fractions) owing to its favourable properties like a constant redox potential (~430 mV) over a large pH range from 4 to 11, a high complex stability ($K = 10^{42}$), and a one-electron reduction into $[Fe(CN)_6]^{4-}$, which can be followed up by UV-VIS spectroscopy (maximal UV-VIS absorption of $[Fe(CN)_6]^{3-}$ at 420 nm) [26, 27]. However, some influence of pH and of the type of functional groups on the reducing capacity of DOM for ferricyanide was observed by Matthiessen [99], by comparing the reducing capacity of hydroquinone and natural organic matter from different soils.

Alternatively, ferric citrate can also be used to study the reducing capacity of DOM. The Fe(III)-citrate reduction (also a one electron reduction) can be monitored by complexation of the produced Fe(II) with ferrozine[14] [Fe(II)-ferrozine$_3$ complex; K = $10^{15.53}$]. This complex can be detected by UV-VIS spectroscopy at 562 nm [100, 102]. Note however that the redox potential of the Fe(III)/Fe(II) citrate couple depends on the speciation of the Fe(III) and Fe(II) citrate complexes. Several complexes (mono-, di- and polycitrate species) can be found in aqueous solutions, each with a different standard redox potential. Furthermore, the speciation of iron citrate is dependent on the pH of the solution. Therefore, the value of the redox potential for Fe(III)/Fe(II)-citrate is dependent on pH and on the ratio of Fe(III) to citrate and can range from ~0.3 to -0.2 V [103, 104].

It should be noted that the use of ferricyanide leads to reported reducing capacity values of natural OM that are about 2 to 10 times higher than those obtained with ferric citrate for the same organic compounds [25, 105]. These differences are attributed to the difference in redox potential of both half reactions, in the chemical structure of the oxidants, and to the effect of pH on the speciation of the Fe(III)-citrate complex. Due to these differences, $K_3Fe(CN)_6$ is able to promote a broader range of oxidation reactions than ferric citrate, leading to a higher reducing capacity of DOM [25, 99, 100]. For this reason, the value for the reducing capacity of OM obtained using ferricyanide is considered to be a 'maximally attainable' value for the reducing capacity (of the tested OM) using an Fe(III) complex as oxidant [101].

5.1.3.2 Measurement of reducing capacity of DOM in RBCW using $K_3Fe(CN)_6$

For the determination of the reducing capacity of DOM in RBCW, a preliminary procedure using ferricyanide as electron acceptor was available from Pirlet [27]. Therefore initially, this oxidant was chosen to work with. The reduction of ferricyanide is represented by equation 1:

$$[Fe(CN)_6]^{3-} + \text{HA (reduced form)} \leftrightarrow [Fe(CN)_6]^{4-} + \text{HA (oxidised form)} \quad (1)$$

According to Pirlet [27], the reduction of ferricyanide to ferrocyanide by RBCW should be monitored spectrophotometrically during 50 hours (or until no further reduction takes place) to determine the reducing capacity of OM. The absorbance values should be recorded regularly after the start of the experiment. The concentration of produced ferrocyanide is calculated using the molar extinction coefficient, the absorbance of the solution at 420 nm, and the initial concentration of ferricyanide in the RBCW solutions. When no further reduction of ferricyanide takes place, the reducing capacity of the RBCW (in meq gC^{-1}) is calculated by dividing the concentration of ferrocyanide (at moment of equilibrium) by the concentration of OM [27].

However, when determining the reducing capacity of DOM in RBCW, care must be taken to avoid bacterial activity, which can disturb the results. For instance, in our preliminary tests (not discussed in this report), the results of the reducing capacity of DOM in RBCW were likely influenced by bacterial activity causing a rapid ferricyanide reduction. Indeed, a wide range of iron-reducing bacteria are able to use ferricyanide as the terminal electron acceptor.

[14] Ferrozine = 3-(2-pyridyl)-5, 6-bis (4-phensylsulfonic acid)-1, 2, 4-triazine monosodium salt

Electrons needed for this bioreduction are usually derived from the microbial oxidation of organic substrates (equation 2), which are passed down the electron transport system [106].

$$CH_2O + H_2O + 4\,[Fe(CN)_6]^{3-} \rightarrow CO_2 + 4\,H^+ + 4\,[Fe(CN)_6]^{4-} \quad (2)$$

To avoid microbial activity in the solutions of clay water with ferricyanide, NaN_3 was added, since azide proved to be an appropriate inhibitor for obtaining abiotic conditions in clay water (Section 6.3.1). In a first series of batch tests with RBCW and $NaNO_3$ (Section 5.4.3.1), the reducing capacity of DOM was determined using ferricyanide, based on the procedure that was adapted from Pirlet [27], including the use of NaN_3 as microbial inhibitor. This procedure was optimised further during later batch tests to limit the uncertainties on this value and to determine the influence of several components, such as NaN_3 and ionic strength. For this optimisation, several supporting tests were performed, which are described by Bleyen *et al.* [26]. The approach that was followed for the optimisation of the procedure is shown in Table 7. The conclusions drawn from these supporting tests are described in Section 6.3.2.1. As the procedure was optimised over several years, different procedures were applied for determining the reducing capacity of DOM in the different batch tests with RBCW. An overview of these procedures is given in Table 8.

Table 7: Approach that was followed to optimise the procedure for the determination of the reducing capacity of DOM for ferrycianide, starting from the procedure of Pirlet [27].

Question to be solved	***Tests/approach to solve the question***
Which reactions take place in a clay water – ferricyanide solution?	Tests with the hydroquinone/benzoquinone model as a standard for dissolved organic matter (DOM).
What is the kinetics of the ferricyanide reduction in clay water solutions?	Measurement at regular times of the ferricyanide concentration in clay water solutions.
What is the optimal ferricyanide/dissolved organic matter (DOM) ratio in clay water – ferricyanide solutions?	Measurement of the reducing capacity in solutions with different ferricyanide/DOM ratios. → The optimal ferricyanide/DOM ratio is established as the lowest ratio for which the maximal reducing capacity of DOM for ferricyanide can be obtained after a certain reaction period.
What is the effect of NaN_3 (bacterial inhibitor) on the ferricyanide reduction in clay water solutions?	Measurement of the reducing capacity in ferricyanide – hydroquinone (or clay water) solutions with and without NaN_3.
What is the effect of the presence of nitrate and nitrite on the ferricyanide reduction in clay water solutions?	Measurement of the reducing capacity in ferricyanide – hydroquinone (or clay water) solutions with and without nitrate or nitrite.
Is there an effect of ionic strength on the reduction of ferricyanide in clay water solutions?	Measurement of the reducing capacity of DOM in clay water with different ionic strength values using ferricyanide. The ionic strength is increased by addition of NaCl.

Table 8: Overview of the adaptations made to the original procedure (adapted from [27]) and the optimised procedures that were / are used, to determine the reducing capacity of DOM for ferricyanide. NaN_3 is added to the solutions to prevent microbial ferricyanide reduction.

	dilution of RBCW solution (in SICZH)	***$[Fe(CN)_6]^{3-}$ concentration (mM)***	***Final NaN_3 concentration (wt%)***	***UV-VIS measurement***	***Used in***	***Problems / interferences***
Procedure from Pirlet (2003)	10 vol%	1	1 wt%	Outside glove box	First series of batch tests with RBCW and nitrate (except for final sampling)	1) High standard uncertainty (up to 70%) due to low OM concentration 2) UV-VIS measurement outside glovebox (possible O_2 contamination and delay in measurements) 3) Interference by NaN_3[a]
Optimised procedure I	50 vol%	0.8	1 wt%	Inside glove box	Final sampling first series of batch tests with RBCW and nitrate	Interference by NaN_3[a]
Optimised procedure II	50 vol%	0.8	0.1 wt%	Inside glove box	Second series of batch tests with RBCW and nitrate First series of batch tests with RBCW and nitrite	Interference by NaN_3[a]

[a] Supporting tests with hydroquinone and RBCW suggest that, in the presence of NaN_3, some of the oxidised functional groups of OM (*e.g.* quinone), produced during the redox reaction between OM and ferricyanide, can be reduced back to their reduced state, resulting in a higher reducing capacity [26].

In general, the reducing capacity of DOM for ferricyanide is determined by monitoring the reduction of ferricyanide by DOM in time. For this, dilutions (with synthetic clay water or SCW[15]) of RBCW are prepared to which ferricyanide and NaN_3 are added. Subsamples of these solutions are taken regularly to determine the concentration of ferricyanide by UV-VIS (absorption peak at 420 nm). The RBCW solution without addition of ferricyanide serves as the blanc. To minimise the delay between sampling and UV-VIS measurement and to prevent air oxidation, the UV-VIS measurements are performed inside a glove box under anaerobic atmosphere (N_2). When the reduction of ferricyanide by DOM is no longer significant, the reducing capacity of DOM (in meq gC^{-1}) is calculated as the decrease in ferricyanide concentration divided by the concentration of DOM present in the solution.

5.1.3.3 Measurement of reducing capacity of DOM in RBCW using ferric citrate

As discussed in Section 5.1.3.1, the reducing capacity of DOM can also be determined with ferric citrate as oxidant. For this, the procedure described by Bauer *et al.* [105] was further adapted for RBCW samples. Similar to the measurements of the reducing capacity using ferricyanide, the effect of several components of the solutions from the batch tests on the reduction of ferric citrate by DOM was investigated in supporting tests, as shown in Table 9 and discussed in detail by Bleyen *et al.* [26]. The conclusions drawn from these tests are described in Section 6.3.2.2.

In the optimised procedure, the reducing capacity of DOM is determined by preparing 50 vol% RBCW solutions (diluted in SICZH) with 1 mM ferric citrate and acidifying the solution to a pH of 4.5 using 2 M HCl. Immediately afterwards, ferrozine (freshly prepared in HEPES[16] buffer; final concentration 0.5 g L^{-1}) is added, which will form a complex with the produced Fe(II) [magenta coloured Fe(II)-$Ferrozine_3$ complex] (equation 3).

$$\text{Fe(III) citrate} + \text{HA (reduced form)} \leftrightarrow \text{Fe(II) citrate} + \text{HA (oxidised form)}$$
$$\downarrow$$
$$\text{Fe(II)-Ferrozine}_3 \qquad (3)$$

Subsamples of these solutions are taken regularly and diluted to 20 vol% with demineralised water to determine the concentration of the produced Fe(II)-$Ferrozine_3$ complex by UV-VIS spectroscopy (absorption peak at 562 nm). Two blancs are included to substract the absorbance of background Fe(II) from the spectra: (1) ferric citrate in demineralised water; (2) 50 vol% RBCW. When a significant reduction of ferric citrate no longer takes place (after max 24 hours), the reducing capacity of DOM is calculated by dividing the concentration of the produced ferrous iron by the concentration of DOM. To minimise the delay between sampling and UV-VIS measurement and to prevent air oxidation, the UV-VIS measurements are performed inside a glove box under anaerobic atmosphere (N_2).

[15] The composition of the used SCW is 0.044 g/l NaCl, 0.012 g/l $MgSO_4$, 0.0015 g/l Na_2SO_4, 0.020 g/l KCl, 0.008 g/l NaF and 1.25 g/l $NaHCO_3$.

[16] 6 wt% HEPES (or 4-(2-hydroxyethyl)-1-piperazineethanesulfonic acid) in demineralised water.

As the reaction is in equilibrium after 20 to 24 hours (Section 6.3.2.2), no microbial inhibitor (*e.g.* NaN_3) has to be added. Indeed, microbial activity would occur only after a certain lag phase, which generally takes longer than the fast abiotic reduction of ferric citrate. Note that, when the reducing capacity of DOM in RBCW solutions from the batch tests was determined, 0.1 wt% NaN_3 was already present in the abiotic test solutions.

Table 9: Approach that was followed to optimise the procedure for the determination of the reducing capacity of DOM for ferric citrate, starting from the procedure of Bauer *et al.* [105].

Question to be solved	***Tests/approach to solve the question***
What is the optimal ferric citrate/DOM ratio?	Measurement of the reducing capacity in solutions with different ferric citrate/DOM ratios.
What is the kinetics of the ferric citrate reduction in clay water solutions?	Follow up of the reaction in detail during the first 72 hours after start.
What is the optimal pH environment for measuring the reducing capacity of DOM in RBCW?	Measurement of the reducing capacity in solutions with different initial pHs
What is the effect of NaN_3 (bacterial inhibitor) on the ferric citrate reduction (in clay water solutions)?	Measurement of the reducing capacity in • ferric citrate – RBCW solutions with and without NaN_3. • ferric citrate solutions with and without NaN_3 (effect on background)
What is the effect of the presence of nitrate and nitrite on the ferric citrate reduction (in clay water solutions)?	Measurement of the reducing capacity in • ferric citrate – RBCW solutions with and without nitrate or nitrite. • Ferric citrate solutions with and without nitrate or nitrite (effect on background)

5.2 Combined percolation and pulse injection tests

5.2.1 Aim

Combined percolation and pulse injection tests have been performed to study the effect of a $NaNO_3$ plume on the physicochemical properties of Boom Clay and its impact on the migration properties of tritiated water (HTO) and two anionic radionuclide species ($^{125\text{-}131}I^-$ and $H^{14}CO_3^-$)[17]. For this, four undisturbed Boom Clay cores were taken at the HADES URL in Mol (Belgium), and loaded to a total stress of 2.75 MPa in oedometer cells. These cores were consecutively percolated with RBCW, first without and then with increasing $NaNO_3$ concentration (0.1, 0.5, and 1 M). Subsequent to each conditioning step, aliquots of tritiated

[17] Previously performed combined percolation and pulse injection tests are described by *e.g.* Moors [101], and Bruggeman *et al.* [34, 37].

water (HTO), $^{125\text{-}131}I^-$, and $H^{14}CO_3^-$ were injected as pulses at the inlet of the percolating water (pulse injection experiments with code name D2), to study the impact of increasing $NaNO_3$ concentrations on the migration parameters.

The dispersion of the injected radionuclides was monitored by following the evolution of their activity in the percolate, and this for each $NaNO_3$ concentration tested. These tests aim at investigating the following (combined) effects of a $NaNO_3$ plume in Boom Clay:

(i) Due to an increase in ionic strength and cation exchange processes between sodium and exchangeable cations of the Boom Clay, the thickness of the EDL can change (Sections 4.1 and 4.2). The variation in EDL thickness could affect the hydraulic conductivity of the clay, the migration parameters of radionuclides (diffusion accessible porosity and apparent diffusion coefficient), the retention degree of (large) mobile organic matter, and could result in an expansion or contraction of the clay.

(ii) Besides an effect on the EDL thickness, an increase in ionic strength could result in a higher radionuclide solubility and a flocculation of mobile organic matter (Section 4.1).

(iii) Furthermore, these tests allow us to check whether nitrate can be reduced by Boom Clay components by (1) analysing the percolated $NaNO_3$ solutions for nitrate, nitrite, ammonium, sulphate, and thiosulphate, and (2) by characterising the clay cores, after having dismantled the cells.

(iv) Finally, the effect of a $NaNO_3$ plume on the compressibility of the clay has been investigated.

5.2.2 Set-up

In 1998, four 'undisturbed' Boom Clay cores (38 mm diameter[18], 30 mm length, labeled H1, H2, V5 and V6) were inserted in stainless steel cells inside a glove box ($[O_2] < 2\times10^{-4}$ vol%) to avoid oxidation of the clay cores. The stratification is these cores[19] is either parallel with ('Horizontal', cores H1 and H2) or perpendicular to ('Vertical', cores V5 and V6) the percolation direction, to check the effect of anisotropy on the hydraulic conductivity and on the migration of the injected radionuclides in the pulse injection tests. Figure 6 shows a schematic graph of the experimental set-up of the percolation tests.

[18] Note that the dismantling of cell V5 revealed that the depth of the cavity hosting the metal filter in the piston was ~3 mm larger than the thickness of 2 mm of the filter. This resulted in a 'ring' of ~3 mm height and internal diameter of 36 mm being pressed in the upper part of the clay, decreasing the effective volume of clay with ~1%. The effect of this locally smaller diameter is expected to be negligibly small.

[19] Cores with identification codes 'AG R4-5' and 'AG R7-8'.

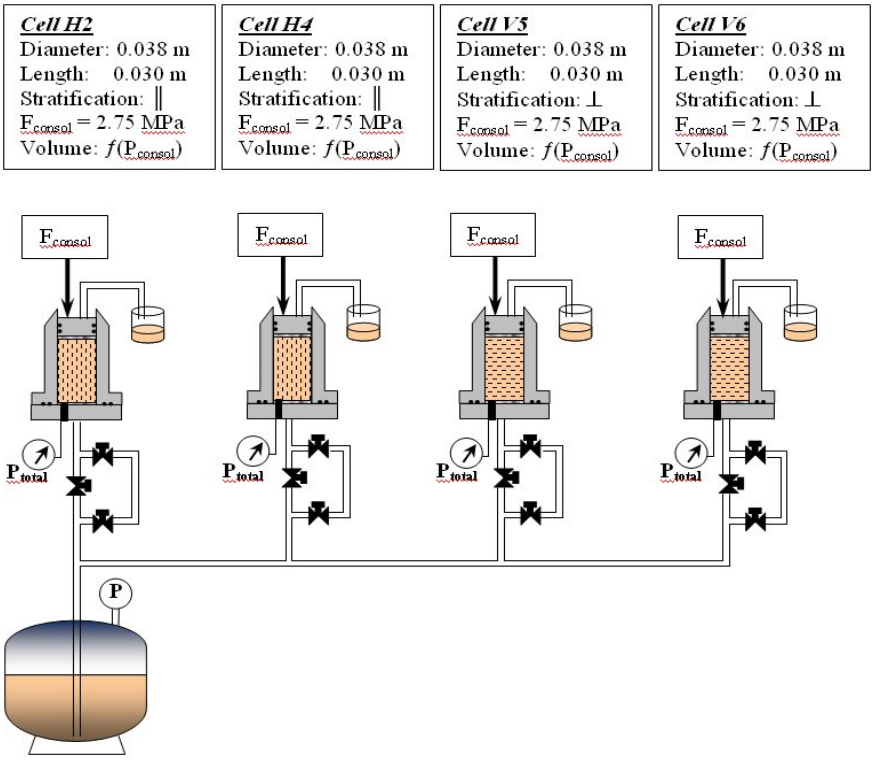

Figure 6: Schematic presentation of the experimental set-up, used to study the effect of a $NaNO_3$ plume on the physicochemical and migration properties of Boom Clay. The percolation solution was supplied from a stainless steel barrel at a water pressure between 0.65 and 1 MPa (adapted from Moors [107]).

The stainless steel cells consist of three parts:

(1) a bottom plate with a sintered stainless steel filter that supports the clay core,
(2) a movable piston with a sintered stainless steel filter that contacts the upper surface of the clay core, and
(3) a 'holder' that is fixed with screws on the bottom plate, and that contains the filters, the clay core, and the piston.

The cells were placed in 'rear loading' oedometers (Wykeham Farrance Ltd.) to apply a constant consolidation pressure of 2.75 MPa on the clay cores. A few months after loading the cores, the (initially undisturbed) clay cores were continuously percolated with RBCW (for composition see Annex 2). Afterwards, the $NaNO_3$ concentration in the RBCW feed water was increased consecutively (Table 10), to equilibrate the cores with the appropriate $NaNO_3$ concentration. The percolation solution was supplied from a stainless steel vessel and was pressurised at an initial pressure of 1 MPa. During the percolation test, the pressure decreased to ~0.65 MPa.

Table 10: Percolation and pulse injection scheme for the four percolation tests, *i.e.* tests H2 and H4 with 'horizontal' cores, and tests V5 and V6 with 'vertical' cores.

Date	*Action*	*Cells on which the action was executed*
05/06/1998	Loading of the clay cores in the oedometer cells (no percolation)	All cells
06/10/1998	Start percolation with RBCW	All cells
18/01/1999	Pulse injection of HTO and $^{131}I^-$	All cells
13/09/1999	Temporary stop of percolation; disconnection of the percolation cells and transport to glove box under inert atmosphere (absence of oxygen)	All cells
01/10/1999	Emplacement of pressure sensor; re-connection of percolation cells in experimental set-up and follow-up of consolidation (no percolation)	All cells
31/01/2000	Continuation of percolation with RBCW	All cells
04/02/2000	Stop of percolation with RBCW	All cells
15/02/2000	Continuation of percolation with RBCW	All cells
14/03/2000	Start percolation with RBCW + 0.1 M $NaNO_3$	All cells
22/09/2000	Pulse injection of $^{125}I^-$	All cells
21/11/2001	Pulse injection of HTO and $H^{14}CO_3^-$	All cells
21/08/2003	Start percolation with RBCW + 0.5 M $NaNO_3$	All cells
16/08/2005	Pulse injection of HTO and $^{125}I^-$	All cells
04/09/2006	Pulse injection of $H^{14}CO_3^-$	H2 and H4
30/07/2007	Start percolation with RBCW + 1 M $NaNO_3$	All cells
21/01/2008	Pulse injection of HTO and $^{125}I^-$	All cells
08/08/2008	Pulse injection of $H^{14}CO_3^-$	H2 and H4
23/02/2010	Stop percolation of RBCW solution (with 1 M $NaNO_3$) to perform compressibility tests	V5 and V6
23/02/2010	Continued percolation with RBCW + 1 M $NaNO_3$	H2 and H4

[a] Between September 1999 and February 2000 there was no percolation of the clay cores.

5.2.2.1 Monitoring of the chemical composition of the percolate and physicochemical properties of the clay

The percolated water was collected regularly during the experiment at the outlet. The samples were stored in a refrigerator to minimise biochemical perturbations of the percolated water in attendance of further analyses (Table 11).

Table 11: Overview of analyses and measurements on the percolate in the four percolation tests.

Analysis/ type of measurement	*Aim*
Measurement of the percolate flow rate, as determined from the weight of the percolated solution over a period of time	Calculation of the hydraulic conductivity from the flow rate, the dimensions of the clay cores, and the applied percolation pressure (0.65 to 1 MPa)
Electrolytic conductivity (EC) measurement of the sampled percolate.	Follow-up of the exchange of the clay cores with the different percolation solutions.
UV-VIS absorption measurement at 266 nm, 280 nm, 360 nm, and 665 nm of the sampled percolate.	Detection of (1) a possible flocculation of dissolved organic matter or (2) a reduced retention degree of (large) mobile organic molecules, due to an increase in ionic strength by $NaNO_3$ and concomitant decrease of the EDL.
pH measurement of the sampled percolate and chemical analysis, for major cations and anions, of a selected set of samples of the percolate.	Evaluation of the effect of a $NaNO_3$ plume on the chemical properties of the Boom Clay (*e.g.* cation exchange between sodium and exchangeable clay cations, see Section 5.2.3.2).
A radiochemical analysis of the sampled percolate during a pulse injection experiment, *i.e.* the measurement of the total gamma and beta activity by means of gamma counters (scintillators, Packard Auto-Gamma 5650 counter, and Packard Cobra Gamma counter) and liquid scintillation counters (Tri-Carb Packard 1900CA).	Evaluation of the effect of a $NaNO_3$ plume on the migration properties of tritiated water (HTO), $^{131}I^-$ or $^{125}I^-$, and $H^{14}CO_3^-$ in Boom Clay (see Section 5.2.3.1)

[a] The internal vertical stress is measured locally (see Figure 6) and is therefore possibly not fully representative for the stress exerted by the clay on the piston.

5.2.2.2 Pulse injection tests

The clay cores were considered to be in equilibrium with the percolation solution once the electrolytic conductivity of the percolate equaled the one of the injected solution and the flow rate (and thus hydraulic conductivity) remained constant. When this steady state was reached, 20 to 25 µl aliquots of radionuclides were injected as pulses at the inlet of the percolation circuit (injection through an inlet-valve-system) (Table 10). Radionuclides from three different groups were tested, *i.e.* HTO (representing unretarded neutral species), iodide ($^{125}I^-$ or $^{131}I^-$) (representing unretarded anions), and $H^{14}CO_3^-$ (representing slightly retarded anions). The dispersion of the injected radionuclides was monitored by following up the evolution of their activity in the percolate, and this for each $NaNO_3$ concentration.

5.2.2.3 Mechanical tests

During the percolation test, the expansion or compression of the clay following a change of the $NaNO_3$ concentration was monitored with a displacement meter on top of the piston. Additionally, pressure sensors were incorporated in the bottom plate, to follow up the internal vertical stress in the clay cores.

After more than 10 years of percolation with $NaNO_3$ solutions, the clay is expected to be converted in a nearly homoionic sodium clay, as predicted by modelling calculations (see Section 6.1.2.1.1). Because of a (about three times) lower flow rate in the vertical cores compared to the horizontal cores, additional pulse injection tests and/or percolation tests would only be performed on the horizontal cores. Therefore, the percolation tests with the vertical cores were stopped in 2010 (Table 10).

Advantage has been taken from the availability of the vertical cores in the oedometers to study the hydromechanical behaviour of a nearly homoionic Na^+-clay, by performing loading-unloading and long-term creep tests prior to dismantling. During the loading-unloading tests, the load on the clay core was increased stepwise to a maximal value of 6.5 MPa (which is slightly higher than the pre-consolidation pressure of Boom Clay of ~6.4 MPa[20]). Each step lasted at least 6 days in order to obtain information concerning the secondary consolidation. Afterwards, long-term creep tests were started at a total vertical stress of 2.0 (core V5) to 2.2 MPa (core V6). The compression (or expansion during unloading) of the clay was studied by measuring the displacement of the piston with a digital dilatometer on top of the piston. The dilatometer was connected to a data acquisition system that continuously measured the position of the piston.

5.2.2.4 Geochemical characterisation of the nearly homoionic Na^+-clay

After the mechanical tests, the cells V5 and V6 were dismantled and the clay cores were pressed out using a manual press. This was performed in a glovebox under Ar atmosphere to avoid oxidation. Each of the cores was cut by hand into 14 cross sections of 2 mm thickness. The water content of each section was determined gravimetrically by weighing the slices before and after overnight drying at 120 °C, and repeating this until a stable weight had been

[20] The preconsolidation stress refers to the maximum effective stress that a soil has experienced throughout its life. The actual *in situ* stress in the Boom Clay at the level of the Underground Research Laboratory (HADES, Mol) is lower than the preconsolidation stress (X. Li, EURIDICE, personal communication, 2010).

reached. Clay powder was prepared from each slice at 70 °C for 1 week in an anaerobic glovebox (under Ar atmosphere) to prevent oxidation. After drying, the clay slices were brought outside the glovebox to be crushed with a mortar and sieved to a grain size of less than 0.125 mm. The samples were stored in a dessicator until characterisation by XRD (X-ray diffraction), determination of the CEC and the clay occupancy and a qualitative analysis of the microstructure of the clay.

XRD was performed on the dried clay powder and on a reference Boom Clay sample, using a Philips X'Pert Pro diffractometer (source was $CuK_{\alpha 1}$ = 1.54060 Å, stepsize 0.017,slit size 0.3667, two-theta range 5-70°, 20s scan step time). The resulting patterns were evaluated with the X'Pert High Score Plus software and the PDF Mineral Database from ICDD (International Centre for Diffraction Data).

The cation exchange capacity (CEC) was determined on the clay powder from 3 positions of the percolated clay cores (top, center and bottom of the core), as well as on reference Boom clay samples from the Mol-1 borehole. The method used was the $[Cu\ Trien]^{2+}$ method in which CEC is determined using a copper (II) triethylenetetramine as an index cation and distilled water as an electrolyte background solution, according to the procedure of Amman *et al.* [108] and previously applied to Boom Clay samples by Honty [18]. The methodology was as follows: a 0.01 M solution of the complex copper(II)-triethylenetetramine or $[Cu\ Trien]^{2+}$ was used to exchange the cations present in the clay with Cu^{2+}. Different amounts of dried clay (100, 200 and 300 mg) were added to 40 mL of distilled water and 10 mL solution of $[Cu\ Trien]^{2+}$. The suspensions of clays were dispersed by an ultrasonic treatment and then shaken for 30 minutes. The supernatant solution was separated by centrifugation and the concentration of $[Cu\ Trien]^{2+}$ was determined by UV-VIS spectrophotometry (Perkin Elmer, Lambda 40). Solution absorbance was measured at 577 nm. The amount of $[Cu\ Trien]^{2+}$ adsorbed was determined using Beer-Lamberts law and a molar absorption coefficient of 0.245 $dm^3\ mol^{-1}\ cm^{-1}$ [18]. The CEC was then calculated as a difference of added and non-adsorbed copper complex and the average CEC was calculated from the values for the different masses of clay [18].

The concentration of the cations Na^+, Ca^{2+}, K^+, Mg^{2+} and Sr^{2+}, which are most commonly found on Boom Clay, was determined in the solutions that were obtained from the CEC measurement. These concentrations were used to calculate the cation occupancy of the Na^+ exchanged clay cores.

A possible deterioration of the clay microstructure due to the high sodium occupancy was investigated by comparing the settlement of the V5 and V6 clay powder in synthetic clay water with that of the reference clay samples from the Mol site used as references for CEC. For this, the clay powder was shaken in synthetic clay water for 4 hours. Afterwards, the suspensions were placed vertically and the settlement of the clay powder was monitored in time.

5.2.3 Combined geochemical and transport modelling

To study the effect of a $NaNO_3$ plume on the migration properties of radionuclides in Boom Clay and on the cation occupancy of the clay, combined transport and geochemical modelling calculations were performed.

5.2.3.1 Modelling of radionuclide migration parameters

To be able to determine the effect of $NaNO_3$ on the migration of some selected radionuclides through the Boom Clay, pulse injection tests were performed on the percolated clay cores. These tests ultimately provide values for the following migration parameters, necessary for performance assessment calculations (see Annex 4 for description):

(i) Chemical retention parameter: retardation factor R (dimensionless), representing the uptake of a radionuclide by the inorganic and organic phases present in the Boom Clay;

(ii) Transport parameters:
- diffusion accessible porosity ε (dimensionless) and its product with the retardation factor: εR;
- the apparent velocity V_{app} (m/s);
- the apparent dispersion coefficient: D^i_{app} (m^2/s).

In fact, fitting (with a least square method) of the evolution of the tracer concentration in the outflowing water, provides values for D^i_{app} and V_{app}. For this, the D2_fit_V2 model was used, which is based on an analytical solution of the transport equation with relevant initial and boundary conditions (more details by Moors [107]). The product εR was calculated based on the values of V_{app} and V_{Darcy}[21]. The latter is related to the hydraulic conductivity, the pressure difference over the clay volume and the core length (see Annex 4, equation A4.2), which can all be obtained from the experimental data. Therefore, to calculate the value of εR accurately, it is important that the pulse injections are performed when the hydraulic conductivity (and thus V_{Darcy}) is constant.

To study the effect of $NaNO_3$ on the radionuclide migration, the obtained values for the migration parameters obtained during percolation with $NaNO_3$, were compared with values from pulse injection experiments in undisturbed Boom Clay cores percolated with RBCW.

5.2.3.2 Modelling of cation concentrations in the outflow of the $NaNO_3$ percolation experiments

Reactive coupled transport modelling with the PHREEQC-2 code was used to describe the experimentally observed elution curves for the cations (as determined by chemical analyses, see Table 11). Solute transport and water-clay interaction mechanisms were accounted for in the model. The model assumes that the variation in cation concentration in the percolate is controlled by fast and reversible cation exchange processes and not by kinetically controlled dissolution/precipitation of clay minerals. This assumption is based on the outcome of a previous experiment [31], which demonstrated that in case of percolation with concrete water with high Na^+ and K^+ concentrations, Na^+ and K^+ elution curves showed a chromatographic pattern typical for cation exchange processes.

[21] $\eta R = V_{Darcy} / V_{app}$.
V_{Darcy} is the total amount of water percolated out of the clay core during the experiment per cross section unit of the clay core and per time unit.

For these calculations, cation exchange parameters previously determined for non-perturbed Boom Clay were used. The reference RBCW composition and the average cation exchange capacity of the clay were taken from De Craen *et al.* [6]. A sensitivity analysis was performed to assess the influence of parameter values (*e.g.* CEC, selectivity coefficients) on the goodness-of-fit of the model to the experimental data. For more details on the database, the model domain, and the parameter values, the reader is referred to a report and paper of Martens *et al.* [35, 109].

5.3 Bioreactor tests

5.3.1 Aim

One of the possible consequences of a $NaNO_3$ and/or $NaNO_2$ plume originating from Eurobitum is the stimulation of microbial nitrate and nitrite reduction. To study this, bioreactor tests were performed, in which the activity of anaerobic microorganisms (endogenous or exogenous to the clay) in Boom Clay slurries with / without $NaNO_3$ and in some cases also Eurobitum degradation products, was investigated.

5.3.2 General set-up

The Boom Clay needed for both bioreactor experiments was cored around the Underground Research Laboratory HADES in Mol, using thin walled stainless steel tubes, smoothly pushed into the clay. To prevent oxidation of the clay as much as possible, the Boom Clay cores were stored anaerobically in the stainless steel tubes, which were hermetically sealed off with flanges.

The reactors were made of two welded 316L stainless steel (reactors S01_A and S01_B and S02_A, S02_B, and S02_C) or carbon steel (reactor S02_D) end caps with an internal volume of ~2.7 L (Figure 7). Pre-calibrated absolute pressure transducers (Druck PTX710) were inserted in the reactors to measure the gas pressure during the experiment regularly. Mixing of the clay slurries was assured by rotating the reactors, which had two blades welded perpendicularly inside the reactor walls. The slurries of both experiments were incubated for 1023 days (series 2, see Section 5.3.4) or 1285 days (series 1, see Section 5.3.3) at room temperature under two different gas atmospheres (N_2 and H_2 for respectively series 1 and 2), which permitted to study the effect of the presence of these gases [due to excavation (N_2), or due to radiolysis and anaerobic corrosion of metal (H_2)] in the clay near the underground repository. Moreover, introducing a H_2 atmosphere in the reactors allowed for the detection of microbial N_2 production.

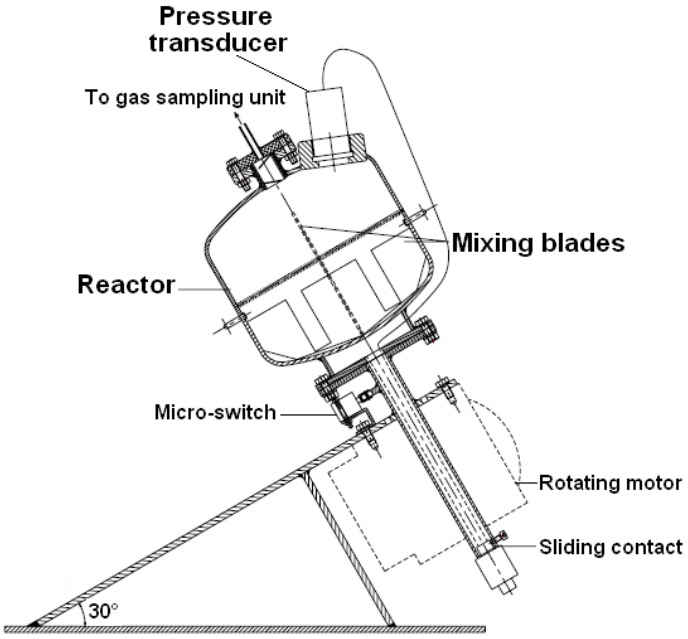

Figure 7: Schematic representation of the reactor used in the bioreactor tests (series 1 and series 2) [110].

5.3.3 First series of bioreactor tests

This series of tests was performed and reported by Ortiz [110]. For each reactor, 1.5 kg Boom Clay was mixed with 2.25 L of SICZH (see Annex 2 for composition) and 50 mM $NaNO_3$[22] for 2 days in a glove box under N_2 atmosphere. These mixtures were then introduced in the anoxic reactors and placed under a N_2 atmosphere at a gas pressure of 1.012 bar and 1.023 bar, respectively for reactor S01_A and S01_B. To the reactor mixture for reactor S01_B an 'Eurobitum radiolytic degradation product' solution (98.3 g or 95.4 mL) was added as well. This degradation product solution contained organic molecules and salts originating from the radiolytic degradation and leaching from Eurobitum (*a.o.* 1.5 mM $NaNO_3$, 25 mM $NaNO_2$, 3 mM $CaSO_4$, 0.15 mM HCOONa, 0.3 mM CH_3COONa, and 0.04 mM $C_2O_4Na_2$; [111]).

The slurries for reactors S01_A and S01_B weighed 2514 and 2618 g and the specific slurry masses were 1.256 g cm^{-3} and 1.258 g cm^{-3}, respectively. The volume of the slurries in the reactors was 2002 mL and 2082 mL, while the gas volumes in both reactors were 663 and 560 mL, respectively. The final solid to liquid weight ratio was 0.487 kg L^{-1} for reactor S01_A and 0.486 kg L^{-1} for reactor S01_B (with added bitumen degradation products and salts).

[22] The modelled $NaNO_3$ concentration profiles in the Boom Clay around a disposal gallery for Eurobitum (Section 3) show that a maximum nitrate concentration of 50 mM will be reached at a distance of about 5 to 6 m from the gallery. Closer to the gallery, the maximum nitrate concentration will be higher, but in time this concentration will also decrease to values equal to (and below) 50 mM.

5.3.3.1 Chemical analysis

At the end of the experiment, the gas phases in both reactors were analysed by gas chromatography (GC) at the Research Institute for Chromatography (Kortrijk, Belgium). A Molsieve column was used for the separation of H_2, O_2, N_2, and CO, while the quantification of the other gases was performed after separation on a PoraPLOT Q column.

The chemical composition of the liquid phase of the clay slurry was determined at the beginning and at the end of the experiment. Hereto, aliquots of the slurries were centrifuged for 2 hours at 27200 g. Chemical analysis was performed in-house by ISE (F^-, NH_4^+), IC (Cl^-, NO_3^-, NO_2^-, HPO_4^{2-}, SO_4^{2-}, $HCOO^-$, CH_3COO^-, and $C_2O_4^{2-}$), GC-MS (minor organic components), ICP-AES (metallic elements), and TOC/TIC analyses. At the start of the experiment and after dismantling the reactors, the pH of both the clay water fractions after sedimentation of the slurries and of the slurries themselves was measured, as well as the redox potential (E_{SHE} or redox potential vs the standard hydrogen electrode) of the Boom Clay slurries.

5.3.3.2 Microbiological analysis

Microbiological analyses were carried out on the slurry samples after dismantling the reactors. The presence of NRP, SRP, TRP, and MPA was investigated by MPN tests as described in Section 5.1.1.1.

5.3.4 Second series of bioreactor tests

Before storing the clay cores anaerobically by vacuum packaging in sterile bags, the clay cores were squeezed to remove the pore water. Prior to the start of the experiment, the outer and therefore most oxidised and contaminated layers were removed. In a glove box under Ar + 0.4% CO_2 atmosphere, 0.4 kg Boom Clay was mixed (for each reactor) with 1.25 L of filtered (with 0.22 µm sterile filter) RBCW for minimum 48 hours, until a homogeneous slurry was obtained. After preparation, the slurries were introduced in the reactors. To two of the slurries (reactors S02_A and S02_B) 0.50 M $NaNO_3$ (final concentration)[23] was added. The specific slurry mass[24] of all slurries was 1.1 g cm^{-3}. The final solid to liquid weight ratio was 0.36 kg L^{-1} in the two reactors with added $NaNO_3$ and 0.32 kg L^{-1} in the two reactors without $NaNO_3$. The volume of the slurries in the reactors was 1.52 L (S02_A and B) and 1.49 L (S02_C and D), while the gas volumes in these reactors were 1.14 L (S02_A and B) and 1.17 L (S02_C and D). A filtered (0.22 µm filter) H_2 gas phase was introduced above the reaction media. The initial gas pressures at the start of the experiment were 1.415 bar, 1.75 bar, 1.585 bar, and 1.670 bar in respectively reactors S02_A, S02_B, S02_C, and S02_D.

[23] The modelled $NaNO_3$ concentration profiles in the Boom Clay around a disposal gallery for Eurobitum (Section 4) show that a concentration of 0.5 M nitrate is reached in the first meter around the gallery.

[24] The specific slurry mass was calculated based on the densities of the liquid and solid phase (density of dry Boom Clay;[6]) and on the concentration of solids in the slurry (in wt%).

5.3.4.1 Chemical analysis

Just before the final sampling of the clay water solutions for chemical analysis, the head space in each reactor was sampled and analysed using gas chromatography (NMi Van Swinden; The Netherlands). The O_2, N_2, CO_2, CH_4, N_2O, CO, C_2H_4, C_2H_6 and H_2 concentrations were measured by GC-Thermal Conductivity Detection.

The chemical composition of the liquid phase of the clay slurries has been determined at the start and at the end of the experiment. For this purpose, aliquots of the slurries were centrifuged for 2 hours at 21000 g (at the beginning of the test) or at 9000 g (after finishing the test) and were subsequently filtered (0.22 µm filter). Similar chemical analyses were performed as for the first series of bioreactor tests (see Section 5.3.3.1). The pH was measured in the clay slurries after finishing the experiment.

5.3.4.2 Microbiological analysis

MPN analysis was performed using specific culture media to detect the presence of NRP and SRP in the Boom Clay slurries, as described in Section 5.1.1.1. To verify these results several (specific) PCR tests were performed to detect the presence of microbial DNA in the clay water and clay slurry samples (Section 5.1.1.2.1). Note however that the PCR tests were only performed 3 to 4 years after finishing the experiment.

5.3.4.3 Characterisation of clay minerals

To determine differences in clay minerals after incubation of the clay slurries with/without nitrate in presence of H_2, XRD was performed, according to the procedure described by Honty [13]. The powder samples (dried out clay slurry) were scanned using the Philips X'Pert Pro System (mask 10 mm, soller slit 0.04, two-theta range 5 to 120°, 20 s/step, CuKα radiation and X'Celerator detector). The resulting patterns were evaluated with the X'Pert High Score Plus software and the PDF Mineral Database from ICDD.

5.4 Batch tests

5.4.1 Aim of the batch tests

In these tests we investigated whether and to which extent nitrate and/or nitrite can oxidise Boom Clay (components) abiotically (at room temperature) or mediated by microbes. Note that a nitrite plume might be caused by the release of radiolytically produced nitrite from Eurobitum, and/or by a (bacterially mediated) nitrate reduction in the Boom Clay.

To allow a clear interpretation of any reaction of nitrate and nitrite with the main reducing components of Boom Clay (dissolved organic matter, kerogen, pyrite), batch experiments with each of these components, and with Boom Clay slurries are being performed. As opposed to the bioreactor tests (Section 5.3), which mainly investigated microbial activity in Boom Clay slurries, the batch tests presented here aim at studying both a purely chemical and a microbially mediated oxidation of Boom Clay components by nitrate or nitrite in separate tests. Until now, batch tests have been carried out with Boom Clay slurries, with

RBCW and with pyrite. In the future, additional batch tests with kerogen and Boom Clay slurries can also be investigated.

5.4.2 Batch tests with Boom Clay slurries

The batch tests with Boom Clay slurries primarily aimed at selecting an appropriate microbial inhibitor for the abiotic batch tests. Nevertheless, these tests also allowed to draw some preliminary conclusions on the abiotic reactivity between nitrate or nitrite and Boom Clay by combining the results of the chemical (nitrate, nitrite, and sulphate analysis) and the microbial analyses. The set-up of these tests has been explained in Section 5.1.2.

5.4.3 Batch tests with RBCW (DOM as electron donor)

For all batch tests with RBCW, Boom Clay pore water was sampled from the EG/BS piezometer (see Section 2). Precautions have been taken to avoid any oxygen contamination during sampling of the RBCW. All test conditions were performed in duplicate.

5.4.3.1 First series of batch tests with RBCW and nitrate

All solutions of this batch test were prepared in an anaerobic glove box (Ar + 0.4% CO_2). Table 12 gives an overview of the number of tests that were started, together with the $NaNO_3$ and NaN_3 concentrations. After preparation of each batch of test solution, the solutions were divided over a series of septum bottles (100 mL, amber glass), each to be opened after a certain reaction period. The $NaNO_3$ concentrations used in these batch tests are considered to be realistic, based on the modelling calculations performed to estimate the $NaNO_3$ concentration profiles in a repository for Eurobitum (see Section 3): (maximum) nitrate concentrations of 0.05 M and 0.2 M are expected to be reached at a distance of about 6 m and 2 m from the gallery wall respectively. Closer to the gallery, the maximum nitrate concentration will be higher, but in time this concentration will decrease as well [29].

As will be discussed in Section 6.3.1, NaN_3 had been identified as the most appropriate inhibitor for NRP. Solutions without NaN_3 were included in this series of batch tests to distinguish between a microbially mediated and an abiotic nitrate reduction (Table 12). Per solution, 16 replicates (~50 mL) were prepared, allowing duplicate analyses after 8 different reaction periods (2, 7, 35, 65, 105, 181, 392, and 700 days). The analyses include chemical analyses (Na^+, Ca^{2+}, NO_3^-, NO_2^-, TIC/TOC), pH measurements, microbial analyses (MPN analysis for NRP detection, as described in Section 5.1.1.1.1) and the determination of the reducing capacity of DOM for ferricyanide as described in Section 5.1.3.2 and Table 13.

Table 12: Overview of the first series of batch tests with RBCW and nitrate (start-up in March 2008). Code ending with x% bact: solutions with x wt% bacteriostatic compound (NaN_3).

$NaNO_3$ concentration (M)	***1 wt% NaN_3 (abiotic tests)***	***No NaN_3 (control tests)***
0	0 M NaNO3_1% bact	0 M NaNO3_0% bact
0.05	0.05 M NaNO3_1% bact	
0.2	0.2 M NaNO3_1% bact	0.2 M NaNO3_0% bact

[a] Control tests for nitrate addition

Table 13: Overview of the composition of the solutions prepared to determine the reducing capacity of DOM for the first series of batch tests with RBCW and nitrate, after a given incubation period in an anaerobic glove box.

Incubation time[a] (days)	***dilution of RBCW solution (in SICZH)***	***$[Fe(CN)_6]^{3-}$ concentration (mM)***	***NaN_3 (wt%)***
0, 2 until 392	10 vol%	1	1
700	50 vol%	0.8	1

[a] Incubation time before analysing the solutions, and thus determining the reducing capacity of the DOM for ferricyanide.

5.4.3.2 Second series of batch tests with RBCW and nitrate

A second series of batch tests with RBCW and $NaNO_3$ has been started up in March 2010. The set-up of these batch tests is similar to the first series of batch tests (see Section 5.4.3.1), but this time lower $NaNO_3$ concentrations were added to the RBCW solutions (Table 14). Additionally, less samplings have been performed at the beginning of the tests, since previously reported studies (Section 4.4), as well as the results of the first batch tests (see Section 6.4.2.1) and preliminary tests with hydroquinone and nitrate [26], did not indicate any chemical reaction between nitrate and DOM. Furthermore, as the results of the optimisation tests with hydroquinone suggest that the addition of azide could result in the reduction of quinone-like species [26], the NaN_3 concentration in the RBCW solutions was limited to 0.2 wt%, which still completely inhibits microbial growth and activity (see Section 6.3.1).

The RBCW solutions (Table 14) were prepared in an anaerobic glove box under N_2 atmosphere. Per solution, 12 replicates [~80 mL (series a) or ~60 mL (series b)] were prepared, allowing duplicate analyses (series a and b) after six different reaction periods (7 days, 1, 3, 6, 18, and ~30 months). At the moment of writing this report, the last sampling has not yet been performed. The same analyses as for the first series of batch tests (with RBCW and $NaNO_3$) were/are performed after each incubation period (see Section 5.4.3.1). The reducing capacity of DOM for $[Fe(CN)_6]^{3-}$ has been determined according to the optimised procedure (see Section 5.1.3.2 and Table 15). For the solutions sampled six months after the start of the batch tests, NaCl was added to the RBCW-ferricyanide solutions, to equal the ionic strength of all solutions during the measurement of the reducing capacity. This was done, to verify the results of the supporting tests (Section 6.3.2.1). No significant influence of ionic strength on the reducing capacity of DOM could be observed for the range of ionic strength of these batch test solutions. For the next sampling, NaCl was therefore not added.

Furthermore, for the samples taken after 18 months, NaN_3 was no longer added to the biotic RBCW-ferricyanide solutions during reducing capacity measurements. In contrast, for these samples, all RBCW-ferricyanide solutions were filter sterilised to prevent microbial ferricyanide reduction. In addition, the reducing capacity of DOM in samples taken after ~18 months of incubation was also determined with ferric citrate (Table 15).

Table 14: Overview of the second series of batch tests with RBCW and nitrate (start-up in March 2010). Code ending with x% bact: solutions with x wt% bacteriostatic compound (NaN_3).

$NaNO_3$ concentration (M)	***0.2 wt% NaN_3 (abiotic tests)***	***No NaN_3 (control tests)***
0[a]	0 M NaNO3_0.2% bact	0 M NaNO3_0% bact
0.005	0.005 M NaNO3_0.2% bact	
0.1	0.1 M NaNO3_0.2% bact	0.1 M NaNO3_0% bact

[a] Control tests for nitrate addition

Table 15: Overview of the composition of the solutions prepared to determine the reducing capacity of DOM for the second series of batch tests with RBCW and nitrate, after a given incubation period in an anaerobic glove box. Only the solutions prepared until the moment of writing this report are included. After 554 days of incubation, both ferricyanide and ferric citrate (FeCit) were used as oxidant to determine the reducing capacity of DOM in the control tests.

Incubation time[a] (days)	***dilution of RBCW solution (in SICZH)***	***$[Fe(CN)_6]^{3-}$ concentration (mM)***	***[FeCit] concentration (mM)***	***NaN_3 (wt%)***	***Ionic strength[b] (M)***
0, 7, 36, 98, 554	50 vol%	0.8	/	0.1	/
189	50 vol%	0.8	/	0.1	Adjusted to ~0.09 M
554	50 vol%	/	1	/[c]	/

[a] Incubation time before analysing the solutions, and thus determining the reducing capacity of the DOM for ferricyanide.

[b] NaCl was added to the solutions to obtain equal ionic strength values in all solutions, to verify that the small differences in ionic strength of the RBCW solutions did not affect the reducing capacity of DOM for ferricyanide (see Section 6.3.2.1).

[c] When determining the reducing capacity of DOM for ferricyanide after 544 days of incubation, NaN_3 was not added to the diluted RBCW from the control tests. To prevent microbial ferricyanide reduction in these RBCW-ferricyanide solutions, all solutions were filter sterilised immediately after preparation.

Furthermore, a gas analysis (by µGC) on the headspace of the samples '0.1M NaNO3_0% bact' and '0.1M NaNO3_0.2% bact' was performed to detect any formation of N_2O due to denitrification. N_2 could not be detected as this is the initial atmosphere in the test bottles (atmosphere of the glove box; an Ar atmosphere could not be used since the UV-VIS spectrophotometer in the glove box cannot work under Ar atmosphere). The concentration of dissolved gases in the interval solution was derived using Henry's law (with k_H (N_2) = 0.00065 M atm^{-1} and k_H (N_2O) = 0.024 M atm^{-1} at 19 °C [112]).

5.4.3.3 First series of batch tests with RBCW and nitrite

A first series of batch tests with RBCW and $NaNO_2$ was started with the same set-up as for the second series of batch tests with RBCW and $NaNO_3$ (see Section 5.4.3.2; Table 16). The RBCW solutions were prepared in an anaerobic glove box (N_2 atmosphere). A more extensive sampling scheme (*i.e.* more sampling during the first six months) was followed compared to the tests with nitrate (Table 17), since there was no indication yet on the kinetics of a reaction between DOM and nitrite, but it was expected to be faster than for nitrate.

For each solution, 16 replicates [~80 mL (series a) or ~60 mL (series b)] were prepared, allowing duplicate analyses (series a and b) after 8 different reaction periods (2 and 7 days, 1, 2, 3, 6, 18, and ~30 months). At the moment of writing this report, the last sampling has not been performed yet. The same analyses as for the second series of batch tests with RBCW and nitrate (see Section 5.4.3.2) have been performed after each reaction period, *i.e.* chemical, microbiological, and gas analyses. The latter was only performed on samples '0.05 M NaNO2_0% bact' and '0.05 M NaNO2_0.2% bact', to detect any formation of N_2O due to reduction of nitrite. As nitrite reduction is studied in these batch tests, NiRP medium was used for the MPN tests. Only for the first MPN tests (at the start and after 2 and 7 days), NRP medium was used as the NiRP medium was not completely optimised yet. Although the use of the NRP medium will not allow us to specifically detect Nitrite Reducing Prokaryotes[25], it will give an indication of the inhibitory effect of azide in the abiotic tests. The reducing capacity of DOM in RBCW for $[Fe(CN)_6]^{3-}$ has been determined according to the optimised procedure (see Section 5.1.3.2 and Table 17). Small adjustments to this procedure were made similar to the analyses for the second series of batch tests with RBCW and nitrate (Section 5.4.3.2 and Table 17). For the samples taken after ~18 months of incubation, the reducing capacity of DOM was determined using ferric citrate as well as ferricyanide (Section 5.1.3.3 and Table 17).

Table 16: Overview of the batch tests with RBCW and nitrite (start-up in March 2010). Code ending with x% bact: solutions with x wt% bacteriostatic compound (NaN_3).

$NaNO_2$ concentration (M)	***0.2 wt% NaN_3 (abiotic tests)***	***No NaN_3 (control tests)***
0	0M NaNO2_0.2% bact	0M NaNO2_0% bact
0.005	0.005M NaNO2_0.2% bact	
0.05	0.05M NaNO2_0.2% bact	0.05M NaNO2_0% bact

[25] The use of NRP medium will not allow to detect specifically Nitrite Reducing Prokaryotes, although certain populations of NRP are capable of using nitrite from the environment as electron acceptor and are thus also considered to be NiRP [70].

Table 17: Overview of the composition of the solutions prepared to determine the reducing capacity of DOM for the first series of batch tests with RBCW and nitrite, after a given incubation period in an anaerobic glove box. Only the solutions prepared until the moment of writing this report are included. After 554 days of incubation, both ferricyanide and ferric citrate (FeCit) were used as oxidant to determine the reducing capacity of DOM in the control tests.

Incubation time[a] (days)	*dilution of RBCW solution (in SICZH)*	*$[Fe(CN)_6]^{3-}$ concentration (mM)*	*[FeCit] concentration (mM)*	*NaN_3 (wt%)*	*Ionic strength[b] (M)*
0, 2, 7, 36, 63, 92, 544	50 vol%	0.8	/	0.1[c]	/
189	50 vol%	0.8	/	0.1	Adjusted to ~0.09 M
554	50 vol%	/	1 mM	/	/

[a] Incubation time before analysing the solutions, and thus determining the reducing capacity of the DOM for ferricyanide.

[b] NaCl was added to the solutions to obtain equal ionic strength values in all solutions, to verify that the small differences in ionic strength of the RBCW solutions did not affect the reducing capacity of DOM for ferricyanide (see Section 6.3.2.1).

[c] When determining the reducing capacity of DOM for ferricyanide after 544 days of incubation, NaN_3 was not added to the diluted RBCW from the control tests. To prevent microbial ferricyanide reduction in these RBCW-ferricyanide solutions, all solutions were filter sterilised immediately after preparation (see Section 5.1.2).

5.4.4 Batch tests with pyrite

For all batch tests with pyrite, commercially available pyrite (from a Peruvian mine, VWR) was used. All pyrite suspensions containing nitrate or nitrite for these batch tests were prepared in an anaerobic glove box (N_2 atmosphere), to prevent air oxidation of pyrite. The suspensions are shaken regularly to allow maximal contact between the pyrite and the electron acceptors (*i.e.* $NaNO_3$ and $NaNO_2$) present in the suspensions.

To assess the oxidation of pyrite by nitrate and nitrite under conditions similar to those in Boom Clay, pyrite suspensions should have been prepared with synthetic clay water (Annex 2). However, as synthetic clay water also contains components (*e.g.* Fe^{2+}), which might affect the outcome of the batch test, the tests were performed in a sodium bicarbonate solution (1.25 g L^{-1} or 15 mM $NaHCO_3$ and flushed with CO_2), close to its concentration in RBCW and with a similar pH. However, due to the presence of bicarbonate during pyrite oxidation, siderite or other ferrous iron carbonate complexes can be produced, which have a higher dissolution limit and thereby tend to prevent the pyrite surface from coating with ferrous hydroxide [113]. To study the effect of bicarbonate on the pyrite oxidation rate, additional batch tests are performed in demineralised water.

Since the required nutrients and microorganisms (NR-SOB, NiR-SOB and/or iron oxidisers (FeOB)) were not sufficiently present in the pyrite suspensions (*i.e.* in the bicarbonate and demineralised water suspensions), microbial activity (and thus microbial pyrite oxidation) was not expected, although microbial contamination from the glove box in which the suspensions were prepared, was possible. To prevent any perturbation of the batch tests by microbial activity, 0.1 wt% NaN_3 was added to some of the abiotic pyrite suspensions (Tables 18 and 19). This compound has frequently been used when investigating pyrite oxidation [60, 62] and preliminary studies indicated that the applied concentration is sufficient to (still) inhibit microbial growth completely (Section 6.3.1). The possible effect of azide on the outcome of

the batch tests with pyrite is studied by including pyrite suspensions in bicarbonate solution without addition of azide (control tests for azide in Tables 18 and 19).

Furthermore, one series of batch tests with pyrite was performed in a bacterial nutrient solution (BNS[26]), spiked with *Thiobacillus denitrificans*, a known nitrate (and nitrite)-dependent autotrophic pyrite oxidiser, which is active at pH 6 to 8 [86, 114, 115]. This microbial species is capable to oxidise both S_2^{2-} and Fe^{2+} from pyrite [115]. Such pyrite suspensions in which nutrients and SOB and/or FeOB are available in sufficiently high quantities would serve as a good positive control for pyrite oxidation.

5.4.4.1 Sample preparation and characterisation

From a pyrite crystal cluster, a fraction was removed for preparation of pyrite powder. This powder was prepared under an argon atmosphere, according to the procedure described by Descostes *et al.* [116]. To remove any oxidation products from the pyrite surface, the samples were completely submerged in 37% HCl for several hours. The pyrite was then introduced into an anaerobic glove box (under Ar + 0.4% CO_2 atmosphere) and rinsed thoroughly with ethanol. Subsequently, the pyrite was grinded in a mortar and sieved again with ethanol (selection of grain sizes < 150 µm). Finally, the pyrite grains were washed with ethanol in an ultrasonic bath and filtered using a cellulose filter (particle retention level of 12.5 µm, Whatman), to remove fine particles adhering to the grain surfaces as much as possible. The pyrite powder was dried and stored anaerobically under an argon atmosphere.

To verify the absence of impurities in the powder, an XRD analysis was performed, according to the procedure described by Honty [13]. The powder samples were scanned using the Philips X'Pert Pro System (mask 10 mm, soller slit 0.04, two-theta range 5-120°, 20 s/step, CuKα radiation and X'Celerator detector). The resulting patterns were evaluated with the X'Pert High Score Plus software and the PDF Mineral Database from ICDD. The spectra obtained by XRD confirmed the presence of predominantly pyrite (Figure 8) in the sample. The XRD pattern only shows two additional small and broad peaks at ~44° two-theta related to an unidentified (and possibly amorphous) phase. Furthermore, no considerable amount (relative to the bulk of the material) of sulfur, iron, FeS, ferrous or ferric sulphates could be detected.

[26] Composition of BNS: 1.5 g/l $NaHCO_3$, 1.5 g/l Na_2HPO_4, 0.3 g/l KH_2PO_4, 0.4 g/l $MgSO_4.7H_2O$, 5.6 mg/l K_2HPO_4, 5.74 mg/l NH_4Cl, 1 mg/l $MgCl_2.6H_2O$, 1 mg/l $MnSO_4.H2O$, 1 mg/l $CaCl_2$, and 1 mg/l $FeCl_2.6H_2O$ at pH 7 (based on Lampe and Zhang [83]).

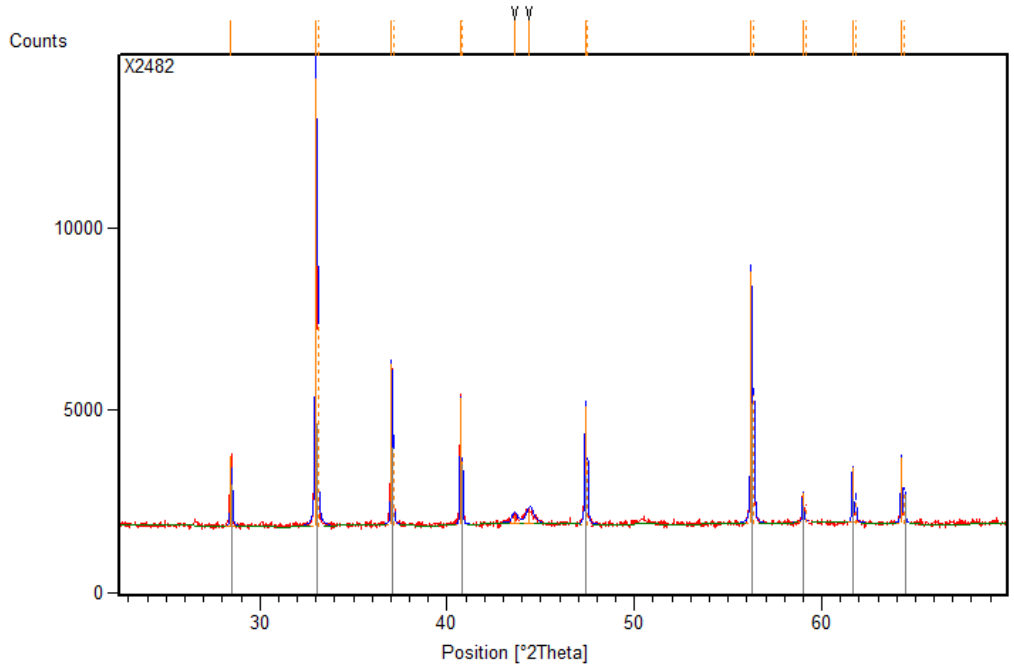

Figure 8: The XRD pattern (20-70° two-theta) of the pyrite powder prepared for the batch tests with pyrite. The obtained diffraction peaks (blue lines) are exactly located at the theoretically expected positions (grey bars; based on PDF database from ICDD, International Centre for Diffraction Data).

The average grain size and distribution were checked with scanning electron microscopy (SEM). The stoichiometric ratio Fe/S was determined by SEM-based energy dispersive X-ray spectroscopy (EDX). For both techniques, a sample of the dry pyrite powder was mounted on copper stubs in the vacuum chamber of a JXA-840 electron microscope (Japan Electron Optics Laboratory Co., Ltd (JEOL), Tokyo, Japan). SEM analyses were performed at 15 kV (300 µA). The SEM images reveal a broad range of pyrite grain sizes, *i.e.* from large grains of ~100 µm in diameter down to high amounts of nanosized particles (0.1 to 1 µm), similar to grains in pyrite framboids present in Boom Clay [117]. The analyses of the pyrite powder with EDX confirmed the composition of the sample as pyrite, but also some SiO_2 was found. Based on the EDX results, the stoichiometric Fe/S ratio (average Fe/S ratio = 0.58 ± 0.14) was slightly higher than expected based on the molecular formula of pyrite (FeS_2 with Fe/S ratio of 0.5). This would suggest that the powder contains also some Fe-S species with a higher Fe to S ratio, *e.g.* FeS, ferrous or ferric (thio)sulphates. Furthermore, slightly elevated $S_2O_3^{2-}$ concentrations (~1 to 2 mg L^{-1}) were found after suspending the pyrite powder in a 15 mM bicarbonate solution. These results suggest the presence of a remainder of the oxidised layer on the pyrite surfaces. Nevertheless, as these species could not be detected by XRD, they are considered to be negligible compared to the large amount of FeS_2 present.

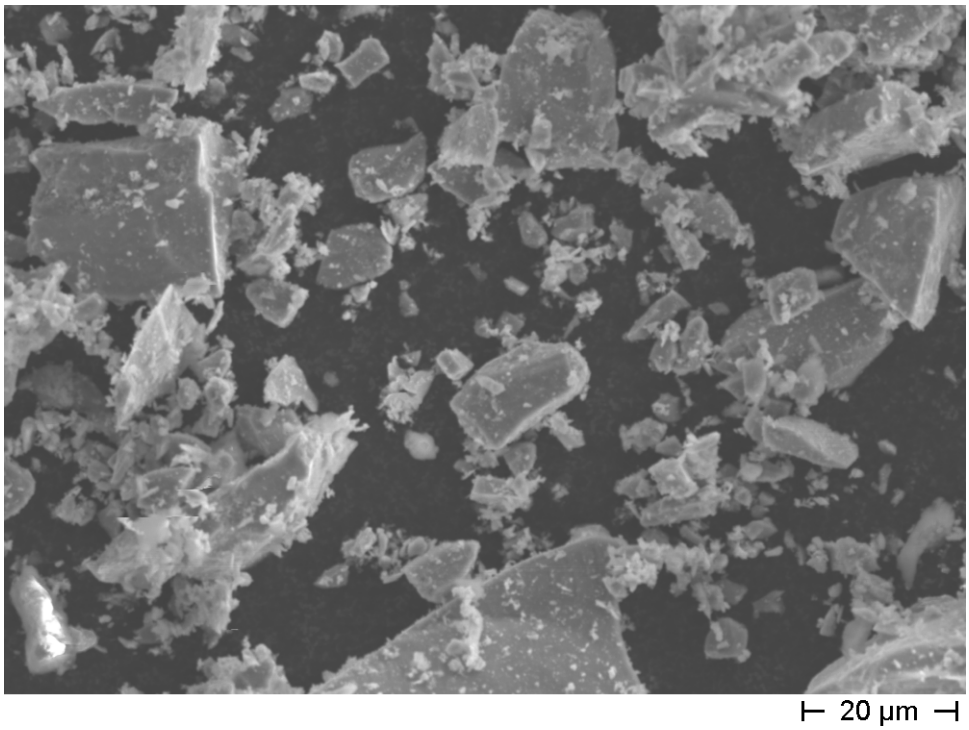

Figure 9: SEM image of the prepared pyrite powder, showing the grain size distribution.

The samples of pyrite were also characterised by BET surface area analysis (based on the Brunauer, Emmett and Teller theory) to determine the specific surface area (SA) of the pyrite grains, using N_2 as the adsorbant. Compared to literature data for similarly prepared pyrite powder (*e.g.* Descostes *et al.* [116]), rather high SA values were obtained for the prepared pyrite, *i.e.* 1.53 ± 0.12 $m^2\ g^{-1}$, which is most likely related to the high amount of nanoparticles in the powder.

5.4.4.2 Batch tests with pyrite and nitrate (started in March 2011)

Table 18 gives an overview of the batch tests with pyrite, in which the oxidation of pyrite by nitrate is studied. In these tests, most of the pyrite suspensions were prepared in a sodium bicarbonate solution (1.25 g L^{-1} or 15 mM $NaHCO_3$ and flushed with CO_2), while the remainder of the test suspensions were prepared in demineralised water, to study the effect of bicarbonate on the pyrite oxidation rate (see Section 5.4.4).

To obtain abiotic conditions, 0.1 wt% NaN_3 was added to some of the solutions (abiotic tests). The effect of NaN_3 on the possible abiotic pyrite oxidation was further investigated by including additional pyrite suspensions without NaN_3 and with/without nitrate or nitrite in the batch tests (control tests for azide). In these solutions, microbial activity was not expected due to a lack of nutrients. MPN tests (for NR-SOB detection; see Section 5.1.1.1.2) were performed to confirm this.

The pyrite suspensions were prepared in an anaerobic glove box (N_2 atmosphere). For this, 70 mL of each test solution (Table 18) was added to a septum bottle (100 mL, amber glass), containing 0.35 g of pyrite powder. The amount of pyrite added to each solution was

weighed, to allow normalisation of the results to the total surface of pyrite available for reaction[27]. Per test condition, 12 duplicates were prepared allowing duplicate analyses after 6 different reaction periods (start, 1, 3, 6, 12, and 24 months), as indicated in Table 18. Only for the test condition without $NaNO_3$, no duplicate samplings were foreseen. At the moment of writing this report, samplings up to 1 year have been performed.

After each incubation period, the chemical composition of the test solution was assessed, *i.e.* the concentrations of NO_3^-, NO_2^-, $S_2O_3^{2-}$, SO_4^{2-}, total iron, NH_4^+, TIC, and/or TOC were determined in the filtrates[28] of the pyrite suspensions. Furthermore, pH and E_{SHE} measurements and microbial analyses (MPN analysis for detection of NR-SOB, as described in Section 5.1.1.1.2) were performed on the pyrite suspensions.

5.4.4.3 Batch tests with pyrite and nitrite (started in March 2011)

Table 18 gives an overview of the batch tests with pyrite, in which the oxidation of pyrite by nitrite is studied. The same set-up as for the batch tests with pyrite and nitrate was applied (see Section 5.4.4.2), *i.e.* (1) preparation of pyrite suspensions in bicarbonate solution or demineralised water; (2) abiotic conditions by addition of 0.1 wt% NaN_3; (3) control tests without azide to study the effect of azide on pyrite oxidation by nitrite. As these batch tests were started at the same time as those with nitrate, the pyrite suspensions without nitrate or nitrite are used as blancs for both batch tests series (Table 18).

[27] Based on the specific surface area (see Section 5.4.4.1), ~0.54 m^2 of pyrite surface is available for oxidation.

[28] The pyrite suspensions were filtered (PURADISC® polyethersulfone membrane filter with 0.45 µm cut off, Whatman) before chemical analysis, to avoid interference of the results by pyrite.

Table 18: Overview of the set-up of the batch tests with pyrite and $NaNO_3$ or $NaNO_2$. All solutions, except for the ones without $NaNO_3$ or $NaNO_2$, were prepared in duplicate. To every solution 5 g L^{-1} of crushed pyrite grains were added.

Code	*$NaNO_3$ or $NaNO_2$ concentration (M)*	*NaN_3 (wt%)*	*Background solution*	*Sampling time (days after start)*
Tests without $NaNO_3$ / $NaNO_2$				
Abiotic tests				
Pyr_0.1% bact_bicarb	0	0.1	15 mM HCO_3^-, pH ~8.4	0, 29, 91, 182, 351, 715
Pyr_0.1% bact_water	0	0.1	Demineralised water, pH ~7	0, 182, 715
Control tests for azide (without addition of SOB)				
Pyr_0% bact_bicarb	0	0	15 mM HCO_3^-, pH ~8.4	0, 29, 91, 182, 351, 715
Tests with $NaNO_3$				
Abiotic tests				
Pyr_0.005M $NaNO_3$_0.1% bact_bicarb	0.005	0.1	15 mM HCO_3^-, pH ~8.4	0, 29, 91, 182, 351, 715
Pyr_0.1M $NaNO_3$_0.1% bact_bicarb	0.1	0.1	15 mM HCO_3^-, pH ~8.4	0, 29, 91, 182, 351, 715
Pyr_0.005M $NaNO_3$_0.1% bact_ water	0.005	0.1	Demineralised water, pH ~7	0, 182, 715
Control tests for azide (without addition of SOB)				
Pyr_0.005M $NaNO_3$_0% bact_bicarb	0.005	0	15 mM HCO_3^-, pH ~8.4	0, 183, 715
Pyr_0.1M $NaNO_3$_0% bact_bicarb	0.1	0	15 mM HCO_3^-, pH ~8.4	0, 29, 91, 182, 351, 715
Tests with $NaNO_2$				
Abiotic tests				
Pyr_0.005M $NaNO_2$_0.1% bact_bicarb	0.005	0.1	15 mM HCO_3^-, pH ~8.4	0, 29, 85, 182, 344, 708
Pyr_0.05M $NaNO_2$_0.1% bact_bicarb	0.05	0.1	15 mM HCO_3^-, pH ~8.4	0, 182, 708
Pyr_0.005M $NaNO_2$_0.1% bact_ water	0.005	0.1	Demineralised water, pH ~7	0, 182, 708
Control tests for azide (without addition of SOB)				
Pyr_0.005M $NaNO_3$_0% bact_bicarb	0.005	0	15 mM HCO_3^-, pH ~8.4	0, 29, 85, 182, 344, 708

The pyrite suspensions with nitrite were prepared similar to the batch tests with pyrite and nitrate (see Section 5.4.4.2). Per test condition, 12 duplicates were prepared allowing duplicate analyses after 6 different reaction periods (start, 1, 3, 6, 12, and 24 months), as indicated in Table 18. At the moment of writing this report, samplings up to 1 year have been performed. The same analyses as for the batch tests with pyrite and nitrate (Section 5.4.4.2) were performed. For the MPN analyses, a specific growth medium for NiR-SOB was used (as described in Section 5.1.1.1.2).

5.4.4.4 Control batch tests to study microbial nitrate/nitrite dependent pyrite oxidation

5.4.4.4.1 Enrichment of Thiobacillus denitrificans

To obtain a sufficiently high concentration of viable and active *T. denitrificans* for spiking the pyrite suspensions of the control batch tests, *T. denitrificans* was purchased from DSMZ (Deutsche Sammlung von Mikroorganismen und Zellkulturen GmbH; strain number DSM 12475) and cultured in growth media LZ_NO3 or LZ_NO2 (depending on the batch test; see Section 5.1.1.1.2).

After two transfers of the grown bacteria to fresh growth medium, ~20 mL of the turbid cultures was centrifuged for 10 min at 4000 rpm. Afterwards, the bacterial pellets were gently resuspended in 20 mL BNS to remove residual nitrate and thiosulphate from the medium. This washing step was repeated 3 times, after which the pellet was resuspended in 5 mL BNS solution. An MPN analysis (using LZ_NO3 and LZ_NO2 media; Section 5.1.1.1.2) was performed to determine the bacterial concentration in these stock solutions. The stock solution with *T. denitrificans* grown in LZ_NO3 contained ~5×10^4 cells mL^{-1}, while the stock solution in LZ_NO2 only contained ~2×10^2 cells mL^{-1}. This already suggests that although *T. denitrificans* can survive (and grow slowly) in a medium containing 7 mM NO_2^-, it prefers to grow in a nitrate-containing medium and/or in the presence of lower concentrations of nitrite. At the start of the microbial control tests, the stock solutions were used to inoculate the pyrite suspensions. Due to the low cell count in the stock solution in LZ_NO2, both stock solutions were used for inoculation of the batch tests with nitrite, while only the stock solution prepared in LZ_NO3 was used for inoculating the tests with nitrate.

5.4.4.4.2 Set-up of the microbial control tests

Table 19 gives an overview of the set-up of the control tests with pyrite and *T. denitrificans*. In contrast to the abiotic batch tests described in Sections 5.4.4.2. and 5.4.4.3, these pyrite suspensions were prepared in a 500 mL volume (DURAN® flask, Schott). Only for the solutions with nitrate or nitrite, a duplicate solution was prepared. The pyrite suspensions were prepared in an anaerobic glove box (N_2 atmosphere), by adding 500 mL of BNS to 2.5 g of pyrite powder. The amount of pyrite added to each solution was weighed, to allow normalisation of the results to the total surface of pyrite available for reaction[29]. In each of these suspensions, *T. denitrificans* was inoculated (initial concentration ~10^2 to 10^3 cells per mL).

[29] Based on the specific surface area (see Section 5.4.4.1), ~3.8 m^2 of pyrite surface is available for oxidation.

Regularly and after each incubation period (as shown in Table 19), the control solutions were shaken until they were completely homogeneous. Afterwards, samples of ~40 mL were taken from the batch test solutions and the same analyses were performed as for the abiotic batch tests with pyrite and nitrate (Section 5.4.4.2). Depending on the electron acceptor in the BNS (nitrate or nitrite), an MPN test using LZ_NO3 or LZ_NO2 (Section 5.1.1.1.2) was performed. At this moment, samplings up to six months have been performed.

Table 19: Overview of the solution compositions of the microbial control batch tests with pyrite and $NaNO_3$ or $NaNO_2$. All solutions, except for the ones without $NaNO_3$ and $NaNO_2$, were studied in duplicate. BNS = Bacterial nutrient solution for *T. denitrificans*.

Pyrite (g L^{-1})	***$NaNO_3$ (M)***	***$NaNO_2$ (M)***	***Background solution***	***Sampling time (days after start)***
Microbial control tests (with addition of *T. denitrificans*)				
Pyr_BNS	0	0	BNS, pH ~8.4	0, 68, 132, 195, 351, 715
Pyr_0.005M $NaNO_3$_BNS	0.005	0	BNS, pH ~8.4	0, 68, 132, 195, 351, 715
Pyr_0.005M $NaNO_2$_BNS	0	0.005	BNS, pH ~8.4	0, 68, 132, 195, 351, 715

5.5 Statistical analysis of results

For all experimental results obtained in the tests described in this report, the expanded uncertainty is given, calculated as the combined standard uncertainty multiplied by the coverage factor k for a 95% confidence (k=2). The combined standard uncertainty is equal to the square root of the total variance obtained by combining all the uncertainty components using the law of propagation of uncertainty or by the spreadsheet method [118].

6 Results and Discussion

6.1 Combined percolation and pulse injection tests

Percolation and pulse injection tests were performed to study the effect of a $NaNO_3$ plume on the physicochemical properties of the Boom Clay and on the migration parameters of radionuclides in Boom Clay perturbed with $NaNO_3$. The effect of an increase in ionic strength (with NaCl) on these properties has been studied previously by Moors [107]. A brief summary of the conclusions from this study is included in Section 6.1.1. The results of the percolation and pulse injection tests studying the impact of $NaNO_3$ are discussed in the following sections:

(i) Impact of a $NaNO_3$ plume on the physicochemical properties of the Boom Clay (Section 6.1.2).
  (a) Impact of a $NaNO_3$ plume on the chemical composition of Boom Clay and on pore water chemistry (Section 6.1.2.1).
  (b) Oxidation of the Boom Clay by a $NaNO_3$ plume (Section 6.1.2.2).
  (c) Impact of a $NaNO_3$ plume on the hydraulic conductivity of Boom Clay (Section 6.1.2.3).

(ii) Impact of a $NaNO_3$ plume on the hydromechanical properties of Boom Clay (Section 6.1.3).

(iii) Impact of a $NaNO_3$ plume on the diffusion properties of HTO, I^- and HCO_3^- (Section 6.1.4).

6.1.1 Observations by Moors on the effect of an increase in ionic strength on physicochemical and migration properties of the Boom Clay

Moors [107] studied the effect of an increase in ionic strength on the physicochemical properties of Boom Clay and the migration parameters of unretarded radionuclides (tritiated water and $^{131}I^-$) in combined percolation and tracer pulse-injection experiments. For this, three Boom Clay cores were consecutively percolated with RBCW, RBCW with 1 M NaCl, RBCW with 0.1 M NaCl, and again with RBCW (set-up similar to Figure 6). Two cores were percolated under constant total vertical stress conditions, *i.e.* mechanically consolidated at 4.65 MPa in oedometer frames, and one core was percolated under constant volume conditions (after applying an initial load to ensure a good contact between cell and sample). When after each switch to a different feed water a (more or less) stable electrolytic and hydraulic conductivity was reached, tracer pulse injection experiments with $^{131}I^-$ and tritiated water (HTO) were carried out. It is important to note that severe corrosion was observed in the cells when they were dismantled at the end of the experiment. This corrosion, resulting in the formation of corrosion products on the cell compounds, has likely hindered the displacement of the piston in the tests under constant total vertical stress conditions, leading to an increase of the consolidation stress during the experiment, or even to constant volume conditions (*i.e.* no displacement of the piston possible). In addition, the percolation was stopped for more than two years during the percolation step with 1 M NaCl, probably resulting in a number of other perturbing processes:

- creep and drained consolidation of the clay (because of open valves at the outlet);
- blockage of filter pores due to creep of clay;
- partial oxidation of the clay (because of open valves at the outlet);
- salt precipitation and corrosion product formation in the filter pores and/or the thin water conduction lines;
- continuation of the cation exchange processes with Na^+.

When the percolation was resumed after more than two years, a sharp decrease of the hydraulic conductivity (25% to even 100%) was observed. Furthermore, it is known that the hydraulic conductivity of clay cores under continuous vertical stress decreases slowly with time (~10% after 6 years; N. Maes, SCK•CEN, personal communication, 2013), probably due to creep of the clay. All this has to be kept in mind when interpreting the results of these tests.

The evolution of the studied physicochemical parameters was consistent for all three Boom Clay cores:

(i) A rapid but slight increase in hydraulic conductivity by ~35% was observed after the switch from RBCW to RBCW with 1 M NaCl, due to the decrease in EDL thickness (Section 4.1). This effect was counteracted in the following weeks by Na^+-M^{2+} cation exchange processes and, to some extent, by the subsequent deterioration of the microstructure ('slaking') due to the ion exchange with sodium. These counteracting processes cause the hydraulic conductivity to decrease again (Section 4.1-3). Note that the deterioration of the microstructure of the clay was applied by Moors [107] to explain the observation that the hydraulic conductivity did not reach its initial value when the cores were percolated again with RBCW at the end of the experiment, *i.e.* a lower hydraulic conductivity – by ~40% to ~100% – was measured at the end of the experiment compared to the initial percolation with RBCW. Considering the 'sudden' decrease of the hydraulic conductivity, by ~25% to even ~100%, after the more than two years lasting percolation stop (see higher), it is not fully clear whether this lower hydraulic conductivity at the end of the experiment is due to the NaCl perturbation, or to the other processes occuring during the percolation stop. In addition, a slight decrease of the hydraulic conductivity is also observed for clay cores that are not subjected to large changes of the ionic strength of the percolation water.

(ii) The effect of ionic strength on the dissolved organic matter concentration was investigated by monitoring the UV absorbance at 280 nm [119] in function of time. A sudden increase in DOC could be observed after each switch to a lower ionic strength, which might be explained by a re-suspension of organic matter that was flocculated during percolation with a high ionic strength (*i.e.* 1 M NaCl) solution (see Section 4.1).

(iii) The evolution of the pH was only fragmentarily recorded in the samples taken after the switches to (1) RBCW with 0.1 M NaCl and (2) back to RBCW. A slight increase in pH (~0.6 pH units) was measured, probably due to (1) a dissolution of calcite (consuming protons) followed by cation exchange between dissolved Ca^{2+} and sorbed Na^+ and (2) a degassing of CO_2 when the percolated solutions came in contact with air.

The observed effects of ionic strength on the transport properties of iodide and tritiated water are summarised as follows:

(i) For iodide, an increase of ηR was observed, ranging from 0.18 when percolating with RBCW, up to 0.33 (unconsolidated core) and 0.24-0.27 (cores consolidated at 4.65 MPa) when percolating with RBCW + 1 M NaCl. As iodide is a non-retarted species (R = 1), this variation is due to the variation in diffusion accessible porosity when the ionic strength is changed. The effect of ionic strength on diffusion accessible porosity of iodide was shown to be reversible.

(ii) As expected for neutral species, the diffusion accessible porosity of tritiated water was not affected by an increase of ionic strength. It is likely that changes in total porosity, by clay consolidation (for the constant vertical stress tests) or by clay expansion (due to exchange with Na^+), were too small to be detected.

(iii) No significant effect of the ionic strength on the apparent diffusion coefficient D_{app} was observed for iodide and tritiated water. With $D_{eff} = \eta R D_{app}$, any effect of the ionic strength on the effective diffusion coefficient D_{eff} of iodide can therefore be attributed to its effect on ηR.

6.1.2 Impact of $NaNO_3$ plume on physicochemical properties of Boom Clay

6.1.2.1 Impact of a $NaNO_3$ plume on the chemical composition of Boom Clay and on pore water chemistry

6.1.2.1.1 Effect on the cation occupancy of the Boom Clay

A selected set of percolate solutions was analysed to determine the concentrations of Na^+, K^+, Mg^{2+}, Ca^{2+}, Sr^{2+}, nitrite, sulphate, and ammonium around the switch to a higher $NaNO_3$ concentration. The results of these analyses are summarised in Figure 10, showing the evolution of the concentration of cations and anions as a function of time (A-B) and as a function of the mass of percolated water (C-D). To be able to mutually compare the evolution for all four cores, the mass of percolated solution at the time of a switch was set equal to that for the H2 core. When plotted as a function of the mass of percolated water, the changes in the ion concentrations for the vertical clay core are more or less comparable with the horizontal clay core. When plotted as a function of time, the concentrations in the vertical core appear to change more slowly compared to the horizontal core. This apparent slower behaviour is caused by the lower hydraulic conductivity in the vertical cores. Because of their ~3 times lower hydraulic conductivity compared to the horizontal cores, ~3 times less solution had percolated through the vertical cores at the time of each switch compared to the horizontal cores.

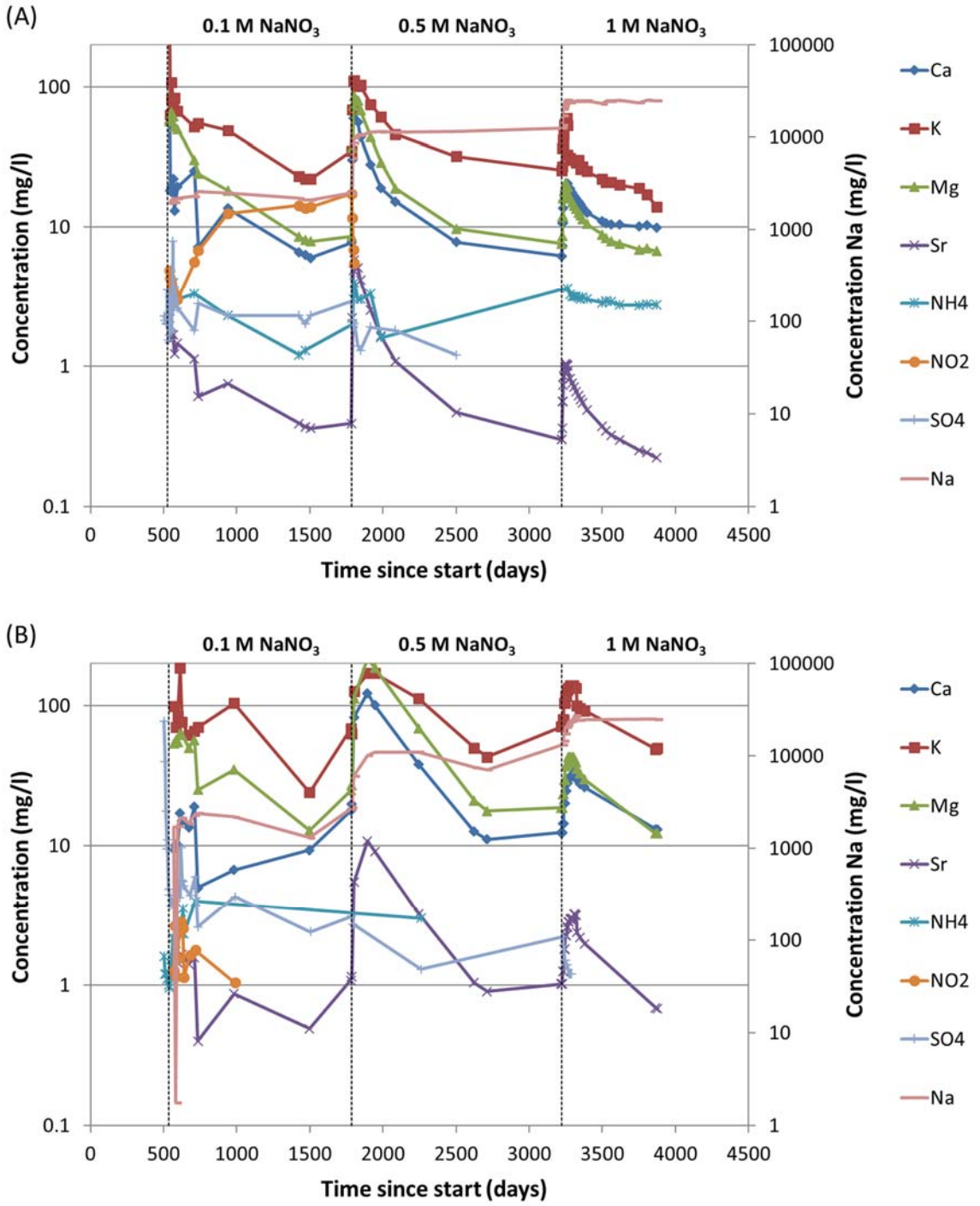

(continued on next page)

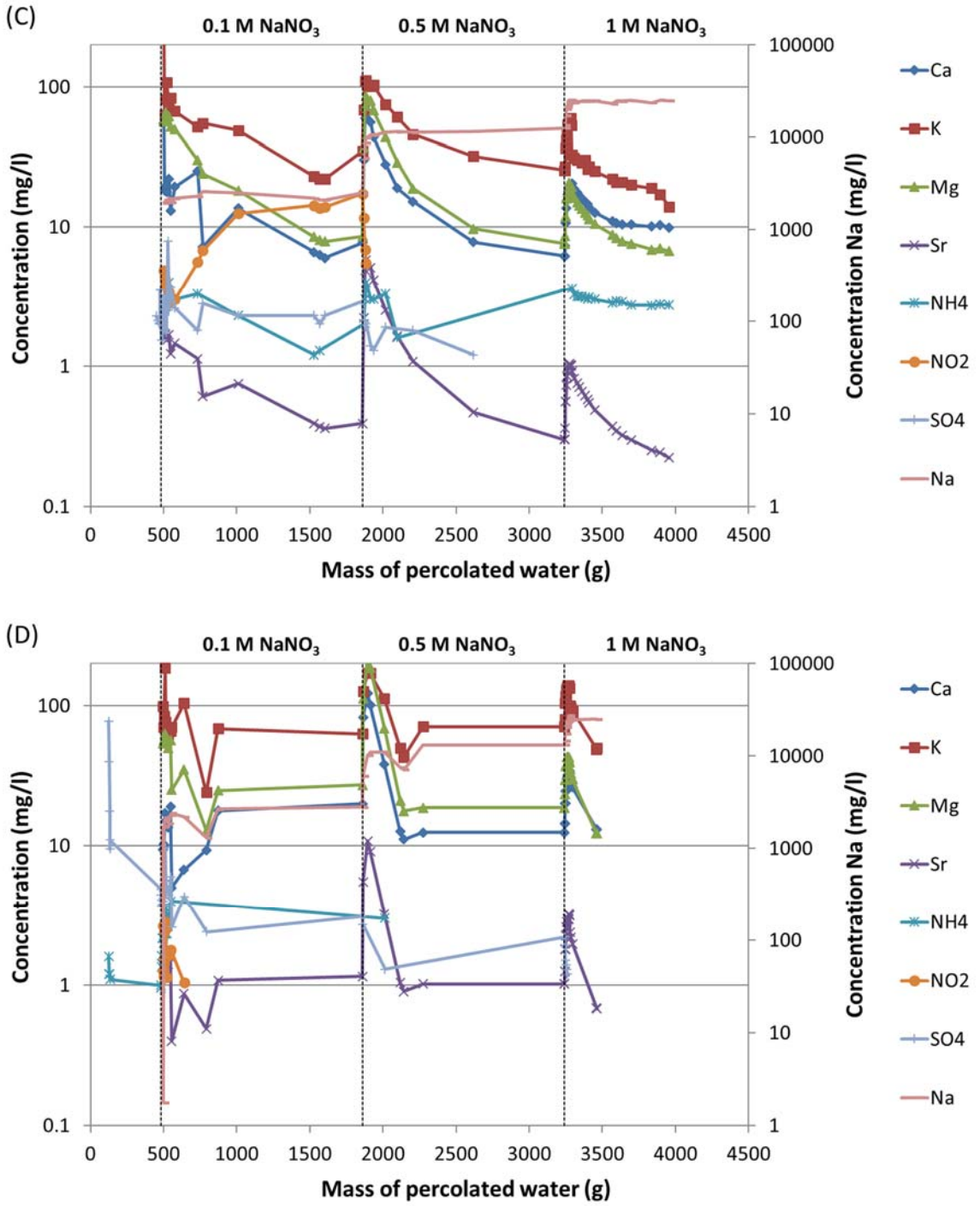

Figure 10: Concentration of Na^+, K^+, NH_4^+, Mg^{2+}, Ca^{2+}, Sr^{2+}, NO_2^-, and SO_4^{2-} in the outflow water as a function of the time (A and B) and as a function of the cumulative mass of solution percolated through the H2 core (C and D) for a horizontal clay core (A and C) and a vertical clay core (B and D). The percolation solution was switched from RBCW to RBCW + 0.1 M $NaNO_3$ after 650 days, to RBCW + 0.5 M $NaNO_3$ after 1905 days and to RBCW + 1 M $NaNO_3$ after 3344 days. For each switch, the mass of percolated solution of V6 was set equal to that of H2 at the time of the switch, to be able to compare the results for all four cores. When the NO_2^-, NH_4^+, or SO_4^{2-} concentration is not indicated, the concentration in the outflow water was below the detection limit (0.5 mg L^{-1} for nitrite; 4 mg L^{-1} for ammonium, and 1 mg L^{-1} for sulphate). The uncertainty on the concentrations is 10% ($[Na^+]$, $[Ca^{2+}]$, $[K^+]$, $[Mg^{2+}]$, $[NH_4^+]$, $[Sr^{2+}]$, 5% ($[NO_3^-]$) or 6% ($[NO_2^-]$).

The results in Figure 10 show a rapid increase of the concentrations of all clay cations immediately after a switch to a higher ionic strength. Except for Na^+, the cation concentrations decreased slowly afterwards. Apart from ammonium (NH_4^+), which is discussed in Section 6.1.2.2, the evolution of the cation concentrations in the percolate can be explained largely by cation exchange with sodium. After increase of the sodium concentration, K^+, Mg^{2+}, and Ca^{2+} are expelled from the clay (in exchange for Na^+), resulting in an increase of the concentration of these cations in the percolate. The observed spread outflow of the cations indicates that it takes quite some time until all K^+, Mg^{2+}, and Ca^{2+} ions are displaced by Na^+. This can be explained by:
(1) the differences in affinity of Na^+, K^+, Mg^{2+}, and Ca^{2+} for the clay minerals[30],

(2) the relatively slow refreshment rate of the solution at some positions in the clay core,

(3) the slower ion exchange and related release of the interlayer cations, and

(4) the participation of desorbed K^+, Mg^{2+}, and Ca^{2+} to ion exchange reactions at other places downstream the percolated core.

For Ca^{2+}, Mg^{2+}, and Sr^{2+}, the concentration in the percolate can be expected to be also controlled by the solubility of carbonate phases, mainly calcite ($CaCO_3$), but also dolomite [$(Ca,Mg)CO_3$], ankerite [$Ca(Fe,Mg,Mn)(CO_3)_2$], $(Ca,Sr)CO_3$, …

A reactive coupled transport model, which takes into account cation exchange processes, was developed with PHREEQC-2 to describe the experimentally observed elution curves for the cations. Note that this model does not take into account other processes (*e.g.* dissolution / precipitation of less soluble minerals). Figure 11 compares the experimental and modelled cation concentrations in the percolate as a function of time for a horizontal (core H2) and a vertical (core V5) clay core.

[30] Within the series of alkaline and alkaline earth elements, the cations with a higher dehydrated radius (K^+, Ca^{2+}, and also Cs^+ and Sr^{2+}) are generally more strongly retained by clay minerals than the cations with a smaller dehydrated radius (Na^+, Mg^{2+}), because of the smaller 'shielding and neutralisation' effect of the hydrating water molecules surrounding the cations. This is related to the lower surface charge density of the larger K^+ and Ca^{2+} cations compared to that of respectively Na^+ and Mg^{2+}. Furthermore, bivalent cations are more strongly adsorbed than monovalent cations.

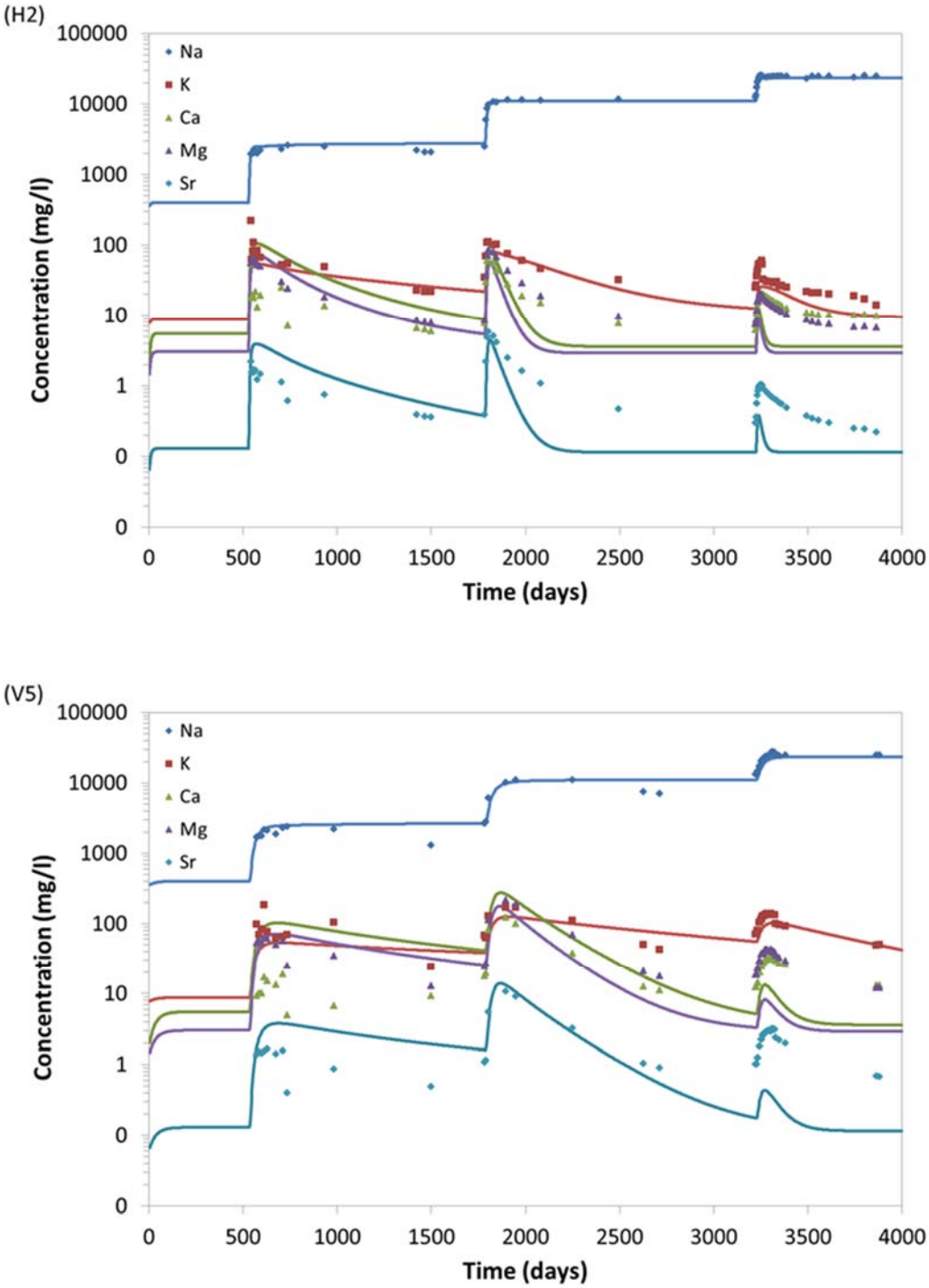

Figure 11: Experimental (symbols) and modelled (lines) Na, K, Mg, Ca, and Sr concentrations in the percolates as a function of time for a horizontal core (H2, top) and a vertical core (V5, bottom). Switch from RBCW to RBCW + 0.1 M $NaNO_3$ after 650 days, switch to RBCW + 0.5 M $NaNO_3$ after 1905 days, switch to RBCW + 1 M $NaNO_3$ after 3344 days.

The comparison between the experimental and modelled results shown in Figure 11 are discussed in detail by Martens *et al.* [35, 109]. Overall, it can be concluded that the cation exchange model is able to reproduce the general tendency of the observations, using independently measured data for undisturbed Boom Clay [6]. The simulated Na^+-K^+ exchange is generally in a good agreement with experimental data. On the other hand, the simulated Na^+-M^{2+} exchange (strongly) underpredicted the eluting concentrations of bivalent cations (Sr^{2+}, Ca^{2+}, Mg^{2+}) during the last injection step with 1 M $NaNO_3$ in the vertical core and during the injection steps with 0.5 and 1 M $NaNO_3$ in the horizontal core. According to Martens *et al.* [109], the underprediction of the eluting concentrations of the bivalent cations is related to:

(i) the assumption of constant selectivity coefficients with values representative for the undisturbed Boom Clay exchange complex [6]. In general, the selectivity coefficient varies as a function of the cation occupancy on the cation exchange complex, as was recently shown quantitatively for Na^+, K^+, Ca^{2+}, Mg^{2+}, and Sr^{2+} on different clay minerals [120].
(ii) the use of the diffusion coefficient of HTO (obtained for undisturbed clay [121]) for all cations, and the neglect of the effect of ionic strength on the transport properties of these cations.

Another important observation in Figure 11 is that the fit of the curves was much better for the vertical core than for the horizontal core, for which the flow rate was three times higher. The lower water flow rate in the vertical clay cores seems to have resulted in a better equilibration of the bulk solution with the water in the double layer and in the dead end pores (*e.g.* 'clay mode' in Appelo *et al.* [122]). This observation thus suggests that kinetics of the diffusion-controlled transport of cations to the exchange sites on the clay surface play an important role.

Figure 12 shows the time evolution of the cation occupancy of the clay in the center of a horizontal and a vertical core, as predicted by the model. It can be seen that the model predicts that the sodium occupancy increases from 47% (value for undisturbed Boom Clay [6]) to 87% and 72% in respectively the horizontal and the vertical core after ~3.4 years of percolation with RBCW + 0.1 M $NaNO_3$ (~1900 days after start of test). Furthermore, after the switch to 0.5 M $NaNO_3$ (horizontal cores) and 1 M $NaNO_3$ (vertical cores), the Boom Clay cores (both vertical and horizontal) would be almost completely transformed into a Na-clay (almost 100% Na-occupancy at the cation exchange sites). This is in agreement with the modelled results shown in Figure 11, *i.e.* only a small increase in bivalent clay cation concentrations can be observed during the final percolation step(s), followed by a fast decrease afterwards. However, for the last two percolation step(s) (0.5 and 1 M $NaNO_3$) the concentration of the bivalent cations was (strongly) underpredicted by the model (see higher), whereas their concentrations were slightly overpredicted during the first percolation step (0.1 M $NaNO_3$). The modelled evolution of the cation occupancy is thus affected accordingly, *i.e.* a somewhat faster increase (compared to reality) of the Na^+ occupancy during the percolation with 0.1 M $NaNO_3$, followed by a slower increase (compared to reality) during the percolation with 0.5 and 1 M $NaNO_3$.

A sensitivity analysis was performed to assess the influence of the parameter values (CEC and selectivity coefficient for the Na^+-K^+ exchange reaction[31]) used in the model on the efficiency of the model to describe the experimental data. This analysis showed that:

(i) of the parameters tested, those from De Craen *et al.* [6] give the best fit of the cation concentrations in the percolate; and

(ii) small changes of the parameters only seem to have minor influences on the predictions.

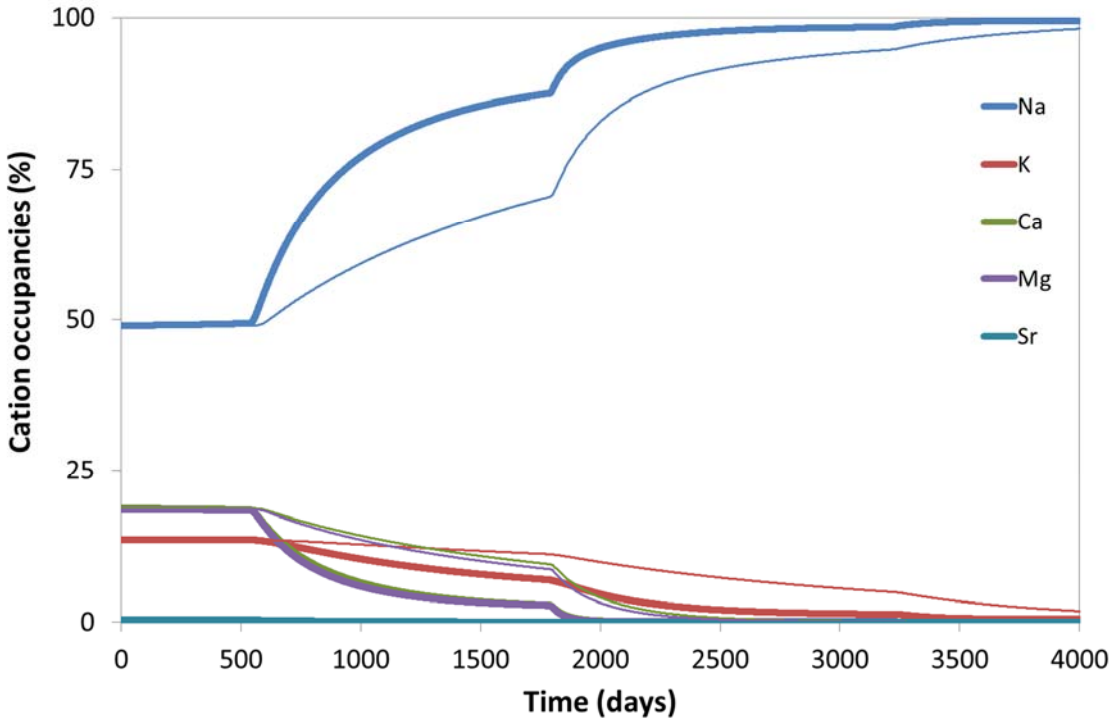

Figure 12: Simulated cation occupancies (%) of the cation exchange complex during the experiment at the middle of the core for the horizontal (H2, thick lines) and the vertical (V5, thin lines) clay cores. Switch from RBCW to RBCW + 0.1 M $NaNO_3$ after 650 days, switch to RBCW + 0.5 M $NaNO_3$ after 1905 days, switch to RBCW + 1 M $NaNO_3$ after 3344 days.

It can thus be concluded that the model, which takes into account solute transport and cation exchange processes, can describe fairly well the experimentally observed cation concentrations in the eluted water, at least for Na^+-K^+ exchange processes and for clay cores percolated at a low flow rate. Furthermore, a good prediction of the Na^+-M^{2+} exchange processes can be made for low $NaNO_3$ concentrations (≤ 0.5 M $NaNO_3$). These results confirm that cation exchange is indeed the dominant mechanism regulating the cation elution in the percolation experiments. Hence, taking into account the limitations mentioned above, the model can be used to estimate the extent of Boom Clay around a disposal gallery disturbed by a $NaNO_3$ plume (see Section 4). Yet, some improvements can be made to the model, by:

[31] The reason for varying the CEC and selectivity coefficient of Na^+/K^+ is because the reported values in the literature are scattered.

(1) using varying selectivity coefficients for Na^+, K^+, Ca^{2+}, Mg^{2+}, and Sr^{2+} as a function of the cation occupancy (as discussed above);
(2) taking into account the difference in diffusion coefficient between different cations [122];
(3) including the impact of ionic strength on the diffusion accessible porosity for radionuclides in highly compacted clay (see Section 6.1.4);
(4) including mechanisms other than cation exchange (*e.g.* dissolution and/or precipitation of poorly soluble phases, *e.g.* $CaCO_3$).

Finally, to investigate the effect of a $NaNO_3$ plume on the cation exchange capacity of Boom Clay, the CEC of the vertical clay cores (V5 and V6) was measured after dismantling of the cells. No significant differences in the CEC values were observed at the different locations in the cores. Average CEC value of respectively 25 ± 2.3 and 26 ± 3.2 meq per 100g clay were found for cores V5 and V6. As a control, previously measured clay powder samples from the Mol site were also measured at the same time. These were in line with the values previously obtained by Honty [18], *i.e.* 13 ± 3.3 to 27 ± 2 meq per 100g clay. The CEC values of the cores percolated with $NaNO_3$ thus were in the same range as the reference Boom Clay cores. In conclusion, increasing the $NaNO_3$ concentration in a clay core to 1 M does not seem to alter the CEC of the clay in a significant way. However, as there was no undisturbed sample available from the clay cores used for the percolation test, small changes in CEC due to the presence of $NaNO_3$ cannot be detected.

The cation occupancy of the dried clay cores of tests V5 and V6 showed an almost complete exchange of the cation holding sites by Na^+. More than 99.9% is occupied by Na^+, followed by ~0.06% Ca^{2+} and 0.01% of K^+ and Mg^{2+}. No significant difference was found between the top, middle and bottom of the cores and between the two clay cores. This results is in agreement with the modelling results discussed above.

To investigate the effect of the high sodium occupancy on the microstructure of the clay, the settlement of the clay powder from cores V5 and V6 in synthetic clay water was compared to that of reference Boom Clay samples. The results showed a faster settlement of the reference Boom Clay powder compared to that of the V5 and V6 cores, suggesting that the V5 and V6 cores consist of smaller sized clay aggregates compared to the undisturbed Boom Clay. This can be explained by slaking of the clay particles (Section 4.3), which could have disturbed the forces that hold the particles together.

6.1.2.1.2 Effect on electrolytic conductivity, pH, and dissolved organic matter concentration of the RBCW

Electrolytic conductivity

In line with the observed increase of the cation concentrations in the percolate (previous section), the change of the electrolytic conductivity (EC) measured in the percolates occurred relatively fast after each switch to a higher ionic strength: not more than about four pore volumes for both the horizontal and the vertical clay cores were needed to reach a steady state EC value in the percolate that equaled the EC value of the feed water (data not shown).

pH

In Figure 13, the evolution of the pH is plotted as a function of time (Figure 13A) or as a function of the cumulative mass of solution percolated through the H2 core (Figure 13B). Switching to a $NaNO_3$ solution with a higher ionic strength was done on the same day for all cores.

Not shown in Figure 13 is the evolution of the pH during the percolation with RBCW. The pH of RBCW was as high as ~9.5. The reason for this high pH is not well known, but is not (only) due to CO_2 degassing [6]. Interaction of this RBCW with the Boom Clay cores in the percolation tests discussed here resulted in a decrease of the pH to a value of 9.1. A pH of ~9 after interaction of RBCW with Boom Clay was also observed in the alkaline plume percolation tests [31]. This value is higher than the value of 8.2 – 8.5 for undisturbed Boom Clay pore water. The reason for the difference is not well known and is being investigated further. One hypothesis is that the percolation rate in these tests was too high to allow full equilibration of the RBCW with the clay (L Wang, SCK•CEN, personal communication, 2013). In view of the different response of the pH when plotted as a function of time (Figure 13A) compared to as a function of mass of percolated solution (Figure 13B), this seems to be a plausible explanation.

The increase of the ionic strength of the RBCW by addition of $NaNO_3$ resulted in a decrease of the pH of the saline clay water to 9.2 (at 0.1 M $NaNO_3$), 8.8 (at 0.5 M $NaNO_3$), and 8.4 (at 1 M $NaNO_3$). Note that these solutions were not equilibrated with 0.4% CO_2, which nowadays is being done if one wants to work under realistic Boom Clay partial CO_2 pressure conditions. Geochemical modelling with the Geochemists' Workbench® also points to a pH decrease when increasing the ionic strength, however with 'only' 0.1 to 0.2 pH units per switch (L. Wang, SCK•CEN, personal communication, 2013). The difference between measured and calculated decreases may (partly) be attributed to the additional release of protons from the dissolved organic matter upon increase of the Na^+ concentration.

Figure 13 demonstrates that increasing the $NaNO_3$ concentration in the percolation solution resulted each time in a fast decrease of the pH of the percolate at the outlet, followed by a less rapid re-increase to more or less the initial pH value. The immediate response of the pH to the increase of the $NaNO_3$ concentration was remarkably similar for all four cores, especially for the first two switches: after the switch, the pH first decreased rapidly to ~8.5 for 0.1 M $NaNO_3$ and ~8.7 for 0.5 and 1 M $NaNO_3$. As the $NaNO_3$ concentration increased and/or as more Na^+ had percolated through the clay cores, the initial pH decrease after the switches thus became smaller.

The pH decrease after each switch is probably to be attributed to the precipitation of calcite following the increase of the Ca^{2+} concentration resulting from the cation exchange between Ca^{2+} and Na^+ (Equation 4) (Figure 10):

$$>X2:Ca + 2\ Na^+ + HCO_3^- \rightarrow 2\ >X:Na + CaCO_3\ (calcite) + H^+ \qquad (4)$$

where >X2:Ca and >X:Na represent Ca^{2+} and Na^+ ion exchange sites on the clay, respectively. In addition, the displacement by Na^+ of (a small fraction of) protons still 'adsorbed' to the amphoteric sites at the edges of the clay sheets and (hydr)oxides of Fe and Al (terminal ferrol and aluminol hydroxylic sites), and on organic matter (hydroxylic and phenolic sites; the

carboxylic sites are mostly dissociated at this pH) may have contributed to the observed pH decrease.

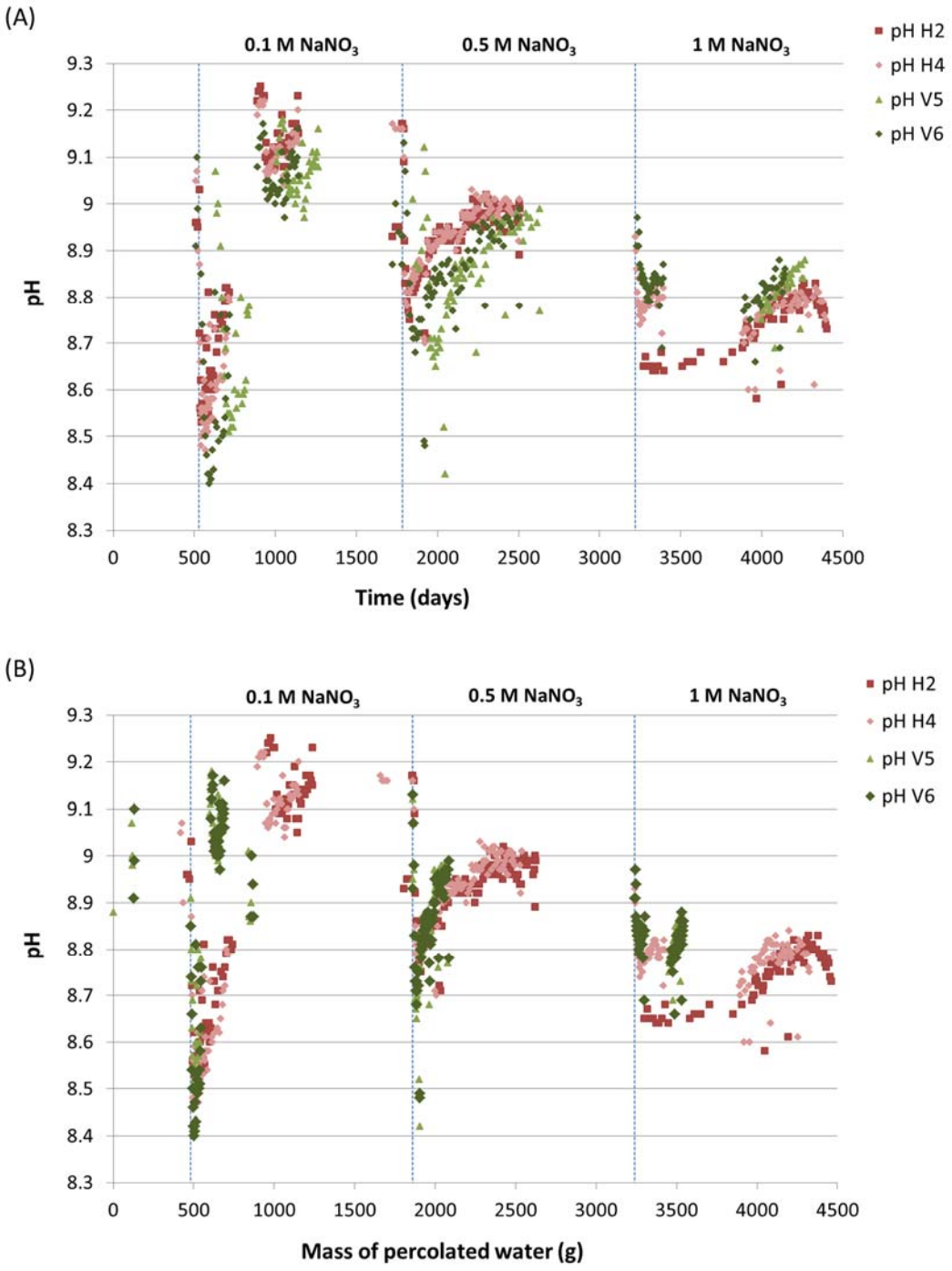

Figure 13: Evolution of the pH as a function of time (A) or as a function of the cumulative mass of solution percolated through the H2 core (B) for the four clay cores during the percolation with RBCW, RBCW + 0.1 M $NaNO_3$ (switch after 650 days), RBCW + 0.5 M $NaNO_3$ (switch after 1905 days), and RBCW + 1 M $NaNO_3$ (switch after 3344 days). For each switch, the mass of percolated solution of H4, V5 and V6 was set equal to that of H2 at the time of the switch, to be able to compare the results for all four cores. The uncertainty on the pH value is considered to be 0.1 pH units.

After this initial decrease, the pH re-increased again to stable values. The re-increase in pH coincided with the observed decrease in Ca^{2+} concentration (Figure 10). During this phase, $CaCO_3$ was most likely no longer formed and the pH re-increased to a value that was controlled by the pH of the injected solution in interaction with the clay. For 0.5 M $NaNO_3$, the pH re-increased to ~9.0, which is higher than the value of 8.8 of the injected solution. In addition, the equilibrium pH for 1 M $NaNO_3$ measured ~8.8, which is also higher than the pH of 8.4 of the initial RBCW with 1M $NaNO_3$. After stabilisation of the pH, small pH variations (up to 0.2 pH units) can still be noticed. These are possibly related to the fact that the pH was not always measured immediately after replacement of the sampling vial, resulting in different degrees of CO_2 degassing and related pH increase. Note also noted that in the first years of percolation, the dissolved CO_2 content in the percolation solution was not kept under control.

Figure 13 further shows that the evolution of the pH is remarkably similar for all four cores when plotted as a function of time. When plotted as a function of mass of percolated solution, it looks like less solution is needed for the pH to re-increase in the vertical cores. This suggests that the evolution of the pH is mainly governed by the contact time of the solution with the clay, and, consequently, that the pH is imposed by the Boom Clay (large buffer capacity) with partly kinetically controlled processes that are not yet fully understood.

Overall, the changes of the pH due to the higher $NaNO_3$ concentrations were relatively small (< 0.7 pH units). Given the large volume of the percolated solution and the gradually lower pH of the high ionic strength solutions, it can be concluded that the Boom Clay buffers the pH well, even if the 'equilibrium' pH of the percolate, *i.e.* the pH reached when the re-increase rate after each ionic strength switch slows down, gradually tends to decrease with increasing ionic strength.

Dissolved organic matter

In RBCW without nitrate, the UV-VIS absorbance at 280 nm correlates well to the concentration of the dissolved organic matter in RBCW [107, 119]. However, the presence of nitrate (as from 0.1 M $NaNO_3$) results in an 'apparent' increase of the absorbance at 280 nm, as confirmed among others for the batch tests with RBCW and nitrate (Section 6.4.2). This increase is caused by the absorbance band of nitrate at 300 nm, which clearly affects the absorbance at 280 nm at high nitrate concentrations. Therefore, to study the effect of the increasing $NaNO_3$ concentration on the TOC in the percolated water, the absorbance was measured at four different wavelengths: 266 nm, 280 nm, 360 nm, and 665 nm. All have proven to show a linear relationship with TOC in RBCW (data not shown). Based on the absorbance spectra with gradually increasing nitrate concentrations, obtained for the batch tests (Section 6.4.2), the absorbance at 360 nm (A360) proved to be the least affected, while maintaining a high enough absorbance to be able to detect significant changes. Note that the UV-VIS absorbance spectrum of nitrite also shows an absorbance maximum at 360 nm and that some nitrite was detected only in core H2 (up to ~0.4 mM NO_2^-) during percolation with 0.1 M $NaNO_3$ (see Section 6.1.2.2). As no significant differences in the evolution of the A360 could be found for both horizontal cores (Figure 14), this low concentration of nitrite did not seem to have affected the A360. As no calibration was performed to quantify TOC based on the A360 at the time of measurement, the evolution of the TOC can only be discussed qualitatively. Figure 14 shows the evolution of the absorbance at 360 nm as a

function of time (Figure 14A) or as a function of the mass of percolated solution (Figure 14B) for the four clay cores.

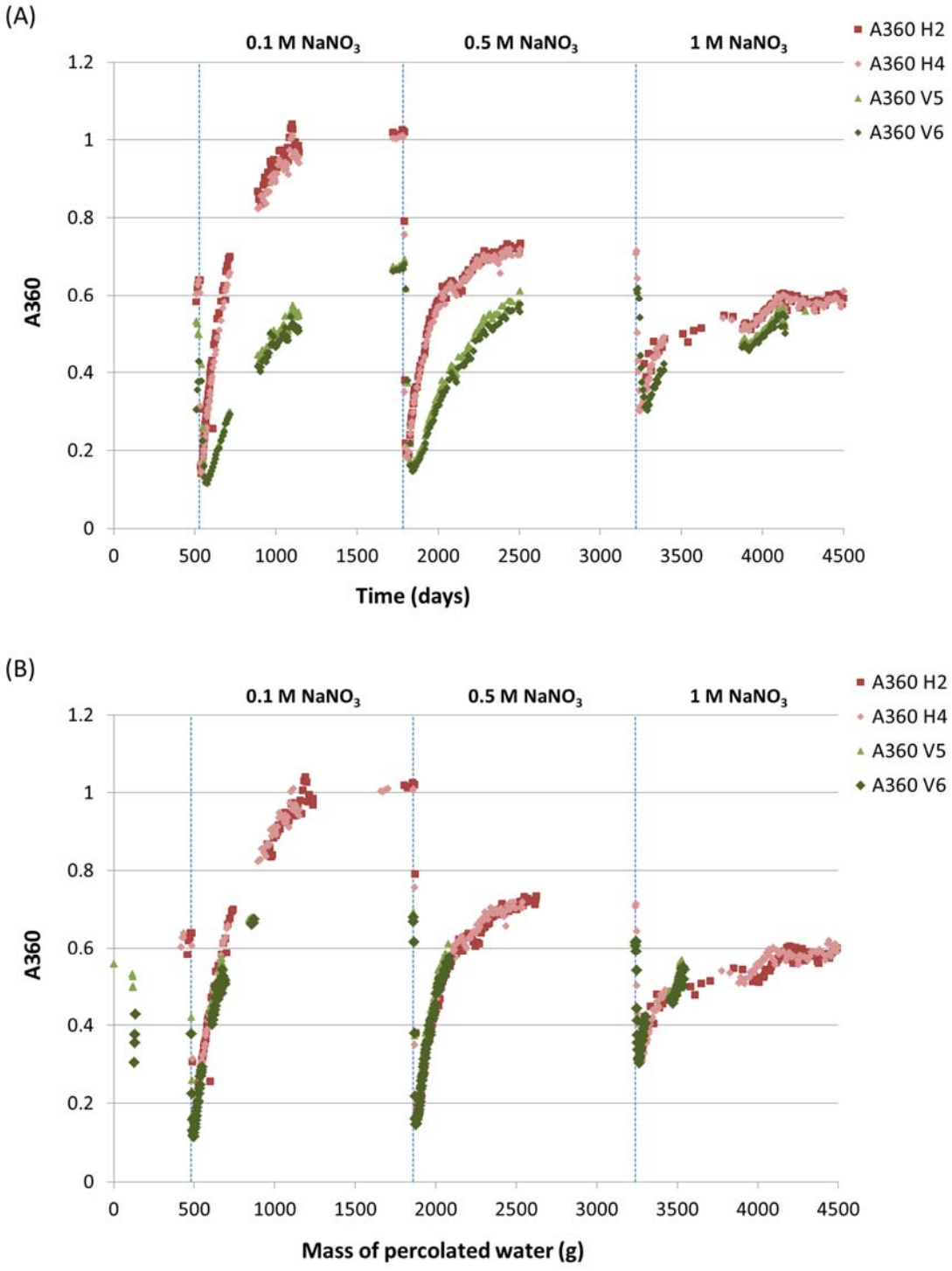

Figure 14: Evolution of the UV absorbance at 360 nm (A360), as a measure of the TOC, as a function of time (A) or as a function of the cumulative mass of solution percolated through the H2 core (B) for the four clay cores during percolation with RBCW, RBCW + 0.1 M $NaNO_3$ (switch after 650 days), RBCW + 0.5 M $NaNO_3$ (switch after 1905 days), and RBCW + 1 M $NaNO_3$ (switch after 3344 days). For each switch, the mass of percolated solution of H4, V5 and V6 was set equal to that of H2 at the time of the switch, to be able to compare the results for all four cores. The uncertainty on the absorbance values is ~1%.

For all cores and after each increase in $NaNO_3$ concentration, more or less the same tendency was observed: an initial rapid decrease of the dissolved organic matter content upon the increase of the $NaNO_3$ concentration was followed by a slower increase to a value slightly higher than or close to the initial value. This behaviour is similar to that observed by Moors [107] (Section 6.1.1) and could be explained by a combination of the following processes:

(i) The increased flocculation of (larger) organic molecules. For large organic molecules, the increasing ionic strength results in a compression of the electrostatic humic double layer (Section 4.1) and thus coagulation of the DOM [46]. This could explain the initial decrease of the DOM concentration, despite the (initial) decrease of the thickness of the EDL due to increase in ionic strength, and the related decrease of the filtration effect of the clay.

(ii) Time-dependent shift in cation balance between Na^+ and Ca^{2+}/Mg^{2+}. Due to an increase of the aqueous concentration of Ca^{2+} and Mg^{2+} (Section 6.1.2.1.1), the sorption of organic molecules increases as well. These bivalent cations form bridges between the negatively charged clay surface and the negative functional groups of the organic molecules (*i.e.* bridging effect), thus facilitating the sorption of organic molecules. As the Ca^{2+} and Mg^{2+} concentration in solution decreases, sorbed Ca^{2+} and Mg^{2+} enter again in solution, resulting in the concomitant desorption of organic molecules. The shift to a more Na^+-dominated pore water composition also seems to cause a release of additional colloids due to microstructure deterioration (see Sections 4.1 and 6.1.3).

It should be noted that when plotted as a function of the mass of percolated water, the evolution of the absorbance at 360 nm for the vertical cores is very similar to that of the horizontal clay cores. This clearly demonstrates that the evolution of the DOM concentration is governed by the number of pore volume replacements, irrespective of the time. It should be reminded that the opposite is seen for the evolution of the pH (Figure 13).

6.1.2.1.3 Effect on the anionic composition of RBCW

The evolution of the NO_3^-, NO_2^-, and SO_4^{2-} concentrations is discussed in the section on the oxidation of the Boom Clay (Section 6.1.2.2), since a change in concentration of these species would indicate an oxidation of Boom Clay components.

Furthermore, it can be noticed that the chloride concentration in the outflow water increased temporarily after the switch to a higher $NaNO_3$ concentration (data not shown), especially for the switch to RBCW with 0.1 M $NaNO_3$ (up to 158 mg L^{-1} for the horizontal and 132 mg L^{-1} for the vertical cores). This observation can be attributed to the release of chloride anions that were trapped in small pores with overlapping EDLs, and that were released as a result of the decreased EDL thickness after the switch to RBCW with 0.1 M $NaNO_3$. Apparently, the decrease in EDL thickness when switching to RBCW with 0.1 M $NaNO_3$ was sufficient to remove most of this trapped chloride, since switching to higher $NaNO_3$ concentrations did not result in a significant increase of the chloride concentration in the horizontal cores, and only in a small increase (by ~20 mg L^{-1} Cl) in the vertical cores.

6.1.2.2 Oxidation of the Boom Clay by a $NaNO_3$ plume

Apart from an increase of the sulphate concentration shortly after the start of the percolation tests[32], the sulphate concentration in the outflow water remained low and did not change significantly during ten years of percolation. Mass balance calculations reveal that the cumulative amount of sulphate in the percolate was only slightly higher than the cumulative amount percolated through the cores (Table 20).

Table 20: Total amount of sulphate present in the feed water (mass $[SO_4^{2-}]_{in}$) and in the percolate (mass $[SO_4^{2-}]_{out}$) of the horizontal clay core H2. Sulphate was supplied to the clay core by continuous percolation with RBCW solutions with a mean sulphate concentration of 0.65 ± 0.9 mg L^{-1} (based on composition of sampled clay water from the EG/BS piezometer [6]). For each value, the combined uncertainty is indicated, which takes into account the uncertainties on the mean concentrations and the percolated volume.

Percolation solution	*mass $[SO_4^{2-}]_{in}$*	*mass $[SO_4^{2-}]_{out}$*
RBCW	0.3 ± 0.4 mg (95% confidence)	1.1 ± 0.4 mg (95% confidence)
0.1 M $NaNO_3$	1 ± 1 mg (95% confidence)	3.6 ± 0.8 mg (95% confidence)
0.5 M $NaNO_3$	1 ± 1 mg (95% confidence)	2.5 ± 0.6 mg (95% confidence)
1 M $NaNO_3$ (status 06/2014)	0.5 ± 0.7 mg (95% confidence)	> 0.8 mg [a]

[a] For this system, the cumulative sampled amount of sulphate could not be calculated since in most samples the concentration of sulphate was below detection limit (< 1-10 mg L^{-1}).

The cumulative amount of sulphate that was supplied to the clay cores was estimated based on the mean sulphate concentration of RBCW [6] and the total volume of percolated water (per percolation solution). The cumulative amount of sulphate in the percolate was calculated based on the mean sulphate concentration in the percolate, determined by chemical analyses of a selected set of percolate samples, and the total volume of percolated water (per percolation solution). The use of a mean sulphate concentration for the whole percolation period (with the same solution) is justified by the fact that variations in sulphate concentration (in the percolate) were almost negligible.

Based on the sulphate concentrations, it can be concluded that there was no important pyrite oxidation. One could argue that care has to be taken in doing so, since sulphate from pyrite oxidation can also (partly) associate with iron oxidation products in the clay and precipitate in the clay as amorphous iron sulphate minerals [123]. Experimental results by the Geological Disposal Research Unit at SCK•CEN indicate that as a result of pyrite oxidation the sulphate concentration in clay water solutions increases always significantly, even in the presence of solid oxidation products like jarosite [124]. Based on these findings and the lack of an observable sulphate increase in the cores during nitrate percolation, the pyrite oxidation by nitrate is considered to be negligible.

[32] For one of the vertical cores, the sulphate concentration has been higher than 100 mg/l shortly after the start of the test (during percolation with RBCW without $NaNO_3$), pointing to some oxidation of the pyrite, probably due to air contamination during the start of the test.

The nitrite concentration in the outflow water during percolation with RBCW containing nitrate was almost always below the detection limit of 5 mg L^{-1}, except in one of the horizontal cores (H2). In this core, nitrite was produced during percolation with 0.1 M $NaNO_3$ (up to ~0.4 mM NO_2^-), indicating some reduction of nitrate to nitrite (see orange curve in Figure 10A). This reaction appears to be inhibited after increasing the $NaNO_3$ concentration further. As microbial nitrate reducers are known to be inhibited at high $NaNO_3$ concentrations[33], these results imply that some microbial dissimilative nitrate reduction to nitrite (DNRN) has taken place. On the other hand, the NH_4^+ concentrations in the outflow water remained rather stable (1-4 mg L^{-1}) during the entire test, implying that no dissimilative nitrate reduction to ammonium (DNRA) has occurred. As the nitrate concentration in the percolate quickly reached the concentration in the feed water, it is unlikely that nitrate was extensively reduced to N_2 or N_2O (through denitrification), although this could not be verified in the current experimental set-up.

As the conditions inside the consolidated clay core H2 would likely be harsh for microorganisms (due to space restriction), it is more probable that these microorganisms were growing and active close to the inlet and outlet of the percolation cell, as well as in the filter, where more space was available. This is supported by the fact that the observed nitrate reduction rate is similar to the one observed in the biotic batch tests studying the nitrate reactivity in RBCW alone (Section 6.4.2), *i.e.* ~0.2 mM NO_2^- day^{-1}.

The oxidative effect of $NaNO_3$ on the mineralogy of the Boom Clay was investigated on the top, center and bottom slices of the dismantled vertical clay cores by XRD analyses. The results are shown in Figure 15.

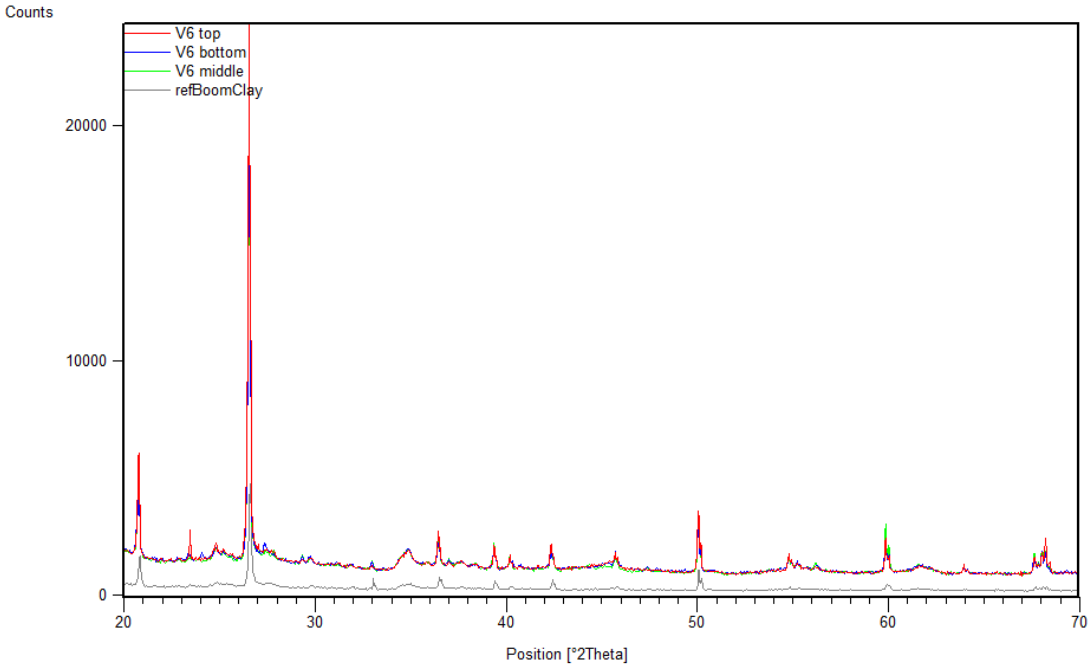

Figure 15: The XRD pattern (20-70° two-theta) of the clay powder obtained from the dismantled V6 core (top, bottom and center slice) after percolation with 1 M $NaNO_3$ solutions. The XRD pattern of a reference Boom Clay sample is also included.

[33] A concentration of ~0.35-0.5 M $NaNO_3$ is considered to be the limit for NRP growth and activity (personal communication M. Libert, CEA, France).

XRD analyses of these samples did not indicate a significant presence of oxidised mineral species (*e.g.* siderite, iron hydroxyde), which is in agreement with the lack of oxidised species (*e.g.* sulphate, thiosulphate) and reduced N species in the percolate. Indeed, compared to the reference sample of Boom Clay, no additional peaks can be detected in the XRD pattern.

6.1.2.3 Impact of a $NaNO_3$ plume on the hydraulic conductivity of Boom Clay

The hydraulic conductivity (K_{hydro}, m/s) was calculated from the flow rate (Q, m^2/s) and the hydraulic pressure gradient (ΔP, Pa) over the core with length L (m) and cross section S (m^2) (see Annex 4, Equation A4.2). The evolution of the hydraulic conductivity, resulting from an increase in $NaNO_3$ concentration in the percolation solution, is shown as a function of time in Figure 16A and as a function of the mass of percolated water in Figure 16B, similar to the previously discussed results.

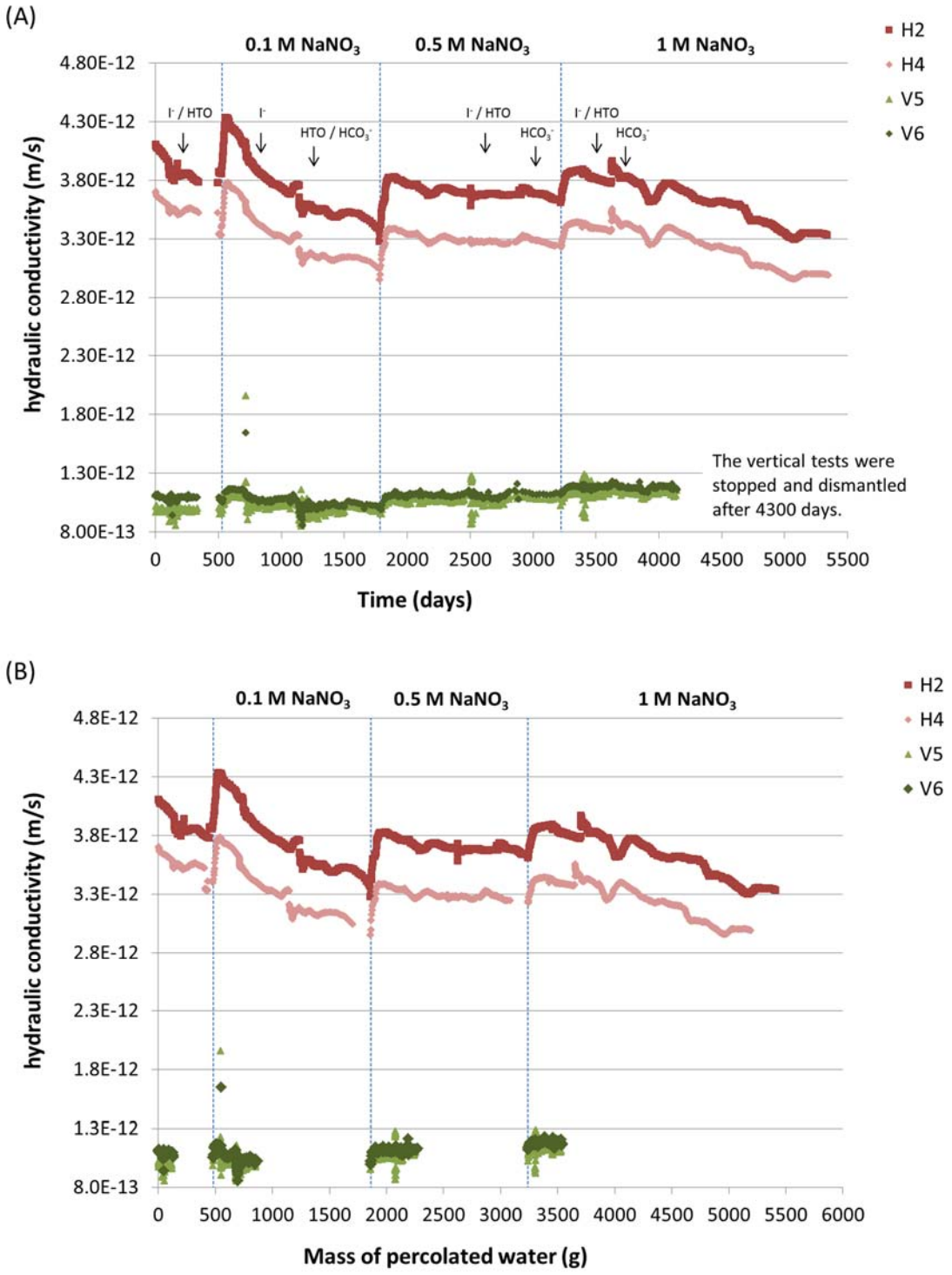

Figure 16: Evolution of the hydraulic conductivity in function of time (A) or as a function of the cumulative mass of solution percolated through the H2 core (B) in all cores (H2 and H4: horizontal cores; V5 and V6: vertical cores). Percolation of the core with RBCW, RBCW + 0.1 M $NaNO_3$ (switch after 650 days), RBCW + 0.5 M $NaNO_3$ (switch after 1905 days), and RBCW + 1 M $NaNO_3$ (switch after 3344 days). For each switch, the mass of percolated solution of H4, V5 and V6 was set equal to that of H2 at the time of the switch, to be able to compare the results for all four cores. For H2, the time at which each pulse injection test started and the corresponding tracer is indicated. The uncertainty on the hydraulic conductivity is generally lower than 3%, taking into account the uncertainties on Q, ΔP, L and S (see equation for hydraulic conductivity in Annex 4).

Figure 16 clearly shows that the hydraulic conductivity in the horizontal cores is approximately three times higher than for the vertical cores, resulting in a three times smaller mass of solution percolated through the vertical cores. The direct consequence of the lower hydraulic conductivity in the vertical cores is the longer equilibration time of the percolated solution with the clay. Another important consequence is that comparison of the evolution of the hydraulic conductivity of the horizontal and the vertical clay cores should not be based on the evolution with time but on the evolution of the mass of percolated solution (Figure 16B).

For all cores, every switch to a higher nitrate concentration was accompanied by an almost immediate increase in hydraulic conductivity. Later on, the hydraulic conductivity slowly re-decreased and stabilised at more or less its initial value. There is however a tendancy towards a slightly higher steady-state hydraulic conductivity while percolating with a higher $NaNO_3$ concentration (Figure 16), especially for the vertical cores. After several years of percolation with 1 M $NaNO_3$, the hydraulic conductivity decreases further and is still dcreasing in time. Overall, for all four cores, the maximum variation in hydraulic conductivity was about 30%, which is very low. For the horizontal cores, the hydraulic conductivity varied between 3.3×10^{-12} to 4.4×10^{-12} m/s, while for the vertical cores it varied between 9.3×10^{-13} and 1.2×10^{-12} m/s. These values are in line with the average hydraulic conductivity of 2.5×10^{-12} m/s that was obtained (under constant volume conditions, thus without an applied counterpressure as for the tests discussed here) for a large set of undisturbed 'vertical' Boom Clay cores taken over the entire thickness of the Boom Clay layer [14, 125]. The effect of increasing the $NaNO_3$ concentration on the hydraulic conductivity in a Boom Clay core therefore appears to be negligible. A similar evolution of the hydraulic conductivity after increasing the ionic strength was observed by Moors [107] while percolating Boom Clay cores with NaCl solutions (with/without applied counter pressure; see Section 6.1.1).

The observed evolution in hydraulic conductivity can be explained in a qualitative way as the overall result of several processes. The initial rapid but small increase in hydraulic conductivity after each switch is likely related to a rapid decrease of the thickness of the EDL upon passage of $NaNO_3$ (increase in ionic strength) in the larger, more easily accessible pores in the interparticle pore space (Chapter 2), resulting in an increase of the easily mobile water fraction (see Annex 1). The subsequent slow decrease in hydraulic conductivity could be to some extent related to the partial re-increase of the EDL thickness caused by cation exchange processes (Section 4.2) and to the deterioration of the microstructure by the sodium attack [55, 56, 107]. The effect of the higher ionic strength in the interlayer porosity likely occurs much more slowly and is counteracted almost instantaneously by cation exchange processes.

The final slow decrease in hydraulic conductivity is similar to what was observed when percolating the cores with RBCW prior to increasing the ionic strength. As the hydraulic conductivity of Boom Clay cores under a constant load also decreases slowly with time in other long-term percolation tests without changing the ionic strength (N. Maes, SCK•CEN, personal communication, 2013), the observed long-term evolution of the hydraulic conductivity does not seem to be linked to changes in the $NaNO_3$ concentration and is more likely related to the test set-up or conditions (*e.g.* partial blockage of the filters, compression of the clay due to long-term consolidation [126]).

Two comments apply for the relevance of the experimentally observed evolution of the hydraulic conductivity to the expected evolution in real disposal conditions. Firstly, in real disposal conditions the increase of the $NaNO_3$ concentration will proceed much slower than in the percolation tests, due to the slow release and dispersion rates. Hence, ion exchange with Na^+ will occur nearly simultaneously with the appearance of $NaNO_3$. Therefore, it can be expected that a sudden but relatively small increase of the hydraulic conductivity, followed by a slow decrease, will not occur. Secondly, together with Na^+ also Ca^{2+} will enter the clay surrounding the disposal gallery[34]. Ca^{2+} will compete with Na^+ for the ion exchange sites on Boom Clay minerals. As a result, the decrease in hydraulic conductivity due to Na^+ ion exchange will be partly levelled off by the presence of small concentrations of Ca^{2+}. The exact overall effect of increased ionic strength and K^+/Ca^{2+} ion exchange is not known, but could be determined experimentally. However, the effect is expected to be limited, as percolation of clay cores with Evolved Cement Water[34] only affects the hydraulic conductivity slightly [31]. Moreover, exploratory calculations of the $NaNO_3$ concentration profiles in Boom Clay around a disposal gallery for Eurobitum suggest that concentrations of 0.5 and 1 M $NaNO_3$ will not be reached in the clay, or only very close (< 0.5 m) to the gallery (Section 3).

6.1.3 Impact of a $NaNO_3$ plume on the hydromechanical properties of Boom Clay

Although it would have been interesting to study whether an increase of the $NaNO_3$ concentration results in a swelling or consolidation of the clay cores, the results of the displacement measurements of the pistons and of the effective pressure measurements[35] cannot be interpreted easily, making it impossible to conclude on a compression or expansion of the clay cores during the percolation tests. First of all, data are lacking on the consolidation and/or creep of the Boom Clay after the loading of the clay cores and after the start of the RBCW percolation. Secondly, sudden displacements and pressure variations were observed that cannot be explained. Possibly, they originate from the sampling or other manipulations. Alternatively, the sudden displacements could be due to a strong friction of the piston, making the displacement to occur in discrete and not in smooth steps. It is not clear whether this is due to corrosion of the internal parts of the percolation cell, as was observed in previous percolation tests by Moors [107] (see Section 6.1.1). In any case, the total displacement of three of the four cells was smaller than 1% (relative to the total length of the clay core). The results of the fourth clay core (V5) are considered unreliable due to the observed large and sudden displacement steps.

To determine the effect of the high sodium occupancy (due to a $NaNO_3$ plume) on the hydro-mechanical properties of the Boom Clay, the percolation of the two vertical clay cores (V5 and V6) with 1 M $NaNO_3$ was stopped about 2.5 years after the last switch of the percolation solution (Table 10). Loading-unloading tests (to a maximal value of 6.5 MPa) and long-term creep tests were performed on these two clay cores to study the hydromechanical behaviour of these nearly homo-ionic sodium clay cores. The hydromechanical properties of the nearly homo-ionic sodium clay cores were compared with those of "intact" Boom Clay cores taken from HADES (URL, Mol, Belgium) and Essen (Essen-1 borehole, Belgium).

[34] The Ca^{2+} concentration is ~2 mM in Young Cement Water and 15-20 mM in Evolved Cement Water.

[35] It was initially not the intention to follow up the consolidation or swelling of the clay cores by means of the displacement meters. As a piston displacement is expected to be accompanied by a variation in effective pressure, the pressure was monitored with time with pressure sensors.

However, to determine these properties, the initial state of the sample before the loading-unloading test needs to be known or assumption have to be made regarding this state. As the ten years of percolation might have changed the structure of the sample, it is difficult to determine this, but since the results on hydraulic conductivity (monitored during the percolation tests) did not reveal significant variations in the hydraulic conductivity during the ~10 years of percolation (see Section 6.1.2.3), we could assume that the porosity was still nearly equal to the initial porosity (~40%).

The results of the loading-unloading tests of the vertical cores are described in detail by Dizier *et al*. [127] and indicate that the hydromechanical properties of the nearly homo-ionic clay cores determined by such mechanical tests, did not differ significantly from these properties of undisturbed Boom Clay, *i.e*. no significant difference in compressibility, secondary consolidation coefficient or in permeability. These results are in agreement with the results from other oedometer tests performed on Boom Clay cores from HADES and from Essen, showing no significant differences in compressibility, secondary consolidation coefficient and permeability, although the Boom Clay pore water in Essen has a relatively high salinity compared to the clay water at HADES [128]. Furthermore, these results are also supported by preliminary observations made by the Polytechnical University of Cataluña (CIMNE-UPC, Spain) when performing a loading-unloading test on Boom Clay cores, which were percolated for ~3 weeks with synthetic clay water containing $NaNO_3$ (0.25M or 0.5M) in an oedometer. In these preliminary tests, no significant effect of the increased $NaNO_3$ concentration in the pore water on the elastic properties (*e.g*. compressibility) of Boom Clay was found (N. Mokni, S. Olivella, UPC, personal communication, 2012).

6.1.4 Impact of a $NaNO_3$ plume on the diffusion properties of HTO, I^-, and HCO_3^-

As described in Chapter 4.1 to 4.3 and in Sections 6.1.1 and 6.1.2, increasing the ionic strength in a clay core with a sodium bearing salt (*e.g*. $NaNO_3$) will result in several processes (most importantly changes in EDL thickness and slaking of the clay), which could have an effect on the migration properties of radionuclides. To assess this effect, radionuclide pulse injection experiments were performed on the clay cores percolated with RBCW with and without $NaNO_3$ (with increasing concentration). These experiments were performed after each switch to a higher $NaNO_3$ concentration, once the hydraulic conductivity remained more or less stable (Table 10 and Figure 16). These tests ultimately provide values for the following migration parameters, necessary for performance assessment calculations (see Annex 4 for description):

(i) Chemical retention parameter: retardation factor R (dimensionless), representing the sorption of a radionuclide by inorganic and organic phases present in the Boom Clay;

(ii) Transport parameters:
- diffusion accessible porosity ω (dimensionless) and its product with the retardation factor: ωR;
- the apparent velocity V_{app} (m/s);
- the apparent dispersion coefficient D^i_{app} (m^2/s).

In fact, fitting the evolution of the tracer concentration in the outflowing water with a least square method, provides values for V_{app} and D^i_{app}. For this, the D2_fit_V2 model was used,

which is based on an analytical solution of the transport equation with relevant initial and boundary conditions (more details in [107]). The product ηR is calculated as the ratio of V_{Darcy} over V_{app} [36]. V_{Darcy} is related to the hydraulic conductivity, the pressure difference over the clay volume, and the core length (see Annex 4, equation A4.2), which can all be obtained from the experimental data. To calculate the value of ηR accurately, it is important that the pulse injections are performed when the hydraulic conductivity (and thus V_{Darcy}) is stable. For all pulse injection experiments, this proved to be more or less the case (Figure 16). Also the reproducibility of the experiments was good, *i.e.* at the same ionic strength the fitted value is approximately the same for both duplicate cores, and this for both the horizontal and the vertical cores. Small differences between duplicate values can be attributed to differences in the hydraulic pressure gradients applied on the clay cores, similar to what was observed by Moors [107].

6.1.4.1 Values of V_{Darcy} and V_{app} for the different pulse injection tests

In Figure 17, the values of V_{Darcy} and V_{app} are shown as a function of the ionic strength for tritiated water, iodide, and bicarbonate. The values for V_{app} are also summarised in Table 22 in Section 6.1.4.3. Note that care should be taken when comparing the values for tritiated water and iodide during percolation with RBCW with the values obtained at higher ionic strengths. Indeed, as mentioned in Table 10, after the pulse injection tests with RBCW, the cores were temporarily withdrawn from the oedometers to install a pressure sensor. These manipulations implied relaxation and re-consolidation of the clay cores, which might have resulted in slightly different boundary conditions. The three 'vertical' V_{Darcy} values for bicarbonate during percolation with RBCW were obtained for three vertical cores [at 219 m, 250 m, and 260 m depth below the drilling table (BDT); Putte members] out of a series of twelve studied cores originating from the Mol-1 drilling [14, 129], for which the properties are probably the most comparable with those of the Boom Clay cores in the $NaNO_3$ percolation tests. Yet, also here care has to be taken when comparing these values with the values for bicarbonate in the vertical cores percolated with RBCW solutions with a higher ionic strength.

Figure 16 shows that V_{Darcy} varied considerably for the different ionic strengths and for all tracers tested, which suggests some dependency of V_{Darcy} with ionic strength. However, when the differences in hydraulic pressure applied at the time of the pulse injections are taken into account (Figure 16), it is clear that the variations in V_{Darcy} are mostly related to the differences in hydraulic pressure.

Furthermore, the values for V_{app} for HTO follow the evolution of the values for V_{Darcy} very well (Figure 16), which is of course expected based on their linear relationship[37]. Taking into account the variation of the hydraulic pressure during the pulse injection experiments at different ionic strengths, the data suggest that no considerable changes in V_{app} occur for HTO when the ionic strength in the clay increases. For iodide and bicarbonate, V_{app} decreases by a factor ~2 as the ionic strength increases to 0.5 and 1 M. This is the result of the increased diffusion accessible porosity for these anionic species, which is discussed further in Section 6.1.4.2.

[36] $\eta R = V_{Darcy} / V_{app}$. V_{Darcy} is the total amount of water percolated out of the clay core during the experiment per cross section unit of the clay core and per time unit.

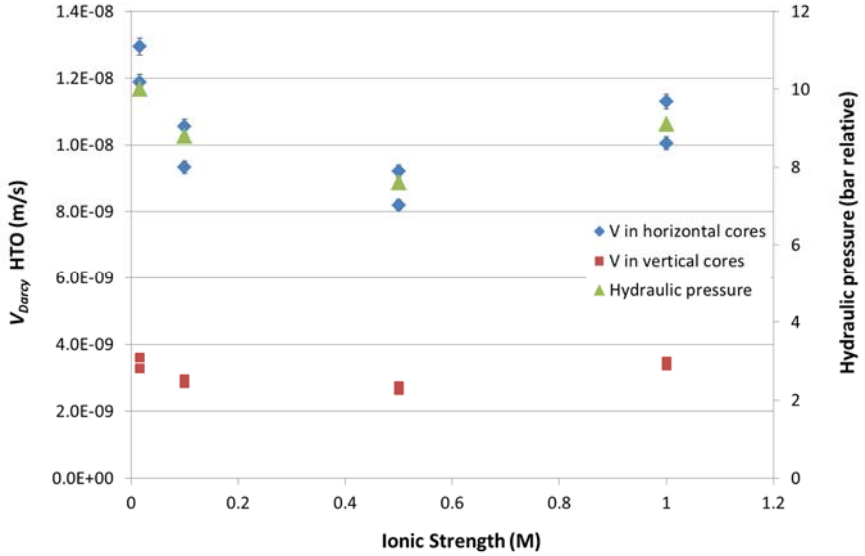
1.4E-08
1.2E-08
1.0E-08
8.0E-09
6.0E-09
4.0E-09
2.0E-09
0.0E+00
12
10
8
6
4
2
0
0
0.2
0.4
0.6
0.8
1
1.2
V_{Darcy} HTO (m/s)
Hydraulic pressure (bar relative)
Ionic Strength (M)
V in horizontal cores
V in vertical cores
Hydraulic pressure

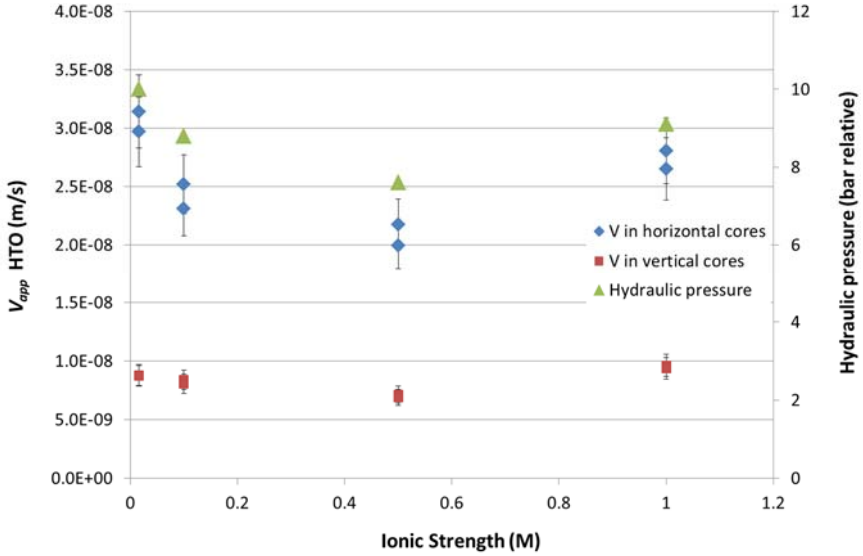
4.0E-08
3.5E-08
3.0E-08
2.5E-08
2.0E-08
1.5E-08
1.0E-08
5.0E-09
0.0E+00
12
10
8
6
4
2
0
0
0.2
0.4
0.6
0.8
1
1.2
V_{app} HTO (m/s)
Hydraulic pressure (bar relative)
Ionic Strength (M)
V in horizontal cores
V in vertical cores
Hydraulic pressure

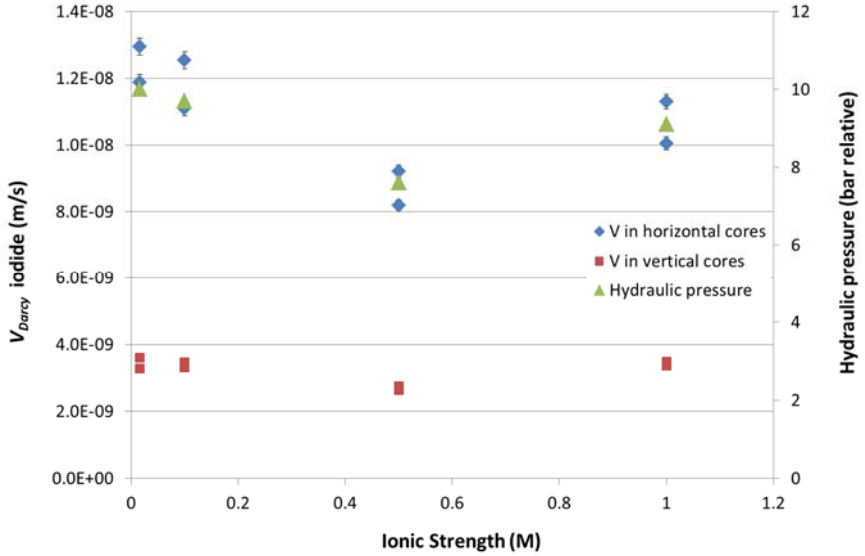
1.4E-08
1.2E-08
1.0E-08
8.0E-09
6.0E-09
4.0E-09
2.0E-09
0.0E+00
12
10
8
6
4
2
0
0
0.2
0.4
0.6
0.8
1
1.2
V_{Darcy} iodide (m/s)
Hydraulic pressure (bar relative)
Ionic Strength (M)
V in horizontal cores
V in vertical cores
Hydraulic pressure

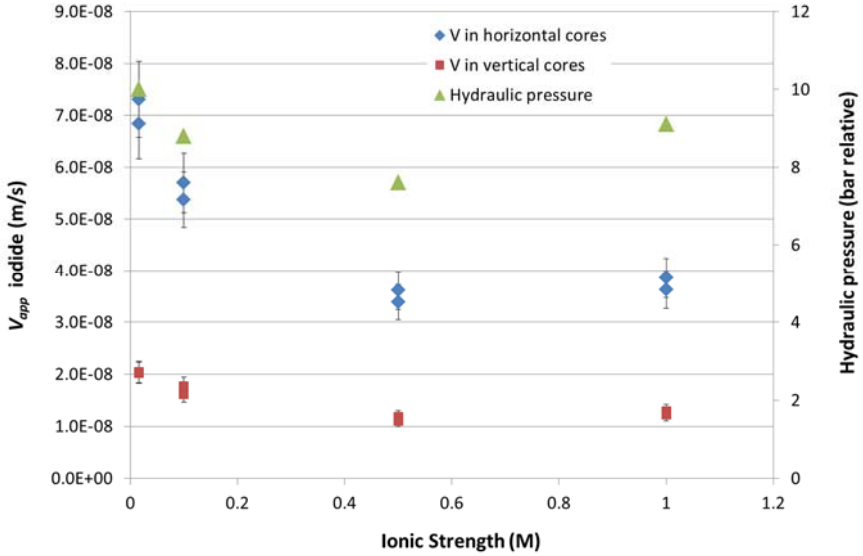
9.0E-08
8.0E-08
7.0E-08
6.0E-08
5.0E-08
4.0E-08
3.0E-08
2.0E-08
1.0E-08
0.0E+00
12
10
8
6
4
2
0
0
0.2
0.4
0.6
0.8
1
1.2
V_{app} iodide (m/s)
Hydraulic pressure (bar relative)
Ionic Strength (M)
V in horizontal cores
V in vertical cores
Hydraulic pressure

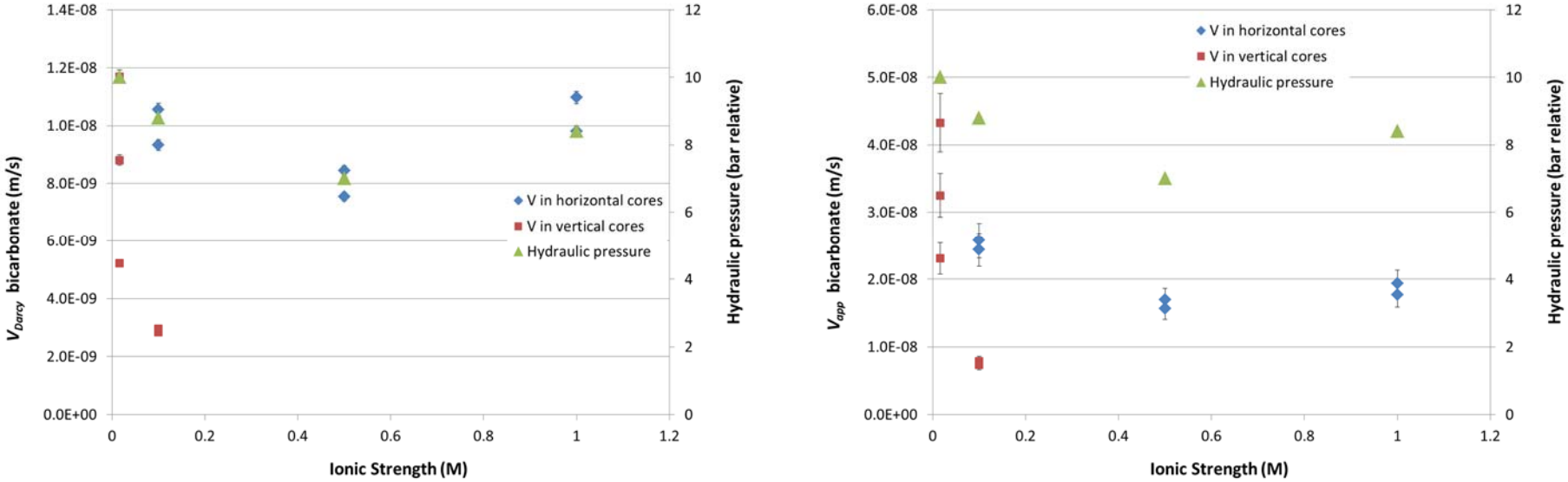

Figure 17: V_{Darcy} (left), V_{app} (right) and hydraulic pressure (all) applied on the percoled solution during pulse injection plotted for different ionic strengths for HTO (top), iodide (middle), and bicarbonate (bottom). The uncertainty on V_{Darcy} and V_{app} is lower than 2% and 10%, respectively. To be conservative, the max uncertainty bars are indicated in the graphs. The uncertainty on the hydraulic pressure is 0.07 bar.

6.1.4.2 Impact on the diffusion accessible porosity and retardation factor

The product ηR is calculated as the ratio of V_{Darcy} (determined experimentally) and V_{app} (determined with the D2_fit_V2 model). Table 21 gives an overview of the product η*R* for HTO, iodide (^{131}I or ^{125}I), and $H^{14}CO_3^-$, as determined for the percolation experiments with $NaNO_3$ (this work) and with NaCl [107]. As the product η*R* is not influenced by the stratification of the clay cores [36, 107], the average values for both the two vertical and the two horizontal cores are shown in Table 21.

Table 21: Overview of the mean values for ηR for HTO, I^-, and $H^{14}CO_3^-$, for the percolation experiments (under consolidated conditions) with $NaNO_3$ (this work) and for NaCl (data from Moors [107]), and for the retardation factor *R* for $H^{14}CO_3^-$. The values for the retardation factor for $H^{14}CO_3^-$ are estimated under the assumption that the same value for η can be used for both iodide and bicarbonate. The uncertainty on the mean ηR is generally < 20%, taking into account the uncertainty on the individual ηR (< 10%) and the standard deviation of the mean. The individual values for the clay core V5 were systematically lower than the values for H2, H4, and V6 (not shown in this table). This is possibly due to the presence of a small metal ring in the percolation cell (see footnote 18).

Percolation solution	*ηR (HTO)*	*ηR ($^{125}I^-$ or $^{131}I^-$)*	*ηR ($H^{14}CO_3^-$)*	*R ($H^{14}CO_3^-$)*
This study:				
RBCW	0.40	0.17	0.26*	1.5
RBCW + 0.1 M $NaNO_3$	0.38	0.21	0.39	1.9
RBCW + 0.5 M $NaNO_3$	0.40	0.24	0.49	2.0
RBCW + 1 M $NaNO_3$	0.38	0.28	0.56	2.0
Moors (2005):				
RBCW	0.35	0.18	n.a.	-
RBCW + 0.1 M NaCl	0.37	0.20	n.a.	-
RBCW + 1 M NaCl	0.38	0.26	n.a.	-

n.a. = not analysed.

* Average value for a large set of tests on vertical and confined clay cores from the Mol-1 drilling campaign [14, 129].

In Table 21, it is seen that the η*R* values for HTO and iodide in $NaNO_3$ percolated cores are in good agreement with the respective values in NaCl percolated cores. Furthermore, the η*R* values for the percolation with RBCW are similar to the values that were determined by Aertsens *et al.* [14, 129] for a large set of 'undisturbed' vertical (confined) Boom Clay cores taken over the entire thickness of the Boom Clay layer, *i.e.* η*R*(HTO) and η*R*(iodide) equal to 0.37 and 0.16, respectively. This gives further evidence that the pulse injection tests reported here have been performed correctly and that the pulse injection tests are reproducible. The values obtained during percolation with RBCW can therefore be used as the background values for HTO and iodide. Furthermore, a background value of 0.26 is given by Aertsens *et al.* [130] for η*R* for $H^{14}CO_3^-$ in vertical Boom Clay cores percolated with RBCW (under confined conditions; cores from the Mol-1 drilling campaign). It can be noted that 0.26 is also the average for the three 'Putte member' vertical cores (at 219 m, 250 m, and 260 m depth BDT) of this Mol-1 drilling, of which the properties are probably the most comparable with those of the Boom Clay cores in the $NaNO_3$ percolation tests.

Tritiated water

Tritiated water is a small, neutral and unretarded (R = 1) radioactive tracer. Because of its neutral charge, it is not subject to electrostatic interactions, and is therefore able to use the entire diffusion accessible pore space. As the hydraulic conductivity at the time of the pulse injection tests was similar to the initial hydraulic conductivity (Figure 16), the diffusion accessible porosity of HTO should not be affected by increases in ionic strength. This is confirmed by the results of the pulse injection tests, *i.e.* no significant difference between values of the diffusion accessible porosity η for HTO for each of the percolation steps (Figure 18). This is also in agreement with the conclusions of Moors [107].

Iodide and bicarbonate

Anions such as iodide are considered to be unretarded (R = 1), since they do not interact significantly with NOM or common soil minerals. Therefore, the retardation factor R for iodide is assumed to be 1 [36]. However, note that for the Toarcian Clay a slight yet significant retardation of iodide has been reported [131].

Due to repulsion forces between anions and the negatively charged clay surface, anions cannot, or only partially, enter the EDL (*i.e.* anion exclusion; see Chapter 2), in contrast to HTO. Hence, the pore space accessible for anions is lower than for water. Anion exclusion is indeed confirmed by the lower average values of ηR (and thus η) for iodide compared to HTO for the clay cores percolated with RBCW. Increasing the $NaNO_3$ concentration in the pore water leads to an overall compression of the EDL, explaining the observed increase of the diffusion accessible porosity η (Figure 18). The value for percolation with 1 M $NaNO_3$ (ηR = 0.28), remains however smaller than the average value of ~0.4 for HTO. The values during percolation with $NaNO_3$ are also well comparable with the results for the percolation with NaCl [107].

On the other hand, for $H^{14}CO_3^-$ – also a negatively charged molecule – the product ηR increases to values that are larger than for HTO. Since due to anion exclusion the diffusion accessible porosity for an anion is smaller than for a neutral species (like for iodide), the retardation factor R must be larger than 1 for $H^{14}CO_3^-$, *i.e.* $H^{14}CO_3^-$ is somewhat retarded in the clay. Based on the results of the pulse injection experiments and assuming that iodide and bicarbonate have the same diffusion accessible porosity, a small retardation factor of 1.5 to 2.0 can be calculated for $H^{14}CO_3^-$. A similar result was reported by Aertsens *et al.* [14, 129], for a large set of tests on vertical and confined clay cores from the Mol-1 drilling campaign. The reason for the retardation is not well known. It is probably not solely related to (bi)carbonate 'sorption' on solid carbonate phases such as calcite and/or siderite [132]. The retardation factor seems to increase with the ionic strength, *i.e.* a 33% increase when the $NaNO_3$ concentration is increased to 1 M. Note that this increase rate depends on the exact value of ηR for $H^{14}CO_3^-$ for an ionic strength of 0.016 M, since the value of 0.26 currently used for the baseline conditions is in fact the average value for three 'Putte member' vertical cores from the Mol-1 drilling campaign [14, 129]. The increase of R with increasing ionic strength cannot be explained yet.

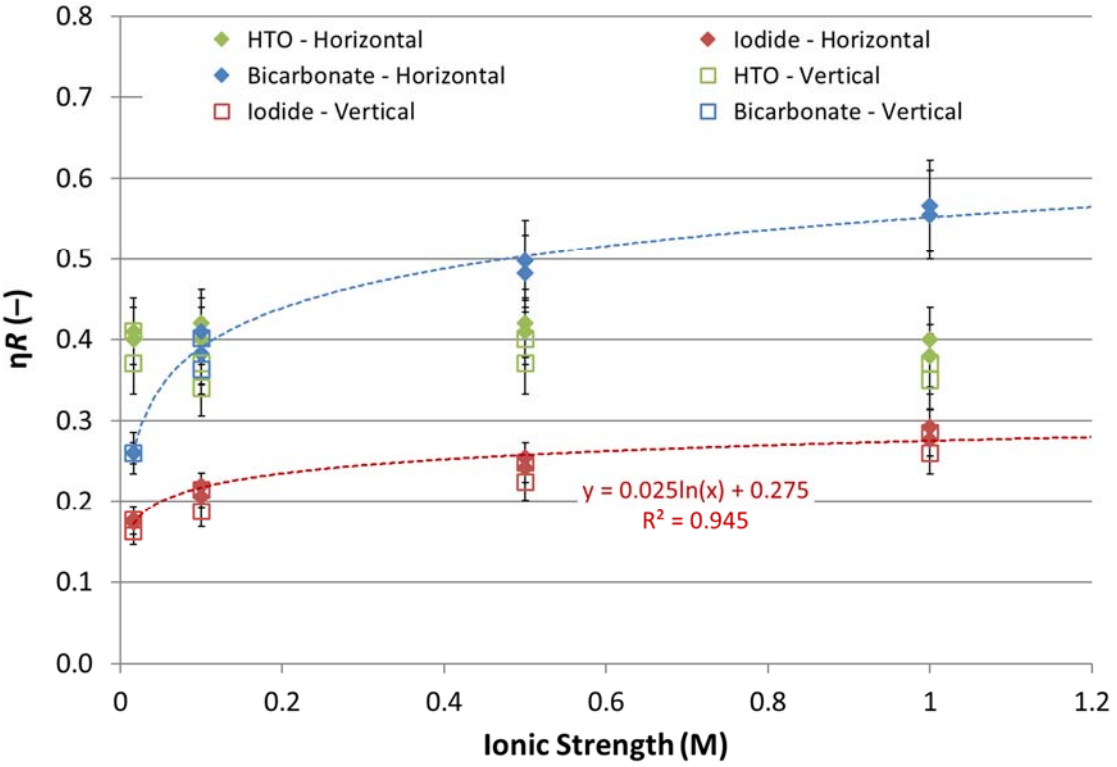

Figure 18: Evolution of the product of the diffusion accessible porosity (η) times the retardation factor *R*, for tritiated water, iodide and bicarbonate, as a function of the ionic strength. The average ηR values for both the horizontal (closed markers) and the vertical (open markers) cores are shown. The uncertainty on ηR is generally < 10%. To be conservative, the uncertainty bars indicated in the graph are 10%. The data for the horizontal cores were fitted using the method of least squares.

Volume of the interparticle pore space

As mentioned in Chapter 2, the pore space in a compacted clay can be subdivided mainly into two types: (i) the interlayer space, *i.e.* the space between individual mineral layers (TOT-layers) in a clay platelet and (ii) the interparticle space, *i.e.* the space located between the clay platelet stacks and/or between other grains of minerals present in the clay material [16, 17, 19]. The relative contribution of the interlayer space to the total pore space increases with increasing bulk dry density of the clay. Pusch *et al.* [19] reported that in a pure Na-montmorillonite at a bulk dry density of 350 kg/m³ the volume of the interlayer water forms only 10% of the total water volume, whereas it makes up more than 90% at a bulk dry density exceeding 1600 kg/m³. At high bulk dry density, such as for the Boom Clay in the percolation tests, and due to the very narrow space, the double layers in the interlayers overlap and the electric potential in the truncated layer becomes large, leading to a complete exclusion of anions from the interlayer [19, 133]. Because the pores of the interparticle pore space are larger, the double layers are more extended and anions are only partly excluded from the latter. Increasing the ionic strength of the free pore solution, however, will decrease the exclusion effect because the double layers are compressed. At high ionic strength (*i.e.* ≥ 1 M), the double layer in the interparticle pore space is so much reduced that anions occupy more or less the total interparticle pore space. These insights made Van Loon *et al.* [16] hypothesise that the diffusion accessible porosity of an unretarded anion (in their case Cl^-) measured at high ionic strength (I ≥ 1 M) represents the interparticle pore space.

Applying this approach to the results of the pulse injection experiments with iodide reported here allows us to assess the interparticle pore space in the Boom Clay cores. Extrapolation of the diffusion accessible porosity of iodide as a function of the ionic strength (Figure 18) yields a value of ~0.30 to ~0.32. Consequently, under the studied conditions (total stress and related bulk dry density) and taking into account the total porosity of 40% in Boom Clay, the interparticle pore space of the Boom Clay cores makes up ~75% to ~80% of the total porosity. This value is considerably higher than the value of 10% reported by Pusch *et al.* [19] for a pure Na-montmorillonite and than the value of ~20% by Van Loon *et al.* [16] for bentonite at a bulk dry density exceeding 1600 kg/m³. We hypothesise that this difference is due to the fact that the mineralogical composition of Boom Clay in Mol consists of only 23 to 59 wt% clay minerals (mainly smectite and mixed layer illite-smectite, kaolinite and illite), and ~75 to ~40 wt% of non-clay constituents [6, 13, 134]. The high contribution of the interparticle pore space to the total pore space can explain the rapid response of the electrolytic conductivity (Section 6.1.2.1.2) and the hydraulic conductivity (Section 6.1.2.3) to the increased ionic strength.

6.1.4.3 Impact on the apparent dispersion coefficient, the apparent diffusion coefficient, and the effective diffusion coefficient

In the pulse injection experiments reported here, radionuclide migration through the Boom Clay is a combination of diffusion and mechanical dispersion, due to the applied hydraulic pressure (0.65 – 1 MPa) on the clay cores (equation A4.1-2). Consequently, fitting of the evolution of the tracer concentration in the outflowing water provides a value for the apparent dispersion coefficient D^i_{app}. Table 22 summarises the average values (for the two cores per stratification) obtained for the apparent dispersion coefficients D^i_{app}, as well as for the apparent velocities V_{app} of HTO, iodide, and $H^{14}CO_3^-$.

Table 22: Overview of the average values for D^i_{app} and V_{app} for HTO, I^-, and $H^{14}CO_3^-$ for both horizontal and vertical cores of the percolation experiments with $NaNO_3$.
The uncertainties on the mean values take into account the uncertainty on the individual values (15% for D^i_{app} and 10% for V_{app}) and the standard deviation of the mean.

Stratification	Percolation solution	HTO		$^{125}I^-$ or $^{131}I^-$		$H^{14}CO_3^-$	
		D^i_{app} ($\times 10^{-10}$ m^2/s)	V_{app} ($\times 10^{-8}$ m/s)	D^i_{app} ($\times 10^{-10}$ m^2/s)	V_{app} ($\times 10^{-8}$ m/s)	D^i_{app} ($\times 10^{-10}$ m^2/s)	V_{app} ($\times 10^{-8}$ m/s)
Horizontal cores	**RBCW**	5.4 ± 0.9	3.1 ± 0.4	3.1 ± 0.6	7.1 ± 0.9	n.a.	n.a.
	RBCW + 0.1 M $NaNO_3$	4.2 ± 0.6	2.4 ± 0.4	2.8 ± 0.4	5.5 ± 0.7	1.0 ± 0.2	2.5 ± 0.3
	RBCW + 0.5 M $NaNO_3$	4.0 ± 0.6	2.1 ± 0.3	2.7 ± 0.5	3.5 ± 0.5	1.2 ± 0.2	1.6 ± 0.2
	RBCW + 1 M $NaNO_3$	4.0 ± 0.6	2.7 ± 0.3	3.0 ± 0.4	3.7 ± 0.5	1.2 ± 0.2	1.9 ± 0.3
Vertical cores	**RBCW**	1.9 ± 0.4	0.88 ± 0.09	1.1 ± 0.2	2.0 ± 0.2	1.2*	3.3*
	RBCW + 0.1 M $NaNO_3$	1.4 ± 0.2	0.82 ± 0.09	1.0 ± 0.1	1.7 ± 0.3	0.4 ± 0.1	0.8 ± 0.1
	RBCW + 0.5 M $NaNO_3$	1.4 ± 0.2	0.70 ± 0.08	1.1 ± 0.2	1.1 ± 0.2	n.a.	n.a.
	RBCW + 1 M $NaNO_3$	1.4 ± 0.2	1.0 ± 0.1	1.1 ± 0.2	1.3 ± 0.2	n.a.	n.a.

n.a. = not analysed.

* Average value for three 'Putte member' vertical and confined cores (taken at 219 m, 250 m, and 260 m depth BDT) from the Mol-1 drilling campaign [14, 129], for which the properties are probably the most comparable with those of the Boom Clay cores in the $NaNO_3$ percolation tests.

Table 22 shows that the increase in ionic strength, followed by the subsequent ion exchange between Na^+ and the clay cations, has no distinct effect on the values of D^i_{app} for the investigated tracers. Similar results were obtained by Moors [107]. Only for HTO, and to a smaller extent I^-, a ~25% (HTO) or ~5-15% (I^-) decrease in D^i_{app} after the first switch to a higher ionic strength (RBCW → 0.1 M $NaNO_3$) can be observed. This is probably due to the re-opening and subsequent re-closure of the percolation cell to install pressure transmitters (Table 10 in Section 5.2.2), which resulted in some densification of the clay cores compared to the situation before opening the percolation cells (because of the smaller diffusion accessible porosity of I^-, the effect is smaller for this anion). Additionally, as V_{app} and therefore also the apparent dispersion coefficient are temperature-dependent, the decrease in D^i_{app} for HTO and I^- might also be attributed to a small extent to the temperature decrease of ~2°C observed during the first switch of the percolations solution to 0.1 M $NaNO_3$.

Furthermore, similar to the hydraulic conductivity, D^i_{app} for all tested radionuclides depends on the orientation of the clay core, demonstrating the effect of anisotropy on the radionuclide dispersion in the Boom Clay. The value of D^i_{app} of HTO and iodide is 2.8 ± 0.1 times higher for the horizontal cores compared to the vertical ones. This observation is similar to those made by Moors [107], who determined an anisotropy effect[37] of 2.3 ± 0.6 for D^i_{app} of HTO and iodide in consolidated (to 4.65 MPa) Boom Clay cores.

If the contribution of the mechanical dispersion is small, the value of the apparent dispersion coefficient can be considered as a good measure of the apparent diffusion coefficient. This can be derived from equation A4.11 (see Annex 4):

$$D^i_{app} = D_{app} + \alpha V_{app} \qquad \text{(A4.11)}$$

in which α (m) is the dispersion length or dispersivity. The contribution of the mechanical dispersion is given by the term αV_{app}. The data in Table 22 indicate that D^i_{app} does not depend much on the ionic strength for a given tracer, whereas V_{app} varied significantly (~50%) between the pulse injection tests. This suggests that the effect of the kinematic dispersion, which is linearly related to V_{app}, on D^i_{app} is limited, and that hence D_{app} for the tracers studied is not much affected by the ionic strength of the percolated solution. Because of this limited effect of the kinematic dispersion on D^i_{app} , the D^i_{app} values can be considered as good yet slightly overestimated value of D_{app}.

Because of the lack of reliable data for the dispersion length, the values for D_{app} and thus also the effective diffusion coefficient (D_{eff}) can however not be calculated using equations A4.11 and A4.12 (see Annex 4). Nevertheless, based on the values of D^i_{app} and applying a similar equation as A4.12, we can calculate values for D^i_{eff}, the effective dispersion coefficient (Equation 5):

$$D^i_{eff} = D^i_{app}\,\eta R \qquad (5)$$

[37] The anisotropy effect is defined here as the ratio D^i_{app} (horizontal core) / D^i_{app} (vertical core). Note that the effect of anisotropy on the D^i_{app} is a combined effect on both D_{app} and V_{app} (based on Equation A4.11).

The calculated D^i_{eff} values include the small contribution of the kinematic dispersion, but offer a good yet slightly overestimated value of the effective diffusion coefficient D_{eff}. They are summarised in Table 23.

As expected, D^i_{eff} for HTO is not affected by the increased ionic strength, apart from the ~25% decrease when switching the ionic strength from 0.016 M to 0.1 M, which was also observed for D^i_{app} and likely caused by the re-opening and subsequent re-closure of the percolation cell (Section 6.1.4.2). In contrast, D^i_{eff} for iodide (both horizontal and vertical cores; Figure 19) and bicarbonate (only horizontal cores; Figure 20) increases by a factor 1.5 to 2 respectively, as the ionic strength increases. For bicarbonate in the vertical cores, this effect is however not clear. This is probably related to the fact that D^i_{eff} at ionic strength 0.016 M were obtained from other clay cores (Section 6.1.4.2 and Table 21), in combination with the fact that data are only available for IS 0.016 M and 0.1 M. The observed behaviour is fully in line with the decrease of the thickness of the EDL upon each increase of the ionic strength, and the related increase of the diffusion accessible porosity (Table 21). Similar results have been reported by, among others, Van Loon *et al.* [16] and Wittebroodt *et al.* [131].

To quantify the dependence of D_{eff} on the ionic strength, rigourous measurements of D^i_{app} for different V_{app} are needed, so that the dispersion length α and the apparent diffusion coefficient D_{app} can be determined for each tracer / sample combination, allowing to clearly separate the effect of diffusion and kinematic dispersion. As this is very time consuming, it has not been done for the pulse injection tests reported here.

Table 23: Overview of the average values for D^i_{app} and D^i_{eff} for HTO, I^-, and $H^{14}CO_3^-$ for both horizontal and vertical cores of the percolation experiments with $NaNO_3$.
The uncertainties on the mean values take into account the uncertainty on the individual values (15% for D^i_{app} and 18% for D^i_{app}) and the standard deviation of the mean.

Stratification	Percolation solution	HTO		$^{125}I^-$ or $^{131}I^-$		$H^{14}CO_3^-$	
		D^i_{app} ($\times 10^{-10}$ m^2/s)	D^i_{eff} ($\times 10^{-10}$ m/s)	D^i_{app} ($\times 10^{-10}$ m^2/s)	D^i_{eff} ($\times 10^{-10}$ m/s)	D^i_{app} ($\times 10^{-10}$ m^2/s)	D^i_{eff} ($\times 10^{-10}$ m/s)
Horizontal cores	**RBCW**	5.4 ± 0.9	2.2 ± 0.4	3.1 ± 0.6	0.6 ± 0.1	n.a.	n.a.
	RBCW + 0.1 M $NaNO_3$	4.2 ± 0.6	1.7 ± 0.3	2.8 ± 0.4	0.6 ± 0.1	1.0 ± 0.2	0.4 ± 0.1
	RBCW + 0.5 M $NaNO_3$	4.0 ± 0.6	1.7 ± 0.3	2.7 ± 0.5	0.7 ± 0.1	1.2 ± 0.2	0.6 ± 0.1
	RBCW + 1 M $NaNO_3$	4.0 ± 0.6	1.6 ± 0.3	3.0 ± 0.4	0.9 ± 0.2	1.2 ± 0.2	0.7 ± 0.1
Vertical cores	**RBCW**	1.9 ± 0.4	0.8 ± 0.1	1.1 ± 0.2	0.19 ± 0.06	1.2*	0.32*
	RBCW + 0.1 M $NaNO_3$	1.4 ± 0.2	0.5 ± 0.1	1.0 ± 0.1	0.20 ± 0.05	0.4 ± 0.1	0.3 ± 0.1
	RBCW + 0.5 M $NaNO_3$	1.4 ± 0.2	0.5 ± 0.1	1.1 ± 0.2	0.25 ± 0.06	n.a.	n.a.
	RBCW + 1 M $NaNO_3$	1.4 ± 0.2	0.5 ± 0.1	1.1 ± 0.2	0.29 ± 0.07	n.a.	n.a.

n.a. = not analysed.

* Average value for three 'Putte member' vertical and confined cores (taken at 219 m, 250 m, and 260 m depth BDT) from the Mol-1 drilling campaign [14, 129], for which the properties are probably the most comparable with those of the Boom Clay cores in the $NaNO_3$ percolation tests.

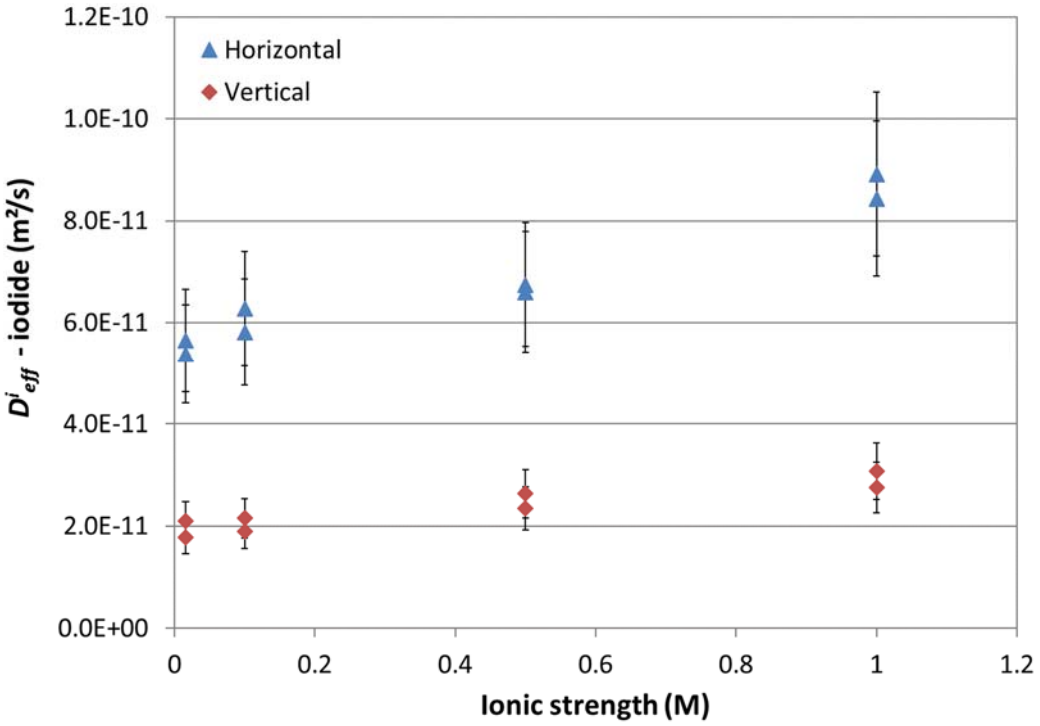

Figure 19: Evolution of the effective dispersion coefficient D^i_{eff} for iodide as a function of the ionic strength. The uncertainty on D^i_{eff} is generally lower than 18%. To be conservative, the max uncertainty bars are indicated in the graphs.

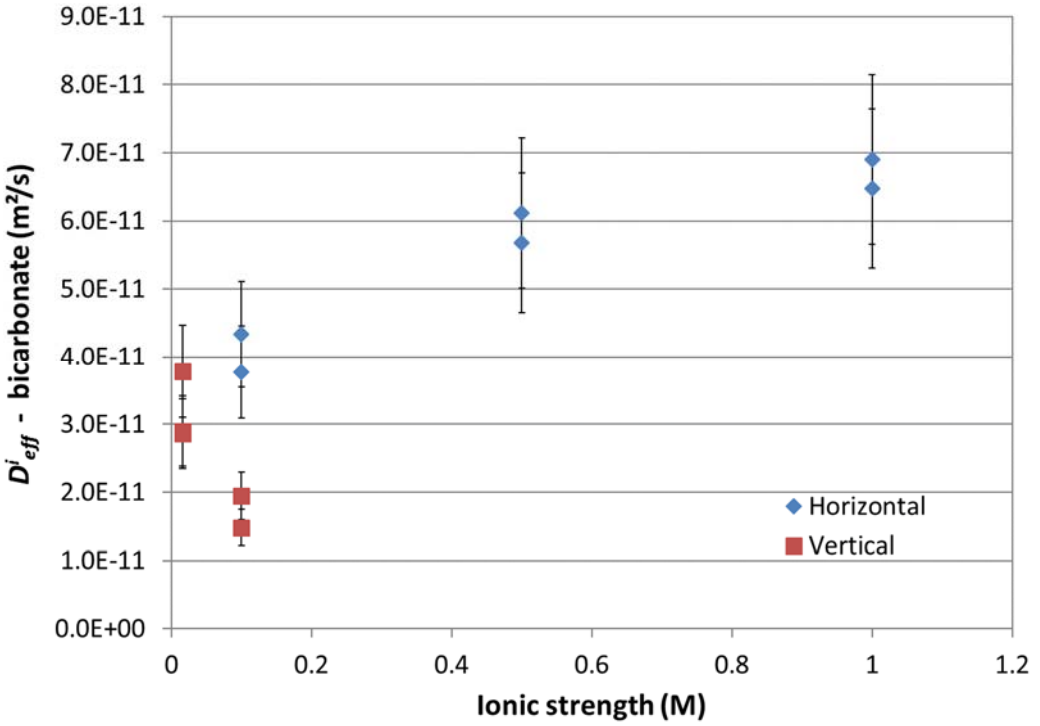

Figure 20: Evolution of the effective dispersion coefficient D^i_{eff} for carbonate as a function of the ionic strength. The uncertainty on D^i_{eff} is generally lower than 18%. To be conservative, the max uncertainty bars are indicated in the graphs.

6.1.5 Conclusions

The results of the combined $NaNO_3$ percolation and radionuclide pulse injection tests reveal that the most important perturbation of the Boom Clay by a $NaNO_3$ plume is the transformation to a clay with a high Na^+ occupancy due to cation exchange reactions with sodium. This transformation as well as the associated evolution of the cationic composition of the percolate in the percolation experiments with $NaNO_3$, can be described relatively well by a combined geochemical and transport model (PHREEQC-2 code) that considers only cation exchange processes.

In principle, the transformation towards a clay with a high Na^+ occupancy might affect the hydromechanical properties of the clay and could therefore affect the number of drums that can be disposed off safely per gallery cross-section [9]. However, loading-unloading and long-term creep tests on nearly 100% Na-clay cores did not reveal any significant differences in hydromechanical properties compared to undisturbed clay cores, which is in agreement with preliminary tests performed by UPC (see Section 4.3). Furthermore, exploratory calculations of the sodium occupancy of the Boom Clay around a disposal gallery for Eurobitum revealed that only the first ~5 meters of clay near the gallery will be transformed into a clay with an increased sodium occupancy compared to undisturbed Boom Clay (Section 3)[38]. Therefore, under real disposal conditions, the hydromechanical perturbation of the Boom Clay due to transformation to a clay with a high Na^+ occupancy, is expected to be very limited.

The other possible effects of a $NaNO_3$ plume in Boom Clay discussed in Section 4, appeared to be negligible and will probably not occur in real repository conditions, or only to a small extent, because of the much lower water flow rate and the slow increase in $NaNO_3$ concentration (Section 3):

(i) Firstly, the percolation experiments showed only a very small effect on the hydraulic conductivity in the clay cores. Initially, a rapid (but small) increase in hydraulic conductivity was observed, likely related to the decreased thickness of the EDL due to ionic strength increase. Afterwards, the hydraulic conductivity decreased again to more or less its initial value.

(ii) Furthermore, only a small effect on the pH and the organic matter content in the percolate was observed, and this primarily immediately after each increase of the $NaNO_3$ concentration in the percolated solution. These observations can be mainly explained by the increase in Na^+ concentration and the related cation exchange processes on the clay and the DOM.

(iii) Thirdly, the stable nitrate concentrations together with the low to very low nitrite and sulphate concentrations suggest that (microbial) nitrate reduction with pyrite or DOM as electron donor did not occur during the nearly ten years that the tests were running. This is confirmed by the results of the XRD analyses.

(iv) Finally, the effect of the $NaNO_3$ plume on the diffusion parameters (for tritiated water, iodide, and bicarbonate) investigated in the pulse injection tests is relatively small. As

[38] Note that these exploratory calculations made use of a transport model, considering cation exchange between sodium and Boom Clay cations. In these calculations, the contribution of the alkaline plume (containing Na^+, K^+, and Ca^{2+}) was not (yet) considered.

expected, for HTO the values of η*R* do not change with ionic strength. The average η*R* value of iodide increases with about 50% when the ionic strength increases to ~1 M. As iodide is considered to be not retarded, this increase is due to the increase in η, and thus related to the decreasing EDL thickness. For $H^{14}CO_3^-$, the average ·*R* value is doubled, which is thought to be due to both an increased diffusion accessible porosity and some retardation (*i.e.* R > 1). The apparent dispersion coefficients of HTO, I^- and $H^{14}CO_3^-$ were not affected by an increase in ionic strength. D^i_{eff} increased with increasing ionic strength for anionic tracers, similar to the results of Moors [107]. Yet, the overall effect of the ionic strength on D^i_{eff} can be considered as relatively small, *i.e.* D^i_{eff} increases by a factor of ~50% (iodide) to 100% (bicarbonate) as the ionic strength increases from 0.016 M to 1 M. Because of the lack of reliable values for the dispersion length, apparent diffusion coefficients and effective diffusion coefficients could not be calculated. However, given the expected low contribution of the kinematic dispersion, the effective dispersion coefficient D^i_{eff}, can be considered as a good yet slightly overestimated value of D_{eff}.

General safety calculations will reveal which redox-sensitive radionuclides (leaching from Eurobitum) can be considered as important contributors to the dose in the biosphere. Based on the outcome of these calculations it can be decided to study the effect of nitrate on the speciation and solubility of these 'problem' radionuclides more in detail, either by exploratory calculations or by additional experiments (*e.g.* percolation and pulse injection tests with these 'problem' radionuclides).

6.2 Bioreactor tests

6.2.1 First series of bioreactor tests (based on data from Ortiz [110])

6.2.1.1 Results

In the first series, microbial nitrate reduction was investigated in two Boom Clay slurries (~0.49 kg L^{-1} solid to liquid weight ratio) mixed with 50 mM $NaNO_3$ under a N_2 atmosphere. To one of the reactors (S01_B), a solution of 'Eurobitum radiolytic degradation products'[39] was added. Table 24 shows the composition of the gas phase in both reactors after ~3.5 years of incubation. The time evolution of the gas pressure during this period is shown in Figure 21. In Table 25, the chemical composition of the clay water fractions at the beginning and at the end of the experiment (after 1285 days or ~3.5 years) are compared, to detect any (microbially induced) changes in the clay slurries.

6.2.1.2 Nitrate reactivity

A few observations can be made from Tables 24 and 25 and Figure 21. Firstly, it seems that nitrate and nitrite were reduced to mainly N_2O and that the N_2O production was higher in the reactor to which organic molecules and salts originating from the radiolytic degradation and leaching of Eurobitum were added (reactor S01_B).

[39] In addition to 50 mM sodium nitrate, this solution contained organic molecules and salts originating from the radiolytic degradation and leaching from Eurobitum (25 mM $NaNO_2$, 3 mM $CaSO_4$, 0.15 mM HCOONa, 0.3 mM CH_3COONa, and 0.04 mM $C_2O_4Na_2$).

In reactor S01_A only a small (and statistically insignificant) amount of nitrate (~2.6 mM NO_3^- or 61 mg N-NO_3^-) was reduced, while mainly N_2O was produced: 437 mg N-N_2O in total (gaseous and dissolved). Nitrite was not detected and only a small increase in ammonium (~0.2 mM NH_4^+) could be observed in this reactor after ~3.5 years. This low concentration of ammonium is similar to what was observed in the percolation tests with $NaNO_3$ (Section 6.1.2.1), implying that the ammonium likely desorbed from the clay due to cation exchange with Na^+. Based on nitrogen mass balance calculations (Figure 22), the production of N_2O cannot be explained by nitrate reduction only. In addition, a decrease in the amount of N_2 was observed, suggesting that part of the N_2 in the gas phase was fixed into ammonium. However, the ammonium released from the clay or biomass might also have served as a nitrogen source. As predominantly N_2O and only low ammonium concentrations were found as the end product in reactor S01_A, we hypothesise that besides denitrification (NO_3^- consumption), also a succession of N_2 fixation (N_2 consumption) and a coupled nitrification-denitrification reaction (N_2O production) had occurred (Annex 3). The latter microbial process is a combination of (partial) nitrification (oxidation of NH_4^+ to nitrite or nitrate) and denitrification, resulting in the formation of nitrogenous gases like N_2 and N_2O [135, 136]. As nitrification requires some oxygen [76], this would suggest a contamination of the slurries with O_2 during the experiment. This is supported by the presence of O_2 in the gas phase at the end of the experiment (Table 24). However, as samples were only taken at the start and the end of the experiment, this hypothesis cannot be verified. To be complete, the anammox process (Anaerobic Ammonium Oxidation by reduction of nitrite) was also considered as an alternative to the nitrification process. However, as this reaction would consume both nitrite and ammonium to produce N_2 [76], this process would not explain the production of N_2O.

In the second slurry (S01_B) nitrite was preferentially reduced (decrease of ~22 mM NO_2^- or 533 mg N-NO_2^-), compared to the nitrate present in the slurry (Table 25). Nitrate only decreased, although not statistically significant, by ~0.5 mM NO_3^- or 12 mg N-NO_3^-, over the course of the experiment. Since nitrite is much more toxic to bacteria than nitrate [137], this preference is probably a mechanism to prevent nitrite toxicity. Moreover, the reduction of nitrite would yield more free energy per transferred electron through denitrification (to N_2O) compared to the reduction of nitrate to N_2O [*e.g.* for oxidation of acetate: $\Delta G^{0'}$ (pH 9) = -81 kJ/electron and -94 kJ/electron for respectively nitrate and nitrite] and is therefore thermodynamically favoured.

Also in slurry S01_B, mainly N_2O was formed and at the end of the experiment the concentration of N_2O in the gas phase was ~70 vol%, which is equivalent to 1525 mg N-N_2O (gaseous and dissolved). Similar to S01_A, the reduced amount of NO_x^- does not explain the net production of N_2O in the slurry. Also here, part of the initially present N_2 seems to have been fixed (statistically significant decrease of 437 mg N-N_2) (Table 24; Figure 22). This again suggests that both denitrification and a combination of N_2 fixation and coupled nitrification-denitrification resulted in the production of N_2O. In this reactor more or less double the amount of N_2 was fixed and ~3.5 times the amount of N_2O was produced compared to S01_A, most likely due to the presence of easily degradable C sources like acetate in reactor S01_B.

In both reactors, the total gas pressure increased (Figure 21), confirming that only part of the produced nitrogen of N_2O was originating from fixed N_2. The total gas pressure increase was more explicit in the reactor S01_B (increase of 0.25 bar) to reactor S01_A (increase of

0.04 bar). This confirms the results of the gas analyses, which also show a higher N_2O production in S01_B compared to S01_A.

The results of the MPN analyses demonstrate the presence of very high concentrations of denitrifying NRP in both clay slurries, in contrast to SRP or TRP (Table 26), which confirms that the ongoing nitrate or nitrite reduction was microbially mediated. In addition, MPA were also found in the reactors (2.5×10^2 and 2.5×10^4 cells/ g slurry in respectively S01_A and B), although at lower concentrations than the denitrifying NRP. However, as methane was not detected (Table 24) and high concentrations of nitrate and/or nitrite were present in the slurries, which are more efficient terminal electron acceptors than CO_2 (See Annex 3), methanogenesis did not seem to occur.

Table 24: Composition (in vol%) and total pressure of the gas phase (P_{total} in bar) in the reactors of the first series of bioreactor tests after ~3.5 years. The initial composition of the gas phase in the reactors was pure N_2 gas (initial pressure of ~1 bar). For each detectable value the combined uncertainty is indicated, taking into account the uncertainty on the dilution factor and on the measured concentration.

Gas component	Reactor S01_A	Reactor S01_B
H_2	<0.1	<0.1
O_2	2.3 ± 0.7	1.3 ± 0.4
N_2	71 ± 19	28 ± 8
CO	<0.1	<0.1
CO_2	3.4 ± 0.9	0.5 ± 0.2
CH_4	<0.1	0.08 ± 0.03
NO	<0.1	<0.1
N_2O	23 ± 6	70 ± 19
NO_2	<0.1	<0.1
H_2S	<0.005	<0.005
NH_3	<0.5	<0.5
P_{total}	1.05 ± 0.05	1.27 ± 0.06

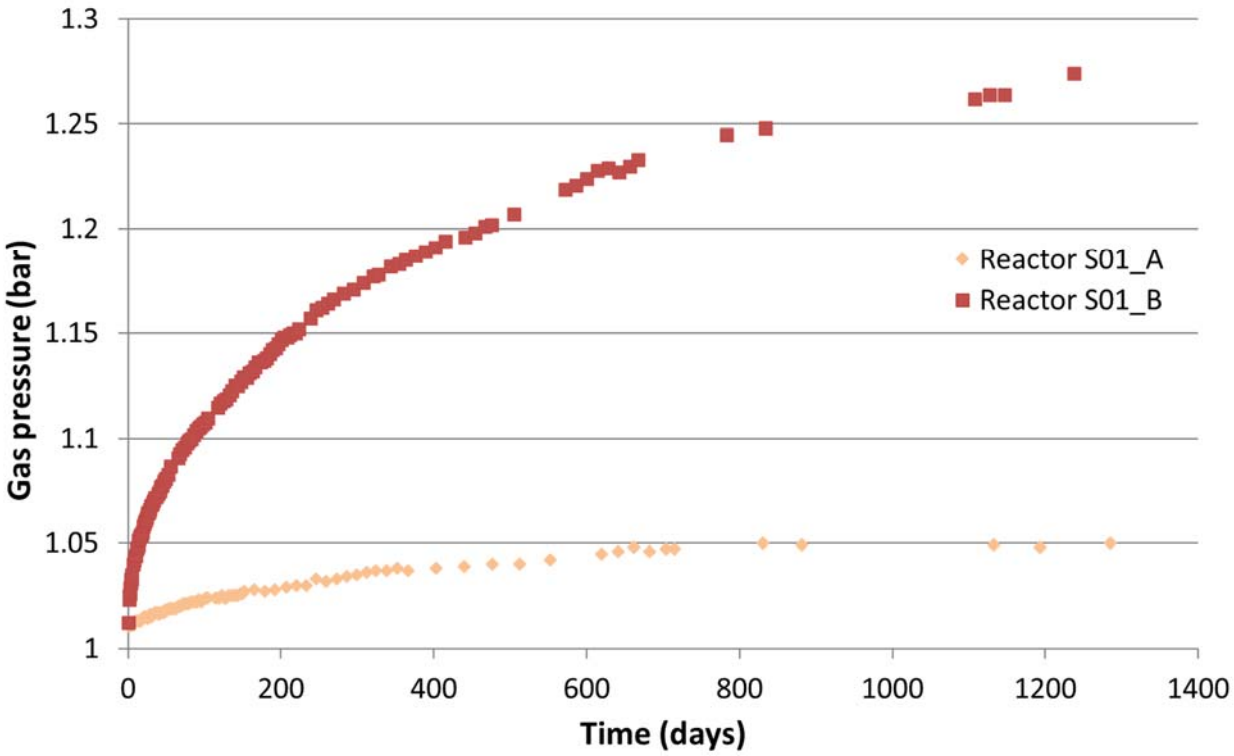

Figure 21: Gas pressure evolution in the first series of bioreactors. Both reactors (S01_A and B) contained Boom Clay slurries mixed with 50 mM $NaNO_3$, while in S01_B also the 'Eurobitum radiolytic degradation product' solution[39] was introduced. The uncertainty on this value is 0.01 bar.

Table 25: Chemical composition (including pH and E_{SHE} results) of the clay water fractions of the first series of bioreactor tests, at the start and the end of the tests. Both reactors contained Boom clay slurries with 50 mM $NaNO_3$ (initial concentration). To reactor S01_B, the 'Eurobitum radiolytic degradation product' solution was added, which contained organic molecules and salts originating from the radiolytic degradation and leaching of Eurobitum[39]. The concentrations are given in mM, except for TIC and TOC (in mg C L^{-1}). The uncertainties on the concentrations are 5% ([NO_3^-], [SO_4^{2-}]), 6% ([Cl^-], [NO_2^-]), 8% ([F^-], [HPO_4^{2-}]), 10% ([Na^+], [Ca^{2+}], [K^+], [Mg^{2+}], [NH_4^+], TIC), 12% ([Si]), 13% ([B]), 14% (TOC, but 47% for reactor S01_B) and 27-35% ([Fe total]).

Chemical species	***Start of the experiment***		***End of experiment (after ~3.5 years)***	
	Reactor S01_A	***Reactor S01_B[b]***	***Reactor S01_A***	***Reactor S01_B***
F^-	0.27	0.362	0.24	0.31
Cl^-	0.683	1.585	0.731	1.6
NO_3^-	47.09	48.22	44.51	47.74
NO_2^-	n.d[a]	25.82	<0.0054	4.22
HPO_4^{2-}	<0.026	<0.026	0.0146	0.0088
SO_4^{2-}	0.0185	2.96	0.0408	3.05
NH_4^+	0.160	0.28	0.24	0.22
Na	55.24	85.30	50.89	62.64
Ca	0.65	0.679	0.454	0.292
Mg	0.934	0.905	0.667	0.263
K	1.01	1.08	1.18	1.46
Si	0.13	0.0830	0.061	0.064
Al	0.015	<0.007	<0.007	<0.007
Fe total	0.0047	0.00288	0.001	0.001
B	0.483	0.515	0.55	0.53
$HCOO^-$	n.d[a]	0.153	n.d[a]	<0.00278
CH_3COO^-	n.d[a]	0.293	n.d[a]	<0.0042
$C_2O_4^{2-}$	n.d[a]	0.0365	n.d[a]	0.0477
TIC	114	109	85	53
TOC	9,26	51,5	30	133
pH slurry	8.74	8.78[c]	8.72	9.36
pH liquid	8.90	8.97[c]	8.90	9.47
E_{SHE} slurry (V)	-0.178	-0.163[c]	+0.009	-0.054

[a] Not determined

[b] The initial concentrations for reactor S01_B have been calculated by proportionally adding the concentrations measured in the 'Eurobitum radiolytic degradation product' solution to those measured in the clay water reactor S01_B prior to the addition of this solution.

[c] The pH and E_{SHE} of the clay water and clay slurry in reactor S01_B were measured before addition of the 'Eurobitum radiolytic degradation product' solution.

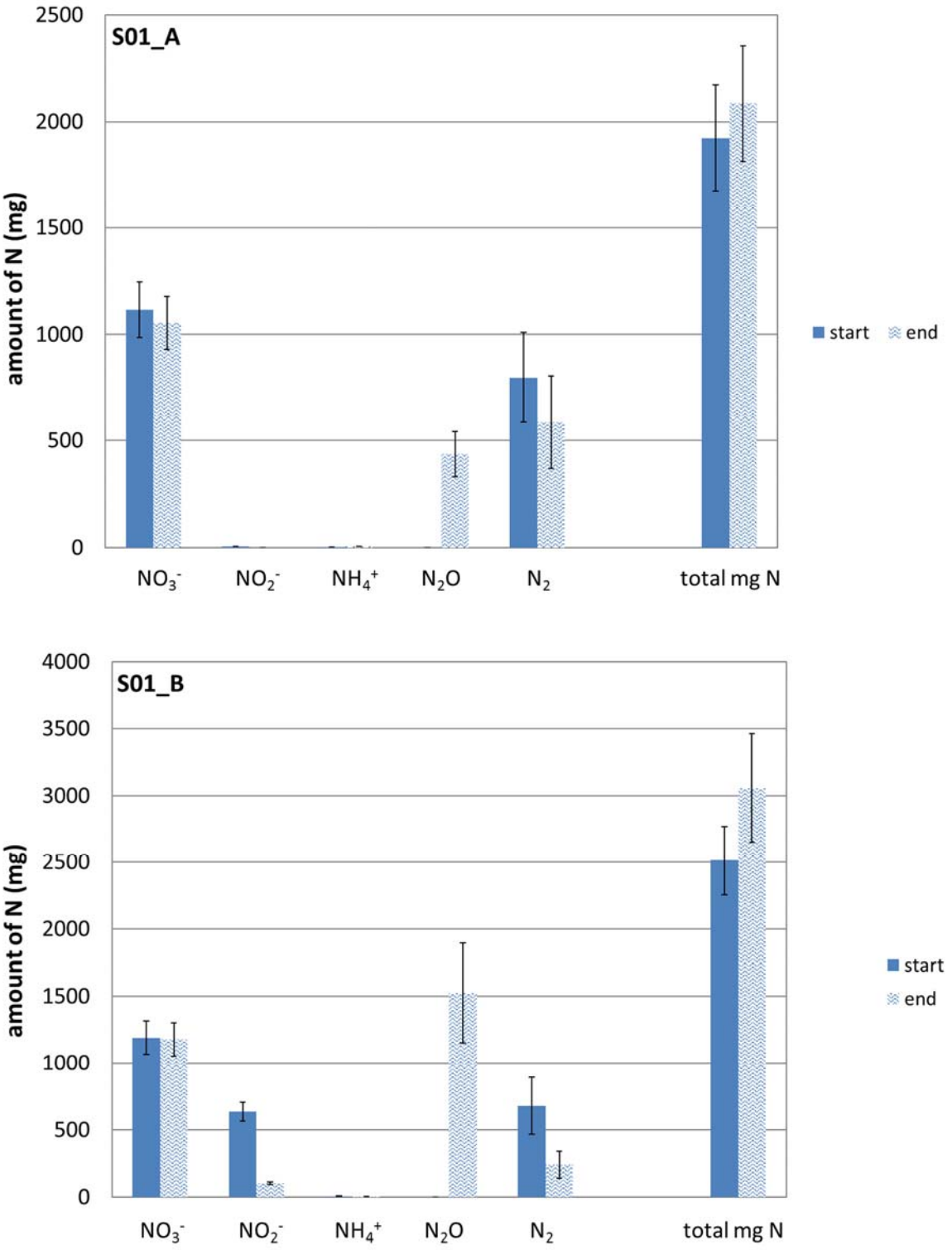

Figure 22: Nitrogen mass balance in the first series of bioreactor tests. Both reactors (S01_A and S01_B) contained Boom Clay slurries mixed with 50 mM $NaNO_3$. S01_B also contained a cocktail of organic and inorganic Eurobitum degradation products. The uncertainty bars indicate the combined uncertainty on the values, taking into account the uncertainty on the concentration, liquid and gas volume and the pressure. The values shown for gaseous compounds are the sum of both the gaseous and dissolved fractions.

Table 26: Results of the microbial analysis (MPN test) performed on the slurry mixtures in reactors S01_A and S01_B at the end of the experiment.

Concentration microorganisms (cells/g slurry)	*S01_A*	*S01_B*
NRP	7.0×10^7	$>1.1 \times 10^6$
SRP	25	2.5
TRP	0.6	0.6
MPA	2.5×10^2	2.5×10^4

The difference in the gas pressure evolution (Figure 3), in the produced amount of N_2O, and in the consumed amount of NO_x^- and N_2 (Tables 4 and 5) between both reactors suggest that the microbial population was not as active in reactor S01_A compared to S01_B. Since the addition of Eurobitum degradation products (especially low molecular weight organic acids and nitrite) to slurry S01_B was the only difference between both reactors, this must have caused the higher denitrification and N_2 fixation rates. Although nitrite is favoured by microbes to be reduced due to its toxicity, addition of nitrite does not seem to cause a significant increase in the published microbial denitrification rates [138] nor in the rates observed in RBCW (see Section 6.4.2). Therefore, the addition of low molecular weight organic acids to S01_B must be the main cause for this faster reaction rate. This is in agreement with the study by Lew *et al.* [139].

6.2.1.3 Electron donors

As high concentrations of heterotrophic nitrate reducers were detected by MPN analyses, heterotrophic NRP activity had likely occurred in both reactors. However, based on the TOC and TIC evolution in the liquid phase, neither autotrophy nor heterotrophy can be excluded:

(i) The low TOC value measured in slurry S01_A (Table 25) at the beginning of the test is in agreement with the dilution of the Boom Clay pore water still present in the clay by addition of synthetic clay water without extra organic matter. For slurry S01_B, the higher initial TOC value (Table 25) is in line with the addition of Eurobitum degradation products (containing 769 mg L^{-1} organic C). No significant leaching of organic compounds from the solid organic fraction in the clay could be observed after 2 days of mixing in either of the slurries. This leaching is however expected to occur in time, based on the results of Maes *et al.* [140], which (partly) explains the increase in TOC concentrations at the end of the of the experiment. However, as no additional TOC measurements occurred during the experiment, it remains uncertain whether any of the DOM from the clay was also used as electron donor or carbon source for nitrate reducers. In reactor S01_B, formate and acetate were consumed, demonstrating that heterotrophs were active in this slurry, at least when formate and acetate were still available.

(ii) In both reactors, a decrease in TIC (Table 25) was observed at the end of the experiment (although not statistically significant in S01_A), suggesting that

autotrophy had taken place in the slurries. However, the TIC is also controlled by the solubility of carbonate phases, mainly calcite and dolomite, which could have precipitated after cation exchange between sodium from $NaNO_3$ and clay cations like Ca^{2+} and Mg^{2+}, thereby (partially) explaining the observed decrease in TIC.

In reactor S01_A, only a small increase in sulphate concentration (~3 mM; Table 25) was observed, indicating that pyrite was oxidised during the experiment, corresponding to a reduction of ~5 mM NO_3^- and a production of ~2.5 mM N_2O or 120 mg N (equation 6).

$$14\ NO_3^- + 4\ FeS_2 + 6\ H^+ \rightarrow 7\ N_2O + 3\ H_2O + 8\ SO_4^{2-} + 4\ Fe^{2+} \quad (6)$$

This reaction however does not explain the observed increase in N_2O (437 mg N), indicating the use of other electron donors besides pyrite: *e.g.* Fe(II) minerals (*e.g.* siderite) could have been used as electron donor, which would have resulted in the precipitation of $Fe(OH)_3$ (at pH 9; not detectable with the applied techniques) and the consumption of CO_2 (autotrophic process). However, the oxidation of other natural electron donors could not be verified further. Most likely, several electron donors and C sources were used simultaneously by the different microbial populations (*i.e.* denitrifiers, nitrifiers, N_2 fixating microorganisms). This, in combination with other processes (*e.g.* magnetite and calcite precipitation; leaching of organic compounds from the solid organic fraction), would have masked the individual outcome of each microbial pathway.

In reactor S01_B, the formate and acetate concentrations decreased until below the detection limit (Table 25), while the oxalate did not decrease in concentration, suggesting that the microbial population present in the slurry preferred using formate and acetate as electron donor and/or C source. In this slurry both nitrate and nitrite were present, but nitrite was preferentially reduced (to N_2O). These results suggest that the denitrifiers present in the clay slurry preferentially consumed nitrite and certain low molecular weight organic molecules (*e.g.* formate, acetate) according to the following reactions:

$$2\ HCOO^- + 2\ NO_2^- + 4\ H^+ \leftrightarrow N_2O + 2\ CO_2 + 3\ H_2O \quad (7)$$

$$CH_3COO^- + 4\ NO_2^- + 5\ H^+ \leftrightarrow 2\ N_2O + 2\ CO_2 + 4\ H_2O \quad (8)$$

The microbial reactions could have been responsible for the observed pH increase in reactor S01_B (increase with ~0.5 unit; Table 25), although that could also be (partly) explained by the degassing of CO_2 from the clay slurry upon equilibration with the N_2 atmosphere.

However, based on the stoichiometry of the above described reactions, these organic compounds alone could not have caused the total observed decrease in nitrite. As hydrogen is produced during N_2 fixation [76], this could have been used as electron donor in case this process had indeed occurred in the reactor, besides the use of natural electron donors from the clay such as organic matter or pyrite (sulphate increase in S01_B similar to S01_A). Due to the limited set of data (samples only from start and end of experiment), this could however not be investigated further.

6.2.2 Second series of bioreactor tests

6.2.2.1 Results

In the second series of bioreactor tests, 4 reactors were filled with Boom Clay slurries (0.32 to 0.36 kg L^{-1} solid to liquid weight ratio) and to two of them (reactors S02_A and S02_B), 0.5 M $NaNO_3$ was added (see Section 5.3.4). Three of the reactors consisted of stainless steel (reactors S02_A, S02_B, and S02_C), while the fourth one was made of carbon steel (S02_D). At the start of the tests, the reactors were pressurised with H_2 at a gas pressure of ~1.8 bar (or ~67 mmol H_2). In contrast to the first series of bioreactor tests, no bitumen degradation products were added.

As for the first bioreactor tests, the composition of the gas phase in the reactors after nearly three years of incubation was analysed and is shown in Table 27. The time evolution of the gas pressure is shown in Figure 23. The chemical composition of the liquid phase in the reactors was analysed before the start and at the end of the experiment (after nearly three years or 1023 days), to be able to detect any (microbially induced) changes (Table 28).

Table 27: Gas composition (in vol%) and pressure (P_{total} in bar) of the gas phase in the reactors of the second series of bioreactor tests after ~3 years. Note that the reactors were filled at the start of the experiment with a pure hydrogen gas phase (at ~1.8 bar).). For each detectable value the combined uncertainty is indicated, taking into account the uncertainty on the dilution factor and on the measured concentration.

Gas component	*Reactor S02_A*	*Reactor S02_B*	*Reactor S02_C*	*Reactor S02_D*
H_2	18 ± 8	<0.6	<1.3	100 ± 6.4
N_2	66 ± 28	3.5 ± 0.2	6.2 ± 1	0.07 ± 0.007
CO_2	0.060 ± 0.004	0.04 ± 0.002	0.009 ± 0.002	0.001 ± 5 x 10^{-5}
CH_4	<0.0007	0.001 ± 0.0002	89 ± 15	0.02 ± 0.001
N_2O	<0.07	87 ± 4	<0.03	<0.006
O_2	7.4 ± 3	8.1 ± 0.4	2.1 ± 0.3	0.9 ± 0.06
CO	<0.002	0.002 ± 0.0005	<0.0008	<0.002
C_2H_4	<0.04	0.0002 ± 3 x 10^{-5}	<0.01	0.0009 ± 1×10^{-5}
C_2H_6	<0.04	0.0002 ± 3 x 10^{-5}	<0.01	0.0004 ± 4×10^{-5}
P_{total}	0.166 ± 0.008	0.6518 ± 0.03	0.379 ± 0.02	1.6135 ± 0.08

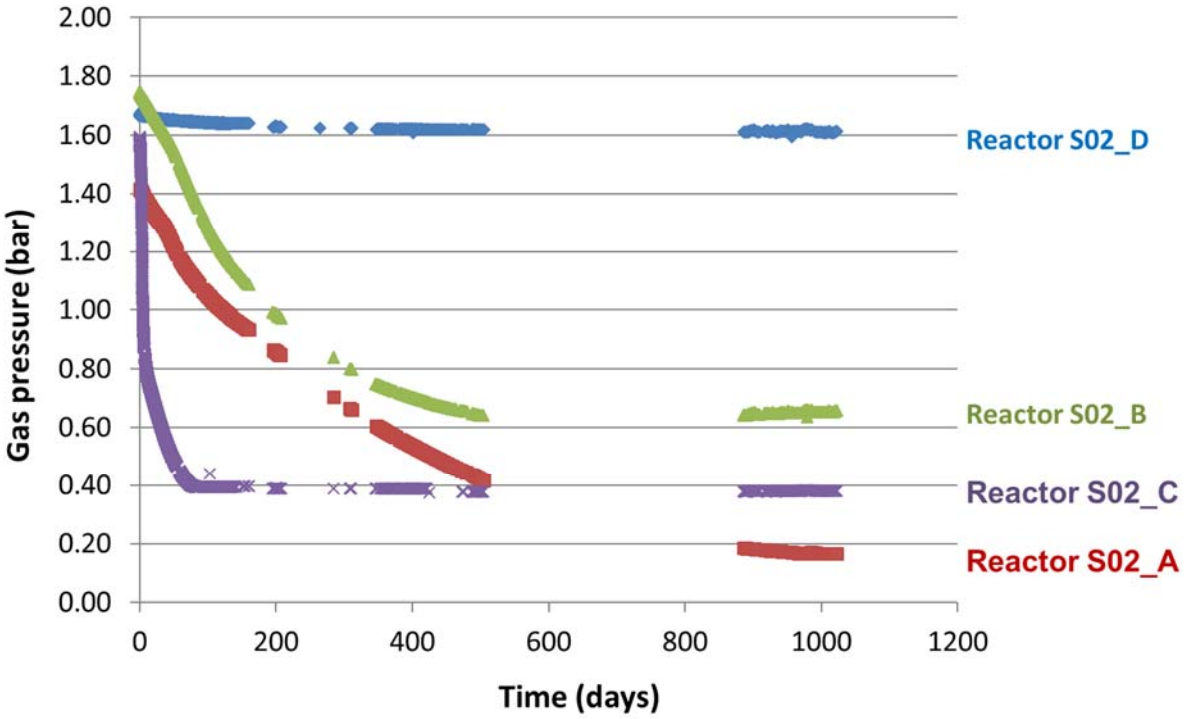

Figure 23: Gas pressure evolution in the bioreactors from series 2. The reactors (S02_A, S02_B, S02_C, and S02_D) contained Boom Clay slurries with (S02_A and S02_B) or without (S02_C and S02_D) 0.5 M $NaNO_3$. The uncertainty on this value is 0.01 bar.

Table 28: Chemical composition of the clay water fractions in the reactors S02_A, B, C and D of the second series of bioreactor tests before the start and after dismantling the experiment (after nearly 3 years). All reactors contained a Boom Clay slurry, and to reactor S02_A and B 0.5 M $NaNO_3$ was added. The concentrations are given in mM, except for TIC and TOC (in mg C L^{-1}). The uncertainties on the concentrations are 5% ($[NO_3^-]$), 6% ($[Cl^-]$), 7% ($[NO_2^-]$, $([SO_4^{2-}])$, 8% ($[F^-]$), 10% ($[Na^+]$, $[NH_4^+]$, $[Ca^{2+}]$, $[K^+]$, $[Si^{4+}]$, [Fe], TIC), 20% $[HPO_4^{2-}]$, 23% ($[Br^-]$) and ~35% (TOC). The uncertainty on the pH is 0.1 units.

Chemical	***Reactor S02_A***		***Reactor S02_B***		***Reactor S02_C***		***Reactor S02_D***	
species	***start***	***end***	***start***	***end***	***start***	***end***	***start***	***end***
F^-	0.12	0.109	0.12	0.166	0.23	0.28	0.23	0.229
Cl^-	0.73	0.711	0.73	0.719	0.79	0.804	1.6	2.3
Br^-	<0.13	<0.13	<0.13	<0.13	0.0060	0.0064	<0.0061	0.0065
NO_3^-	437.07	445.13	456.42	340.30	<0.0040	0.0182	<0.0040	<0.0040
NO_2^-	<0.01	<0.01	0.33	44.78	<0.0054	<0.0054	<0.0054	<0.0054
HPO_4^{2-}	<0.01	<0.005	<0.01	<0.01	0.022	<0.01	<0.005	0.055
SO_4^{2-}	0.030	0.0395	0.026	0.0272	0.026	0.0084	0.162	0.383
$S_2O_3^{2-}$	<0.02	<0.02	<0.02	0.025	<0.01	<0.01	<0.01	<0.01
NH_4^+	0.34	9.42	0.40	1.74	0.028	0.035	0.052	0.050
Na	456.72	443.67	461.07	448.02	18.4	10.2	15.3	11.1
Ca	3.97	0.284	4.44	0.0719	0.262	0.447	0.21	0.0369
K	4.45	2.71	4.78	3.40	0.478	0.17	0.381	0.16
Si	0.13	0.13	0.12	0.12	0.71	0.33	1.0	0.090
Fe	n.a.	0.00093	n.a.	0.00265	n.a.	0.0476	n.a.	0.0010
$HCOO^-$	0.0073	0.073	0.0058	0.016	<0.0056	0.013	0.49	0.69
CH_3COO^-	0.11	0.025	0.16	0.017	<0.008	0.61	1.6	2.00
$C_2O_4^{2-}$	<0.006	<0.006	<0.006	0.026	<0.0028	<0.0028	0.056	0.194
TIC	187	128	185	600	204	69	118	41
TOC	87	97	660	140	242	590	9700	9300
pH	n.a.	9.31	n.a.	9.55	n.a.	9.64	n.a.	9.42

The difference in detection limits for the anions is due to the high nitrate concentrations in reactors S02_A and S02_B. Mainly the detection of Br^- is disturbed by the high nitrate concentrations.

n.a.: not analysed

6.2.2.2 Nitrate reactivity in Boom Clay slurries with H_2 (reactors S02_A and S02_B)

In both reactors to which nitrate was added, clear indications for microbial nitrate reduction were observed, *i.e.* production of reduced N species (Tables 27 and 28), hydrogen consumption (Table 27) and the presence of NRP (see further). However, although the slurries were considered to be duplicates, different microbial processes had taken place in both reactors.

A total gas pressure decrease due to net gas consumption was observed in both reactors (Figure 23). Based on the hydrogen concentration in the gas phase of both reactors (Table 27), this pressure decrease is caused by hydrogenotrophic processes. Figure 23 shows that the gas pressure decrease occured in both reactors at more or less the same rate during the first ~500 days of the experiment. Afterwards, the total gas pressure decreased further in reactor S02_A, while it remained rather stable in reactor S02_B. Only at the end of the experiment, the pressure in reactor S02_A also stabilised. In reactor S02_A, a small amount of hydrogen gas (18 vol% or ~1.4 mmol H_2) was still present at the end of the experiment, in contrast to reactor S02_B (Table 27). This could explain why the gas pressure in reactor S02_B stabilised earlier than in S02_A, *i.e.* in this reactor, the microbial process had ceased, most likely due to the limitation in H_2.

In slurry S02_A, the concentration of N_2 in the gas phase increased during the experiment, to a final concentration of 66 vol% (Table 27) or 144 mg N-N_2 in total (in gas and solution). Furthermore, high concentrations of ammonium were detected at the end of the experiment in reactor S02_A (increase with 159 mg N-NH_4^+; Table 28). These results suggest that both denitrification and DNRA took place in this reactor, although no statistically significant decrease in nitrate concentration could be detected at the end of the test. This decrease is most likely masked by the high uncertainty on the high nitrate concentrations, which is ~22 mM NO_3^- or ~300 mg N (at 95% confidence level). During the experiment, the atmosphere in the reactor changed from ~100 vol% H_2 to 18 vol% H_2, indicating the activity of hydrogenotrophic nitrate reducers, similar to what was observed by Libert *et al.* [141]. In total, 66 mmol H_2 has been consumed over the course of the experiment in S02_A, which is in agreement with the observed amount of produced N-species (taking into account the measurement uncertainties; Tables 26 and 27) and the stoichiometry of the following hydrogenotrophic nitrate reduction processes:

$$NO_3^- + H^+ + 2.5\ H_2 \leftrightarrow 0.5\ N_2 + 3\ H_2O \quad \text{hydrogenotrophic denitrification} \qquad (9)$$

$$NO_3^- + 2\ H^+ + 4\ H_2 \leftrightarrow NH_4^+ + 3\ H_2O \quad \text{hydrogenotrophicDNRA} \qquad (10)$$

The observed decrease in H_2 and TIC concentration in the liquid phase of S02_A (Table 28) over the course of the experiment, confirms that hydrogenotrophic microbes, which grow autotrophically when using H_2 as electron donor [76], dominated the system. The TOC value measured at the beginning of the test is more or less in agreement with the concentration measured in the Boom Clay pore water used in this experiment. As for the first series of bioreactor tests, no significant leaching of organic compounds from the solid organic fraction in the clay could be observed after 2 days of mixing in either of the slurries, although this could have been masked by (partial) flocculation of (larger) organic compounds due to the addition of a high amount of $NaNO_3$ (ionic strength effect) [46].

In slurry S02_B, ~25% of the initial nitrate content (2032 mg $N\text{-}NO_3^-$) was predominantly reduced to both nitrite (778 mg $N\text{-}NO_2^-$) and N_2O [1183 mg $N\text{-}N_2O$ (gaseous and dissolved)], although also ammonium (23 mg $N\text{-}NH_4^+$) and N_2 [104 mg $N\text{-}N_2$ (gaseous and dissolved)] were formed (Tables 26 and 27). Furthermore, all hydrogen gas in the gas phase of the reactor was consumed (~82 mmol H_2), demonstrating that also here hydrogenotrophic processes had taken place, with the following reactions as the dominant ongoing metabolisms.

$$NO_3^- + H^+ + 2\ H_2 \leftrightarrow 0.5\ N_2O + 2.5\ H_2O \quad \text{hydrogenotrophic denitrification} \qquad (11)$$

$$NO_3^- + H_2 \leftrightarrow NO_2^- + H_2O \quad \text{hydrogenotrophic DNRN} \qquad (12)$$

Based on the stoichiometry of reactions 9 to 12 and the observed production of N species, hydrogen cannot account for all of the nitrate that has been reduced, *i.e.* ~250 mmol H_2 would have been needed to produce the observed amounts of N species. This indicates that some of the nitrate was reduced with a natural electron donor from the clay. In addition, a significant decrease in TOC and increase in TIC (Table 28) was observed, suggesting the use of DOM in as the electron donor for the remainder of the nitrate reduction processes. This is in contrast to other experiments that have demonstrated that nitrate reduction with Boom Clay electron donors such as DOM is characterised by very slow kinetics (see Sections 6.2.1 and 6.4.2). In addition, the initial DOC concentration in this reactor is 2 to 8 times higher than the one expected, based on DOC values known for Boom Clay pore water (78 to 263 mg C L^{-1} [6]), even taking into account the possible leaching of DOC from the solid phase (~100 mg C/l expected based on Maes *et al.* [140]). These observations suggest that the slurry of reactor S02_B was contaminated with easily biodegradable organic compounds (*e.g.* ethanol used for cleaning of the reactors prior to the experiment), which were used by the nitrate reducing microorganisms as electron donor when H_2 was depleted. This contamination would also explain the heterogeneity in the microbial processes observed for the duplicate reactors S02_A and S02_B, as it was not the case in S02_A.

Although its reduction is thermodynamically favoured, nitrite was still largely present at the end of the test in slurry S02_B, in contrast to S02_A. It seems that the presence of a limited amount of easily biodegradable organic compounds and the excess of nitrate have partially favoured DNRN over denitrification. This is in agreement with the results of Oh and Silverstein [67], which demonstrated the accumulation of nitrite in slurries with a low C/N ratio. Furthermore, nitrate reductase can use electrons derived from acetate oxidation preferentially compared to nitrite reductase, which also favours the DNRN reaction over the subsequent denitrification pathway [66].

In both reactors, the consumed and produced amount of nitrogen was in balance, taking into account the uncertainty on the measurements. Furthermore, as more gas was consumed (H_2) compared to the produced gas (N_2 and N_2O), the observed H_2 consuming reactions (equations 9-12) were responsible for the decrease in gas pressure (Figure 23), *i.e.* a decrease of 1.25 and 1.09 bar in reactors S02_A and B respectively, even though denitrification occurred.

It can be noted here that the occurrence of a pure chemical reaction between nitrate and hydrogen, catalysed by the surface of the stainless steel reactor vessels, cannot be excluded. However, this purely chemical reaction would only generate ammonium as the end product

[142, 143]. As only ~1.3 mM NH_4^+ was produced in reactor S02_B, we assume that the reactions observed in these reactors are mainly microbially mediated.

Nevertheless, after finishing the bioreactor tests, MPN analyses did not show a significant concentration of NRP in either of the reactors. As this was not expected and a problem with the MPN analyses could not be excluded (*i.e.* also very low concentrations in the positive control), molecular biology techniques were applied to investigate this further. The PCR analyses performed on the solid and/or liquid phase of these reactors about 4 years after the end of the experiment, still showed the presence of bacterial DNA in both slurries. More specific PCR analyses demonstrated the presence of microorganisms containing the *nirS* gene (coding for nitrite reductase) in reactor S02_B. This demonstrates that microbes capable of denitrification were present in this reactor, explaining the observed increase in gaseous N species. On the other hand, this gene could not be detected in reactor S02_A, although also here, the gas composition clearly indicates that denitrification had taken place. Possibly, the dominant denitrifying population present in reactor S02_A was genetically different from the one in reactor S02_B, using a different, structurally different nitrite reductase encoded by *nirK* [94]. It is also possible that the denitrifying population had died significantly before DNA extraction was performed, due to a lack of some of the essential nutrients for microbial activity and survival, and could therefore not be detected anymore. As no samples for microbiological analysis were taken during the experiment, it remains impossible to characterise the active bacterial population, which was present in the reactors.

6.2.2.3 Chemical evolution in Boom Clay slurries without nitrate (reactors S02_C and S02_D)

The evolution in chemical composition of the gas and liquid phase of the slurries without $NaNO_3$ was clearly different in reactors S02_C and S02_D, although these reactors were duplicates, except for the reactor material.

In slurry S02_C, a severe increase in low molecular weight organic compounds and a decrease in H_2 concentration was observed (Tables 27 and 28), *i.e.* mainly methane (17 mmol CH_4 or 201 mg C), but also some acetate (~0.8 mmol acetate or 9 mg C) was produced, while hydrogen gas was consumed completely (~77 mmol H_2). The TOC had significantly increased (by 348 mg C), while the TIC had decreased (by 135 mg C), indicating the consumption of inorganic carbon, while organic compounds were produced (*e.g.* acetate, methane, Tables 27 and 28). Note that part of the observed TOC increase was probably due to leaching of organic compounds from the solid organic fraction in the clay slurry [140]. Additionally, the total gas pressure in reactor S02_C decreased severely (by 1.20 bar) within the first 100 days of the experiment and remained more or less stable afterwards (Figure 23).

These results indicate that CO_2 was reduced to methane by MPA, resulting in the observed high amounts of methane in the gas phase and the severe decrease in DIC in this reactor. As hydrogen was completely consumed during this process, these results suggest that a H_2 / CO_2 dependent methanogenesis had occurred in this reactor [144], which also explain the decrease in TIC (Table 28):

$$4\ H_2 + CO_2 \leftrightarrow CH_4 + 2\ H_2O \qquad (13)$$

Furthermore, as the acetate concentration increased significantly, also a microbial H_2 / CO_2 dependent acetogenesis [145] seems to have occurred in this reactor:

$$4\ H_2 + 2\ CO_2 \leftrightarrow CH_3COOH + 2\ H_2O \quad (14)$$

Only MPA could have produced methane at ambient temperature by the H_2 / CO_2 dependent mechanism [76, 144] in reactor S02_C, although this could not be confirmed by microbiological analyses, as MPN analyses for MPA were not performed. However, since the gas pressure only decreased significantly in the first few months of the experiment and stabilised later on (Figure 23), the microbial activity appears to have ceased during the final years of the experiment. This was also suggested by PCR analyses, as no bacterial or archaeal DNA could be detected ~4 years after the end of the test. It is thus likely that the MPA in the reactor were only actively growing during the first few months and severely diminished in numbers afterwards due to a lack of nutrients.

In contrast to reactor S02_C, methanogenesis was suppressed in the reactors to which nitrate was added [reactors S02_A and S02_B, but also S01_A and S01_B (first series of bioreactor tests, discussed in Section 6.3.1)], although in some of these reactors (*i.e.* S01_A and S01_B) MPA could be detected. In the latter reactors, nitrate served as the most important electron acceptor available, as this oxidant is more energetically favourable compared to CO_2 (Figure A3.1).

In the carbon steel reactor S02_D, the second reactor to which no nitrate was added, only small changes in the chemical composition of the clay water (Table 28) and of the gas phase (Table 27) were observed. Besides a small increase in sulphate concentration (by 0.22 mM), possibly caused by an oxygen contamination resulting in pyrite oxidation, no oxidation/reduction products or considerable changes in their concentrations could be detected over the course of the experiment (Table 28). On the other hand, relatively high concentrations in organic compounds (formate, acetate, and oxalate; TOC) were measured in the clay water of this reactor (Table 28). Furthermore, the gas pressure and composition remained rather unchanged over three years (Table 27), indicating that little to no gas producing or consuming microbial activity had occurred in this slurry. Possibly, in this reactor (S02_D) traces of organic cleaning products or of previously present clay slurries remained in the porous iron (hydr)oxide layer of the carbon steel, causing the likely (although not verified) low microbial activity in the reactor. Therefore, this reactor should in fact not be regarded as a duplicate for the control reactor S02_C.

6.2.2.4 Characterisation of the clay slurries

As H_2 is considered as the main electron donor in the bioreactors S02_A, S02_B, and S02_C, little oxidation of the clay components is expected. To verify this, all clay fractions from the reactors were characterised by XRD. For all reactors (with and without added $NaNO_3$), the analysed clay samples had a similar mineralogical composition, which was also similar to the one reported for undisturbed Boom Clay [134]. Only the presence of dolomite was more prominent in slurry S02_B compared to S02_A. This might be linked to the observed production of inorganic carbon in the former reactor, which may have precipitated to some extend with the Ca^{2+} and Mg^{2+} present in the clay water.

6.2.3 Conclusions

The experiments reported here demonstrate that nitrate reducing prokaryota can grow and become active in disturbed Boom Clay in the presence of nitrate. These microorganisms can use Boom Clay components (pyrite, dissolved organic matter, …), organic carbon sources originating from Eurobitum (preferentially acetate and formate) or from another external source, as well as H_2 – generated during radiolysis of Eurobitum or from anaerobic corrosion of the metal in the gallery – as electron donor. The products of these microbial reactions can be several different reduced N species (depending on the reaction), *i.e.* N_2O and N_2 (through denitrification), NH_4^+ (through DNRA), and NO_2^- (through DNRN).

When denitrification occurs, gaseous products will be formed and, depending on the electron donor (*e.g.* using organic compounds) in this process, the gas pressure might increase. Too high gas pressures could influence the radionuclide transport through the clay [68], *i.e.* a gas-driven transport of water and radionuclides could be caused, or even fracturing of the clay would be possible. Yet, when H_2 is used as the electron donor (by hydrogenotrophic microorganisms), gas will be consumed by nitrate or nitrite reduction. H_2 could be present in and near the gallery, as a result of anaerobic corrosion of metallic components or radiolysis of Eurobitum. Hydrogenotrophic nitrate or nitrite reduction resulting in a gas pressure decrease, might therefore occur in and near the disposal gallery for Eurobitum – as far as microbial activity would not be hindered or made impossible because of other limiting factors (pH, available space, …).

Besides denitrification, also DNRN and/or DNRA took place in the presence of nitrate, resulting in the formation of nitrite and ammonium, respectively. Accumulation of nitrite may be due to competition during the different stages of denitrification or due to a lack of appropriate enzymes present in the microbial population. Usually, this nitrite accumulation is only temporary, due to its toxicity for microorganisms (see first series of bioreactor tests; Section 6.2.1), although in some cases nitrite could remain present at rather high concentrations [66, 146]. Many soil nitrate reducing microorganisms appear to have the ability to perform both denitrification and DNRA. DNRA is preferentially performed under strong reducing conditions and when the ratio of electron donor to electron acceptor is high [147] (see second series of bioreactor tests; Section 6.2.2). This ammonium can then be converted into organic N-compounds (biomass) or into other N species (*e.g.* nitrification). However, when present in the clay, ammonium can also sorb onto the clay minerals and compete with some radionuclides for sorption sites [70].

In the absence of nitrate, other microorganisms can grow and become active, utilizing different substrates. As no considerable decrease in the sulphate concentration was observed in these slurries, probably no SRP activity has taken place, most likely due to the low sulphate concentration in the RBCW. When H_2 was present, MPA activity (methane production) was demonstrated in the absence of nitrate, hereby typically utilizing CO_2 and H_2, which also results in a gas pressure decrease. Furthermore, some acetate was produced as well, which could later on be used by other microorganisms as an easily biodegradable C source.

Although there is no doubt that microorganisms will be present, there exists considerable uncertainty regarding their activity in the repository for Eurobitum. The confined spaces of undisturbed Boom Clay are likely too small for the growth and activity of microorganisms, as the porosity of this clay is smaller than the expected size of active microorganisms [73, 74,

117]. Therefore, only the pores or voids in the primary waste packages, the engineered barrier system [except the small pores in the (high-density) concrete], and around the liner of the disposal gallery are possible sites for microbial activity. However, the conditions here will be far from ideal for microbial growth and activity (see Annex 3). Nevertheless, certain microbial populations could be able to adapt themselves and might therefore survive (sometimes as spores) or even be metabolically active in these harsh conditions (*e.g.* at high pH conditions), until the circumstances become more favourable [76, 77, 79, 80, 148].

Additional bioreactor tests are required to study the nitrate and nitrite reactivity in Boom Clay further under laboratory and (more) realistic disposal conditions. This would allow us to obtain more insights in the factors that are controlling the bacterial activity, *i.e.* (highly) alkaline conditions, presence of easily degradable C-sources and salts that will be released from Eurobitum, presence of H_2 gas, ...

6.3 Development of analysis techniques

6.3.1 Appropriate inhibition of bacterial growth or activity

From all different chemical inhibitors that were tested ($HgCl_2$, CH_2O, NaN_3, Triclosan, and Chloramphenicol), NaN_3 was selected as the most appropriate inhibitor for the following reasons:

- Based on the results of the MPN analyses (Table 29), NaN_3 has a bacteriostatic efficiency comparable to that of $HgCl_2$ and CH_2O, in contrast to Triclosan and Chloramphenicol (both broad-spectrum antibiotics), which were not able to inhibit microbial growth. As seen in the MPN tests, a concentration of 0.1 wt% NaN_3 is already sufficient to significantly inhibit the microbial growth.
- The NRP activity in the Boom Clay slurries (1/10 and 1/100 g Boom Clay per g RBCW) with nitrate (and bacterial inhibitor) was followed over time (3, 7, and 17 weeks) by analysing the nitrate and nitrite concentration (Table A5.2). While the nitrate and nitrite concentrations remained constant in the slurries with NaN_3, $HgCl_2$, and CH_2O, microbial nitrate reduction to nitrite was observed in the blank solutions and in those with Triclosan and Chloramphenicol. These results indicate that the former three inhibitors cause a total inhibition of the NRP population. In contrast, Triclosan and Chloramphenicol seem to promote the microbial nitrate reduction (transient enhanced inhibition), as a higher amount of nitrate was reduced in the Boom Clay slurries with 0.1 M $NaNO_3$ when Triclosan or Chloramphenicol was added (see Section 6.4.1 and Annex 5). This is most likely due to instability of the compounds in aqueous solutions due to hydrolysis or light[40]. Possible degradation products of the antibiotics were likely used as carbon sources for microorganisms, thereby stimulating the microbial growth and/or activity [97].
- The addition of Na^+ from NaN_3 to Boom Clay suspensions results in ion exchange reactions that are quantitatively understood [84, 97] and similar to the response seen in the percolation tests (see Section 6.1.2.1.1).

[40] Chloramphenicol is only 4 days stable in aerobic aqueous solutions. In absence of strong bases or acids, Triclosan is susceptible to degradation via aqueous photolysis, with a half-life of less than 1 hour under abiotic conditions (United States Environmental Protection Agency, DP barcode 343543, 2008).

Table 29: Results of MPN analyses on Boom Clay slurries with 0.1 M $NaNO_3$ (after 7 weeks of incubation). The sample name consists in the solid to liquid weight ratio (1/10 or 1/100) and the type and concentration of the inhibitors added to the slurries (see Table 5) [84]. The lower and upper detection limit are equal to respectively 3 and 1.1×10^3 cells mL^{-1}.

Sample	*MPN[b] (cells mL^{-1})*	*Sample*	*MPN[b] (cells mL^{-1})*
1/10 blank	> 1099	1/100 blank	> 1099
1/10 0.1 wt% $HgCl_2$	7 ±	1/100 0.1% $HgCl_2$	< 3.0
1/10 0.5 wt% $HgCl_2$	9	1/100 0.5% $HgCl_2$	21
1/10 0.1 wt% NaN_3	292	1/100 0.1% NaN_3	28
1/10 1 wt% NaN_3	150	1/100 1% NaN_3	11
1/10 0.1 wt% CH_2O	7	1/100 0.1% CH_2O	7
1/10 1 wt% CH_2O	9	1/100 1% CH_2O	11
1/10 20 mg L^{-1} Chlor.	> 1099	1/100 20 mg L^{-1} Chlor.	> 1099
1/10 200 mg L^{-1} Chlor.	> 1099	1/100 200 mg L^{-1} Chlor.	> 1099
1/10 1000 mg L^{-1} Chlor.	> 1099	1/100 1000 mg L^{-1} Chlor.	> 1099
1/10 10 µM Tricl.	< 3.0	1/100 10 µM Tricl.	> 1099
1/10 100 µM Tricl.	> 1099	1/100 100 µM Tricl.	7
1/10 1000 µM Tricl.	> 1099	1/100 1000 µM Tricl.	> 1099

[a] Number of positive tubes (out of three replicates) for the three serial decimal dilutions.
[b] Most probable number (microbial concentration) calculated from the number of positive tubes.

- N_3^- proves to be stable in the Boom Clay geochemical conditions: no significant changes in N_3^- concentration in the slurries after 3, 7, and 17 weeks of incubation were observed.
- The presence of NaN_3 in a 1 wt% concentration increases the uncertainty on the nitrate concentration (due to interference of the measurement by ion chromatography) from ~6% to 10-20% [84, 97].
- Based on the results of the batch tests with RBCW (Section 6.4.2), the presence of NaN_3 (up to 1 wt%) appears not to interfere with the DOM content in RBCW. However, for Boom Clay slurries a significant decrease in TOC with increasing NaN_3 concentrations can be observed in the supernatans of the clay slurry after centrifugation. This is likely caused by increased flocculation of DOM due to the release of bivalent cations from the clay by cation exchange processes and the subsequent bridging of DOM molecules. In addition, the higher degree of shielding of the negatively charged functional groups of DOM by Na^+ has likely resulted in an increased interaction between the flocculated DOM and clay particles.

Although $HgCl_2$ and CH_2O are slightly more efficient in inhibiting the growth of NRP in slurries compared to NaN_3 (based on results of MPN in Table 21), they were not selected to be used in the batch tests under abiotic conditions, for the following reasons [84, 97]:

- The addition of $HgCl_2$ results in cation exchange reactions and in a significant decrease in TOC values (probably due to flocculation). Indeed, the concentration of Hg^{2+} is considerably lower than the added concentration of $HgCl_2$, indicating that there is an interaction between Hg^{2+} and organic matter (flocculation) and/or solid particles (cation exchange). These interactions are to be avoided in batch tests where the reactivity between nitrate (or nitrite) and Boom Clay (thus also DOM) is

investigated. Furthermore, the presence of Hg^{2+} might have an effect on the redox potential of the Boom Clay, *i.e.* redox reactions between Hg^{2+} and Boom Clay are possible [84, 97].
- The use of CH_2O as inhibitor strongly affects the TOC values of the slurries [84, 97], which would make it difficult to investigate the reactivity of nitrate with DOM.

Initially, NaN_3 was added to the RBCW solutions of the batch tests to a final concentration of 1 wt%. Later, this concentration was decreased to 0.2 wt% for reasons mentioned in Section 6.3.2. As MPN tests on the RBCW solutions with 0.2 wt% NaN_3 demonstrated that NRP growth and activity only re-started after several dilutions of the solution in NRP medium (Section 6.4.2.2), this lower concentration of NaN_3 is sufficient to suppress the NRP activity and growth in the RBCW solutions.

An alternative for a chemical bacterial inhibitor, to be used in future batch tests with RBCW, was also investigated, *i.e.* filter sterilisation using a sterile 0.22 µm filter and an autoclaved recipient. Several observations indicate that this technique can be used in future tests with RBCW:

- The TOC content in the RBCW did not significantly decrease due to filter sterilisation, indicating that there is no loss of organic matter due to filtration.
- MPN analysis of the unfiltered and filtered RBCW solutions with and without $NaNO_3$ confirm the absence of NRP in the filtered solutions, while NRP are present (in high concentrations) in the unfiltered solutions (Figure 24).
- Chemical analyses of the RBCW solutions with $NaNO_3$ show that microbial nitrate reduction only takes place in the unfiltered solution, at a similar rate as the one observed for the batch tests with RBCW (See Section 6.4.2). In the filtered RBCW solution with nitrate, no nitrite was formed after 6 months.

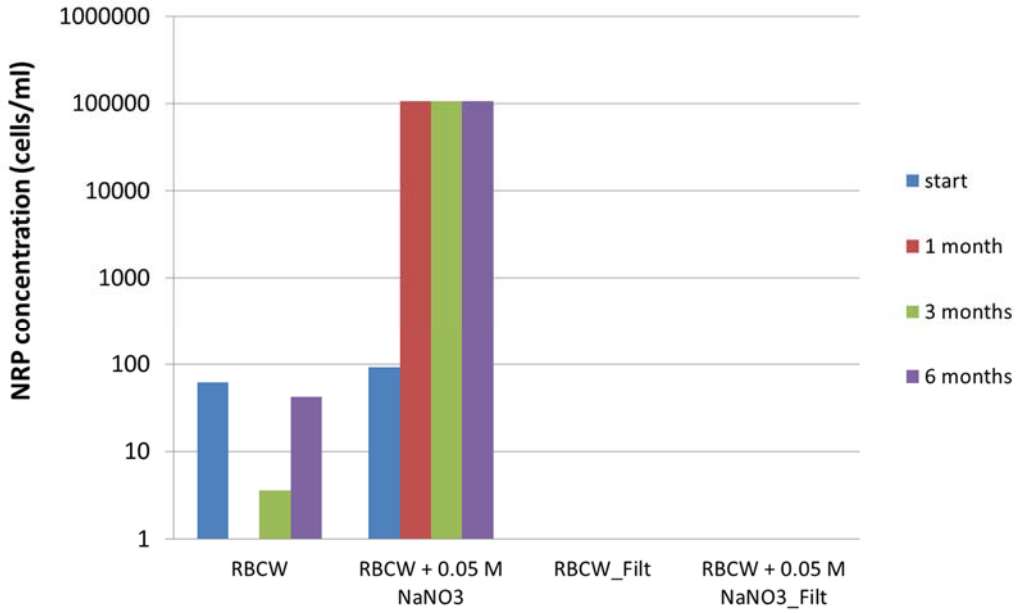

Figure 24: Evolution of the NRP concentration (measured by MPN analyses) in the unfiltered solutions (RBCW and RBCW + 0.05 M NaNO3) and in the filtered solutions (RBCW_Filt and RBCW + 0.05 M NaNO3_Filt) in function of time. The lower and upper detection limit of these MPN analyses are equal to respectively 3 and 1.06×10^5 cells mL^{-1}.

6.3.2 Determination of the reducing capacity of organic matter

The supporting tests to optimise the procedure to determine the reducing capacity of DOM for both ferricyanide and ferric citrate are described in detail by Bleyen *et al*. [26]. In this section, a summary of these results is given.

6.3.2.1 Reducing capacity of organic matter (from RBCW) for ferricyanide

Based on the results of the supporting tests [Table 7; both with RBCW and with hydroquinone (a model for DOM)], the following conclusions can be drawn:

(i) **Reaction kinetics of ferricyanide reduction by DOM:**
- The evolution of the reduction of ferricyanide by hydroquinone indicates that ~80% of this phenolic compound is oxidised (with an optimal molar ferricyanide/hydroquinone ratio of 1/1) to benzoquinone by ferricyanide within the first few minutes after mixing, while the remainder is oxidised over the next few days at a slower rate. This slower rate is probably due to the formation of quinhydrone complexes[41], resulting in less available oxidisable groups [149].
- The reduction of $Fe(CN)_6^{3-}$ by DOM of RBCW is characterised by two reaction mechanisms: an initial fast reaction process (within 24-50 hours) that is attributed to the oxidation of phenolic functional groups of DOM (*e.g.* hydroquinones) and a second slower reaction process (lasting over ~500 h) that involves the less available functional groups.
- In the optimised procedure, clay water is diluted to 50 vol% (~50 mgC L^{-1}) by SCW containing ferricyanide (final concentration 0.8 mM). This optimal ferricyanide to DOM ratio was established as the lowest ratio for which the maximal reducing capacity of DOM for ferricyanide can be obtained after a certain reaction period.
- The value of the reducing capacity of DOM is always determined after 50 h, *i.e.* after the switch to the slower reaction process. This allows us to compare the values of the reducing capacities of DOM in RBCW, obtained at different sampling times. Furthermore, possible misinterpretation of the results due to formation of quinhydrone-like species in the RBCW solutions after longer incubation periods is prevented.

(ii) The **uncertainty** of an individual reducing capacity value using the optimised procedure for ferricyanide (optimised procedure II in Table 8) is 10-20%, and is calculated for each value based on uncertainties on the TOC value and on the ferricyanide concentration.

(iii) The reducing capacity of DOM in RBCW ranges from 3.4 to 6.1 meq gC^{-1}. Its value varies slightly depending on the batch of RBCW taken from the EG/BS piezometer, similar to the differences in TOC and functional groups observed for different batches of RBCW [22, 150].

(iv) **Effect of nitrate and nitrite on the reducing capacity of DOM for ferricyanide:**

[41] Note that the combination of hydroquinone (reduced quinone) and benzoquinone (oxidised quinone) results in the formation of quinhydrone through ring stacking [26].

- No reaction between $[Fe(CN)_6]^{3-}$ or $[Fe(CN)_6]^{4-}$ and nitrite or nitrate could be observed after 300 hours.
- Addition of 0.1 M $NaNO_3$ does not have an effect on the reducing capacity of hydroquinone for ferricyanide. As hydroquinones are important redox-active functional groups in the DOM of RBCW, these results already suggest that nitrate will have little oxidative effect on the dissolved organic matter (in the absence of bacteria).
- A slow and small degree of oxidation of hydroquinone by 0.1 M nitrite can be observed after ~100 hours, suggesting that nitrite, in contrast to nitrate, does have some oxidative effect on dissolved organic matter. However, as this reaction is only observed after ~100 hours, the influence of nitrite on the reducing capacity value of DOM in RBCW is expected to be small.

(v) **Effect of azide on the reducing capacity of DOM for ferricyanide:**

- The presence of NaN_3 appears to result in higher reducing capacities of both hydroquinone and DOM in RBCW, most likely due to reduction of oxidised organic functional groups (*e.g.* phenolic compounds [151]). Because of this effect, the NaN_3 concentration in the $K_3Fe(CN)_6$ solutions was lowered from 1 wt% in the original procedure to 0.1 wt% in the optimised procedure II in Table 8.
- To eliminate NaN_3 in the ferricyanide solutions completely, supporting tests demonstrate that the RBCW-ferricyanide solutions can be filter sterilised (0.22 µm filter) when the reducing capacity is determined. Based on these results, no significant difference is shown between the reducing capacity of DOM of filtered and non-filtered RBCW solutions. However, as the abiotic solutions from the batch tests with RBCW (see Sections 5.4.3 and 6.4.2) already contain NaN_3 during incubation, the effect of azide on the reducing capacity of DOM cannot be completely avoided.

(vi) For a range of **ionic strength**s comprising all ionic strengths of the solutions of the batch tests with RBCW (second series with nitrate and first series with nitrite), only increasing the ionic strength of the ferricyanide-RBCW solutions above 0.1 M leads to somewhat faster initial ferricyanide reduction kinetics and a higher reducing capacity of DOM (though not statistically significant). This result suggests a (slightly) higher availability of easily oxidisable functional groups (*e.g.* phenols) at higher ionic strength. However, for the batch tests with RBCW (second series with $NaNO_3$ and first series with $NaNO_2$), even the highest ionic strength in the ferricyanide-RBCW solutions is below 0.1 M, indicating that no adjustment of the ionic strength is needed.

The main conclusions from these supporting tests are summarised in Table 30.

Table 30: Overview of the conclusions drawn from the supporting tests to investigate the effect of several components on the determination of the reducing capacity of DOM using ferricyanide [26].

Investigated component	*Influence on ferricyanide reduction by DOM*	
	Effect on ferricyanide / ferrocyanide	Effect on DOM during determination of the reducing capacity
Nitrate	No	No
Nitrite	No	Yes (only significant after ~100 hours[a])
Microorganisms	Yes	Yes
NaN_3	No	Yes (+ possible reaction between azide and nitrite)
Differences in ionic strength	No	Yes: increasing overestimation of the reducing capacity of DOM with increasing ionic strength (but only at ionic strength > 0.1 M)

[a] For hydroquinone solutions

6.3.2.2 Reducing capacity of organic matter (from RBCW) for ferric citrate

The procedure for the determination of the reducing capacity determination using ferric citrate as oxidant was optimised starting from the procedure described by Bauer *et al.* [105]. Based on the results of these supporting tests (performed with RBCW) described in detail by Bleyen *et al.* [26], the following conclusions can be drawn:

(i) **Reaction kinetics of Fe(III) reduction by DOM:**
- The evolution of the reduction of Fe(III) from ferric citrate by DOM of RBCW is characterised by two reaction mechanisms, similar to the reaction kinetics observed for ferricyanide by DOM (Section 6.3.2.1), *i.e.* an initial fast reduction of Fe(III) due to reaction with phenolic groups (within 1 hour) followed by a slow reduction of Fe(III).
- Less ferric citrate can be reduced by DOM from RBCW compared to ferricyanide, which is in agreement with previous studies [25, 105]. In addition, the reduction of Fe(III) by iron-oxidisable DOM reaches its thermodynamic equilibrium faster than for ferricyanide, *i.e.* within 24 hours a stable Fe(II) concentration is reached. The value of the reducing capacity of DOM is therefore determined for each sample after ~24 hours.
- In the optimised procedure, 50 vol% clay water (~50 mgC L^{-1}) is mixed with 1 mM ferric citrate to determine the reducing capacity of DOM in RBCW. This optimal ferric citrate / DOM ratio results in the maximal reducing capacity of DOM for ferric citrate.

(ii) The value of the reducing capacity of DOM, using ferric citrate, is **pH dependent**. This can be explained (at least in part) by the difference in speciation of the Fe(III) and Fe(II) citrate complexes and in the standard redox potential of the corresponding reduction reaction. A lower pH of the solution seems to render a ferric citrate complex

with a higher standard redox potential, and thus a higher oxidising capacity towards DOM [103, 104]. To measure the reducing capacity of DOM in RBCW, the ferric citrate-RBCW solution is therefore acidified to pH 4.5 prior to addition of ferrozine, which generates a higher value of the reducing capacity of DOM than when the solution remains at pH 7.

(iii) The **uncertainty** of an individual reducing capacity value using the optimised procedure for ferric citrate is 12-15% (at pH 4.5 and after ~24h) and is based on uncertainties on the TOC value and on the produced Fe(II) concentration.

(iv) The reducing capacity of DOM in RBCW using ferric citrate ranges from 0.8 to 1.3 meq gC^{-1} (measured at pH 4.5). Similar to what has been observed for ferricyanide, the value of the reducing capacity of DOM in RBCW using ferric citrate varies slightly depending on the batch of RBCW.

(v) **Effect of nitrate and nitrite on the reducing capacity of DOM for ferric citrate:**

- Addition of nitrate to RBCW does not have an effect on the value of the reducing capacity of DOM in RBCW, using ferric citrate (both at pH 4.5 and pH 7).
- On the other hand, nitrite appears to have a significant effect on the measurements of the reducing capacity of DOM:
  - Nitrite slowly oxidises some of the DOM, as described above. However, as the reducing capacity is measured within ~24 hours, the effect of this slow reaction during this measuring period is considered to be negligible.
  - At pH 4.5, nitrite is mainly present as HNO_2, which is able to oxidise Fe(II) from the ferrous citrate complex, once this is produced [139, 140]:

$$Fe^{2+} + HNO_2 + H^+ \rightarrow Fe^{3+} + NO + H_2O \quad (15)$$

Based on the reducing capacity of DOM in clay water solutions to which 0.05 M $NaNO_2$ is freshly added, this reaction interferes severly with the results: Fe(III) reduction by DOM cannot be observed. On the other hand, at pH 7, Fe(II) oxidation by nitrite occurs more slowly, allowing some of the produced Fe(II) to be detected during the measurement. However, some Fe(II) would still be oxidised by nitrite, rendering the results unreliable as well.

- Addition of nitrite at a low concentration (≤ 0.2 mM), similar to the nitrite produced by microbial nitrate reduction in RBCW during 1.5 year (see Section 6.4.2.2), does however not result in a lowering of the reducing capacity of DOM for ferric citrate.

(vi) **Effect of azide on the reducing capacity of DOM for ferric citrate:**

- Addition of azide to ferric citrate at pH 4.5 causes a decrease of the background or produced Fe(II) concentration. This in turn would lead to an understimation of the reducing capacity value of DOM.
- On the other hand, NaN_3 can also (to some extent) reduce oxidised functional groups of DOM, as described in Section 6.3.2.1. However, addition of fresh azide does not result in a statistically significant increase in the value of the reducing capacity of DOM (measured at pH 4.5), in contrast to the measurements with ferricyanide. This might be due to the counteracting effect of azide on DOM and on Fe(II).
- When fresh nitrite and azide are both added, azide appears to block part of the effect of nitrite on the Fe(III) reduction by DOM (when acidified to pH 4.5).

Possibly, part of the nitrite is used to decompose azide under acidic conditions, resulting in the generation of N_2 and N_2O [152, 153]:

$$N_3^- + HNO_2 + H^+ \rightarrow N_2 + N_2O + H_2O \quad (16)$$

Although a higher reducing capacity of DOM was measured when both fresh nitrite and azide were added to RBCW, compared to only adding nitrite, the reducing capacity of DOM in these solutions was still lower than expected (without nitrite or azide), indicating that using ferric citrate to determine the reducing capacity of DOM will not provide reliable values for the batch tests with RBCW and nitrite (Section 6.4.2.3).

The main conclusions from these supporting tests are summarised in Table 31. Based on the results of these tests, it is clear that ferric citrate can only be used in the batch tests with RBCW to determine the reducing capacity of DOM in RBCW with nitrate and not with nitrite (Section 6.4.2.2).

Table 31: Overview of the conclusions drawn from the supporting tests to investigate the effect of several components on the determination of the reducing capacity of DOM using ferric citrate [26].

Investigated component	***Influence on Fe(III) reduction by DOM***	
	Effect on Fe(III) or Fe(II)	Effect on DOM during determination of the reducing capacity
Nitrate	No	No
Nitrite	Yes	Yes: underestimation of the reducing capacity of DOM (only significant for nitrite concentrations ≥ 1 mM)
Microorganisms	No significant effect (due to lag phase)	
NaN_3	No	No significant effect (but counteracting reactions with azide, DOM and Fe) + reaction between azide and nitrite

6.4 Batch tests

As discussed in Annex 3, the conditions in the Boom Clay are far from ideal for bacterial activity. Hence, it is of importance to study whether and to which extent nitrate or nitrite can be reduced abiotically in Boom Clay. To allow a clear interpretation of any reactivity of nitrate and nitrite with the main reducing components of Boom Clay (dissolved organic matter, kerogen, pyrite), batch experiments with each of these components were and are being performed, both in biotic and in abiotic conditions. Abiotic conditions were obtained by adding NaN_3 to the clay slurries, pyrite, or clay water. Here, the results of batch tests with Boom Clay slurries (Section 6.4.1), RBCW (Section 6.4.2), and pyrite (Section 6.4.3) are discussed.

6.4.1 Batch tests with Boom Clay slurries

The main purpose of the tests with Boom Clay slurries was the selection of an appropriate inhibitor for denitrifying bacteria and other NRP (Section 6.3.1). Nevertheless, these tests also allow us to draw preliminary conclusions on the abiotic reactivity between nitrate or nitrite and Boom Clay. The results of the chemical analyses of these batch tests are shown in Annex 5: tests with Boom Clay slurries (with or without microbial inhibitor) and 100 mM $NaNO_2$ (Table A5.1), or 100 mM or 1 M $NaNO_3$ (Table A5.2) after 3, 7 or 17 weeks of incubation in anaerobic conditions. Table A5.3 gives the results of the chemical analysis of the supernatant of Boom Clay slurries with and without 1 M $NaNO_3$ after one year of anaerobic incubation.

Nitrate was only reduced to nitrite in the Boom Clay slurries with 0.1 M nitrate containing a high microbial concentration (MPN values above 1099, Table 29), *i.e.* slurries without inhibitor and slurries to which the antibiotics Triclosan and Chloramphenicol were added (Table A5.2). In some of the Boom Clay slurries with Triclosan and Chloramphenicol, all nitrate (0.1 M) was reduced after 3 to 17 weeks of incubation to mainly nitrite, but also to other nitrogen components, as the produced nitrite concentration is lower than the reduced nitrate concentration. In the clay slurries without these antibiotics, less than 1% of the nitrate content was reduced in nitrite. This demonstrates that long-term incubation of clay slurries with unstable antibiotics (Triclosan and Chloramphenicol) enhances the microbial activity, as the degradation products of the antibiotics (and/or solvent) could have been used as carbon sources and electron donors [97] (see also Section 6.3.1). Compared to easily degradable organic compounds, the Boom Clay reducing components appear to be (relatively) poor electron donors for microorganisms, which is in agreement with the results from the first series of bioreactor tests (see Section 6.2.1).

In contrast, no significant nitrite reduction (chemically nor microbially) could be observed in the Boom Clay slurries with 0.1 M nitrite (Table A5.1) during 17 weeks of incubation, although small decreases of the nitrite concentration may have been undetectable due to the high uncertainty on the nitrite concentration, and because the presence of other N species with a lower or negative valency was not verified. The lack of microbial nitrite reduction is most likely due to the high nitrite concentration (100 mM) added to the slurries, which is highly toxic to a microbial population [137].

In the Boom Clay slurries with 1 M $NaNO_3$, both without inhibitor [solid to liquid ratios of 1/3 (Table A5.3) and 1/10 (Table A5.2)] and with CH_2O (Table A5.3) or $HgCl_2$ (Table A5.2) as inhibitors, there was no significant nitrate reduction and no nitrite was detected in the slurries

with a solid to liquid ratio of 1/10 (in the other slurries nitrite was not measured). These observations confirm the results of other studies, in which it is shown that high salt concentrations inhibit microbial activity as well [76]. $NaNO_3$ concentrations of 0.35 to 0.5 M have been shown to inhibit NRP growth and activity severely [141]. The limit of resistance appears to be depending on the microbial species.

In none of the slurries, including the ones where nitrate was reduced, the sulphate concentration increased significantly, suggesting that pyrite was not oxidised by nitrate, nor biotically, nor abiotically (*i.e.* purely chemically) or only at a slow rate. Note however that besides sulfate, other pyrite oxidation products were not measured or might have precipitated (*e.g.* $FeCO_3$) in the slurry.

In summary, it can be concluded that no considerable abiotic reduction of nitrate and nitrite had occurred in the batch tests with Boom Clay slurries (within 17 weeks of incubation). Microbially mediated nitrate reduction was observed and was enhanced by addition of a carbon source in the form of (instable) antibiotics (Triclosan and Chloramphenicol) [97].

6.4.2 Batch tests with Real Boom Clay Water

6.4.2.1 First series of batch tests with RBCW and nitrate

In a first series of batch experiments with RBCW, five different clay water solutions were prepared in duplicate (Table 12): (1) RBCW, (2) RBCW with 0.2 M $NaNO_3$, (3) RBCW with 1 wt% NaN_3, (4) RBCW with 1 wt% NaN_3 and 0.05 M $NaNO_3$, and (5) RBCW with 1 wt% NaN_3 and 0.2 M $NaNO_3$. Any reaction between nitrate and the dissolved organic matter in RBCW was monitored in time, by analysing each solution after different reaction periods. The complete set of results from the chemical analyses and pH measurements is given in Annex 6. Figure 25 shows the evolution of the nitrate and nitrite concentrations in the RBCW solutions with 0.2 M $NaNO_3$, to which no microbial inhibitor (NaN_3) was added.

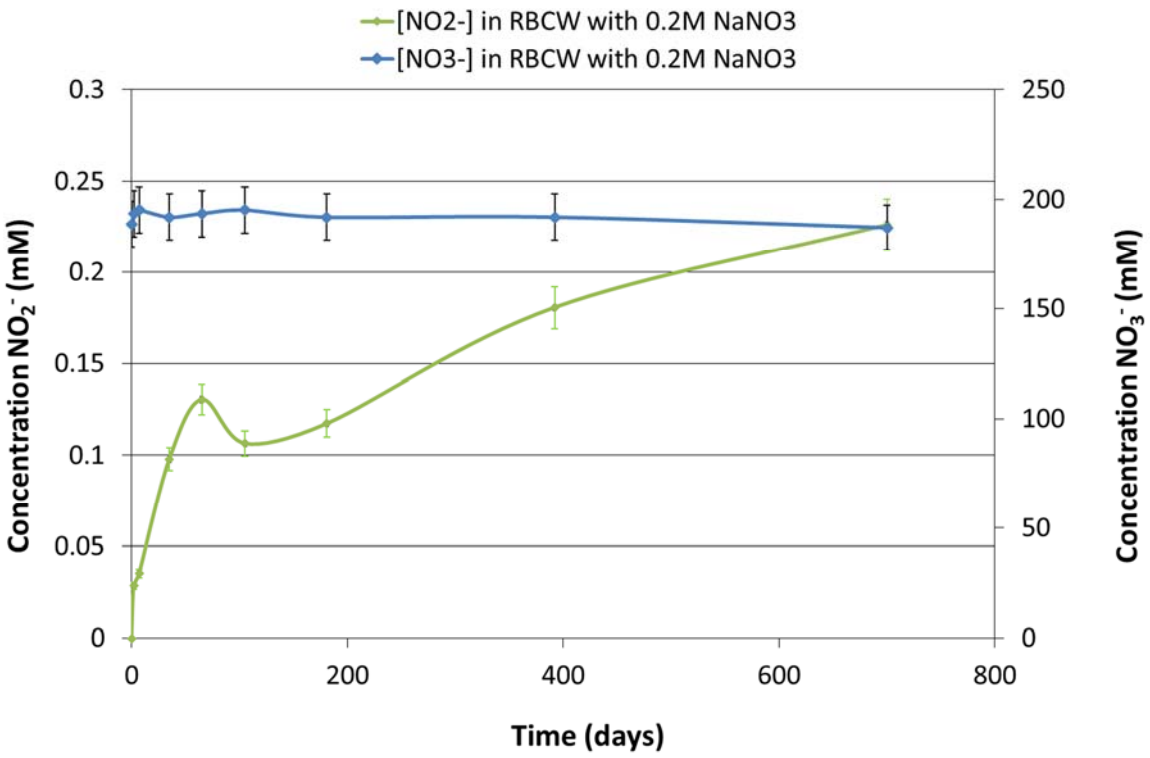

Figure 25: Evolution of the nitrate and nitrite concentrations in one series of the RBCW solutions with 0.2 M $NaNO_3$ and to which no microbial inhibitor (NaN_3) was added. Similar results were observed in the duplicate solution. The uncertainty on the NO_2^- and NO_3^- concentrations is 5-6%.

There were no significant variations in time of the Na^+ concentration and of the TOC and TIC values. Slightly increasing Ca^{2+} concentrations were measured in the solutions that were analysed after more than one year of storage in the glove box, due to leaching of Ca^{2+} from the glass bottles. The pH fluctuations with time were very limited and not linked to nitrate reactivity (similar fluctuations for all solutions). In none of the solutions with nitrate, a significant decrease in the nitrate concentration was observed, suggesting that there was no important nitrate reduction (Tables A6.2, 4 and 5). However, in the RBCW solutions with 0.2 M $NaNO_3$ but without microbial inhibitor (NaN_3), the nitrite concentration was increasing slowly (Figure 25). Note that in some samples (opened after different reaction periods), there was a lower nitrite production rate, resulting in the fluctuations of the nitrite concentration in time. After about two years of reaction, 0.23 to 0.33 mM nitrite was formed, corresponding to a reduction of only 0.12 to 0.18 mol% of the initial nitrate content.

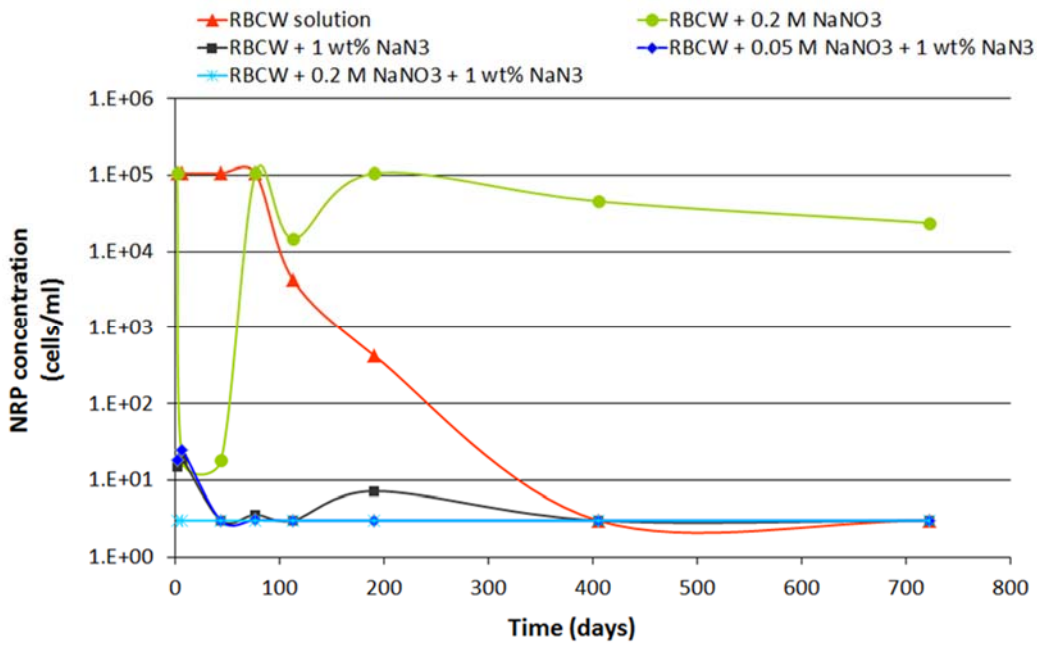

Figure 26: Time evolution of the concentration of viable cells in the five different clay water solutions, as measured with MPN analyses of one series of samples per type of solution. The lower and upper detection limits are equal to respectively 3 and 1.1×10^5 cells mL^{-1}. The concentration of viable cells in the Boom Clay water solution (RBCW) after 2, 7, 36, and 65 days of reaction, and in the Boom Clay water solution with 0.2 M $NaNO_3$ (RBCW + 0.2 M $NaNO_3$) after two days of reaction was higher than the upper detection limit.

Figure 26 shows the concentration of viable cells in the five different solutions, as measured with an MPN analysis after each reaction period. The microbial analyses were performed on only one series of samples per type of solution. As a high concentration of viable cells (~10^5 cells mL^{-1} clay water) was detected in the clay water solutions in which nitrite was produced (0.2 M $NaNO_3$ solutions without microbial inhibitor), it is likely that the production of nitrite was microbially mediated (*i.e.* DNRN). The low nitrate reduction rates in these solutions indicate a low microbial activity, probably due to the low concentration or availability of (easily degradable) electron donors in RBCW. It can be remarked that in two samples with nitrite formation (RBCW with 0.2 M $NaNO_3$, samples analysed at 7 and 44 days after start of the batch test, see Figure 26), almost no viable cells were detected (~ 18 cells mL^{-1}) although nitrite was produced. Possibly, during the preparations of the RBCW solutions, the NRP population was disturbed, which could have resulted in (some) microbial death. After an adjustment phase (lag phase), the microbial concentration increased again to its original value. However, as nitrite was produced during this phase, the NRP activity might not have been as low as implied by the concentration measured by MPN analysis.

The decrease in NRP concentration in the RBCW solution (without $NaNO_3$ and NaN_3) after two to three months of incubation is probably linked to the consumption of certain essential nutrients in the RBCW, which finally resulted in the death of the NRP (Figure 26). In the Boom Clay water solutions to which NaN_3 was added, no significant number of viable cells were detected (MPN values close to or below the lower detection limit of 3 cells mL^{-1}), confirming the efficiency of 1 wt% NaN_3 as microbial inhibitor. In none of the solutions with NaN_3 an abiotic reduction of nitrate into nitrite was detected, as indicated by the stable nitrate concentrations and the lack of nitrite production in these solutions (see Annex 6).

In Figure 27, the results of the determination of the reducing capacity of DOM in RBCW after about two years of contact with or without nitrate is shown[42].

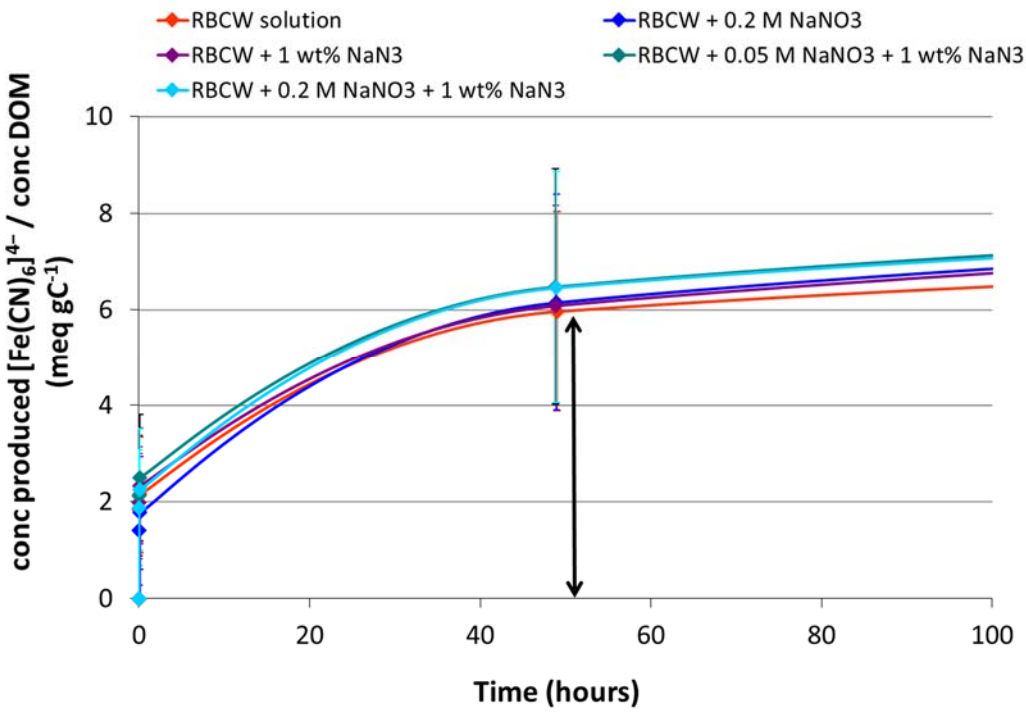

Figure 27: Results of the determination of the reducing capacity of DOM (in RBCW, after ~2 years of contact with or without nitrate) for $[Fe(CN)_6]^{3-}$, using ferricyanide (optimised procedure I; see Section 5.1.3.2). The reducing capacity of DOM in these solutions was determined after ~50 hours of reaction between ferricyanide and DOM (indicated by the arrow). The uncertainty bars take into account the uncertainty on the decrease in ferricyanide and on the TOC concentration.

The results of the other measurements (on clay water solutions analysed after shorter reaction periods) are not presented here, as they were obtained with the original procedure to determine reducing capacities of Boom Clay water (Table 8), resulting in high uncertainties. Figure 27 shows that the reducing capacity of the DOM in the five different RBCW solutions (after ~2 years of storage in an anaerobic glove box) is similar and equals ~6 to 6.5 meq gC^{-1} (measured after ~50 hours, pH of the solutions ~8.1, and with 1 wt% NaN_3).

A lower reducing capacity was not measured for the RBCW solutions in which some of the nitrate was reduced into nitrite (RBCW + 0.2 M $NaNO_3$ without NaN_3). As the mean nitrite concentration measured in these solutions at the end of the experiment was 0.27 mM (mean concentration for two replicates), the reducing capacity of the RBCW solutions should have decreased with 5.7 meq gC^{-1}, in the assumption that all functional groups of DOM that can

[42] Due to a lack of sufficient solution to prepare the $K_3Fe(CN)_6$ solutions with the optimised procedure I (Table 8; $K_3Fe(CN)_6$ solutions with 50 vol% clay water instead of 10 vol%), the duplicate solutions (a and b) were poured together and the reducing capacity of the mixture (containing 80 vol% of solution a and 20 vol% of solution b) was determined.

be oxidised by nitrate can also be oxidised by ferricyanide. Several explanations were investigated as to why this decrease could not be observed:

(i) A possible **reaction between nitrite and ferricyanide**?
However, the unexpected high reducing capacity of the clay water solutions in which nitrite was formed, cannot be explained by an additional reduction of ferricyanide by nitrite. Indeed, no redox reactions between nitrite and ferricyanide were observed after one month in control $K_3Fe(CN)_6$ solutions with nitrite (in demineralised water) (Section 6.3.2.1).

(ii) The interference of the measurements due to the **presence of azide** in the solutions?
As remarked in Section 6.3.2.1 and by Bleyen *et al.* [26], the presence of NaN_3 in the ferricyanide-RBCW solutions appears to result in higher reducing capacities of DOM. To investigate this further, the reducing capacity of DOM in the RBCW solutions with 0.2 M $NaNO_3$ ('0.2M NaNO3_0% bact', see Table 12) was determined, after ~2 years of storage in the glove box, with and without addition of NaN_3 (1 wt%) to the ferricyanide solutions. The reducing capacity of DOM (determined after ~50 hours) in the ferricyanide solutions with 1 wt% NaN_3 was ~28% higher (although not statistically significant) than in the ferricyanide solutions without NaN_3 (Figure 28).
The kinetics of the reaction until 500 hours after the start (Figure 28) suggest that the difference in reducing capacity is mainly caused by a higher degree in oxidation of the phenolic functional groups, which supports the possible conversion of quinone-like groups into hydroquinone-like groups by azide (Section 6.3.2.1), *i.e.* N_3^- could have reduced (some of) the functional groups of dissolved organic matter that were previously oxidised by nitrate.

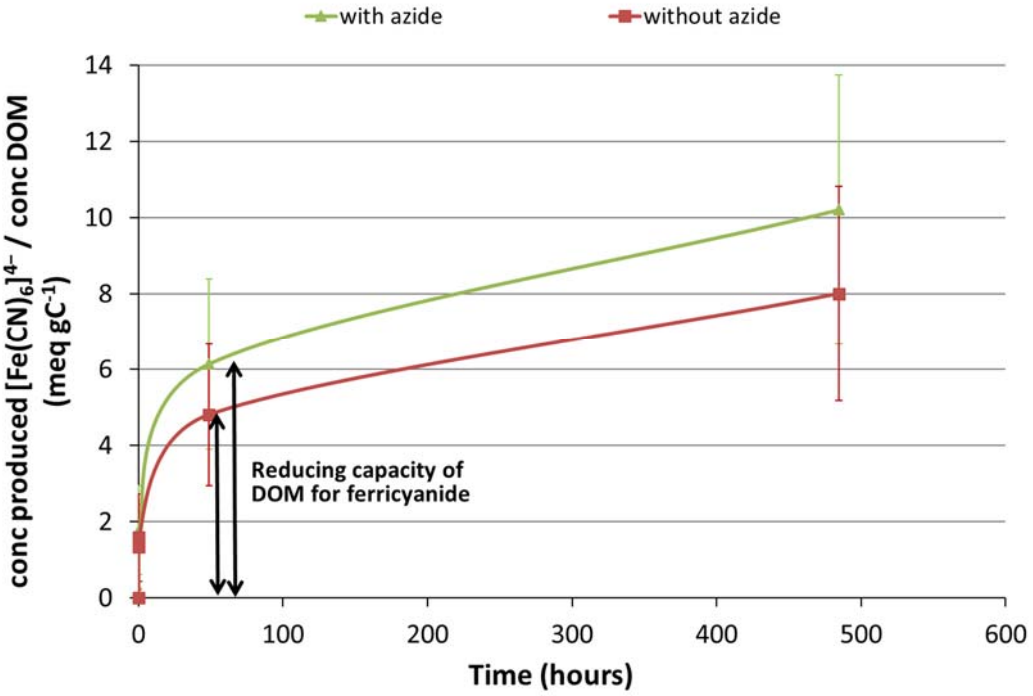

Figure 28: Results of the determination of the reducing capacity of DOM (in RBCW, after ~2 years of contact with 0.2 M nitrate) for $[Fe(CN)_6]^{3-}$, to study the effect of addition of NaN_3 (1 wt%) on the value of the reducing capacity. To this end, the reduction of ferricyanide by DOM was followed up in a 50 vol% RBCW solution (prepared from RBCW incubated for ~2 years with 0.2 M $NaNO_3$) with 0.8 mM $K_3Fe(CN)_6$ and 0 or 1 wt% NaN_3 (as indicated in the legend). The reducing capacity of DOM in these solutions is determined after ~50 hours of reaction between ferricyanide and DOM (indicated by the arrow). The uncertainty bars take into account the uncertainty on the decrease in ferricyanide and on the TOC concentration.

(iii) **A difference in functional groups oxidised by ferricyanide and nitrate**?
Considering the higher redox potential of the redox couple $[Fe(CN)_6]^{3-}/[Fe(CN)_6]^{4-}$ at pH 9 ($E^{0'}$ = 0.430 V) compared to the redox couple NO_3^-/NO_2^- ($E^{0'}$ at pH 9 = 0.3 V), it can be expected that significantly more functional groups will be oxidised by ferricyanide compared to nitrate. This hypothesis is in agreement with the results of the preliminary batch test in which RBCW was oxidised by air [26]. In this test, a decrease in the value of the reducing capacity of DOM was detected after oxidation for several weeks by air. This is explained by the standard redox potential of O_2/OH^- ($E^{0'}$ at pH 9 = 0.7 V), which is higher to the one of the $[Fe(CN)_6]^{3-}/[Fe(CN)_6]^{4-}$ redox couple, demonstrating that all (and more) oxidisable functional groups of DOM that can be oxidised by ferricyanide will also be oxidised by oxygen.

Due to the effect of azide, the oxidation potential of ferricyanide, the high uncertainty (35%) on the reducing capacity value and because the reducing capacity is determined after 50h (before complete oxidation of DOM by ferricyanide), the expected decrease in reducing capacity of DOM in RBCW solutions in which microbial nitrate reduction took place, could have been too small to detect.

6.4.2.2 Second series of batch tests with RBCW and nitrate

In the second series of batch tests with Boom Clay water, the same set-up as for the first experiment has been applied, but lower concentrations of $NaNO_3$ and NaN_3 (for abiotic test conditions) were added to the RBCW solutions (Table 14). Any reaction between nitrate and the dissolved organic matter in RBCW was followed up by analysing each solution in duplicate after different reaction periods. The complete set of results of the chemical analyses and pH measurements is given in Annex 6. Figure 29 shows the evolution of the concentration of nitrate and nitrite in the RBCW solutions with 0.1 M $NaNO_3$ without microbial inhibitor (NaN_3).

Firstly, the results of the chemical analyses were similar to the ones obtained with the first series of batch tests with RBCW and nitrate (Section 6.4.2.1), *i.e.* no significant variations in time of the Na^+ concentration, and of the TOC and TIC values, a small increase in the Ca^{2+} concentration and very limited fluctuations in time of the pH. Secondly, nitrite was again only produced in the RBCW solutions with 0.1 M $NaNO_3$ to which no microbial inhibitor was added (Figure 29 and Annex 6): after about 18 months of incubation, ~0.1 mM nitrite was formed. Furthermore, no significant production of N_2O could be detected in the RBCW solutions with 0.1 M $NaNO_3$ and with nor without NaN_3.

Based on these results, only 0.1 mol% (or ~0.1 mM) of the initial nitrate content has been reduced to nitrite in the biotic RBCW solution with 0.1 M $NaNO_3$ after ~18 months of reaction, which is too low to be detected due to the high uncertainties on the high nitrate concentration (*i.e.* 5.5%). These results are completely in agreement with the results that were obtained in the first series of batch tests, in which a reduction of ~0.1 mol% of the initial nitrate content (0.2 M) (Section 6.4.2.1, Figure 25) was observed in the solutions with 0.2 M $NaNO_3$ (no inhibitor) after about 1.5 years of incubation (calculation based on interpolation of results). Hence, these tests confirm that an abiotic nitrate reduction by DOM in RBCW is not possible or is characterised by extremely slow kinetics, as was observed in the first series

of batch tests with RBCW and $NaNO_3$ (see Section 6.4.2.1) and in the supporting test with hydroquinone and $NaNO_3$ (see Section 6.1.2.4).

Note that the amount of N_2 that might have been produced in these solutions as well could not be detected due to the initial N_2 atmosphere in the septum bottles[43]. However, as the gas pressure in the bottles of RBCW with 0.1 M $NaNO_3$ and with/without NaN_3 did not change over time, as well as the nitrate concentration, the formation of N_2 is not expected to be considerable.

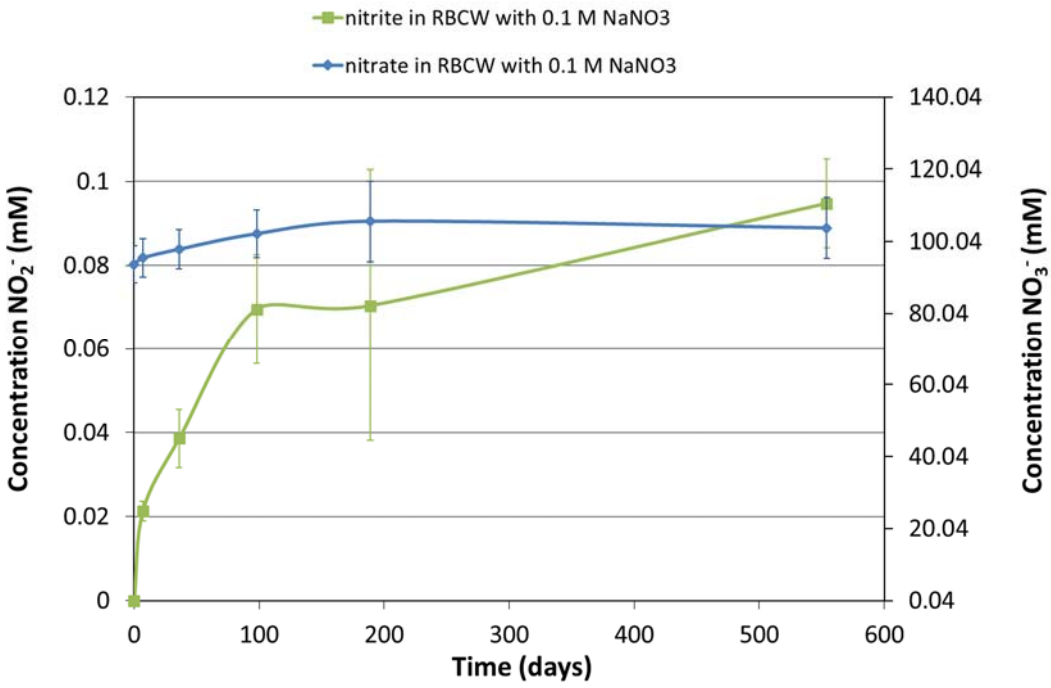

Figure 29: Evolution of the mean nitrate and nitrite concentrations in duplicate series of the Boom Clay water solutions with 0.1 M $NaNO_3$, to which no microbial inhibitor (NaN_3) was added. The indicated uncertainty bars represent the combined uncertainty, taking into account the standard deviation of the mean and the uncertainty of the individual values (5-6%).

Figure 30 shows the time evolution of the concentration of viable NRP cells in the five different clay water solutions (one of the two replicates per type of solution). In all solutions without NaN_3 high concentrations of viable NRP (~10^4 to 10^5 cells mL^{-1} clay water) were present. Hence, the nitrite production in the solutions with 0.1 M $NaNO_3$ and without NaN_3, as measured by chemical analysis, is due to microbial nitrate reduction to nitrite. In contrast to the previous batch test with RBCW and nitrate, the (possible) disturbance of the NRP growth after the start of the test in the solutions without inhibitor (and with nitrate) (see Section 6.4.2.1), did not occur in this batch test (high concentrations of viable NRP after 7 and 36 days).

The RBCW solutions containing 0.2 wt% NaN_3 showed very low to undetectable (< 3 cells mL^{-1}) NRP concentrations (Figure 30). Furthermore, microbial growth and activity

[43] As the measurement of the reducing capacity required an anaerobic atmosphere and the UV-VIS did not function under an Ar atmosphere, the atmosphere inside the glove box was N_2.

was only possibly in the MPN growth medium when the RBCW solutions (and thus the azide concentration) were diluted at least 1/1000, which confirms the efficiency of NaN_3 as a microbial inhibitor, even in lower concentrations (0.2 wt%; see also Section 6.3.1.).

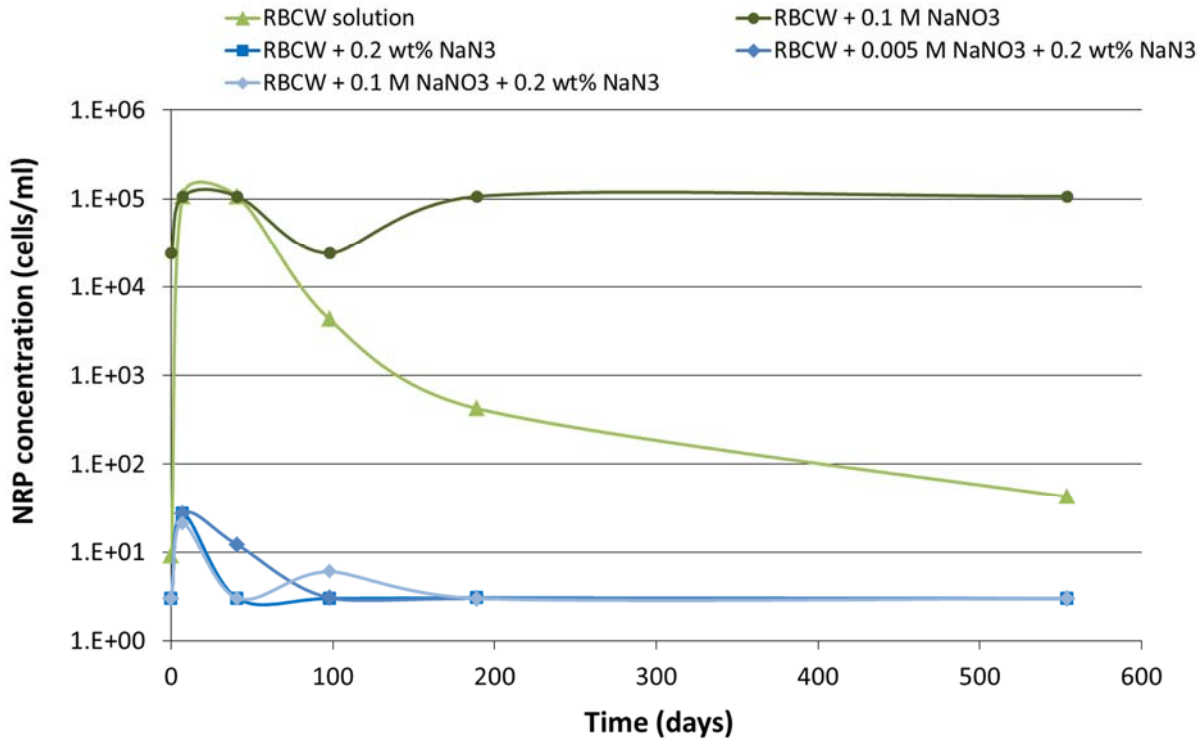

Figure 30: Time evolution of the concentration of viable cells in the five different clay water solutions, as measured with MPN analyses of one series of samples per type of solution (similar results obtained with duplicate solution). The lower and upper detection limits are equal to respectively 3 and 1.1×10^5 cells mL^{-1}.

For all subsamples, the reducing capacity of DOM in RBCW was measured using ferricyanide according to the optimised procedure (see Section 5.1.3.2 and Table 15). Figure 31 shows an overview of the measured reducing capacity for all solutions ('a' series) in function of time. As the reduction of ferricyanide by DOM could not be determined after 50 hours for the samples taken one and three months after the start of the batch tests, these values are not included here. However, an estimation of the reducing capacity values for these samples, based on the ferricyanide concentration after 30 and 120 hours, suggests that these values are similar to the initial values for the RBCW solutions.

After ~1.5 years of incubation, no significant differences were observed between the values of the reducing capacity of DOM in all RBCW solutions. Furthermore, the reducing capacity of DOM in the RBCW solutions with 0.1 M $NaNO_3$ after 18 months (in which ~0.1 M nitrite was formed; Figure 29) was not significantly lower than the reducing capacity that was measured at the start of the experiment. The microbial oxidation of the DOM by nitrate could thus not be demonstrated by a significant decrease in reducing capacity of the DOM in the RBCW solutions with 0.1 M $NaNO_3$ (without NaN_3), using ferricyanide as oxidant (Figure 31). Nevertheless, as ~0.1 mM nitrite was produced in these solutions after ~18 months, the total

reducing capacity of DOM for ferricyanide in these RBCW solutions should have decreased with ~1.7 meq gC^{-1}, assuming that all functional groups that can be oxidised by nitrate can also be oxidised by ferricyanide (Section 6.4.2.1). However, as already suggested in Section 6.4.2.1, it is likely that considerably more functional groups of DOM can be oxidised by ferricyanide than by nitrate, based on their redox potential. Furthermore, the addition of azide during the reducing capacity measurements has likely influenced the results as well (Section 6.4.2.1; [26]). It therefore seems that the procedure II to determine the reducing capacity of DOM using ferricyanide as oxidant does not allow the detection of a small degree in oxidation of DOM by nitrate.

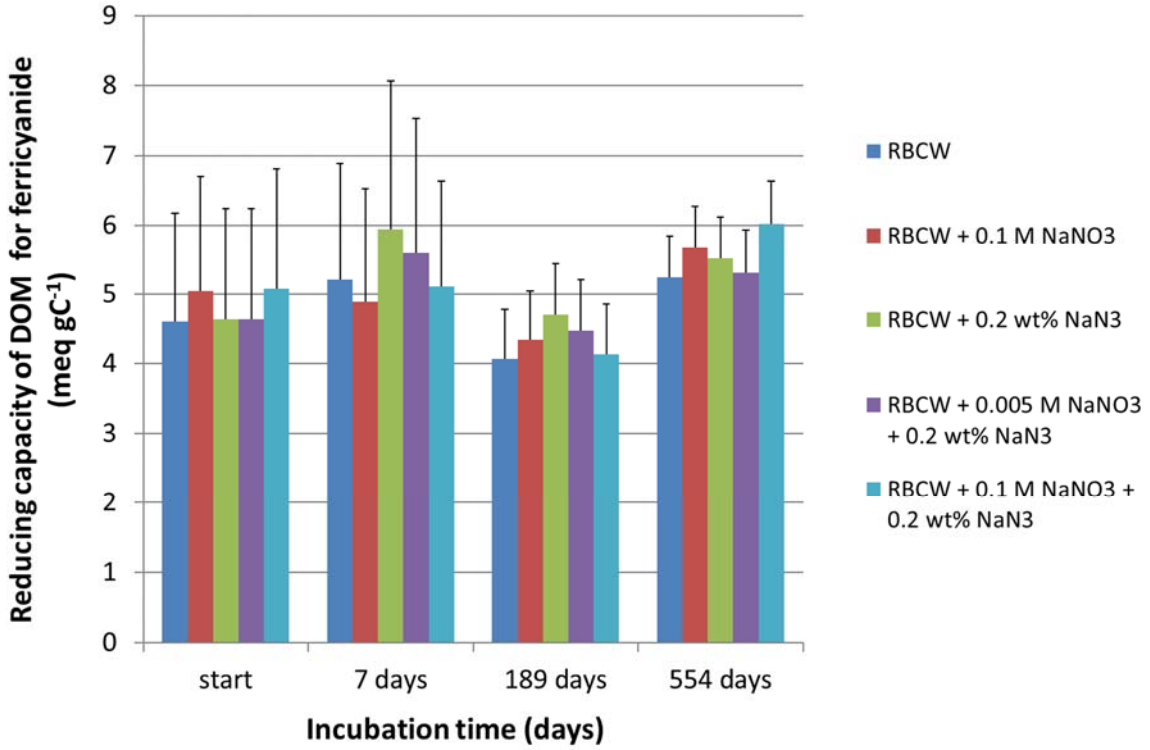

Figure 31: Overview of the reducing capacity values of DOM (in one of the duplicate solutions of the second series of batch tests with RBCW and nitrate), measured with ferricyanide, in function of the incubation time. The indicated uncertainties take into account the uncertainty on the TOC values and on the decrease of the ferricyanide concentration. The optimised procedure II as described in Section 5.1.3.3 was applied, except for the adjustment of the ionic strength of the solutions for solutions analysed after 189 days.

To be able to detect the expected decrease in reducing capacity of DOM due to microbial nitrate reduction, another oxidant was used to determine the reducing capacity, *i.e.* ferric citrate (Section 6.3.2.2). Due to interference of NaN_3 on the measurements with ferric citrate (Section 6.3.2.2), this method was performed only on the biotic solutions of the batch tests (sampled after 1.5 years). Figure 32 clearly shows that the reducing capacity value of the RBCW solution incubated with nitrate decreases when nitrite is produced: the reducing capacity was 1.7 ± 0.2 meq gC^{-1} at the beginning and decreased to 0.53 ± 0.1 meq gC^{-1} after 1.5 years (mean concentrations for both duplicates). This decrease in reducing capacity (1.1 ± 0.2 meq gC^{-1}) is similar to, yet somewhat lower than the expected decrease due to the

formation of nitrite (~1.7 meq gC^{-1}). This suggests that there are also some differences in organic functional groups that can be oxidised by Fe(III) citrate, on the one hand, and nitrate, on the other hand, which is in line with the differences in redox potential of the redox couples NO_3^-/NO_2^- ($E^{0'}$ at pH 9 = 0.3 V) and ferric citrate/ferrous citrate (~0.1 to -0.2 V for solutions with pH ≥ 4.5 [103]). In any case, these results indicate that ferric citrate can be used as oxidant to detect a decrease in reducing capacity of DOM in RBCW induced by microbial DOM oxidation, although the effect can possibly not be determined quantitatively.

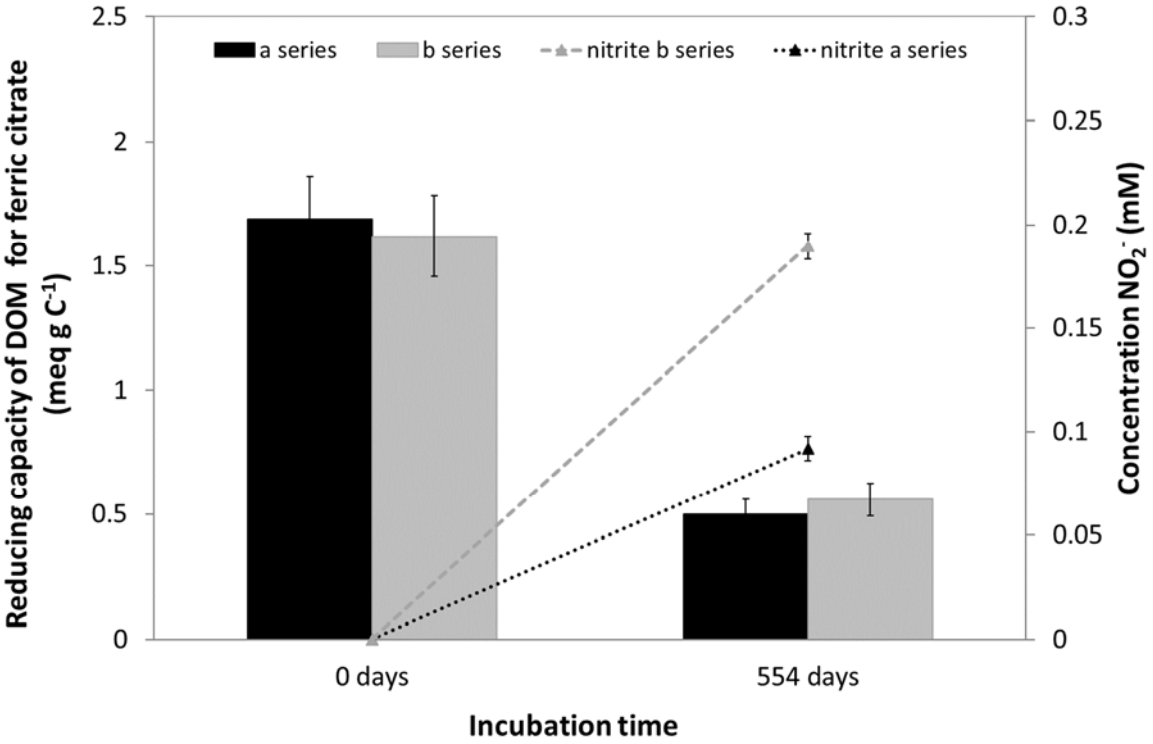

Figure 32: Evolution of the reducing capacity of DOM determined using ferric citrate as oxidant and the production of nitrite in RBCW with $NaNO_3$ (in the solutions of the second series of batch tests with RBCW and nitrate), as a function of the incubation time. Black and grey represent the two duplicates. The indicated uncertainties on the reducing capacity take into account the uncertainty on the TOC values and on the increase in ferrous iron. The uncertainty on the nitrite concentration is ~6%.

6.4.2.3 First series of batch tests with RBCW and nitrite (started in March 2010)

In the first series of batch tests with RBCW and nitrite, the same set-up as for the previous batch tests was followed (see Section 5.4.3.3; Table 16). Any reaction between nitrite and the dissolved organic matter in RBCW was followed up in time, by analysing each solution in duplicate after different reaction periods. The complete set of results of the chemical analyses and pH measurements is given in Annex 6. No considerable changes in the cation composition nor in pH were observed in the RBCW solutions after ~18 months, similar to the previously described batch tests with RBCW and nitrate (Sections 6.4.2.1 and 6.4.2.2).

Figure 33 shows the time evolution of the concentration of viable NRP or NiRP in the five different clay water solutions, as measured with MPN analyses in NRP (first three months) and NiRP medium (remainder of the samplings) for one series of samples per type of

solution[44]. High concentrations of viable NRP and NiRP (~10^4 cells mL^{-1} clay water) were present in RBCW containing nitrite and without NaN_3, except in the samples that were analysed after two and seven days of incubation (~100 to 300 cells mL^{-1} clay water). The results of the MPN analyses of these solutions after two and seven days of incubation resemble the results from the first series of batch tests with nitrate. As mentioned in Section 6.4.2.1, this disturbance of the microbial growth could have occurred during the preparations of the RBCW solutions, leading to partial death of the population. These results also suggest that the NiRP concentration (detected as from three months after the start) in the RBCW solution with 0.05 M $NaNO_2$ was similar to the NRP concentration (detected during the first months of the test).

Furthermore, in the solutions with 0.2 wt% NaN_3, NRP and NiRP growth could only be observed when the sample was diluted at least 100-fold, demonstrating the inhibitory effect of NaN_3 on the NiRP population.

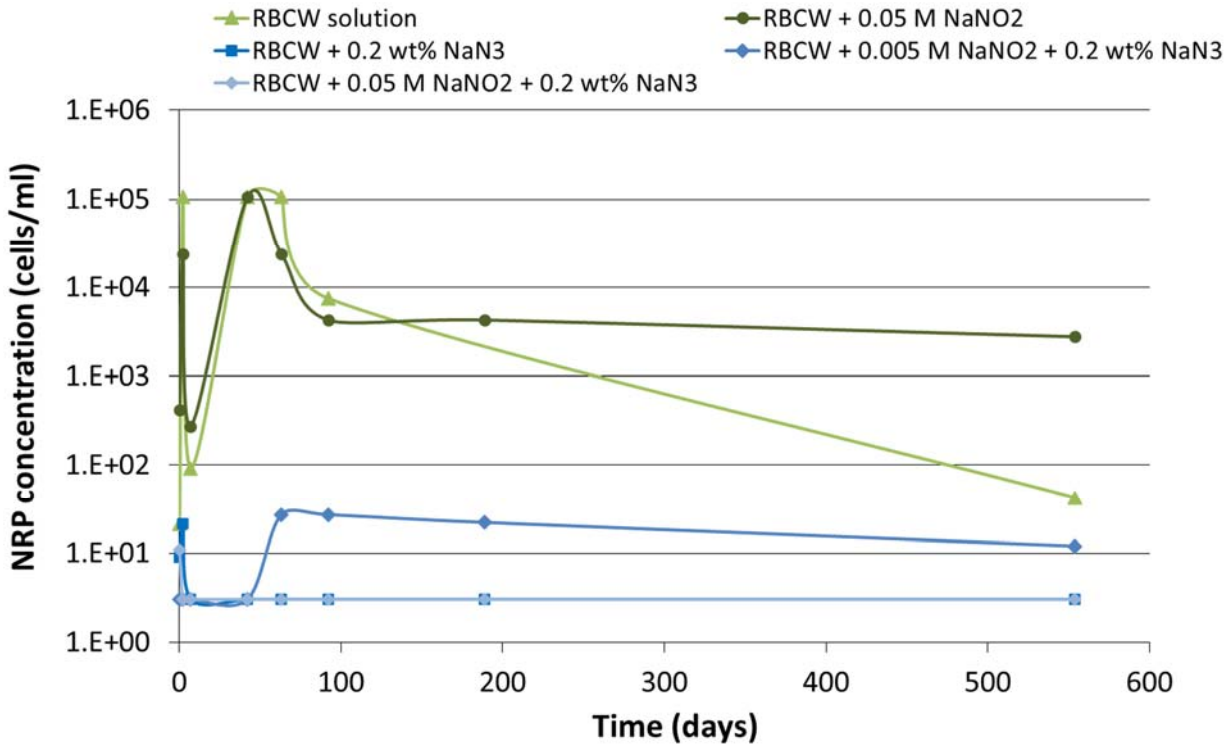

Figure 33: Time evolution of the concentration of viable NRP (first 3 months) and NiRP (final samplings) in the five different clay water solutions, as measured with MPN analyses (in NRP medium) of one series of samples per type of solution (similar results in duplicate solution). The lower and upper detection limits are equal to respectively 3 and 1.1×10^5 cells mL^{-1}.

[44] Initially, the NRP medium was used for detection of denitrifyers (both reduction of nitrate and nitrite) in the RBCW solutions. However, after optimisation of the MPN test with NiRP medium, this growth medium was used for the remainder of samples taken from the batch tests with RBCW and nitrite, to be able to specifically detect NiRP in the solutions.

Figure 34 shows the evolution of the nitrite concentration in the RBCW solutions with 0.005 and 0.05 M $NaNO_2$, and with or without microbial inhibitor (0.2 wt% NaN_3). No significant decrease in the nitrite concentration in the solutions with $NaNO_2$ can be observed (Figure 34), although any decrease smaller than the uncertainty on the measurements (~6%) could still have occurred. Furthermore, no significant increase in ammonium concentration could be detected (Annex 6), indicating that no significant reduction of nitrite to ammonium (abiotically or microbially) had taken place.

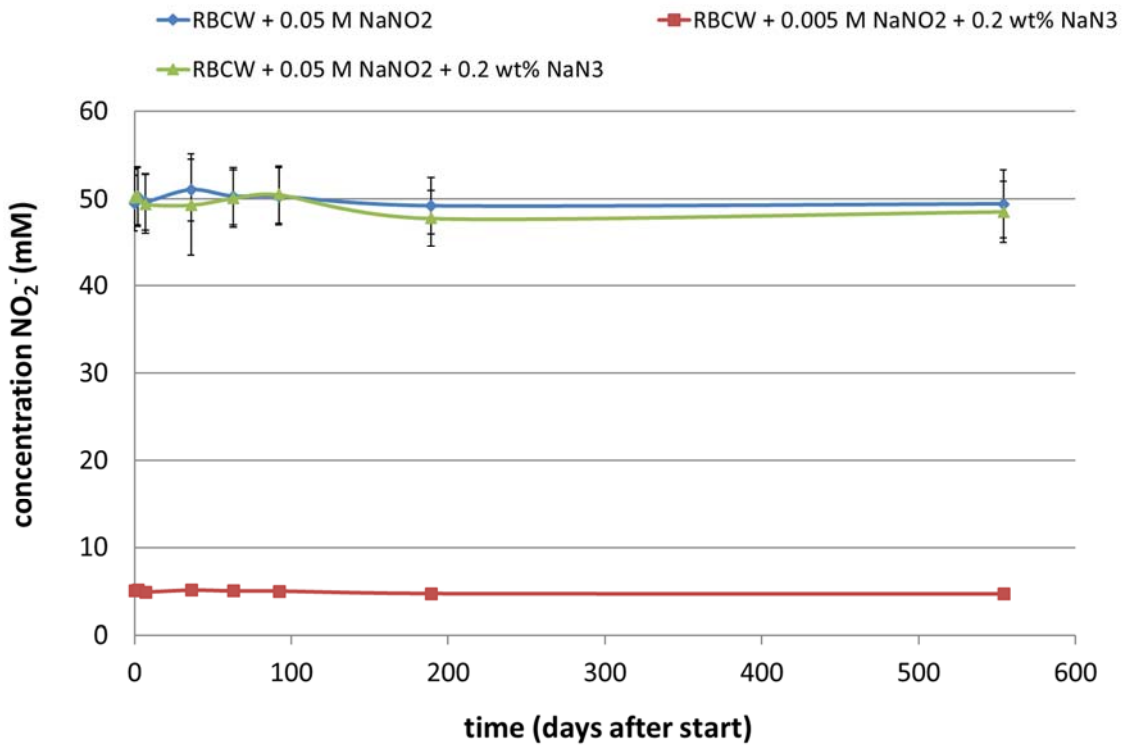

Figure 34: Evolution of the mean nitrite concentrations in the Boom Clay water solutions with $NaNO_2$ (see concentrations in the legend), and with/without NaN_3. Similar results were observed in the duplicate solutions. The indicated uncertainty takes into account the uncertainty on the individual NO_2^- concentrations (~6%) and the standard deviation of the mean.

After 189 and 554 days of incubation, a gas analysis was performed on the head space of the RBCW solutions with the highest nitrite concentration ('0.05 M $NaNO_2$_0% bact' and '0.05 M $NaNO_2$_0.2% bact'; see Table 16), to detect any formation of N_2O in these solutions. The results of these analyses indicate that N_2O was formed in both the biotic and the abiotic RBCW solution with nitrite (Figure 35), suggesting that in these solutions nitrite is reduced – albeit slowly – either microbially (biotically) or chemically (abiotically).

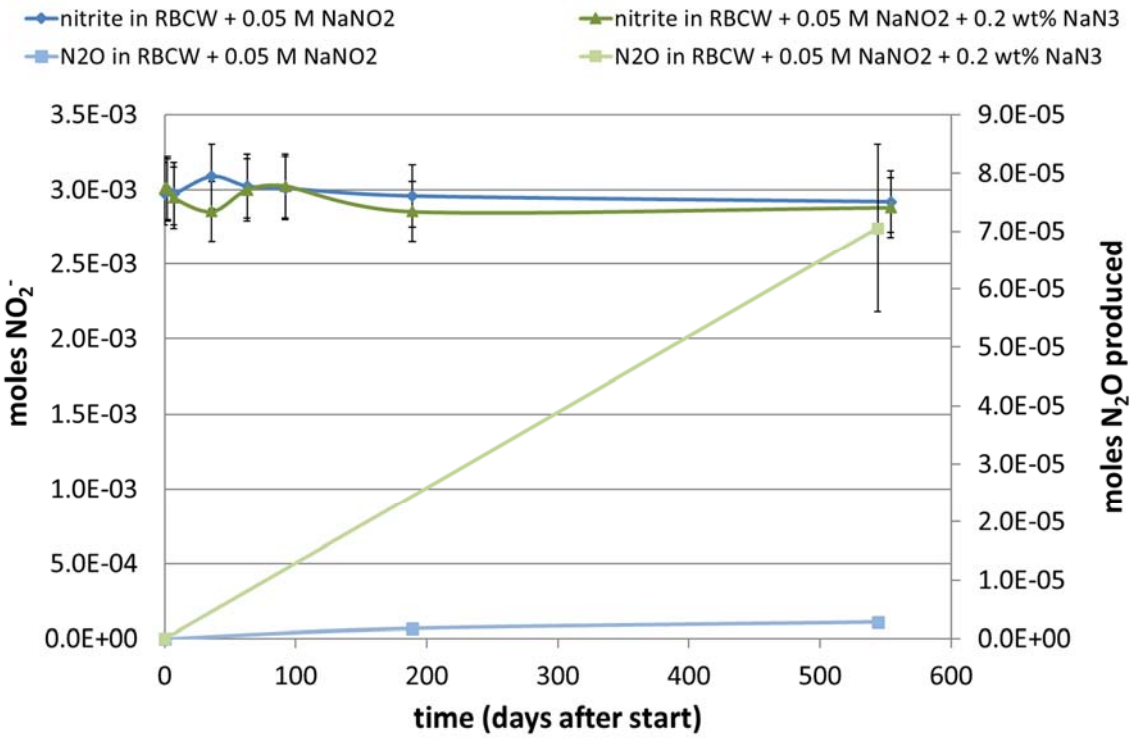

Figure 35: Evolution of the amount of nitrite and N_2O produced in one series of the Boom Clay water solutions with $NaNO_2$ and with/without azide (indicated in the legend). The indicated uncertainty for the amount of N_2O takes into account the uncertainty on the measurement (including uncertainty on dilution factor), on the pressure in the headspace and on the liquid volume. The amount of N_2O in the headspace of the RBCW bottles at the start of the test is based on the theoretical amount present in the N_2 atmosphere of the glove box.

Based on the partial gas pressure of N_2O in the headspaces of the RBCW solutions (*i.e.* 1 mbar in the RBCW solution with 0.05 M $NaNO_2$ and 25 mbar in the solution with 0.05 M $NaNO_2$ and 0.2 wt% NaN_3), it seems that the nitrite reduction in the abiotic test solution is kinetically faster than in the biotic test solution. As both abiotic and microbially mediated reaction can take place in the latter solution, the higher N_2O concentration in the abiotic test solution suggests that nitrite has reacted with azide rather than with DOM.

As described in Section 6.3.2.2, azide is known to decompose with nitrite under acidic conditions, resulting in the generation of N_2 and N_2O (equation 16). Although several authors presume that this reaction does not occur at neutral pH or higher [154, 155], this has not been investigated yet in a long-term experiment (order of magnitude of our batch tests). A slow azide decomposition could therefore indeed have occurred in the RBCW solutions with nitrite and azide. Based on the N_2O produced in the system with the highest nitrite concentration and azide ('0.05 M NaNO2_0.2% bact'), about 1.1 mM azide and nitrite would have been used to generate the amount of N_2O observed. This decrease in both azide or nitrite concentration would not have been visible, due to their high initial concentration (~32 ± 3 mM N_3^- and ~50 ± 3 mM NO_2^-).

Yet, a slow oxidation of hydroquinone by nitrite was observed in the respective supporting tests [26]. Hence, some of the production of N_2O might also have resulted from chemodenitrification, in which DOM was oxidised by nitrite [64]. However, based on the

significantly higher amount of N_2O formed under abiotic (with azide) compared to biotic (without azide) conditions, decomposition of azide by nitrite can be assumed to be dominating the system.

In the test solutions containing RBCW and nitrite without azide, ~0.1 mM nitrite has been reduced to N_2O after 1.5 years, based on the N_2O content in the headspace of these solutions. This means that only 0.2 mol% of the initial nitrite content (0.05 M) was reduced to N_2O by microbes after about 1.5 years of reaction. However, nitrite may also have been reduced to N_2 though this could not be verified due to the initial N_2 atmosphere present in the gas phase of the septum bottles. Yet, as no significant increase in total gas pressure could be observed after 18 months for the test solutions containing RBCW and nitrite without azide, we can assume that no considerable amount of NO_2^- had been reduced to N_2 (*i.e.* less than 0.7 mM NO_2^- assuming that the produced N_2 concentration was lower than 1 vol%). These results indicate that microbial nitrite reduction with DOM as electron donor is characterised by slow kinetics, which suggests again that DOM from Boom Clay water is a poor electron donor for microbial activity.

For all subsamples, the reducing capacity of DOM in RBCW was measured using ferricyanide according to the optimised procedure II (see Section 5.1.3.2) and Table 19 (Section 5.4.3.3). Figure 36 shows an overview of the reducing capacity values of all solutions in function of time. As the reduction of ferricyanide by DOM was not determined after 50 hours for samples taken two days and three months after the start of the batch tests, these values are not included here. However, an estimation of these values, based on the ferricyanide concentration after 30 and 120 hours, suggests that these values are in agreement with the results shown in Figure 36.

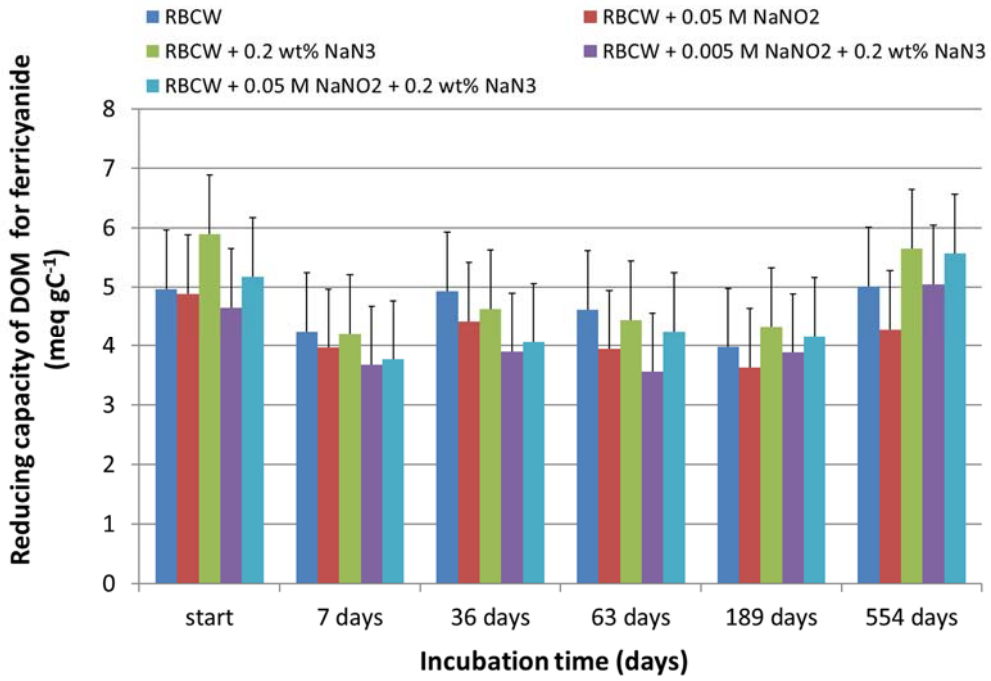

Figure 36: Overview of the reducing capacity values of DOM (in the solutions of the first series of batch tests with RBCW and nitrite), measured with ferricyanide, in function of the incubation time. The indicated uncertainties take into account the uncertainty on the TOC values and on the decrease of the ferricyanide concentration. The optimised procedure II as described in Section 5.1.3.3 was applied, except for the adjustment of the ionic strength of the solutions for solutions analysed after 189 days.

After 1.5 years of incubation (*i.e.* ~18 months of storage in an anaerobic glove box), no significant differences were observed in the reducing capacities of DOM in the RBCW solutions with or without $NaNO_2$ (Figure 36). Furthermore, no significant differences in reducing capacity of DOM in the RBCW solutions with nitrite could be detected over time. However, based on the amount of N_2O measured in the head space of the biotic RBCW solution containing nitrite, a decrease in reducing capacity of DOM (using ferricyanide) of ~1.6 meq gC^{-1} was expected, assuming that all functional groups that can be oxidised by nitrite can also be oxidised by ferricyanide. However, based on the redox potential of the redox couple $Fe(CN)_6]^{3-}/[Fe(CN)_6]^{4-}$ at pH 9 ($E^{0'}$ = 0.43 V) compared to the redox couple NO_2^- /NO ($E^{0'}$ at pH 9 = 0.11 V), it can be expected that significantly more functional groups will be oxidised by ferricyanide compared to nitrite. Furthermore, addition of azide during the measurements might have influecned the results as well (see Section 6.4.2.1). As was seen in the batch tests with RBCW and nitrate (Sections 6.4.2.1 and 6.4.2.2), this probably explains why the use of ferricyanide as oxidant for the determination of the reducing capacity of DOM (with procedure II in Table 8) does not allow the detection of the (small) oxidation of DOM by nitrite.

In addition, as nitrite interferes with the reducing capacity measurements using ferric citrate, this oxidant cannot be used either for these batch tests. The expected decrease in reducing capacity of DOM due to microbial nitrite reduction in the RBCW solutions incubated for 1.5 years with nitrite can therefore not be confirmed.

To be able to study abiotic nitrite reduction with DOM without the effect of azide on the results, new batch tests with RBCW and nitrite should be performed, in which abiotic conditions should be created by filter sterilisation.

6.4.3 Batch tests with pyrite

6.4.3.1 Batch tests with pyrite and nitrate

6.4.3.1.1 Abiotic batch tests with pyrite and nitrate

Abiotic pyrite oxidation by nitrate is investigated under anaerobic conditions in two different background solutions with/without $NaNO_3$ (0.005 M and 0.1 M): (1) a bicarbonate solution with a similar pCO_2 as RBCW; (2) demineralised water. Abiotic conditions were created by adding 0.1 wt% NaN_3 to the solutions (Table 18). Control tests to study possible effects of azide were performed with pyrite and $NaNO_3$ (0 M, 0.005 M, and 0.1 M) in 15 mM $NaHCO_3$ without addition of NaN_3. Pyrite oxidation by nitrate was monitored by analysing the chemical and microbial composition of the solutions after different reaction periods. The complete set of results from the chemical analyses and pH measurements is given in Annex 7. Figures 37 and 38 show the evolution of the sulphate and thiosulphate concentrations in the pyrite suspensions with/without nitrate and with/without azide.

The MPN analyses performed on one of the duplicate samples (a series) per type of solution at each sampling period showed that no nitrate reducing pyrite oxidising bacteria were present in the abiotic and control batch tests solutions with pyrite (*i.e.*, below detection limit of 3 cells mL^{-1}), even in the absence of NaN_3. Hence, this demonstrates that all tests without additional bacteria, both with and without NaN_3, can be considered as abiotic.

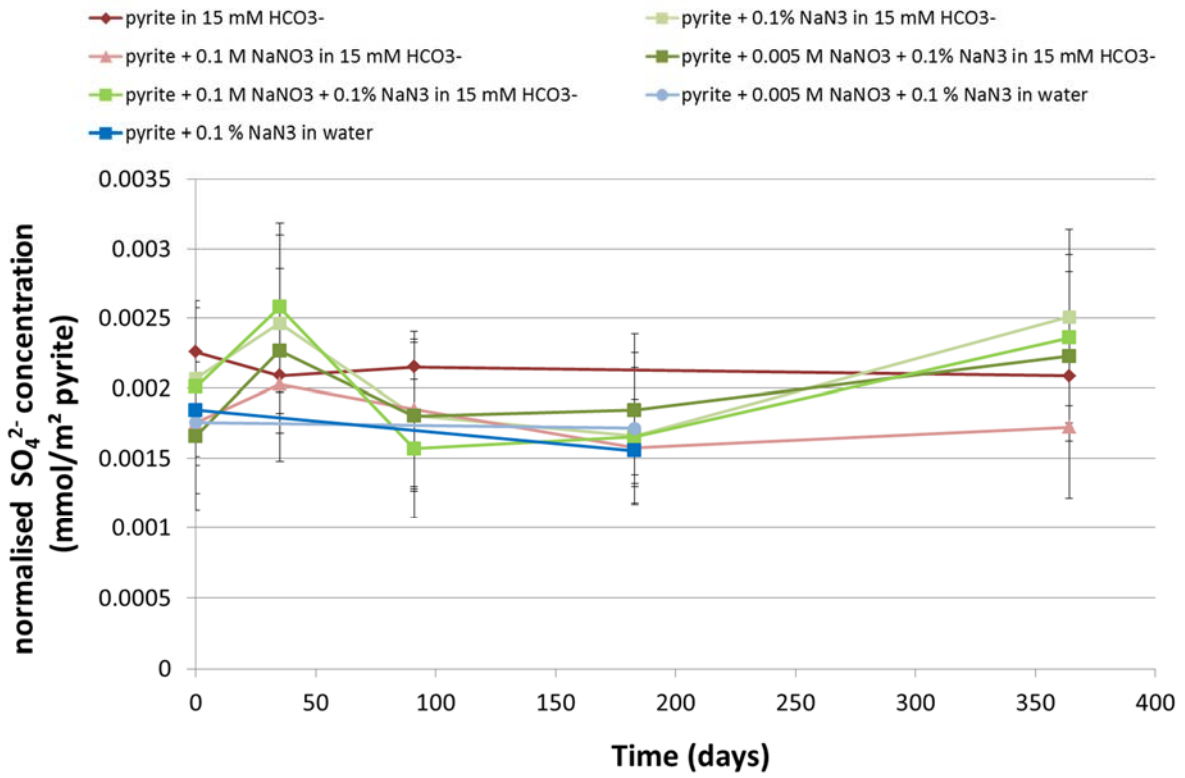

Figure 37: Evolution in time of the sulphate concentrations, normalised to the total specific surface area of the added pyrite, in one series of the pyrite suspensions with or without $NaNO_3$ and with or without microbial inhibitor (NaN_3). Similar results were observed in the duplicate solution. Green: bicarbonate solutions with NaN_3; Red: bicarbonate solutions without NaN_3; Blue: aqueous solutions with NaN_3. The indicated uncertainty takes into account the uncertainty on the individual sulphate concentration (10%) and on the surface area to volume ratio (~8%).

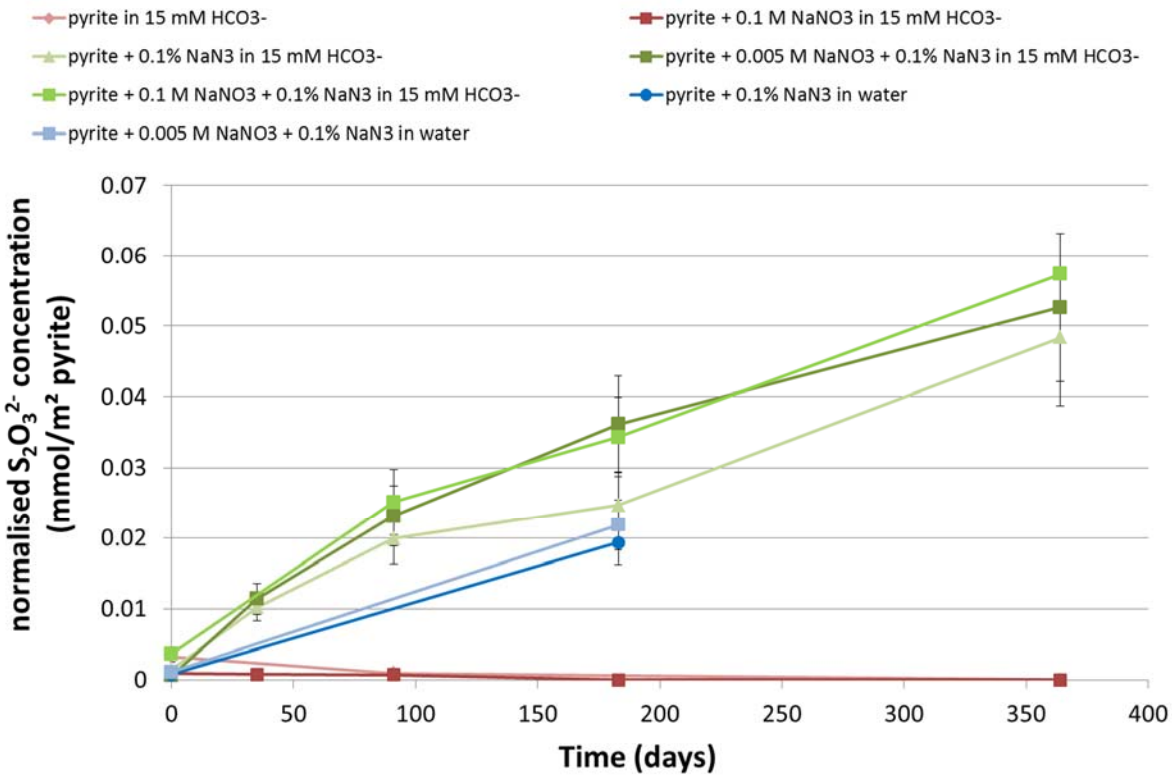

Figure 38: Evolution in time of the thiosulphate concentrations, normalised for the total specific surface area of the added pyrite, in one series of the pyrite suspensions with/without $NaNO_3$ and with/without microbial inhibitor (NaN_3), as shown in the legend. Green: bicarbonate solutions with NaN_3; Red: bicarbonate solutions without NaN_3; Blue: aqueous solutions with NaN_3. Similar results were observed in the duplicate solution. The indicated uncertainty takes into account the uncertainty on the individual thiosulphate concentration (~4-5%) and on the surface area to volume ratio (~8%).

In none of the solutions, a significant decrease in nitrate concentration nor an increase in nitrite concentration can be detected (Annex 7). These results suggest that no significant abiotic nitrate reduction by pyrite (at pH 7-8) has occurred during one year of incubation. This outcome is in agreement with previous studies [62, 63], which show that nitrate does not significantly oxidise pyrite within one month of incubation.

However, in the solutions containing azide, the thiosulphate concentration (Figure 38) and pH (Annex 7) increase over time, while this is not the case in the solutions without azide [below detection limit for thiosulphate (0.5 mg L^{-1}) and within the uncertainty range (± 0.1) for pH]. This increase is clearly not linked to the nitrate concentration, as the thiosulphate concentration also increases in the absence of nitrate (but in presence of azide). For the pyrite suspensions in water, a high pH increase (~3 pH units after six months) can be noticed, while for the bicarbonate solutions only a slight pH increase (~0.3 pH units after six months) can be observed, due to the presence of the bicarbonate buffer. These results suggest that pyrite oxidation by azide has occurred when azide is present. As both NH_4^+ and N_2 could be produced based on the redox half-reactions of azide [152, 156], this reaction will be investigated further in the future by analysis the ammonium and azide concentration and the gas pressure evolution in the septum bottles. Detection of N_2 production is however not possible, as N_2 is the background atmosphere in the glove box in which these batch tests are

being performed. As the sulphate concentration remains stable in all solutions with NaN_3, thiosulphate appears not to be oxidised further by N_3^-.

According to Moses and Herman [157], Fe^{2+} would be adsorbed onto the pyrite surface after oxidation of S^- (*i.e.* partial pyrite oxidation). When also Fe^{2+} from pyrite is oxidised to Fe^{3+} (*i.e.* complete pyrite oxidation), this is followed by precipitation of ferric hydroxide onto the surface, leading to the formation of a protective layer against further pyrite oxidation, thus slowing down this reaction. However, in the presence of bicarbonate (*i.e.*, ~15 mM HCO_3^- in the bicarbonate solution of the batch tests), ferrous carbonate 'complexes' like $FeCO_3$ will be produced after partial pyrite oxidation. These complexes will not be adsorbed onto the pyrite surface [113]. The presence of bicarbonate therefore prevents surface coating and thus passivation, leading to a faster pyrite oxidation rate. This would explain why pyrite oxidation by azide occurs at a higher rate in the bicarbonate solutions compared to in water (Figure 38).

6.4.3.1.2 Biotic batch tests with pyrite and nitrate, with addition of T. denitrificans

Biotic batch tests with pyrite and $NaNO_3$ (0 M and 0.005 M) were started in a bacterial nutrient solution (BNS) and spiked with *T. denitrificans*, which is known to perform nitrate-dependent pyrite oxidation [115]. Microbial pyrite oxidation coupled to nitrate reduction was monitored in time, by analysing subsamples taken after different reaction periods. The MPN analyses performed on the subsamples taken from each pyrite suspension at each sampling period show that high concentrations of *T. denitrificans* are present in these batch test solutions (10^4 – 10^5 cells mL^{-1}), both in the presence and the absence of $NaNO_3$ (Figure 39).

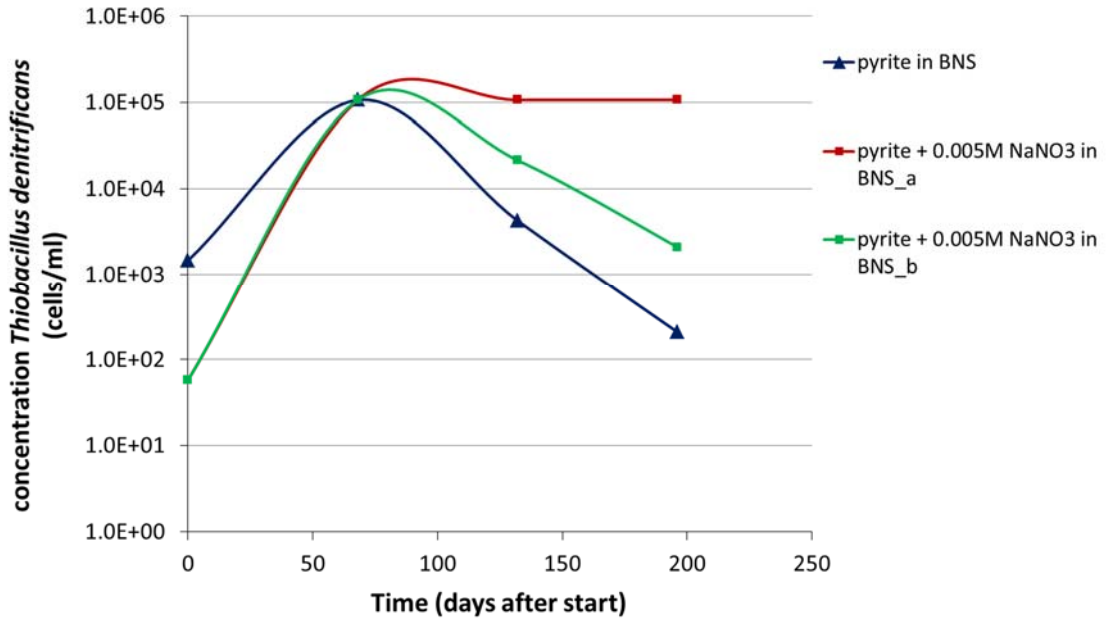

Figure 39: Time evolution of the concentration of viable *T. denitrificans* in the three bacterial nutrient solution (BNS) with pyrite and with/without nitrate, as measured with MPN analyses (using LZ_NO3 medium). The lower and upper detection limits are equal to respectively 3 and 1.1×10^5 cells mL^{-1}.

The complete set of results from the chemical analyses and pH measurements is given in Annex 7. Figures 39 and 40 show the evolution of the pH, nitrite, sulphate, and thiosulphate concentrations in the bacterial nutrient solution with pyrite and with/without nitrate.

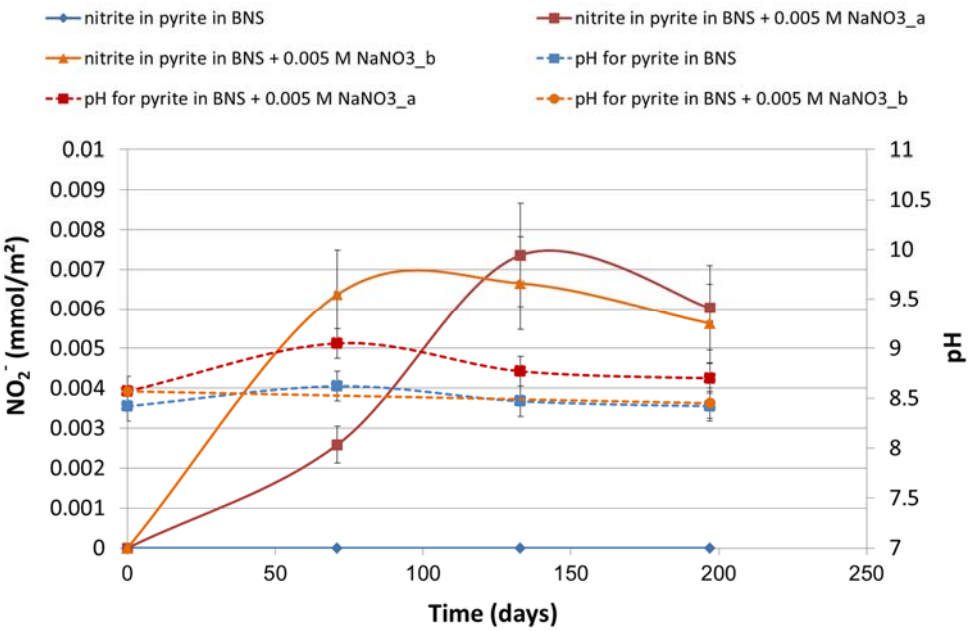

Figure 40: Time evolution of the normalised nitrite concentrations and pH in the bacterial nutrient solutions (BNS) with pyrite and with/without 0.005M $NaNO_3$. The indicated uncertainty takes into account the uncertainty on the individual concentrations (~6%) and on the surface area to volume ratio (~8%).

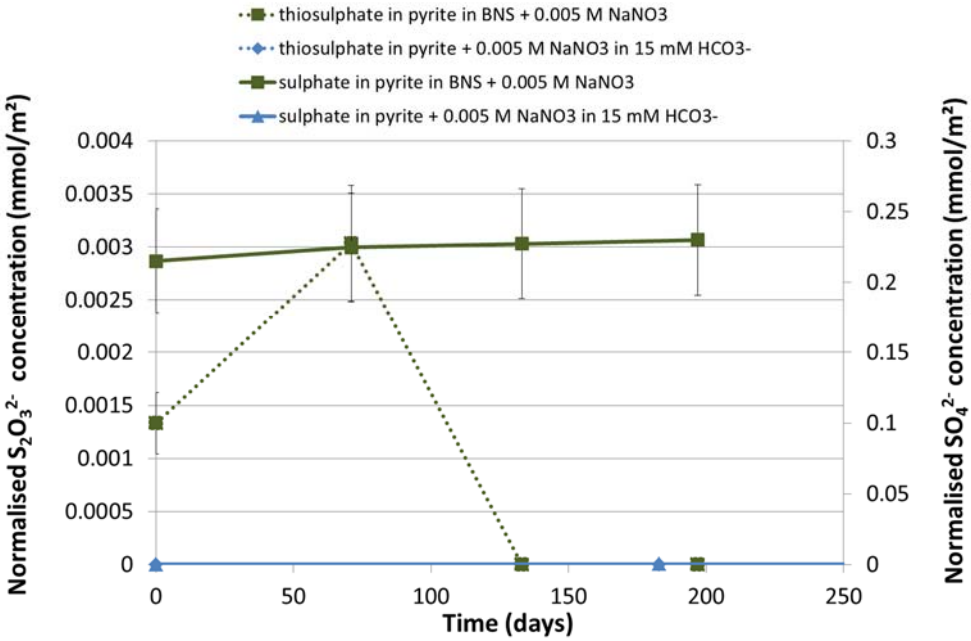

Figure 41: Time evolution of the normalised thiosulphate and sulphate concentrations in one of the bacterial nutrient (BNS) or bicarbonate (HCO3-) solutions with pyrite and with 0.005M $NaNO_3$ (as indicated in the legend). Similar results were observed in the duplicate solutions. The indicated uncertainty takes into account the uncertainty on the individual concentrations (5-10% for SO_4^{2-} and 4-5% for $S_2O_3^{2-}$) and the uncertainty on the surface area to volume ratio (~8%).

In none of the solutions with nitrate, a significant decrease in nitrate concentration can be observed, although a trend to decrease is visible (Annex 7). Also nitrite production (~0.006 mmol nitrite per m^2 pyrite surface) in the bacterial nutrient solutions with nitrate was noticed after ~2 months (Figure 40). The sulphate concentration increased in time although this increase is not statistically significant due to the high background sulphate concentration in the solution. Thiosulphate was produced initially, but decreased again after ~2 months Figure 41).

Based on the above mentioned results and given the fact that abiotic nitrate- and azide-free solutions did not show any pyrite oxidation, the observed reaction could only be attributed to microbial nitrate-dependent pyrite oxidation, though at a low rate. *T. denitrificans* is known to use both S^- and Fe^{2+} as electron donor (complete pyrite oxidation), which would result in the production of both sulphate and Fe^{3+} (equation 19; [115]). Thiosulphate is only formed as an intermediate S species during microbial pyrite oxidation, which is in agreement with our results.

$$2\ FeS_2 + 15\ NO_3^- + H_2O \rightarrow 15\ NO_2^- + 2\ Fe^{3+} + 4\ SO_4^{2-} + 2\ H^+ \quad (19)$$

After about two months of reaction, ~0.006 mmol nitrite per m^2 pyrite surface was formed in both solutions with nitrate, corresponding to a reduction of 0.9 mol% of the initial nitrate content and an increase of ~0.05 mol% of sulphate. Due to the uncertainties on the nitrate and sulphate concentrations, these changes could however not be detected. As no additional nitrite production was observed after the first 2 months, nitrite was probably converted further into gaseous N species (through denitrification). This would be in agreement with the main reaction performed by *T. denitrificans* (equation 20; [115, 158]):

$$2\ FeS_2 + 6\ NO_3^- + 4\ H^+ \rightarrow 3\ N_2 + 2\ Fe^{3+} + 4\ SO_4^{2-} + 2\ H_2O \quad (20)$$

Based on the stoichiometry of equation 21 and the nitrate, nitrite, and sulphate concentrations after six months of reaction, ~0.007 mmol/m^2 N_2 could have been produced, corresponding to a decrease in nitrate concentration of ~2.5 mol% NO_3^-. This decrease would still be masked by the uncertainty on the nitrate concentration.

SEM photographs, taken after four months of incubation, did not show the formation of visual corrosion pits on the surface of the pyrite that was in contact with nitrate (data not shown). There was no clear difference between the pyrite grains that were incubated in BNS with and without $NaNO_3$. Based on the amount of nitrate reduced, ~10% of the outer pyrite layer would be oxidised (assuming that only the outermost layer is reactive). As during microbial pyrite oxidation the smallest pyrite particles (0.1-1 µm) would be oxidised at a faster rate then larger pyrite grains [115], most of the oxidised layers are expected on the former particles. Due to the small size of the particles, the formation of the corrosion pits on the surface of these nanoparticles might not have been clearly visible by SEM.

6.4.3.2 Batch tests with pyrite and nitrite

6.4.3.2.1 Abiotic batch tests with pyrite and nitrite

Abiotic batch experiments were performed with pyrite and $NaNO_2$ (0 M, 0.005 M, and 0.05 M) in both bicarbonate solution (15 mM HCO_3^-) and water, all containing 0.1 wt% NaN_3. Control

tests to study any effect of azide were performed with pyrite and $NaNO_2$ (0 M and 0.005 M) in bicarbonate solution without addition of NaN_3. Any pyrite oxidation by nitrite was monitored in time, by analysing each solution after different reaction periods. The MPN analyses performed on one series of samples per type of solution at each sampling period confirmed the absence of nitrite reducers in all solutions (same results as for the batch tests with nitrate, see Section 6.4.3.1.1), demonstrating that in all the above mentioned test conditions, even in absence of azide, abiotic pyrite oxidation is studied.

The complete set of results from the chemical analyses and pH measurements is given in Annex 7. Figures 41 and 42 show the evolution of the sulphate and thiosulphate concentrations in the solutions with pyrite and with/without nitrite or azide. In all solutions a significant decrease or decreasing trend in nitrite concentration can be noticed (Annex 7), which is more clear in the bicarbonate solutions containing pyrite and 0.005M $NaNO_2$ (17 mol% and 12 mol% decrease in nitrite in the presence and the absence of azide, respectively) then in water with pyrite and 0.005 M $NaNO_2$ (~5 mol% decrease for solutions with azide) after about six months of incubation. Furthermore, both the sulphate and the thiosulphate concentrations increased significantly in all bicarbonate solutions containing nitrite. On the other hand, in the bicarbonate solution with pyrite and azide (without $NaNO_2$), but also in all suspensions of pyrite in water and NaN_3 (with and without $NaNO_2$), only an increase in thiosulphate can be noticed.

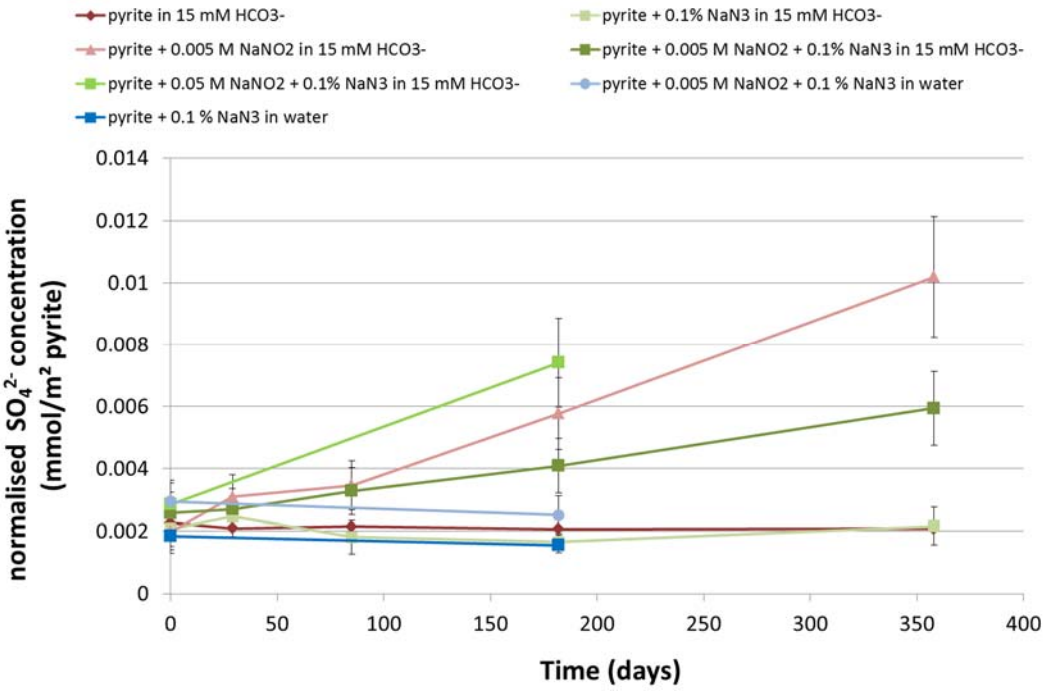

Figure 42: Evolution in time of the sulphate concentrations, normalised to the total specific surface area of the added pyrite, in one series of the pyrite suspensions with/without $NaNO_2$ and with/without microbial inhibitor (NaN_3), as shown in the legend. Similar results were obtained in the duplicate solution. Green: bicarbonate solutions with NaN_3; Red: bicarbonate solutions without NaN_3; Blue: aqueous solutions with NaN_3. The indicated uncertainty takes into account the uncertainty on the individual sulphate concentration (5-10%) and on the surface area to volume ratio (~8%).

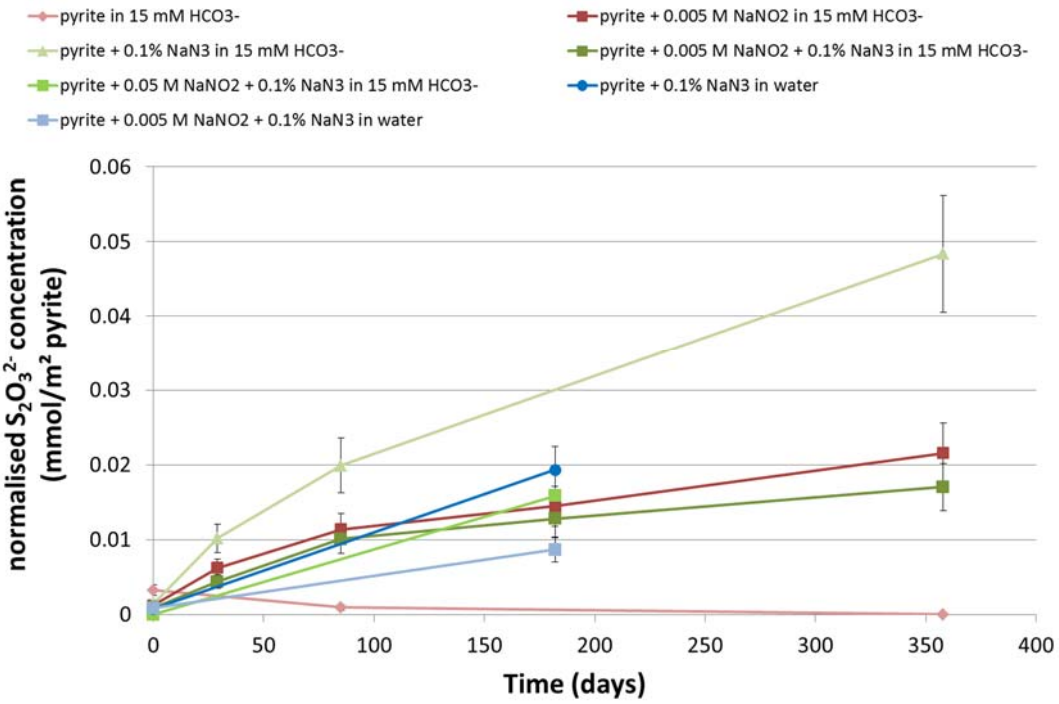

Figure 43: Evolution in time of the thiosulphate concentrations, normalised to the total specific surface area of the added pyrite, in one series of the pyrite suspensions with/without $NaNO_2$ and with/without microbial inhibitor (NaN_3), as shown in the legend. Similar results were observed in the duplicate solution. Green: bicarbonate solutions with NaN_3; Red: bicarbonate solutions without NaN_3; Blue: aqueous solutions with NaN_3. The indicated uncertainty takes into account the uncertainty on the individual thiosulphate concentration (4-5%) and on the surface area to volume ratio (~8%).

Based on the results of the bicarbonate solution with pyrite and nitrite (without azide), an abiotic pyrite oxidation by nitrite can occur, resulting in the production of both thiosulphate and sulphate. The produced thiosulphate is most likely an intermediate product in the oxidation of pyrite to sulphate (end product). This reaction will be investigated further in the future by analysing the gas composition (production of N_2O) and pressure.

In the pyrite suspensions with azide and without nitrite (both water and bicarbonate solution), the sulphate concentration remained constant, while pyrite was oxidised to thiosulphate, similar to what is observed in the abiotic batch tests with pyrite and $NaNO_3$ containing azide (Section 6.4.3.1.1). On the other hand, in the suspensions containing both azide and nitrite, the sulphate and thiosulphate concentrations increased slower than in pyrite suspensions with nitrite but without azide. Furthermore, the thiosulphate concentration in these suspensions (with azide and nitrite) increased more slowly than in the presence of only azide (Figures 41 and 42). This indicates that the addition of nitrite to the pyrite suspensions with azide results in a lower pyrite oxidation rate compared to the rate observed in pyrite suspensions with either nitrite or azide. This difference can be explained by azide decomposition by nitrite (equation 16), similar to what is observed in the abiotic batch tests with RBCW and nitrite (Section 6.4.2.3), resulting in a lower availability of both electron acceptors for pyrite oxidation. These hypotheses will be investigated further in the future, by analysing the ammonium and azide concentrations and the gas pressure evolution in the septum bottles of these batch tests.

Comparing the results of the pyrite suspensions with azide and 0.005 M $NaNO_2$ in both water and bicarbonate solutions, a higher nitrite reduction rate can be observed in the presence of bicarbonate, which is most likely due to the prevention of the formation of an Fe^{3+} surface coating of the pyrite grains (*i.e.* passivation layer), as explained previously (see Section 6.4.3.1.1).

To study these reactions further, XRD analyses were performed on the pyrite grains obtained from the samples taken after six months. However, the formation of new minerals, *e.g.* siderite or other iron minerals, could not be observed, which is likely due to the low of amount of pyrite (maximally 0.2 mol%) that was oxidised in the solutions. This XRD analysis, as well as a SEM-EDX and XPS analysis, will be performed again on pyrite obtained from the final samples of these batch tests.

6.4.3.2.2 Biotic batch tests with pyrite and nitrite, with addition of T. denitrificans

To study microbial pyrite oxidation coupled to nitrite reduction, biotic batch tests with pyrite and $NaNO_2$ (0 M or 0.005 M $NaNO_2$) are being performed in bacterial nutrient solution spiked with *T. denitrificans*. This bacterial species was grown on LZ_NO2 growth medium before inoculation of the biotic tests, showing its ability to use nitrite as electron donor in place of nitrate. However, based on the growth rate in LZ medium with nitrite or nitrate (see Section 5.4.4.4), *T. denitrificans* appears to be rather sensitive to nitrite (at a concentration of 7 mM NO_2^-).

The complete set of results from the chemical analyses and pH measurements is given in Annex 7. Figure 44 shows the evolution of the pH and the nitrite, sulphate, and thiosulphate concentrations in the BNS with pyrite and nitrite. Although statistically not significant, nitrite seems to have been reduced in both solutions with nitrite, while sulphate and/or thiosulphate (depending on the series) was produced. In the "a" series, nitrite decreased by 0.04 mmol/m² and both sulphate and thiosulphate increased with 0.01 mmol/m² after ~6 months of incubation. In contrast, in the "b" series, 0.09 mmol/m² nitrite was consumed, while 0.03 mmol/m² sulphate was produced. In the latter series, the thiosulphate concentration initially increased (similar to what was seen in the biotic control tests with pyrite and $NaNO_3$ (see Section 6.4.3.1.2), but decreased afterwards, while the sulphate concentration increased, indicating the further oxidation of thiosulphate into sulphate.

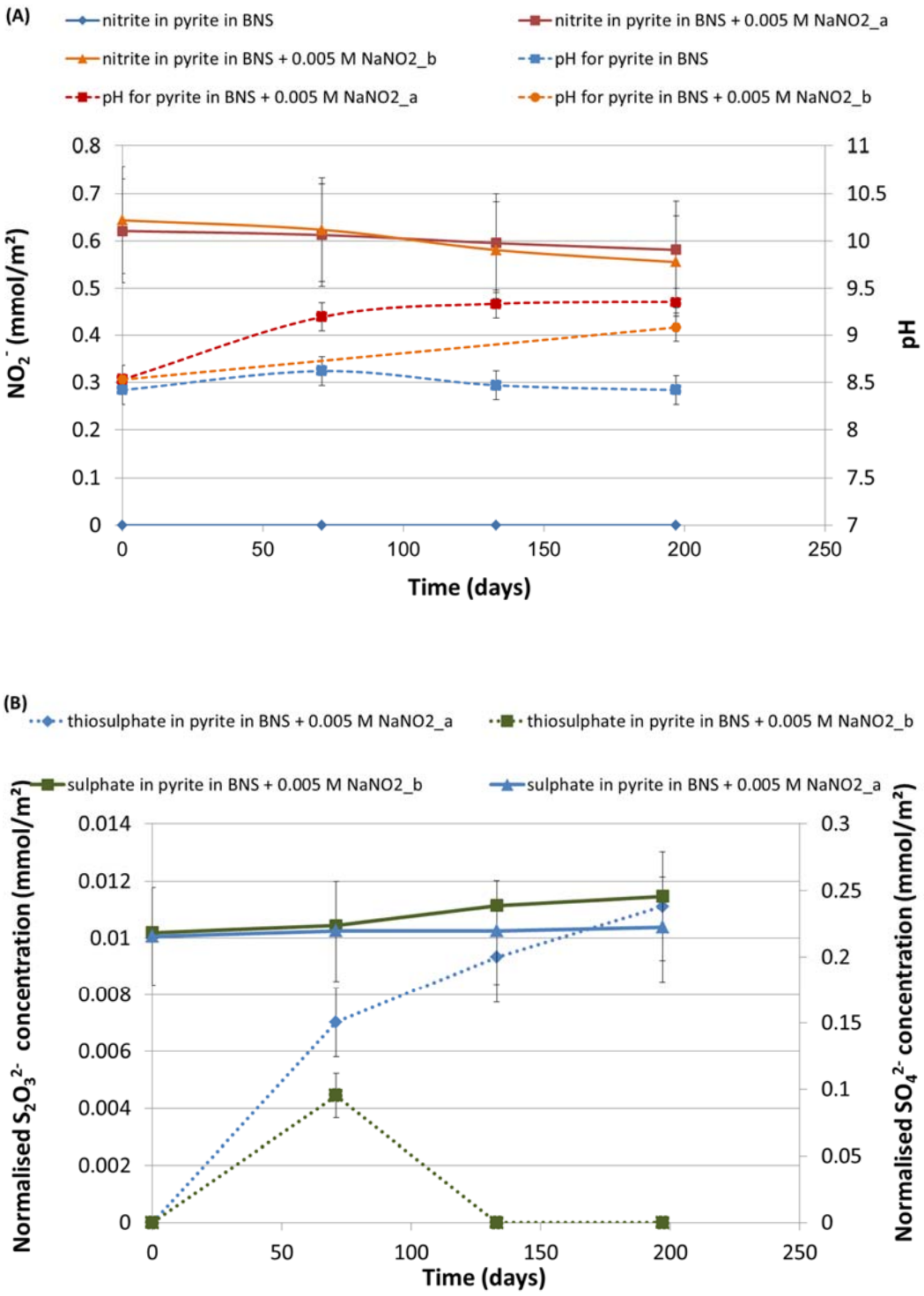

Figure 44: Time evolution of the pH and normalised nitrite (A), thiosulphate, and sulphate concentrations (B) in both of the bacterial nutrient solutions (BNS) containing pyrite and 0.005M $NaNO_2$. The indicated uncertainty takes into account the uncertainty on the individual concentrations and on the surface area to volume ratio.

Based on the MPN analyses (Figure 45), *T. denitrificans* can be found in both nitrite solutions, though only at very low concentrations, *i.e.* ~10^1 to 10^2 cells mL^{-1}. No growth of these microorganisms was observed over a period of six months, although the bacteria appear to survive in the BNS solution with nitrite. This suggests that the added concentration of nitrite inhibits the growth of this strain of *T. denitrificans*. This is in agreement with the results of previous studies [115, 159], which indicate that nitrite already causes a slight inhibition at concentrations as low as 0.4 mM.

In the "a" series, both thiosulphate and sulphate were produced during nitrite reduction (Figure 44), similar to the abiotic pyrite oxidation by nitrite (Section 6.4.3.2.1). As this suspension also contained the lowest concentration of *T. denitrificans* (even close to the detection limit of 3 cells mL^{-1}), both thiosulphate and sulphate are most likely formed due to (predominantly) abiotic processes. The observed nitrite reduction rate is also similar to the reduction rate under abiotic conditions (see Section 6.4.3.2.1).

On the other hand, in the "b" series thiosulphate appears to be oxidised further to sulphate (Figure 44). The difference in end products between both series is most likely due to the combination of abiotic pyrite oxidation by nitrite and a microbial use of thiosulphate or pyrite as electron donor, performed by the low concentration of *T. denitrificans* in the "b" series.

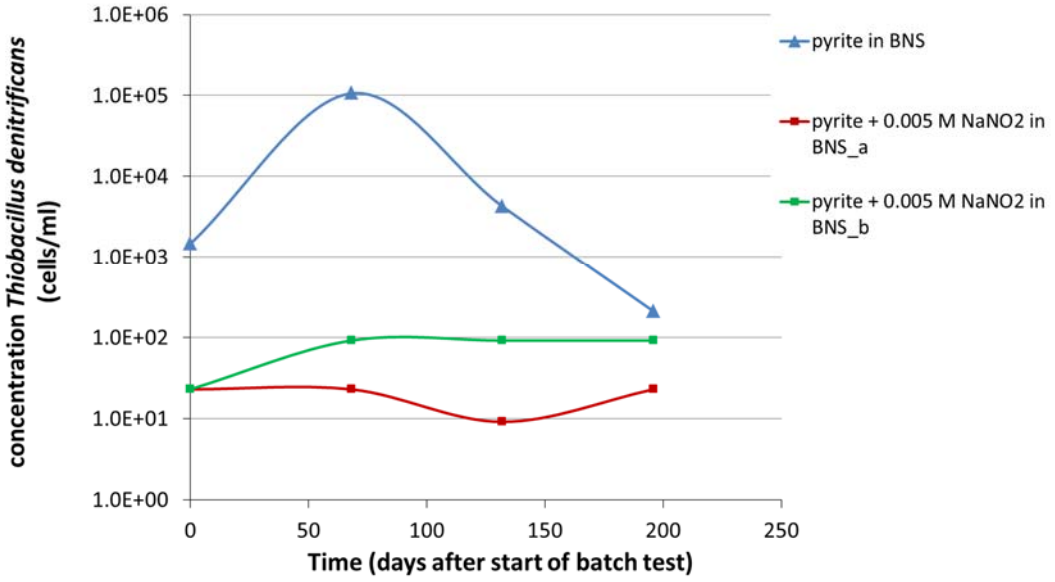

Figure 45: Time evolution of the concentration of viable *T. denitrificans* in the three bacterial nutrient solution (BNS) with pyrite and/or nitrite, as measured with MPN analyses (using LZ_NO2 medium). The lower and upper detection limits are equal to respectively 3 and 1.1×10^5 cells mL^{-1}.

The SEM photographs of the pyrite grains in contact with nitrite for four months did not clearly show the formation of a visual oxidation layer on the surface of the pyrite. Based on the amount of nitrite reduced, ~40% of the outer pyrite layer would be oxidised (assuming that only the outermost pyrite layer is oxidised). However, as explained in Section 6.4.3.1.2, the smallest (nano-sized) pyrite particles will most likely oxidise at a faster rate then the larger

grains, because of the difference in specific surface area [115]. This would explain why pyrite oxidation by nitrite could not be demonstrated (yet) by SEM.

6.4.4 Conclusions

The batch tests aim at investigating whether and to which extent abiotic reduction of nitrate and nitrite can occur in Boom Clay. This knowledge is required to conclude on a perturbation of the reducing capacity of Boom Clay towards redox-sensitive radionuclides by a $NaNO_3$ plume around a disposal gallery for Eurobitum bituminised waste when microbial activity in the clay formation is impossible or strongly limited.

Neither in the batch tests with the Boom Clay slurries [with $NaNO_3$ (0.1 and 1 M)] nor in the tests with RBCW [with 0.05 and 0.2 M $NaNO_3$ (first series) or with 0.005 and 0.1 M $NaNO_3$ (second series)], a purely chemical nitrate reduction was observed after 4 months to 2 years of incubation. Similar to this, no decrease of nitrate or production of (thio)sulphate could be observed in the abiotic batch tests with pyrite and $NaNO_3$ (without additional NaN_3), indicating that an abiotic pyrite oxidation by nitrate does not occur, at least not to a significant extent, within 1 year of reaction.

In contrast, when microbial activity was allowed in Boom Clay slurries, microbial nitrate reduction was observed and was enhanced by the presence of an additional easily degradable carbon source and/or electron donor, *e.g.* unstable antibiotics (Triclosan and Chloramphenicol). Without addition of easily degradable organic compounds to Boom Clay slurries, less than 1% of the nitrate content was reduced to nitrite after 17 weeks. These results suggest that the dissolved organic matter in Boom Clay is a poor carbon source and/or electron donor for the microbial nitrate reducers present. In contrast, no nitrate reduction was observed in Boom Clay slurries with 1 M $NaNO_3$, suggesting that 1 M $NaNO_3$ inhibits – at least temporarily – the microbial activity as well.

Furthermore, in RBCW with 0.1 M or 0.2 M $NaNO_3$ (without microbial inhibitor), only a very slow microbially mediated nitrate reduction rate was observed, *i.e.* ~0.1 mol% nitrate was reduced per year (independent of the initial nitrate concentration). This microbial nitrate reduction was coupled to the oxidation of DOM in RBCW, which resulted in a decrease in reducing capacity of DOM in RBCW for ferric citrate. On the other hand, when ferricyanide was used to determine this reducing capacity, no decrease in reducing capacity of DOM (due to microbial oxidation) could be observed. This is mainly related to the fact that ferricyanide oxidises more functional groups of DOM compared to nitrate and ferric citrate. Furthermore, the addition of azide during the reducing capacity measurements has likely influenced the results as well.

In the biotic batch tests with pyrite and $NaNO_3$, which were spiked with *T. denitrificans*, a microbial nitrate-dependent pyrite oxidation could be observed, at a rate of ~7 mol% per year (extrapolated from the currently known data). This microbial reaction results in the formation of sulphate and nitrite, although most likely also other (unquantified) N species were formed.

In the batch tests with RBCW and $NaNO_2$ (with 0.005 or 0.05 M $NaNO_2$), an abiotic nitrite reduction to N_2O was observed, probably mainly caused by the slow decomposition of azide

(used as microbial inhibitor) by nitrite in the abiotic RBCW solutions with nitrite. However, a slow and less important oxidation of DOM by nitrite cannot be excluded completely, as a slow oxidation of hydroquinone by nitrite was observed during preliminary tests. A small scale batch test with filter sterilised RBCW and nitrite will be performed to investigate this further. In the batch tests with pyrite, a purely chemical pyrite oxidation by nitrite could be observed after one year, resulting in the formation of both thiosulphate (intermediate product) and sulphate (end product). After 1 year of reaction, ~12 mol% of the initial nitrite concentration (0.005 M) was reduced by pyrite.

Similar to the tests with nitrate, in the RBCW solutions with 0.05 M $NaNO_2$ in which microbial activity was allowed, a very slow microbially mediated nitrite reduction was observed. Under these biotic conditions, only ~0.2 mol% of the initial nitrite content (0.05 M) was reduced within one year, indicating the slow kinetics of the microbial nitrite reduction with DOM as electron donor.

In the biotic batch tests with pyrite and $NaNO_2$ (0.005 M $NaNO_2$), which were spiked with *T. denitrificans*, the growth (and possibly activity) of *T. denitrificans* was inhibited by the addition of 5 mM nitrite to the suspensions. In the pyrite suspension with the highest *T. denitrificans* concentration, a combination of abiotic pyrite oxidation by nitrite and a microbial use of thiosulphate or pyrite as electron donor was observed. These processes result in the production of sulphate, while thiosulphate was formed only as intermediate product.

The experiments reported here thus demonstrate that abiotic nitrate reduction in Boom Clay does not occur, or only at a very slow rate. Nitrite on the other hand is more reactive than nitrate, although also here the rates are rather low and likely limited to the availability of the electron donor (*e.g.* reactive surface of pyrite). When microbes would be active in the Boom Clay, they can indeed use pyrite and dissolved organic matter as electron donors for the reduction of nitrate and nitrite, as already observed in the batch reactor tests (Section 6.2). However, without an additional source of C and/or electron donors, these reactions are still rather slow, although significantly faster than the purely chemical reaction.

7 General conclusions

To investigate the compatibility of Eurobitum bituminised waste with the Boom Clay, the possible disturbances of the barrier function of the clay by the disposal of Eurobitum are studied. Both a geomechanical and a geochemical perturbation of the clay are to be expected as a result of an osmosis-induced water uptake – and related swelling – of the waste and gas generation, and due to the release of large amounts of salts – mainly $NaNO_3$ – in the clay, respectively. In this report, the possible geochemical perturbation of the clay by such a $NaNO_3$ plume is discussed.

$NaNO_3$ concentration profiles were calculated to estimate the extent of the $NaNO_3$ plume around a disposal gallery for Eurobitum. The concentration profiles were determined for a fairly realistic release rate of $NaNO_3$, which was derived from upscaling $NaNO_3$ release rates that were measured in water uptake tests with small Eurobitum samples [9]. Diffusive transport was simulated, taking into account sorption of Na^+ on the concrete and the backfill in the gallery, and cation exchange with Na^+ in the clay. These exploratory calculations suggest that only the first ~5 meters of clay near the gallery will be transformed into a clay with an increased sodium occupancy compared to undisturbed Boom Clay. Furthermore, the maximum nitrate concentrations would be limited to 0.5 to 1 M at the gallery interface, and about 0.1 M at a distance of 5 meter from the gallery. Note that these values are conservative due to the assumptions in the model (Section 3).

Three different types of experiments were performed to assess the impact of a $NaNO_3$ plume in the Boom Clay, namely combined $NaNO_3$ percolation and radionuclide pulse injection experiments, bioreactor tests, and batch tests.

The combined $NaNO_3$ percolation and radionuclide pulse injection tests aimed at investigating the disturbances of the physicochemical properties and their effect on the transport properties of the clay. Cation exchange with sodium revealed to be the most important effect of a $NaNO_3$ plume. These cation exchange processes transform the clay into a clay with a high Na^+ occupancy, which appears not to affect its hydromechanical properties significantly and thus also the hydro-chemical-mechanical interaction between the swelling Eurobitum and the clay [9]. A combined geochemical and transport model (PHREEQC-2 code), in which only cation exchange reactions are considered, was applied and proved to be able to reproduce relatively well the cationic composition of the percolate in the percolation experiments with $NaNO_3$. The possible impact of a $NaNO_3$ plume on the other geochemical properties of the clay appear to be negligible. Observed effects on the hydraulic conductivity of the clay cores, and on the pH and the organic matter content in the percolate, were relatively small, and are expected to be even smaller in real disposal conditions because of the much slower increase of the ionic strength and the Na^+ concentration. There was no significant reduction of nitrate in the clay, and no oxidation of pyrite could be detected.

The effect of the $NaNO_3$ plume on the migration of tritiated water, iodide, and bicarbonate is small as well. Only for the anionic species a significant yet modest increase by about 50% in diffusion accessible porosity was measured when the ionic strength in the percolation solution increased from 0.016 M to 1 M. As the effective dispersion coefficient depends on the diffusion accessible porosity, this parameter increased also with increasing ionic strength

for anionic species: by ~50% for iodide, and ~100% for bicarbonate, when increasing the ionic strength from 0.016 M to 1 M. These observations can be explained mostly by the effect of the increased ionic strength on the EDL thickness. Because of the lack of reliable values for the dispersion length, the effective diffusion coefficient could not be calculated. However, given the low contribution of the kinematic dispersion, the effective dispersion coefficient can be used as a conservative estimate of the effective diffusion coefficient.

In the bioreactor tests we assessed the possibility and the consequences of the stimulation of microbial activity in Boom Clay slurries when nitrate or nitrite is added. More specifically, we investigated whether and to which extent a microbially mediated redox reaction occurs between nitrate or nitrite and Boom Clay components and what the outcome and extent would be. In the two series of reactor tests that were performed so far, microbially mediated denitrification, DNRA, and DNRN were observed, and revealed to be enhanced by the addition of formate and acetate as carbon sources. In the second series of reactor tests, which were initially pressurised with H_2, hydrogen was mainly used as electron donor for these processes, *i.e.* nearly all hydrogen gas was consumed during microbial nitrate reduction processes, leading to the production of nitrate into N_2, N_2O, ammonium, and nitrite. The consumption of hydrogen gas resulted in a gas pressure decrease, whilst in the first series of tests (where the gas phase was initially filled with nitrogen gas) an increase in gas pressure was observed by the production of mainly N_2O. Hence, the hydrogen gas that will be produced in the near field of a disposal gallery due to radiolysis of Eurobitum and water and due to anaerobic steel corrosion, might be consumed by microorganisms, thus lessening the possible mechanical perturbation of the clay due to gas generation. Note that this conclusion holds no statement about the actual occurrence of microbial activity in or around the disposal gallery after its closure. Mainly because of the highly alkaline pH, the high salt concentration at the gallery interface, and the low space available for growth of bacterial cells, the extent of the microbial activity remains uncertain.

Batch tests with Boom Clay slurries or with two of the main redox-active components of Boom Clay, *i.e.* dissolved organic matter and pyrite, were (and are still being) performed to study whether and to which extent nitrate or nitrite can be reduced abiotically in the Boom Clay. No purely chemical reduction of nitrate has been observed so far in batch tests with Boom Clay slurries (after one year of anaerobic incubation), RBCW (after two years of anaerobic incubation), and pyrite (after one year of anaerobic incubation). On the other hand, a very slow oxidation of DOM by nitrite might have occurred in the batch tests with RBCW, although this should be investigated further. Furthermore, a clear abiotic nitrite reduction by pyrite was observed after one year of anaerobic incubation, resulting in the formation of both thiosulphate and sulphate.

In biotic test conditions (with Boom Clay slurries, RBCW, and pyrite) both nitrate and nitrite were reduced at (very) low rates by microbes. The addition of readily available carbon sources and/or electron donors (thought to be formed by degradation of the antibiotics that were added as microbial inhibitor) considerably enhanced the microbially mediated nitrate reduction, which is in agreement with observations from the bioreactor tests. Based on the microbial reaction rates observed in the batch tests in the absence of easily oxidisable organic compounds, the Boom Clay natural organic matter and also pyrite appear to be poor electron donors for microorganisms.

8 Open questions and recommendations

The results of the experiments that were discussed in this report allow us to obtain better insights in the potential perturbation of the Boom Clay by a $NaNO_3$ plume, with respect to the barrier function of the Boom Clay towards radionuclides (*i.e.* limitation of the migration of radionuclides leaching from the waste). The results that are available so far do not reveal an important disturbance of the Boom Clay. Still some open questions remain:

1) The results of the bioreactor tests, where the microbially mediated nitrate reduction is studied, demonstrate the complexity of these processes. A parametric study such as applied for the currently performed batch tests (Section 6.4) with sufficient duplicates will allow us to better understand the reactivity of the different compounds (nitrate, nitrite, different natural/introduced electron donors) in absence but also in presence of microbes. In particular, additional batch tests should be performed to study the effect of $NaNO_3$/$NaNO_2$ on the following redox-active components in the Boom Clay:
    a. DOM: investigation of a possible oxidation of DOM by nitrate/nitrite without interference of azide.[45]
    b. Pyrite: additional batch tests with Boom Clay pyrite and nitrate/nitrite could be performed to assess the effect of the crystal structure and origin on the reactivity with nitrate and nitrite.[45]
    c. Kerogen.
    d. Boom Clay slurries: assessment of nitrate and nitrite reactivity in the presence of a combination of redox-active Boom Clay components.

    This will support a first evaluation of the effect of a nitrate plume on the reducing capacity of the Boom Clay and thus on the migration of redox-sensitive radionuclides. Eventually the obtained knowledge on the separate Boom Clay redox-active components and the Boom Clay slurry could be tested in ternary system experiments consisting of Boom Clay, $NaNO_3$ and redox-sensitive radionuclides. To study the (bio)geochemical processes under more realistic repository conditions, the expected high pH and ionic strength are to be considered as important parameters as well.

    To a lesser extent this could be complemented by an evaluation of the effect of the presence of hydrogen and Fe (nanoparticles) on nitrate reduction under repository conditions. Indeed, Truche *et al.* [142, 160] observed an abiotic reduction of nitrate and sulphate by hydrogen in the presence of catalysts like C-steel, stainless steel 316 L, and Hastelloy C276, but it should be stressed that these observations were made at high temperatures (90-150°C).

2) The model that has been been used in Section 3 to determine the order of magnitude of the $NaNO_3$ concentrations in the near field, had to use several assumptions due to the lack of detailed data, such as transport parameters of $NaNO_3$ through the EBS and the use of Rb^+-sorption data instead of Na^+ data. The model (and the assumptions) could be improved by performing specific experiments. It seems unlikely this will change the conclusions, but this can give more insight into the extent of the perturbed zone in the clay, in which Na^+ will have an increased occupancy. This could

[45] These tests are ongoing at the moment of finalisation of this report (version 2018).

furthermore be complemented with sorption studies of cationic radionuclide species to gain knowledge on the effect of the increased competition with Na^+.

3) The nitrate plume will not be the only perturbation of the Boom Clay close to the Boom Clay - Gallery interface. For example, due to the presence of large amounts of cementitious materials in the EBS, an alkaline plume will also perturb the clay. The effect of combined perturbations – if expected to happen at the same timescale in the evolution of the geological disposal facility – or sequential perturbations, will need to be assessed.

9 References

1. Boulanger, D. (2011). Source term for the Safety and Feasibility Case 1. NIROND TR-2011-68. ONDRAF/NIRAS, Brussels, Belgium.

2. Stankovskiy, A. (2011). Calculation of decay power release, activity and absorbed dose in Eurobitum intermediate level waste. External Report SCK•CEN-ER-181. SCK•CEN, Mol, Belgium.

3. Pottier, P. (1989). Handbook of Reference Medium Active Waste (RMA). Volume 12482 of Euratom publications. Commission of the European Communities.

4. Demonie, M. (1996). Chemische samenstelling van het gebitumineerd product van de fluxen E1 tot en met EX. Belgoprocess Note ref. AFB-96-390. Belgoprocess, Dessel, Belgium.

5. Smith, P., Cornélis, B., Capouet, M., Depaus, C., and Van Geet, M. (2009). The long-term safety assessment methodology for the geological disposal of radioactive waste. SFC1 level 4 report. ONDRAF/NIRAS, Brussels, Belgium.

6. De Craen, M., Wang, L., Van Geet, M., and Moors, H. (2004). Geochemistry of Boom Clay pore water at the Mol site. Status 2004. Scientific report SCK•CEN-BLG-990. SCK•CEN, Mol, Belgium.

7. Marivoet, J. and Weetjens, E. (2009). Impact of advanced fuel cycles on geological disposal. Proceedings to the MRS conference, 1193: 117-126.

8. Valcke, E., Marien, A., and Van Geet, M. (2009). The methodology followed in Belgium to investigate the compatibility with geological disposal of Eurobitum bituminized intermediate-level radioactive waste. Proceedings to the MRS conference, 1193: 105-116.

9. Mariën, A., Bleyen, N., and Valcke, E. (2013). The swelling of Eurobitum by water uptake and its geo-mechanical consequences. External Report SCK•CEN-ER-218. SCK•CEN, Mol, Belgium.

10. Yu, L., Weetjens, E., Valcke, E., and Mariën, A. (in preparation). Evaluation of the gas source term for Eurobitum. External Report SCK•CEN-ER-211. SCK•CEN, Mol, Belgium.

11. Valcke, E. and Mariën, A. (2009). Geochemical perturbations in Boom Clay: $NaNO_3$. Restricted Contract Report SCK•CEN-R-4850. SCK•CEN, Mol, Belgium.

12. Valcke, E. and Marien, A. (2009). Further studies on the compatibility of Eurobitum bituminised waste with the geological disposal medium (EUROCOMPAT I and II). Restricted Contract Report SCK•CEN-R-4846. SCK•CEN, Mol, Belgium.

13. Honty, M. (2008). SMARAGD. The study of mineral alterations of clay barriers used for Radwaste storage and its geological disposal. External Report SCK•CEN-ER-58. SCK•CEN, Mol, Belgium.

14. Aertsens, M., Dierckx, A., Put, M., Moors, H., Janssen, K., Van Ravestyn, L., Van Gompel, M., and De Cannière, P. (2005). Determination of the hydraulic conductivity, the product ηR of the porosity η and the retardation factor R, and the apparent diffusion coefficient Dp on Boom Clay cores from the Mol-1 drilling. Restricted Contract Report SCK•CEN-R-3503. SCK•CEN, Mol, Belgium.

15. Bradbury, M.H. and Baeyens, B. (2002). Porewater chemistry in compacted re-saturated MX-80 bentonite: physicochemical characterisation and geochemical modelling. PSI Bericht Nr. 02-10. PSI, Villigen, Switzerland.

16. Van Loon, L.R., Glaus, M.A., and Müller, W. (2007). Anion exclusion effects in compacted bentonites: towards a better understanding of anion diffusion. Applied Geochemistry, 22: 2536-2552.

17. White, R.E. (1997). Principles and practice of soil science: the soil as a natural resource (3rd edition). Blackwell Science, UK.

18. Honty, M. (2010). CEC of the Boom Clay – a review. External Report SCK•CEN-ER-134. SCK•CEN, Mol, Belgium.

19. Pusch, R., Karnland, O., and Hökmark, H. (1990). GMM – a general microstructural model for qualitative and quantitative studies of smectite clays. SKB Technical Report 90-43. SKB, Stockholm, Sweden.

20. Kele, S., Van Geet, M., and De Craen, M. (2006). Geochemistry of Boom Clay pore water and its dissolved gasses. Internal Report SCK•CEN-I-78. SCK•CEN, Mol, Belgium.

21. De Craen, M. (1998). The formation of septarian carbonate concretions in organic-rich argillaceous sediments. Ph.D. thesis. K.U.Leuven, Leuven, Belgium.

22. Van Geet, M. (2004). Characterisation of Boom Clay organic matter: mobile and immobile fraction. Restricted Contract Report SCK•CEN-R-3884. SCK•CEN, Mol, Belgium.

23. Blanchart, P. (2011). Influences de l'oxydation et de la biodegradation anaerobie sur la matière organique de l'argile oligocène de Boom (Mol, Belgique): conséquences sur la formation d'espèces organiques hydrosolubles. Ph.D. thesis. Institut National Polytechnique de Lorraine, Nancy, France.

24. Bruggeman, C. and De Craen, M. (2012). Boom Clay natural organic matter. External Report SCK•CEN-ER-206. SCK•CEN, Mol, Belgium.

25. Peretyazhko, T. and Sposito, G. (2006). Reducing capacity of terrestrial humic acids. Geoderma, 137: 140-146.

26. Bleyen, N., Vasile, M., Marien, A., and Valcke, E. (2016). Methods to determine the reducing capacity of dissolved organic matter in Boom Clay pore water. External Report SCK•CEN-ER-283. SCK•CEN, Mol, Belgium.

27. Pirlet, V. (2003). The investigation of the neptunium complexes formed upon interaction of high-level waste glass and Boom Clay medium. Ph.D. thesis. Université de Liège, Liège, Belgium.

28. Mariën, A. and Valcke, E. (2012). Scoping calculations on the oxidation of Boom Clay by nitrate. Technical Note TN-26. SCK•CEN, Mol, Belgium.

29. Weetjens, E., Valcke, E., and Mariën, A. (2010). Sodium nitrate release from EUROBITUM bituminised radioactive waste. Scoping calculations. External Report SCK•CEN-ER-146. SCK•CEN, Mol, Belgium.

30. Wacquier, W. and Humbeeck, H.V. (2009). B&C concept and open questions (draft version March 2009). ONDRAF/NIRAS Report 2009-0146. ONDRAF/NIRAS, Brussels, Belgium.

31. Wang, L., Jacques, D., and De Cannière, P. (2010). Effect of an alkaline plume on the Boom Clay as a potential host formation for geological disposal of radioactive waste. External Report SCK•CEN-ER-28. SCK•CEN, Mol, Belgium.

32. Sneyers, A. and Van Iseghem, P. (1998). The leaching behavior of bituminised waste in the geologic disposal conditions of the Boom Clay formation. Proceedings to the MRS conference, 506: 565-572.

33. Valcke, E., Marien, A., Smets, S., Li, X., Mokni, N., Olivella, S., and Sillen, X. (2010). Osmosis-induced swelling of Eurobitum bituminized radioactive waste in constant total stress conditions. Journal of Nuclear Materials, 406: p. 304-316.

34. Bruggeman, C. (2009). Preparation of topical reports as a basis for the Data Collection Forms. Management Report. Restricted Contract Report SCK•CEN-R-4792. SCK•CEN, Mol, Belgium.

35. Martens, E., Wang, L., and Jacques, D. (2008). Modelling of cation concentrations in outflow of NaNO3 percolation experiments through Boom Clay cores. External Report SCK•CEN-ER-85. SCK•CEN, Mol, Belgium.

36. Bruggeman, C., Aertsens, M., Maes, N., and Salah, S. (2010). Iodine retention and migration behaviour in Boom Clay. External Report SCK•CEN-ER-119. SCK•CEN, Mol, Belgium.

37. Bruggeman, C., Maes, N., Aertsens, M., Govaerts, J., Martens, E., Jacops, E., Van Gompel, M., and Van Ravestyn, L. (2010). Technetium retention and migration behaviour in Boom Clay. External Report, SCK•CEN-ER-101 SCK•CEN, Mol, Belgium.

38. Bruggeman, C., Salah, S., and Maes, N. (2010). Americium retention and migration behaviour in Boom Clay. External Report, SCK•CEN-ER-201. SCK•CEN, Mol, Belgium.

39. Bruggeman, C., Maes, N., Aertsens, M., and De Cannière, P. (2013). Tritiated water retention and migration behaviour in Boom Clay. SFC1 level 5 report: First full Draft – status 2009. External Report SCK•CEN-ER-248. SCK•CEN, Mol, Belgium.

40. Maes, N. (2007). Uranium retention and migration behaviour in Boom Clay – status 2004. NIROND-TR report 2007- 10. ONDRAF/NIRAS, Brussels, Belgium.

41. Maes, N., Salah, S., Bruggeman, C., Aertsens, M., and Martens, E. (2011). Caesium retention and migration behaviour in Boom Clay. Topical report – first draft. External Report SCK•CEN-ER-153. SCK•CEN, Mol, Belgium.

42. De Cannière, P., Maes, A., Williams, S., Bruggeman, C., Beauwens, T., Maes, N., and Cowper, M. (2010). Behaviour of Selenium in Boom Clay. External Report SCK•CEN-ER-120. SCK•CEN, Mol, Belgium.

43. Qu, W. and Li, D. (2000). A model for overlapped EDL fields. Journal of Colloid and Interface Science, 224: 397-407.

44. Sparks, D.L. (2003). Environmental soil chemistry (2nd edition). Academic Press, Elsevier Science, USA.

45. McCarthy, J.F. and Zachara, J.M. (1989). Subsurface transport of contaminants. Environmental science & technology, 23: 496-502.

46. Jones, M.N. and Bryan, N.D. (1998). Colloidal properties of humic substances. Advances in Colloid and Interface Science, 78: 1-48.

47. Tang, C.Y., Kwon, Y.-N., and Leckie, J.O. (2007). Fouling of reverse osmosis and nanofiltration membranes by humic acid—effects of solution composition and hydrodynamic conditions. Journal of Membrane Science, 290: 86-94.

48. Zazouli, M., Nasseri, S., Mahvi, A., Gholami, M., Mesdaghinia, A., and Younesian, M. (2008). Retention of humic acid from water by nanofiltration membrane and influence of solution chemistry on membrane performance. Journal of Environmental Health Science & Engineering, 5: 11-18.

49. Chang, S., Ryan, M., and Gupta, R. (1993). The effect of pH, ionic strength, and temperature on the rheology and stability of aqueous clay suspensions. Rheologica Acta, 32: 263-269.

50. Kretzschmar, R. and Sticher, H. (1997). Transport of humic-coated iron oxide colloids in a sandy soil: Influence of Ca2+ and trace metals. Environmental Science & Technology, 31: 3497-3504.

51. Grenthe, I. and Wanner, H. (2000). Guidelines for the extrapolation to zero ionic strength. Thermodynamic database report TDB-2. OECD Nuclear Energy Agency, Issy-les-Moulineaux, France.

52. Garavito, A.M., De Canniere, P., and Kooi, H. (2007). In situ chemical osmosis experiment in the Boom Clay at the Mol underground research laboratory. Physics and Chemistry of the Earth, 32: 421-433.

53. Lide, D.R. and Frederikse, H.P.R. (1995). CRC Handbook of Chemistry and Physics (76th edition). CRC Press, Boca Raton, USA. 2624.

54. Conway, B.E. (1981). Ionic Hydration in Chemistry and Biophysics. Elsevier Scientific Publishing Company, Amsterdam, The Netherlands.

55. Shainberg, I. and Singer, M. (1990). Soil response to saline and sodic conditions. In: Agricultural salinity assessment and management. Tanji, K.K. (Ed.). Am. Soc. Of Civil. Eng. Manuals and Reports on Engineering Practice. ASCE, New York, USA, pp. 91-112.

56. Churchman, G., Skjemstad, J., and Oades, J. (1993). Influence of clay minerals and organic matter on effects of sodicity on soils. Soil Research, 31: 779-800.

57. Cervantes, F., Monroy, O., and Gomez, J. (1998). Accumulation of intermediates in a denitrifying process at different copper and high nitrate concentrations. Biotechnology Letters, 20: 959-961.

58. Conrad, R. (1996). Soil microorganisms as controllers of atmospheric trace gases (H_2, CO, CH_4, OCS, N_2O, and NO). Microbiological reviews, 60: 609-640.

59. Cabello, P., Roldan, M.D., and Moreno-Vivian, C. (2004). Nitrate reduction and the nitrogen cycle in archaea. Microbiology, 150: 3527-46.

60. Jørgensen, C.J., Jacobsen, O.S., Elberling, B., and Aamand, J. (2009). Microbial oxidation of pyrite coupled to nitrate reduction in anoxic groundwater sediment. Environmental Science & Technology, 43: 4851-4857.

61. Hartog, N. (2003). Reactivity of Organic Matter and other Reductants in Aquifer Sediments. Ph.D. thesis. University of Utrecht, Utrecht, the Netherlands.

62. Schippers, A. and Jørgensen, B. (2001). Oxidation of pyrite and iron sulfide by manganese dioxide in marine sediments. Geochimica et Cosmochimica Acta, 65: 915-922.

63. Schippers, A. and Jørgensen, B.B. (2002). Biogeochemistry of pyrite and iron sulfide oxidation in marine sediments. Geochimica et Cosmochimica Acta, 66: 85-92.

64. Van Cleemput, O. and Samater, A.H. (1996). Nitrite in soils: accumulation and role in the formation of gaseous N compounds. Fertilizer Research, 45: 81-89.

65. De Cannière, P., Moors, H., Lolivier, P., De Preter, P., and Put, M. (1996). Laboratory and in situ migration experiments in the Boom Clay. Report EUR-16927. European Commission.

66. Almeida, J., Reis, M., and Carrondo, M. (1995). Competition between nitrate and nitrite reduction in denitrification by Pseudomonas fluorescens. Biotechnology and Bioengineering, 46: 476-484.

67. Oh, J. and Silverstein, J. (1999). Acetate limitation and nitrite accumulation during denitrification. Journal of Environmental Engineering, 125: 234-242.

68. Mallants, D. and Jacques, D. (2007). Modelling multi-phase flow phenomena in concrete barriers used for geological disposal of radioactive waste. Proceedings of the 11th International Conference on Environmental Remediation and Radioactive Waste Management. American Society of Mechanical Engineers, pp. 741-749.

69. Harrington, J., Milodowski, A., Graham, C., Rushton, J., and Cuss, R. (2012). Evidence for gas-induced pathways in clay using a nanoparticle injection technique. Mineralogical Magazine, 76: 3327-3336.

70. Staunton, S., Dumat, C., and Zsolnay, A. (2002). Possible role of organic matter in radiocaesium adsorption in soils. Journal of Environmental Radioactivity, 58: 163-73.

71. Oremland, R.S., Blum, J.S., Bindi, A.B., Dowdle, P.R., Herbel, M., and Stolz, J.F. (1999). Simultaneous reduction of nitrate and selenate by cell suspensions of selenium-respiring bacteria. Applied and Environmental Microbiology, 65: 4385-4392.

72. Ortiz-Bernad, I., Anderson, R.T., Vrionis, H.A., and Lovley, D.R. (2004). Resistance of solid-phase U (VI) to microbial reduction during in situ bioremediation of uranium-contaminated groundwater. Applied and Environmental Microbiology, 70: 7558-7560.

73. Boivin-Jahns, V., Ruimy, R., Bianchi, A., Daumas, S., and Christen, R. (1996). Bacterial diversity in a deep-subsurface clay environment. Applied and Environmental Microbiology, 62: 3405-3412.

74. Velimirov, B. (2001). Nanobacteria, Ultramicrobacteria and Starvation Forms: A Search for the Smallest Metabolizing Bacterium. Microbes and Environments, 16: 67-77.

75. Krulwich, T.A. and Guffanti, A.A. (1983). Physiology of acidophilic and alkalophilic bacteria. Advances in Microbial Physiology, 24: 173-214.

76. Madigan, M.T., Martinko, J.M., and Parker, J. (2000). Brock Biology of Microorganisms (9th edition). Prentice-Hall, New Jersey, USA.

77. Miller, W., Alexander, R., Chapman, N., McKinley, J.C., and Smellie, J. (2000). Geological disposal of radioactive wastes and natural analogues. Vol. 2. Elsevier Scientific Publishing Company, Amsterdam, The Netherlands.

78. Stott, J. and Herbert, B. (1986). The effect of pressure and temperature on sulphate-reducing bacteria and the action of biocides in oilfield water injection systems. Journal of Applied Bacteriology, 61: 57-66.

79. Pedersen, K. (2000). Microbial processes in radioactive waste disposal. Technical Report TR-00-04. SKB, Stockholm, Sweden.

80. Pedersen, K., Nilsson, E., Arlinger, J., Hallbeck, L., and O'Neill, A. (2004). Distribution, diversity and activity of microorganisms in the hyper-alkaline spring waters of Maqarin in Jordan. Extremophiles, 8: 151-164.

81. Guillaumont, R., Fanghanel, T., Neck, V., Fuger, J., Palmer, D., Grenthe, I., and Rand, M.H. (2003). Update on the chemical thermodynamics of uranium, neptunium, plutonium, americium and technetium. Elsevier Scientific Publishing Company, Amsterdam, The Netherlands.

82. Swanson, K.M.J., Petran, R.L., and Hanlin, J.H. (2001). Culture methods for enumeration of microorganisms. In: Compendium of methods for the microbiological examination of foods. Downes, F.P. and Ito, K. (Eds). APHA, Washington, USA, pp. 58-61.

83. Starr, M.P., Stolp, H., Trüper, H.G., Balows, A., and Schlegel, H.G. (1981). The prokaryotes: a handbook on habitats, isolation, and identification of bacteria. Vols I and II. Springer Verlag GmbH & Co, Berlin, Germany.

84. Aerts, S. (2008). Use of inhibitors to prevent bacterial artefacts in experiments. External Report SCK•CEN-ER-65. SCK•CEN, Mol, Belgium.

85. Drysdale, G., Kasan, H., and Bux, F. (2000). Assessment of nitrite denitrification behaviour by denitrifying heterotrophic organisms in a NDBEPR activated sludge system. Proceedings of the WISA 2000 Biennial Conference 2000: 1-6.

86. Lampe, D.G. and Zhang, T.C. (1996). Evaluation of sulfur-based autotrophic denitrification. Proceedings of the HSRC/WERC Joint Conference on the Environment: 1-15.

87. Aerts, S., Jacops, E., and Dewel, A. (2009). Microbial activity around the connecting gallery (2nd edition). External report SCK•CEN-ER-61. SCK•CEN, Mol, Belgium.

88. Labat, M. and Garcia, J.-L. (1986). Study on the development of methanogenic microflora during anaerobic digestion of sugar beet pulp. Applied Microbiology and Biotechnology, 25: 163-168.

89. Martin-Laurent, F., Philippot, L., Hallet, S., Chaussod, R., Germon, J., Soulas, G., and Catroux, G. (2001). DNA extraction from soils: old bias for new microbial diversity analysis methods. Applied and Environmental Microbiology, 67: 2354-2359.

90. Sagova-Mareckova, M., Cermak, L., Novotna, J., Plhackova, K., Forstova, J., and Kopecky, J. (2008). Innovative methods for soil DNA purification tested in soils with widely differing characteristics. Applied and Environmental Microbiology, 74: 2902-2907.

91. Wouters, K., Moors, H., Boven, P., and Leys, N. (2013). Evidence and characteristics of a diverse and metabolically active microbial community in deep subsurface clay borehole water. FEMS Microbiology Ecology, 86: 458-473.

92. Lane, D.J. (1991). 16S/23S rRNA sequencing. In: Nucleic acid techniques in bacterial systematics. Stackebrandt, E. and Goodfellow, M. (Eds). John Wiley and Sons, Chichester, UK, pp. 115-175.

93. Friedrich, M.W. (2002). Phylogenetic analysis reveals multiple lateral transfers of adenosine-5'-phosphosulfate reductase genes among sulfate-reducing microorganisms. Journal of Bacteriology, 184: 278-289.

94. Braker, G., Fesefeldt, A., and Witzel, K.P. (1998). Development of PCR primer systems for amplification of nitrite reductase genes (*nirK* and *nirS*) to detect denitrifying bacteria in environmental samples. Applied and Environmental Microbiology, 64: 3769-3775.

95. Luton, P.E., Wayne, J.M., Sharp, R.J., and Riley, P.W. (2002). The *mcrA* gene as an alternative to 16S rRNA in the phylogenetic analysis of methanogen populations in landfillb. Microbiology, 148: 3521-3530.

96. Oremland, R.S. and Capone, D.G. (1988). Use of "specific" inhibitors in biogeochemistry and microbial ecology. In: Advances in microbial ecology. Springer, USA, pp. 285-383.

97. Mariën, A., Bleyen, N., Aerts, S., and Valcke, E. (2011). The study of abiotic reduction of nitrate and nitrite in Boom Clay. Physics and Chemistry of the Earth, 36: 1639-1647.

98. Benz, M., Schink, B., and Brune, A. (1998). Humic acid reduction by Propionibacterium freudenreichii and other fermenting bacteria. Applied and Environmental Microbiology, 64: 4507-4512.

99. Matthiessen, A. (1995). Determining the redox capacity of humic substances as a function of pH. Vom Wasser, 84: 229-235.

100. Bauer, I. and Kappler, A. (2009). Rates and extent of reduction of Fe(III) compounds and O_2 by humic substances. Environmental Science & Technology, 43: 4902-4908.

101. Wolf, M., Kappler, A., Jiang, J., and Meckenstock, R.U. (2009). Effects of humic substances and quinones at low concentrations on ferrihydrite reduction by Geobacter metallireducens. Environmental Science & Technology, 43: 5679-5685.

102. Stookey, L.L. (1970). Ferrozine - a new spectrophotometric reagent for iron. Analytical Chemistry, 42: 779-781.

103. Wang, Z., Liu, C., Wang, X., Marshall, M.J., Zachara, J.M., Rosso, K.M., Dupuis, M., Fredrickson, J.K., Heald, S., and Shi, L. (2008). Kinetics of reduction of Fe(III) complexes by outer membrane cytochromes MtrC and OmcA of Shewanella oneidensis MR-1. Applied and Environmental Microbiology, 74: 6746-6755.

104. Vukosav, P., Mlakar, M., and Tomišić, V. (2012). Revision of iron (III)–citrate speciation in aqueous solution. Voltammetric and spectrophotometric studies. Analytica Chimica Acta, 745: 85-91.

105. Bauer, M., Heitmann, T., Macalady, D.L., and Blodau, C. (2007). Electron transfer capacities and reaction kinetics of peat dissolved organic matter. Environmental Science & Technology, 41: 139-145.

106. Morris, K., Zhao, H., and John, R. (2005). Ferricyanide-mediated microbial reactions for environmental monitoring. Australian Journal of Chemistry, 58: 237-245.

107. Moors, H. (2005). Topical report on the effect of the ionic strength on the diffusion accessible porosity of Boom Clay. External Report SCK•CEN-ER-02. SCK•CEN, Mol, Belgium.

108. Ammann, L., Bergaya, F., and Lagaly, G. (2005). Determination of the cation exchange capacity of clays with copper complexes revisited. Clay Minerals, 40: 441-453.

109. Martens, E., Jacques, D., Wang, L., De Canniere, P., Van Gompel, M., Marien, A., and Valcke, E. (2011). Modelling of cation concentrations in the outflow of NaNO3 percolation experiments through Boom Clay cores. Physics and Chemistry of the Earth, 36: 1693-1699.

110. Ortiz, L. (2005). Influence of a NaNO3 plume: microbial denitrification study (NRM039A and NRM039B experiments). Restricted Contract Report SCK•CEN-R-4263. SCK•CEN, Mol, Belgium.

111. Valcke, E., Sneyers, A., and Iseghem, P.V. (2000). The effect of radiolytic degradation products of Eurobitum on the solubility and sorption of Pu and Am in Boom Clay. Proceedings of the MRS conference, 663: 141-149.

112. Wilhelm, E., Battino, R., and Wilcock, R.J. (1977). Low-pressure solubility of gases in liquid water. Chemical Reviews, 77: 219-262.

113. Descostes, M., Beaucaire, C., Mercier, F., Savoye, S., Sow, J., and Zuddas, P. (2002). Effect of carbonate ions on pyrite (FeS_2) dissolution. Bulletin de la Société géologique de France, 173: 265-270.

114. Nugroho, R. (2011). Effect of nitrite on denitrification of wastewater by autotrophic bacteria. Jurnal Air Indonesia, 2: 163-168.

115. Bosch, J., Lee, K.-Y., Jordan, G., Kim, K.-W., and Meckenstock, R.U. (2012). Anaerobic, nitrate-dependent oxidation of pyrite nanoparticles by Thiobacillus denitrificans. Environmental Science & Technology, 46: 2095-2101.

116. Descostes, M., Vitorge, P., and Beaucaire, C. (2004). Pyrite dissolution in acidic media. Geochimica et Cosmochimica Acta, 68: 4559-4569.

117. Hemes, S., Desbois, G., Urai, J.L., De Craen, M., and Honty, M. (2011). Comparative study on porosity in fine- and coarse-grained Boom Clay samples (Mol-Dessel reference site, Belgium). External Report SCK•CEN-ER-157. SCK•CEN, Mol, Belgium.

118. Eurachem/CITAC (2012). Quantifying uncertainty in analytical measurement (3rd edition). Eurachem/CITAC Guide CG 4. Available on http://www.citac.cc.

119. Maes, N. (2006). Technical note concerning the relationship between TOC and UV in Boom Clay Waters. Internal Report SCK•CEN-I-87. SCK•CEN, Mol, Belgium.

120. Tournassat, C., Gailhanou, H., Crouzet, C., Braibant, G., Gautier, A., and Gaucher, E.C. (2009). Cation exchange selectivity coefficient values on smectite and mixed-layer illite/smectite minerals. Soil Science Society of America Journal, 73: 928-942.

121. Aertsens, M., Put, M., and Dierckx, A. (1999). An analytical model for pulse injection experiments. In: Modelling of transport processes in soils at various scales in time and space. Wageningen Pers, Wageningen, the Netherlands.

122. Appelo, C., Van Loon, L., and Wersin, P. (2010). Multicomponent diffusion of a suite of tracers (HTO, Cl, Br, I, Na, Sr, Cs) in a single sample of Opalinus Clay. Geochimica et Cosmochimica Acta, 74: 1201-1219.

123. Clague, J.C. (2013). Denitrification in the shallow groundwater system of two agricultural catchments in the Waikato, New Zealand. Ph.D. thesis. Lincoln University, Christchurch, New Zealand.

124. De Craen, M., Van Geet, M., Wang, L., and Put, M. (2004). High sulphate concentrations in squeezed Boom Clay pore water: evidence of oxidation of clay cores. Physics and Chemistry of the Earth, 29: 91-103.

125. Wemaere, I., Marivoet, J., and Labat, S. (2008). Hydraulic conductivity variability of the Boom Clay in north-east Belgium based on four core drilled boreholes. Physics and Chemistry of the Earth, 33: S24-S36.

126. Rao, S.N. and Mathew, P.K. (1995). Effects of exchangeable cations on hydraulic conductivity of a marine clay. Clays and Clay Minerals, 43: 433-437.

127. Dizier, A., Yu, H., and Li, X.L. (in preparation). Interpretation of the long-term creep tests on two Boom Clay cores percolated with 1 M $NaNO_3$. External Report. SCK•CEN, Mol, Belgium.

128. De Craen, M., Wemaere, I., Labat, S., and Van Geet, M. (2006). Geochemical analyses of Boom Clay pore water and underlying aquifers in the Essen-1 borehole. External Report SCK•CEN-ER-19. SCK•CEN, Mol, Belgium.

129. Aertsens, M., Van Gompel, M., De Cannière, P., Maes, N., and Dierckx, A. (2008). Vertical distribution of transport parameters in Boom Clay in the Mol-1 borehole (Mol, Belgium). Physics and Chemistry of the Earth, 33: S61-S66.

130. Aertsens, M., Dierckx, A., Moors, H., De Cannière, P., and Maes, N. (2010). Vertical distribution of H14CO3- transport parameters in Boom Clay in the Mol-1 borehole (Mol, Belgium) and comparison with data from independent measurements. External Report SCK•CEN-ER-66. SCK•CEN, Mol, Belgium.

131. Wittebroodt, C., Savoye, S., Frasca, B., Gouze, P., and Michelot, J.-L. (2012). Diffusion of HTO, $^{36}Cl^-$ and $^{125}I^-$ in Upper Toarcian argillite samples from Tournemire: Effects of initial iodide concentration and ionic strength. Applied Geochemistry, 27: 1432-1441.

132. Van Cappellen, P., Charlet, L., Stumm, W., and Wersin, P. (1993). A surface complexation model of the carbonate mineral-aqueous solution interface. Geochimica et Cosmochimica Acta, 57: 3505-3518.

133. Bolt, G.H. and de Haan, F.A.M. (1982). Anion exclusion in soil. In: Soil Chemistry: B. Physcio-chemical Models. Bolt, G.H. (Ed.). Elsevier, Amsterdam, The Netherlands.

134. Honty, M. and De Craen, M. (2012). Boom Clay mineralogy− qualitative and quantitative aspects: Status 2011. External Report SCK•CEN-ER-187. SCK•CEN, Mol, Belgium.

135. Nugroho, S.G. and Kuwatsuka, S. (1990). Concurrent observation of several processes of nitrogen metabolism in soil amended with organic materials: I. Effect of different organic materials on ammonification, nitrification, denitrification, and N_2 fixation under aerobic and anaerobic conditions. Soil Science and Plant Nutrition, 36: 215-224.

136. Zhu, X., Burger, M., Doane, T.A., and Horwath, W.R. (2013). Ammonia oxidation pathways and nitrifier denitrification are significant sources of N_2O and NO under low oxygen availability. Proceedings of the National Academy of Sciences, 110: 6328-6333.

137. Bollag, J.-M. and Henninger, N.M. (1978). Effects of nitrite toxicity on soil bacteria under aerobic and anaerobic conditions. Soil Biology and Biochemistry, 10: 377-381.

138. Akunna, J.C., Bizeau, C., and Moletta, R. (1993). Nitrate and nitrite reductions with anaerobic sludge using various carbon sources: glucose, glycerol, acetic acid, lactic acid and methanol. Water Research, 27: 1303-1312.

139. Lew, B., Stief, P., Beliavski, M., Ashkenazi, A., Svitlica, O., Khan, A., Tarre, S., de Beer, D., and Green, M. (2012). Characterization of denitrifying granular sludge with and without the addition of external carbon source. Bioresource Technology, 124: 413-420.

140. Maes, A., Bruggeman, C., Geraedts, K., and Vancluysen, J. (2003). Quantification of the interaction of Tc with dissolved boom clay humic substances. Environmental Science & Technology, 37: 747-753.

141. Libert, M., Bildstein, O., Esnault, L., Jullien, M., and Sellier, R. (2011). Molecular hydrogen: An abundant energy source for bacterial activity in nuclear waste repositories. Physics and Chemistry of the Earth, 36: 1616-1623.

142. Truche, L., Berger, G., Albrecht, A., and Domergue, L. (2013). Engineered materials as potential geocatalysts in deep geological nuclear waste repositories: a case study of the stainless steel catalytic effect on nitrate reduction by hydrogen. Applied Geochemistry, 35: 279-288.

143. Choe, S., Liljestrand, H.M., and Khim, J. (2004). Nitrate reduction by zero-valent iron under different pH regimes. Applied Geochemistry, 19(3): p. 335-342.

144. Zinder, S.H. (1993). Physiological ecology of methanogens. In: Methanogenesis. Springer, USA, pp. 128-206.

145. Chen, A.C., Ohashi, A., and Harada, H. (2003). Acetate synthesis from H_2/CO_2 in simulated and actual landfill samples. Environmental Technology, 24: 435-43.

146. Almeida, J., Julio, S., Reis, M., and Carrondo, M. (1995). Nitrite inhibition of denitrification by Pseudomonas fluorescens. Biotechnology and Bioengineering, 46: 194-201.

147. Rütting, T., Boeckx, P., Müller, C., and Klemedtsson, L. (2011). Assessment of the importance of dissimilatory nitrate reduction to ammonium for the terrestrial nitrogen cycle. Biogeosciences, 8: 1779-1791.

148. Roadcap, G.S., Sanford, R.A., Jin, Q., Pardinas, J.R., and Bethke, C.M. (2006). Extremely alkaline (pH > 12) ground water hosts diverse microbial community. Groundwater, 44: 511-517.

149. Kappelmeyer, U., Kuschk, P., and Stottmeister, U. (2003). Model experiments on the influence of artificial humic compounds on chemodenitrification. Water, Air, and Soil Pollution, 147: 317-330.

150. Van Geet, M., Maes, N., and Dierckx, A. (2003). Characteristics of the Boom Clay organic matter, a review. Professional paper 2, nr 298. Geological survey of Belgium.

151. Couladouros, E.A., Plyta, Z.F., Haroutounian, S.A., and Papageorgiou, V.P. (1997). Efficient synthesis of aminonaphthoquinones and azidobenzohydroquinones: mechanistic considerations of the reaction of hydrazoic acid with quinones. An overview. The Journal of Organic Chemistry, 62: 6-10.

152. Betterton, E.A. (2003). Environmental fate of sodium azide derived from automobile airbags. Critical Reviews in Environmental Science and Technology, 33: 423-458.

153. McIlvin, M.R. and Altabet, M.A. (2005). Chemical conversion of nitrate and nitrite to nitrous oxide for nitrogen and oxygen isotopic analysis in freshwater and seawater. Analytical Chemistry, 77: 5589-5595.

154. Aulakh, M. and Rennie, D. (1985). Azide effects upon N2O emission and transformations of N in soils. Canadian Journal of Soil Science, 65: 205-212.

155. Sidransky, E., Walter, B., and Hollocher, T. (1978). Studies on the differential inhibition by azide on the nitrite/nitrous oxide level of denitrification. Applied and Environmental Microbiology, 35: 247-250.

156. Dilworth, M.J. and Thorneley, R.N. (1981). Nitrogenase of *Klebsiella pneumoniae*. Hydrazine is a product of azide reduction. Biochemical Journal, 193: 971-983.

157. Moses, C.O. and Herman, J.S. (1991). Pyrite oxidation at circumneutral pH. Geochimica et Cosmochimica Acta, 55: 471-482.

158. Zhang, Y.-C., Slomp, C.P., Broers, H.P., Passier, H.F., and Van Cappellen, P. (2009). Denitrification coupled to pyrite oxidation and changes in groundwater quality in a shallow sandy aquifer. Geochimica et Cosmochimica Acta, 73: 6716-6726.

159. Baalsrud, K. and Baalsrud, K.S. (1954). Studies on Thiobacillus denitrificans. Archiv für Mikrobiologie, 20: 34-62.

160. Truche, L., Berger, G., Albrecht, A., and Domergue, L. (2013). Abiotic nitrate reduction induced by carbon steel and hydrogen: implications for environmental processes in waste repositories. Applied Geochemistry, 28: 155-163.

161. Froelich, P.N., Klinkhammer, G., Bender, M.a.a., Luedtke, N., Heath, G.R., Cullen, D., Dauphin, P., Hammond, D., Hartman, B., and Maynard, V. (1979). Early oxidation of organic matter in pelagic sediments of the eastern equatorial Atlantic: suboxic diagenesis. Geochimica et Cosmochimica Acta, 43: 1075-1090.

162. Konhauser, K. (2007). Introduction to geomicrobiology. Blackwell Publishing, Oxford, UK.

163. Till, B.A., Weathers, L.J., and Alvarez, P.J. (1998). Fe(0)-supported autotrophic denitrification. Environmental Science & Technology, 32: 634-639.

164. Hauck, S., Benz, M., Brune, A., and Schink, B. (2001). Ferrous iron oxidation by denitrifying bacteria in profundal sediments of a deep lake (Lake Constance). FEMS Microbiology Ecology, 37: 127-134.

165. Cardoso, R.B., Sierra-Alvarez, R., Rowlette, P., Flores, E.R., Gómez, J., and Field, J.A. (2006). Sulfide oxidation under chemolithoautotrophic denitrifying conditions. Biotechnology and Bioengineering, 95: 1148-1157.

166. Zumft, W.G. (1997). Cell biology and molecular basis of denitrification. Microbiology and molecular biology reviews, 61: 533-616.

167. Kimura, M. (2000). Anaerobic microbiology in waterlogged rice fields. Soil Biochemistry, 10: 35-138.

168. Sorensen, J. (1978). Capacity for denitrification and reduction of nitrate to ammonia in a coastal marine sediment. Applied and Environmental Microbiology, 35: 301-305.

169. Henault, C., Devis, X., Page, S., Justes, E., Reau, R., and Germon, J. (1998). Nitrous oxide emissions under different soil and land management conditions. Biology and Fertility of Soils, 26: 199-207.

170. Forsythe, S., Dolby, J., Webster, A., and Cole, J. (1988). Nitrate-and nitrite-reducing bacteria in the achlorhydric stomach. Journal of Medical Microbiology, 25: 253-259.

171. Rabus, R., Hansen, T.A., and Widdel, F., Dissimilatory sulfate-and sulfur-reducing prokaryotes, in The prokaryotes, Dworkin, M., Falkow, S., Rosenberg, E., Schleifer, K.H., and Stackebrandt, E., Editors. 2006, Springer Science, Singapore. p. 659-768.

172. Greene, E., Hubert, C., Nemati, M., Jenneman, G., and Voordouw, G. (2003). Nitrite reductase activity of sulphate-reducing bacteria prevents their inhibition by nitrate-reducing, sulphide-oxidizing bacteria. Environmental Microbiology, 5: 607-617.

173. Marietou, A., Richardson, D., Cole, J., and Mohan, S. (2005). Nitrate reduction by Desulfovibrio desulfuricans: a periplasmic nitrate reductase system that lacks NapB, but includes a unique tetraheme c-type cytochrome, NapM. FEMS Microbiology Letters, 248: 217-225.

174. Madden, A.S., Smith, A.C., Balkwill, D.L., Fagan, L.A., and Phelps, T.J. (2007). Microbial uranium immobilisation independent of nitrate reduction. Environmental Microbiology, 9: 2321-2330.

175. Griffault, L., Merceron, T., Mossmann, J.R., Neerdael, B., De Cannière, P., Beaucaire, C., Daumas, S., Bianchi, A., and Christen, R. (1996). Acquisition et régulation de la chimie des eaux en milieu argileux pour le projet de stockage de déchets radioactifs en formation géologique: projet "Archimède argile". Final report EUR-17454 FR. European Commission.

176. Bernier, F., Li, X.L., Bastiaens, W., Ortiz, L., Van Geet, M., Wouters, L., Frieg, B., Blümling, P., Desrues, J., Viaggiani, G., Coll, C., Chanchole, S., De Greef, V., Hamza, R., Malinsky, L., Vervoort, A., Vanbrabant, Y., Debecker, B., Verstraelen, J., Govaerts, A., Wevers, M., Labiouse, V., Escoffier, S., Mathier, J.F., Gastaldo, L., and Bühler, C. (2006). SELFRAC: fractures and self-healing withing the excavation disturbed zone in clays. Final report EUR-22585. European Commission.

177. Lin, L.C., and Beuchat, L.R. (2007). Survival of *Enterobacter sakazakii* in infant cereal as affected by composition, water activity, and temperature. Food Microbiology, 24, 767-777.

178. Rizoulis, A., Steele, H.M., Morris, K., Lloyd, J.R. (2012). The potential impact of anaerobic microbial metabolism during the geological disposal of intermediate-level waste. Mineralogical Magazine, 76: 3261-3270.

179. Padan, E., Bibi, E., Ito, M. and Krulwich, T.A. (2005). Alkaline pH homeostasis in bacteria: New insights. Biochimica et Biophysica Acta, 1717: 67-88.

10 Acknowledgements

This work is undertaken in close co-operation with, and with the financial support of ONDRAF/NIRAS, the Belgian Agency for the Management of Radioactive Waste and Enriched Fissile Materials, as part of its programme on geological disposal of medium-level long-lived waste.

The authors wish to acknowledge Sven Aerts, Marc Aertsens, Christophe Bruggeman, Katrien Hendrix, Norbert Maes, Hugo Moors, Mirela Vasile, Lian Wang, and Eef Weetjens (all SCK•CEN), Pierre De Cannière (FANC; ex-SCK•CEN), Maarten Van Geet (ONDRAF/NIRAS; ex-SCK•CEN), and Evelien Martens (ex-SCK•CEN) for their contributions to the experimental and/or modelling work and/or for the discussions on the results. The technical assistance of Patrick Boven, Marc Van Gompel, Louis Van Ravesteyn, Steven Smets, and Wim Verwimp (SCK•CEN) is greatly appreciated. Christophe Bruggeman, Hugo Moors, Karine Ferrand, and Norbert Maes are thanked for the review of the report.

Annex 1: Electrical Double Layer (EDL) theory to estimate the thickness of the EDL [43]

The Electrical Double Layer (EDL) theory allows to obtain concentration profiles of cations and anions as a function of the distance from the clay surface. These concentration profiles are related to the electrical potential profile near the surface. Based on the classical Gouy-Chapman EDL-theory, an expression for the electrical potential profile can be derived from a combination of the Poisson equation and the Boltzmann equation. Other approaches (based on the Gouy-Chapman model) could also be followed to derive similar expressions for the concentration profiles (*e.g.* Sparks [44]; Moors [107]). However, these approaches will not be discussed in this report.

The **Poisson equation** describes the relationship between the electrical potential ψ (J C^{-1}) at a distance x of the clay surface and the local net charge density ρ_e (C m^{-3}).

$$\frac{d^2\psi}{dx^2} = -\frac{\rho_e}{\varepsilon} \qquad \text{(A1.1)}$$

where ε (F m^{-1}) is the dielectric constant of the solution.

For a single clay surface in equilibrium with the bulk solution, the electrochemical potential of the ions is constant. This ultimately results in the **Botzmann equation**:

$$n_i = n_i^0 \exp\left(-\frac{z_i e\psi}{k_b T}\right) \qquad \text{(A1.2)}$$

where n_i and n_i^0 are the number of ions of type i, respectively near and far away from the clay surface, $z_i e$ is the ionic charge of ion i, k_b is the Boltzmann constant and T is the temperature.

Note that this equation is valid for a single clay surface in an (theoretically) infinitely large liquid phase so that in the liquid phase far away from the charged surface the electrical potential is zero and the ionic concentrations are equal to the bulk ionic concentrations (boundary conditions). The net charge density per unit is proportional to the local concentration difference between cations and anions:

$$\rho_e = \sum_i z_i n_i e \qquad \text{(A1.3)}$$

By introducing equations A1.2 and A1.3 in equation A1.1, assuming symmetrical electrolytes (in clay water), and introducing the Debye-Hückel approximation, *i.e.* assuming a low surface charge density, the Poisson equation can be rewritten as:

$$\frac{d^2\psi}{dx^2} = \kappa^2\psi \qquad \text{(A1.4)}$$

where the parameter κ (m^{-1}) was introduced to simplify the equation, and is proportional to the square root of the ionic strength:

$$\kappa = \sqrt{\frac{2e^2 \sum_i z_i^2 n_i}{\varepsilon k_b T}} \quad \text{(A1.5)}$$

Equation A1.4 can be solved to obtain the electrical potential profile $\psi(x)$:

$$\psi = \psi_0 e^{-\kappa x} = \psi_0 e^{-a\sqrt{I}x} \quad \text{(A1.6)}$$

where ψ_0 (J C^{-1}) is the surface potential, a (m^{-1}) is a proportionality constant, and I is the ionic strength. The physical constant κ can be seen as an "equivalent Double Layer Thickness", since the potential at $x = \kappa^{-1}$ is decayed to ψ_0/e. The concentration profiles of the cations and anions near the clay surface can then be calculated by introducing equation A1.6 in the Boltzmann distribution (equation A1.2).

The electrical potential profile (equation A1.6) allows to draw the following conclusions on the effect of increased ionic strength and valence of the cations on the EDL thickness:

(i) The thickness of the EDL layer decreases as the ionic strength increases;
(ii) The EDL layer is thinner for higher valence clay cations.

Annex 2: Overview of the chemical composition of RBCW, sampled from the EG/BS piezometer [6]

Over the years, 74 pore water samples from the EG/BS piezometer[46] were analysed, resulting in a large dataset. In Table A2.1, the minimum, maximum, mean and median values of the ionic concentrations are given.

Table A2.1: Chemical composition of RBCW sampled from the EG/BS piezometer [6]. Min. = minimum; Max. = maximum; n/a = not analysed.

	Concentration (mg L^{-1})			
Chemical element	***Min.***	***Max.***	***Mean***	***Median***
Ca	3.1	5.4	3.9	3.9
Fe	0.5	4.6	1.1	1.0
Mg	1.7	4.0	3.0	3.0
K	5.2	13.1	9.3	9.4
Si	1.2	21.2	3.0	2.3
Na	390	467	410	410
F^-	2.7	4.3	3.2	3.1
Cl^-	23.5	34.8	26.0	25.9
Br^-	0.5	0.8	0.5	0.5
SO_4^{2-}	0.3	1.5	0.6	0.4
HCO_3^-	728	4425	1048	871
TIC	143	871	206	171
DOC	78	160	96	89

The composition of SICZH (Synthetic Boom Clay Water) is:

0.11 mM $MgCl_2.6H_2O$, 0.34 mM KCl, 0.17 mM NaCl, 13.93 mM $NaHCO_3$, 0.70 mM H_3BO_3, 0.18 mM SiO_2, 0.039 mM $Na_2HPO_4.12H_2O$, 0.26 mM NaF and 0.02 mM $FeCl_2.4H_2O$.

[46] The EG/BS piezometer was one of the first piezometers installed in the HADES Underground Research Laboratory (Mol, Belgium). It is installed at a depth of -260 m and in contact with the silty layer of the Boom Clay formation. After the installation of the piezometer, the borehole was filled with an uncharacterised material (gravel). EG/BS clay water (or RBCW) is considered, with the exception of the Na^+ concentration, to be a good reference model water for Boom Clay [6].

Annex 3: Microorganisms in the Boom Clay surrounding a disposal gallery for Eurobitum

There are several ways in which microorganisms could become part of the repository environment. By far, the most likely is external contamination, *i.e.* introduction of microorganisms during the construction of the disposal facility. In addition to this, any indigenous microbial species still present in niches of the Boom Clay might be stimulated to grow and become active due to physico-chemical changes during excavation and the operational stage of the disposal facility (*e.g.* oxygen, large space, …). In these aerobic conditions, aerobic respiration is the primary metabolic pathway, as it generates the largest free energy yield per mol electron donor (*e.g.* organic carbon; Figure A3.1). Furthermore, aerobes are equipped with a range of enzymes capable of degrading complex organic molecules. The trapped oxygen is however expected to be consumed rather quickly by oxidation of metal, organic matter and pyrite, as well as radiooxidation of bitumen. Upon depletion of oxygen, the microbial community will shift to a rather anaerobic community, which could use NO_3^-, NO_2^-, Mn(IV), Fe(III), SO_4^{2-} or CO_2 as electron acceptor, depending on their availability and with a preference towards the acceptor (and reduction mechanism) yielding the highest amount of energy. The latter explains why methanogenesis only occurs when all other electron acceptors are exhausted (Figure A3.1; [161]). Because of the expected rapid resaturation of the gallery and the leaching of $NaNO_3$ from Eurobitum, nitrate may appear relatively early at the interface of the gallery with the clay [29], thereby stimulating Nitrate Reducing Prokaryotes in the Boom Clay surrounding the disposal gallery. Once all nitrate is reduced, other microbial species would become more dominant, such as Sulphate Reducing Prokaryotes (or related species) consuming the sulphate which is expected to leach from Eurobitum and be produced from pyrite oxidation. Finally, Methane Producing Archaea are expected to become active when all other electron acceptors are depleted. The presence of a disposal facility for Eurobitum in the clay would also result in the leaching of radionuclides into the clay, which could be reduced by Metal-Reducing Prokaryotes.

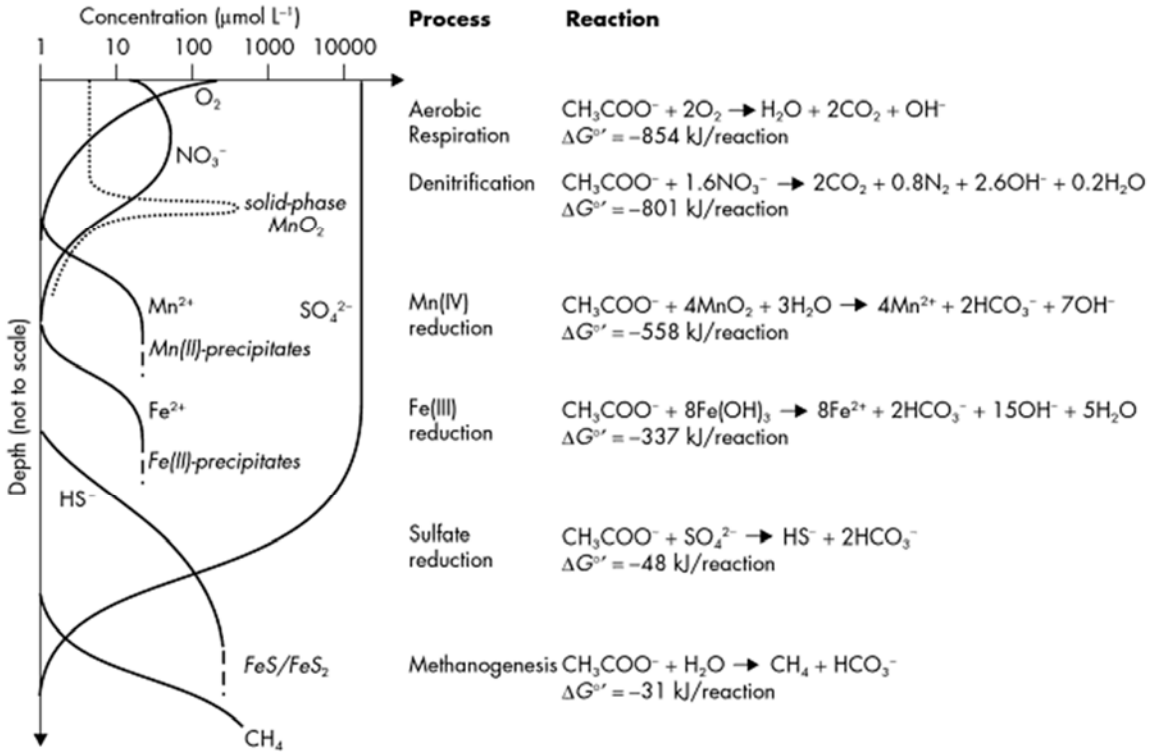

Figure A3.1: Idealised pore water and solid phase concentration profiles of O_2, nitrate, manganese, iron, sulphate, methane and some of their reduced compounds in a marine sediment. The calculations are based on the theory of successive utilisation of terminal electron acceptors during decomposition of organic matter (adapted from Froelich *et al.* [161] by Konhauser [162]). The depth at which the different processes occur can vary extensively. The Gibbs free energy changes were calculated at standard conditions and at the biochemical reference state (pH 7).

Nitrate and Nitrite Reducing Prokaryotes

In anaerobic soils, nitrate is an important electron acceptor and can be reduced to nitrite and subsequently converted to more reduced N species like NO_2^- (through DNRN or dissimilative nitrate reduction to nitrite), NO, N_2O, N_2 (through denitrification or through anammox or anaerobic ammonium oxidation in the presence of NH_4^+), or NH_3 (through DNRA or dissimilative nitrate reduction to ammonium). FeS_2, Fe(0), Fe(II), H_2, reduced inorganic sulphur compounds or organic compounds can all serve as electron donors for nitrate and nitrite reducers [57, 58, 60, 115, 163-165]. Furthermore, microbial nitrate (and nitrite) reduction is performed both by heterotrophic and autotrophic microorganisms, respectively using organic C and inorganic C sources [76].

The end products of denitrification are usually N_2 or N_2O, as microorganisms tend to minimise the accumulation of high concentrations of toxic intermediate products like nitrite or NO [58], although accumulation of nitrite has also been observed under certain conditions [66, 67]. The DNRA process is a reduction of nitrate or nitrite to ammonium, followed by the excretion of NH_4^+ (or NH_3 under high pH conditions) into the medium [59, 166]. Studies have shown that in soils microbial populations capable of DNRA are slightly more numerous than those of denitrifiers [147, 167, 168]. Whether denitrification or DNRA would occur in a soil is

principally related to the soil oxidation status and the C/NO_3^- ratio, *i.e.* an excess of biodegradable DOM compared to nitrate and more reducing conditions appear to promote DNRA over denitrification. Indeed, under these conditions, DNRA has the advantage over denitrification since more electrons can be transferred per mol NO_3^-, making the energy yield per mol nitrate is higher for DNRA [147].

All of the above mentioned microbial nitrate reduction processes are applied to generate energy (dissimilative pathways, Figure A3.2). On the other hand, nitrate and N_2 can also be reduced to an organic nitrogen source (assimilative nitrate reduction), which can be used for biosynthesis (assimilative pathway, Figure A3.2) [76].

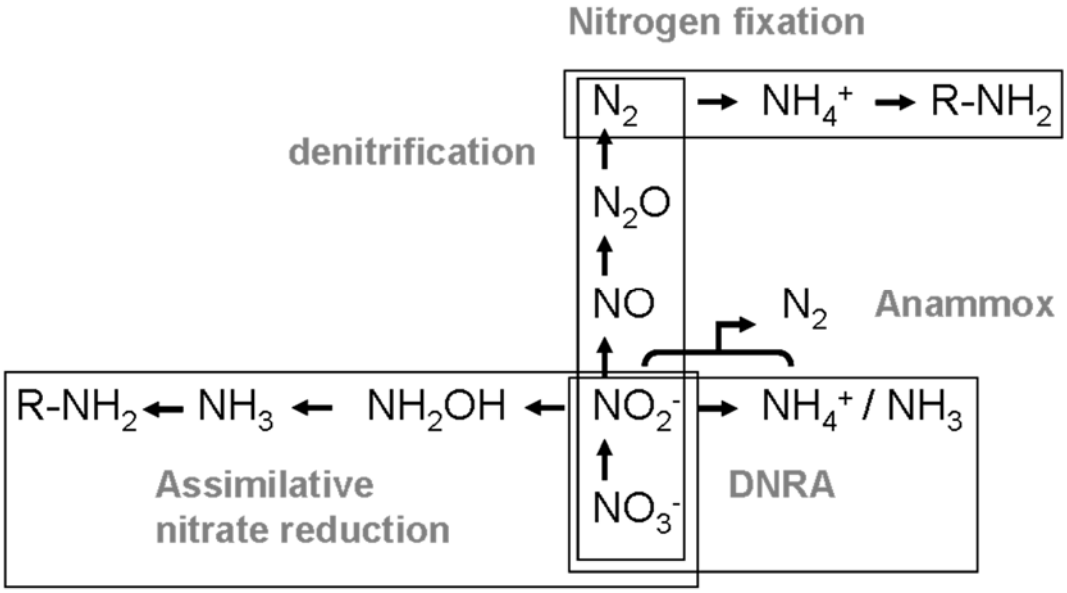

Figure A3.2: Overview of the some of the metabolic reactions of the nitrogen cycle, performed by anaerobic microorganisms. The assimilative pathway (assimilative nitrate reduction) leads to the incorporation of nitrogen atoms into organic molecules in the cell during biosynthesis. All other indicated reactions are dissimilative pathways, *i.e.* denitrification, dissimilative nitrate reduction to ammonium (DNRA) and anaerobic ammonium oxidation (anammox), which all lead to the production of ATP during anaerobic respiration [59, 76, 166]. Usually, only part of the reactions indicated here can be performed by one type of microorganism, as the enzymes needed for completing the entire metabolism are generally not present in one microbial species.

Only a few prokaryotic genera (both anaerobic as aerobic) are able to use nitrogen gas as a source of nitrogen for their biosynthesis, a process called nitrogen fixation. In the microbial N_2 fixation process, N_2 is reduced to ammonium, which is subsequently converted to an organic N compound (Figure A3.2). Due to the stability of the nitrogen triple bond in N_2, this molecule is extremely inert and its activation is a very energy-demanding process [76].

As a range of specific enzymes is necessary to perform these microbial pathways, a combination of different microbial species is required to perform the entire N cycle in the soil [76, 169]. Some of these microbial species are able to express multiple enzymes, which are used in different pathways. These species can therefore choose to perform the reaction for which the oxidised nitrogen compound is present and which would generate the most energy [58, 76]. A distinction should be made between Nitrate and Nitrite Reducing Prokaryotes (respectively NRP and NiRP). Some microbial species can reduce both nitrate and

nitrite, although in some of them, the potential rate of nitrate reduction appears to be considerably higher than that of the nitrite reduction. Conversely, some Nitrite Reducing Prokaryotes are only able to reduce nitrite and not nitrate to gaseous N compounds [170].

Sulphate- and Thiosulphate- Reducing Prokaryotes

Assimilative sulphate reduction, which is widespread in prokaryotes and plants, yields reduced sulphur for biosynthesis, which is only released into the environment upon decay of the biomass. On the other hand, dissimilative sulphate reduction directly produces free sulphide. The reduction of sulphate to sulphide proceeds via various intermediates, but – in contrast to denitrification – the excretion of the intermediate oxidation states is extremely rare, implying that in nearly all cases the final product is sulphide [Figure A3.3].

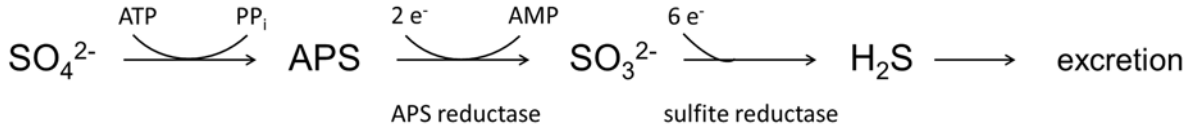

Figure A3.3: Dissimilatory reduction of sulphate to sulphide adapted from Madigan *et al.* [76]. PP_i: pyrophosphate; APS: adenosine 5'-phosphosulphate; AMP: adenosine monophosphate.

Certain variations on the general metabolism can however be observed. Several bacteria are unable to reduce sulphate (through a dissimilative process) but can instead reduce sulphite, thiosulphate or elemental sulphur to sulphide. Furthermore, certain SRP (or related organisms) are capable of generating energy via disproportionation. In this inorganic sulphur-based fermentation process, part of the S-compounds will end up more oxidised, while the remaining S will be more reduced [171].

These microbial species are a very heterogeneous group, which are capable of utilizing a wide range of low-molecular mass organic compounds (alcohols, polar aromatics, aliphatic acids, hydrocarbons), but also H_2, as possible electron donors. Furthermore, besides the use of sulphur species as electron acceptor, some of them are also able to reduce nitrate or nitrite to ammonium [171-173]. This is most likely evolved as a defence mechanism against inhibition of dissimilatory sulphate reduction by toxic N species (*i.e.* nitrite and in high concentrations also nitrate) [172].

Methane-producing Archaea or MPA

A large variety of Archaea can produce methane gas as part of their energy metabolism. Methanogens only grow under strictly anaerobic conditions, and depending on the species, can be autotroph or heterotroph [76]. Through a combination of syntrophic bacteria and methanogens, virtually any organic compound can eventually be reduced to methane [58].

Several substrates can be used by different populations of methanogens to produce methane and can therefore be divided into three classes, *i.e.* CO_2-type substrates (*e.g.* H_2 combined with CO_2 as most important substrate), methyl-containing substrates, and acetate. H_2 is one of the most important precursors of methane in anoxic soils, contributing to ~10 to 50% of the total CH_4 production. In anoxic soils, the production of H_2 due to fermentation of organic matter can be intensive, but most of the produced H_2 and CO_2 can immediately be converted to CH_4 by methanogens, thereby preventing its accumulation [58, 145].

Nevertheless, due to its low energy yield (Figure A3.1), microbial methane production can normally only occur when CO_2 or organic compounds with only one or a few carbon atoms (*e.g.* formate, acetate, methylated substrates) are the only remaining electron acceptors in the environment [58, 161], and would therefore not occur in the presence of nitrate and/or nitrite.

Metal-reducing Prokaryotes

Metal–reducing Prokaryotes, which can be present and active in clay, are able to reduce and thereby immobilise dissolved U(VI) from their surroundings (bioimmobilisation). However, a high nitrate concentration often hinders the activity of these bacteria is. Nonetheless, some of these species are nitrate-indifferent, which allows them to reduce uranium despite a nitrate presence [72, 174].

Factors restricting microbial growth and activity in and around the disposal gallery for Eurobitum

The chemical composition of the Boom Clay (pore water) in combination with leached inorganic (NO_3^-, NO_2^-, SO_4^{2-}, …) and organic Eurobitum (acetate, formate, oxalate, …) degradation products as well as H_2 (from radio-oxidation of bitumen and anaerobic corrosion of steel) would provide sufficient nutrients, electron donors and acceptors for microbial growth and activity in the disturbed Boom Clay surrounding the disposal gallery for Eurobitum. Nevertheless, other factors will restrict microbial activity and growth in the repository.

First of all, in undisturbed conditions, the low permeability and small pore sizes of the Boom Clay acts as a barrier to the microbial movement. Indeed, as the smallest active microorganisms measure ~1 µm in diameter and ultramicrobacteria (UMB; small non-growing but active prokaryotes) can even be smaller than 0.3 µm in size [74], they are too large to move freely through the pores of the Boom Clay (mean pore size 35-45 nm [117]). Furthermore, the pore size distribution likely also impacts the microbial cell growth and activity. Because of the restrictions in space, bioavailable nutrients, and/or electron donors in the undisturbed clay formation, prokaryotes will be present when possible, but likely in an inactive dormant state such as endospores (diameter smaller than pore size Boom Clay). This explains also why bacteria were found in 'undisturbed' Boom Clay' by molecular and conventional microbiological (culturing and microscopic observations) techniques, although the concentration was rather low (about 10^3 bacteria per gram clay) [73, 175].

The excavation of a disposal gallery results in the formation of an excavation damaged zone (EDZ), characterised by the creation of fissures and the general increase of the porosity upon relaxation of the clay. As observed in a microbial study previously carried out in disturbed Boom Clay, microorganisms can readily contaminate the clay near a gallery during this excavation process. The bacterial concentration appears to decrease as a function of distance from the gallery, with only a few bacteria detectable at more than 80 cm from the wall [73]. These results can be explained by the disturbances of the clay in the EDZ (excavation damaged zone) during the mining process, which probably allowed the ingress of the microorganisms into this zone and/or the 'awakening' of dormant microbes, following the creation of fissures and the general increase of the porosity upon relaxation of the clay. However, as self-sealing of fractures occurs in a relatively short time in the Boom Clay, thereby restoring the porosity [176], it can be expected that the zone in which the microorganisms can be active in the Boom Clay will also decrease accordingly in time. Yet, it is likely that small but nonetheless sufficiently large niches will remain to exist, enabling microbial activity in the clay layer surrounding the disposal gallery for Eurobitum.

A second important factor restricting the microbial growth and activity in Boom Clay is the low bioavailability of nutrients, *i.e.* nutrients are only available through dissolution of minerals and diffusion through the pores. Therefore, microbial growth and activity in Boom Clay without influx of extra nutrients and electron donors/acceptors is assumed to be limited [73]. In the case of the clay surrounding the repository of Eurobitum, additional electron donors and acceptors will be provided by the waste form (*i.e.* leached nitrate, bitumen degradation products such as acetate). However, the leaching of salts from the Eurobitum waste in the repository will result in a (locally) increased salt concentration in the Boom Clay pore water and therefore in a decrease in water activity (or water availability for microorganisms). Most microorganisms are unable to cope with very low water activities and either die or become dehydrated and dormant under such conditions. Gram-negative bacteria are generally not able to grow and be active below water activity values of 0.96, while most Gram-positive bacteria are hindered below a water activity of 0.9 [177]. On the other hand, some microorganisms (halophilic species) grow optimally under lower water activity (0.8-0.9) [76]. Expect for spore-forming bacteria, most prokaryotes cannot survive water activities below 0.6, although a few exceptions exist which are able to survive at extremely low water activities [76, 177]. As shown in Section 3, the maximum $NaNO_3$ concentration in the Boom Clay (at the interface with the gallery) is expected to be ~1 M $NaNO_3$, corresponding to a water activity of ~0.97. The expected $NaNO_3$ plume would therefore not (substantially) restrict the microbial growth and activity in the Boom Clay, although it might inhibit growth of osmosensitive species, thereby reducing the biodiversity of the microbial population. On the other hand, the rather high $NaNO_3$ in the Boom Clay at the interface with the disposal gallery (*i.e.* 1 M $NaNO_3$) could inhibit the nitrate reducing activity, as observed in the batch tests with Boom Clay slurries (Section 6.4.1) and in the percolation tests (Section 6.1.2.2). Note however that the limit of resistance appears to be depending on the microbial species.

Thirdly, the alkaline environment in and around the disposal gallery might restrict microbial activity. Indeed, the Belgian concept for the geological disposal of radioactive waste considers the use of high amounts of cement in the design of the repository for Eurobitum, highly alkaline (pH > 12.5) cement-equilibrated water will fill the voids in the disposal gallery during at least several thousands of years. Most non-extremophilic bacteria grow over a broad range of external pH values, from 5.5– 9.0 [179]. Under highly alkaline conditions (pH >

12.5) microbial activity, growth and even survival is limited to certain extreme alkaliphilic microorganisms [76, 148]. To be able to survive in alkaline conditions, microorganisms must maintain a near-neutral cytoplasmic pH, which is done by a number of possible adaptive strategies: (1) increased metabolic acid production; (2) increased production of ATP synthase that couples proton entry to ATP generation; (3) changes in cell surface properties; and (4) increased expression and activity of monovalent cation/proton antiporters [179]. In certain microorganisms, adaptation to a high pH can thus at some level stimulate certain microbial metabolic processes. Depending on the extent of the adaptive strategies, every alkaliphilic species has its specific external pH range optimal for growth. Outside of this pH range, growth and activity is assumed to decrease since the microbial species would not be able to maintain its cytoplasmic pH. Whether or not the microbial population present in a disposal gallery for Eurobitum will be viable and active at pH above 12.5 and the extent of this activity seems to be depending on the species, their potential to work together in the community and their optimal pH for growth [76, 148, 178] as well as other restricting factors such as appropriate nutrient availability, space restriction, ...

A less alkaline pH is expected however at the boundary between the concrete liner and the Boom Clay (pH 10 to 10.5), and an even lower pH of 8 to 9 is expected further in the Boom Clay [31]. These pH conditions allow growth and activity of (nitrate reducing) microorganisms as was observed for the microbial population obtained from a natural high pH sediment (pH ~11) analogous to the host rock surrounding a repository [178]. Note that certain alkaliphilic microorganisms (mostly archaea) are also halophilic and could therefore survive both under high ionic strength and high pH conditions (thus inside the disposal gallery) [76].

Lastly, small increases in pressure above atmospheric pressure can stimulate microbial growth and activity. However, when the pressure continues to increase, the microbial metabolic processes will eventually be completely inhibited at higher pressures (threshold depending on the species *e.g.* 65 MPa for SRP [78]). This implies that the relatively low hydrostatic pressure (2.2 MPa) in the Boom Clay at a depth of -220 m should not be a barrier to the microbial activity.

In conclusion, at the boundary between the concrete liner and the Boom Clay, the space conditions are the most favourable for microbial growth and activity compared to the undisturbed clay formation. Here, the expected maximum $NaNO_3$ concentration could however inhibit microbial activity, although this is depending on the species. Both the $NaNO_3$ plume and the alkaline plume are expected not to inhibit the microbial population completely, but rather cause a shift towards a less diverse alkaliphilic population. The extent of the microbial activity will depend on the microbial community present and their adaptation to high pH, as well as other restricting factors such as appropriate nutrient availability. This should be investigated further.

Annex 4: Brief overview of transport parameters [36]

During percolation tests, the transport of a solute through a clay volume is dispersion-driven. Dispersive transport is a combination of diffusion and mechanical dispersion of solute. The standard one-dimensional flux of a solute (J_x) through a clay volume is therefore described as the sum of the advective flux ($J_{x,a}$) and the dispersive flux ($J_{x,d}$):

$$J_x = J_{x,a} + J_{x,d} = V_{Darcy}C - \eta D^i_{pore}(\delta C/\delta x) \quad \text{(A4.1)}$$

With V_{Darcy} the Darcy velocity (m s^{-1}), C the liquid phase solute concentration (mol L^{-1}), η the diffusion accessible porosity (-) and D^i_{pore} the pore dispersion coefficient. According to Darcy's law, the Darcy velocity is the water flow out of the clay volume:

$$V_{Darcy} = K_{hydro}\, \Delta P/(L\, \rho.g) \quad \text{(A4.2)}$$

with K the hydraulic conductivity (m s^{-1}), ΔP the pressure gradient exerted over the clay (in Pa), L the length of the clay volume (m), ρ is the density of the solution (kg m^{-3}) and g is the gravity (m s^{-2}).

As solute transport inside the clay volume can only occur through the pores, the pore velocity V_{pore} and the pore dispersion coefficient D^i_{pore} are introduced, similar to equation A4.1.

$$V_{pore} = V_{Darcy}/\eta \quad \text{(A4.3)}$$

$$D^i_{pore} = D_{pore} + \alpha V_{pore} \quad \text{(A4.4)}$$

with D_{pore} the pore diffusion coefficient and α (m) the dispersion length.

Based on equations A4.1-4 and under conditions where a constant V_{Darcy}, η and D^i_{pore} are valid, the rate of mass change through a clay volume is described as the standard one-dimensional advection-dispersion equation:

$$\delta C/\delta t = D^i_{pore}\, \delta^2 C/\delta x^2 - V_{pore}\, \delta C/\delta x \quad \text{(A4.5)}$$

However, when the solute is retarded due to sorption, the equation takes into account the adsorbed solute concentration C_{ads} (mol kg^{-1}):

$$\delta C/\delta t + \rho_b/\eta\, \delta C_{ads}/\delta t = D^i_{pore}\, \delta^2 C/\delta x^2 - V_{pore}\, \delta C/\delta x \quad \text{(A4.6)}$$

with ρ_b the dry bulk density of the clay (kg m^{-3}) and C_{ads} the adsorbed solute concentration, which is expressed as K_dC (with K_d the solid-liquid distribution coefficient) when linear and reversible sorption of the solute is assumed.

For retarded solutions, the following one-dimensional advection-dispersion equation can therefore be derived (equation A4.7) when following parameters are introduced (equations A4.8-10):

$$\delta C/\delta t = D^i_{app}\, \delta^2 C/\delta x^2 - V_{app}\, \delta C/\delta x \quad \text{(A4.7)}$$

hereby introducing the retardation factor R, the apparent dispersion coefficient D^i_{app} and the apparent velocity V_{app}:

$$R = 1 + \rho_b K_d/\eta \quad \text{(A4.8)}$$

$$D^i_{app} = D^i_{pore}/R \quad \text{(A4.9)}$$

$$V_{app} = V_{pore}/R \quad \text{(A4.10)}$$

Similar to equation A4.4, D^i_{app} is a linear function of V_{app}:

$$D^i_{app} = D_{app} + \alpha V_{app} \quad \text{(A4.11)}$$

with D_{app} expressed as D_{pore}/R.

Another frequently used diffusion parameter is the effective diffusion coefficient, D_{eff} ($m^2\ s^{-1}$), which describes the diffusive behaviour of a species in the porous medium as a whole:

$$D_{eff} = D_{app}\, \eta R = D_{pore}\, \eta \quad \text{(A4.12)}$$

Annex 5: Batch tests with Boom Clay slurries: complete set of results of chemical analysis

Table A5.1: Chemical analysis of the supernatant of Boom Clay slurries with 100 mM $NaNO_2$ after 3, 7 or 17 weeks of incubation in an anaerobic glove box. The slurries had a solid to liquid weight ratio of 1/100 g Boom Clay per g RBCW. No microbial inhibitor was added to the blank sample. Values denoted by "-" were not measured. All values are given in mg L^{-1}. The uncertainty on the concentrations is 6% (in presence of N_3^- up to 20%) for $[NO_2^-]$ and $[NO_3^-]$ and 4% for $[SO_4^{2-}]$.

Inhibitor	*$[NO_2^-]$ (mg L^{-1})*			*$[NO_3^-]$ (mg L^{-1})*			*$[SO_4^{2-}]$ (mg L^{-1})*		
	3	*7*	*17*	*3*	*7*	*17*	*3*	*7*	*17*
blank	4.44 10^3	4.36 10^3	4.32 10^3	30.4	30.5	31.6	< 0.25	< 0.25	0.31
0.1 wt% $HgCl_2$	4.46 10^3	4.85 10^3	4.36 10^3	689	672	686	< 0.25	0.41	0.58
0.5 wt% $HgCl_2$	4.34 10^3	4.50 10^3	4.34 10^3	123	124	124	0.35	0.35	0.83
0.1 wt% NaN_3	4.32 10^3	3.51 10^3	4.08 10^3	30.2	31.4	31.4	< 0.25	< 0.25	0.38
1 wt% NaN_3	4.37 10^3	4.10 10^3	4.32 10^3	44.8	47.1	48.0	1.24	< 0.25	0.32
0.1 wt% CH_2O	4.38 10^3	4.07 10^3	4.34 10^3	45.4	49.3	47.1	< 0.25	< 0.25	0.26
1 wt% CH_2O	4.21 10^3	3.88 10^3	4.06 10^3	38.8	39.6	39.4	< 0.25	< 0.25	0.40

	$[N_3^-]$ (mg L^{-1})			*[Hg] (mg L^{-1})*		
	3	*7*	*17*	*3*	*7*	*17*
blank	-	-	-	-	-	-
0.1 wt% $HgCl_2$	-	-	-	67	50	26
0.5 wt% $HgCl_2$	-	-	-	1.38 10^3	1.05 10^3	0.92 10^3
0.1 wt% NaN_3	0.69 10^3	0.70 10^3	0.66 10^3	-	-	-
1 wt% NaN_3	6.1 10^3	6.2 10^3	6.1 10^3	-	-	-
0.1 wt% CH_2O	-	-	-	-	-	-
1 wt% CH_2O	-	-	-	-	-	-

Table A5.2: Chemical analysis of the supernatant of Boom Clay slurries with 100 mM $NaNO_3$ or1 M $NaNO_3$ in the last two samples (denoted in the table)] after 3, 7 or 17 weeks of incubation in an anaerobic glove box. The slurries had a solid to liquid weight ratio of 1/10 or 1/100 g Boom Clay per g RBCW (denoted as 1/10 or 1/100 in the table). No microbial inhibitor was added to the blank samples. Values denoted by "-" were not measured. All values are given in mg L^{-1}. The uncertainty on the concentrations is 6% (in presence of N_3^- up to 20%) for [NO_2^-] and [NO_3^-] and 4% for [SO_4^{2-}]. Tricl. = Triclosan; Chlor. = Chloramphenicol; % = wt%.

Inhibitor	*[NO_3^-] (mg L^{-1})*			*[NO_2^-] (mg L^{-1})*			*[SO_4^{2-}] (mg L^{-1})*		
	3	*7*	*17*	*3*	*7*	*17*	*3*	*7*	*17*
1/10 clay slurry with 100 mM $NaNO_3$									
blank_a	6.41 10^3	6.41 10^3	6.64 10^3	37.8	35.6	40.6	0.97	0.95	1.65
0.1% $HgCl_2$	5.92 10^3	5.97 10^3	6.14 10^3	30.6	19	10.8	2.06	0.85	0.93
0.5% $HgCl_2$	6.04 10^3	6.03 10^3	6.22 10^3	< 0.5	< 0.5	< 2.5	1.53	1.82	2.88
0.1% NaN_3	5.95 10^3	6.29 10^3	6.23 10^3	< 0.25	< 0.25	< 0.25	0.66	0.63	0.8
1% NaN_3	5.63 10^3	6.10 10^3	6.13 10^3	< 0.25	< 0.25	< 0.25	0.66	0.61	0.76
0.1% CH_2O	6.00 10^3	6.02 10^3	6.28 10^3	< 0.25	< 0.25	< 0.25	0.64	0.61	0.66
1% CH_2O	5.99 10^3	6.00 10^3	6.30 10^3	< 0.25	< 0.25	< 0.25	0.77	0.7	0.87
blank_b	6.35 10^3	6.21 10^3	6.21 10^3	32.4	30.9	31.1	0.66	1.17	2.94
10 µM Tricl.	6.11 10^3	5.94 10^3	5.79 10^3	< 0.25	< 0.25	< 0.25	0.39	0.45	0.33
100 µM Tricl.	5.51 10^3	4.31 10^3	< 0.25	512	1.08 10^3	2.78 10^3	< 0.25	< 0.25	< 0.25
1000 µM Tricl.	4.76 10^3	1.98 10^3	< 0.25	0.90 10^3	2.39 10^3	2.83 10^3	< 0.25	< 0.25	1.42
20 mg L^{-1} Chlor.	4.76 10^3	1.64 10^3	1.33 10^3	0.91 10^3	2.58 10^3	2.73 10^3	< 0.25	< 0.25	4.23
200 mg L^{-1} Chlor.	4.32 10^3	482	< 0.25	1.16 10^3	3.30 10^3	252	< 0.25	< 0.25	< 0.25
1000 mg L^{-1} Chlor.	5.50 10^3	4.05 10^3	0.99 10^3	583	1.02 10^3	3.07 10^3	< 0.25	< 0.25	1.74
1/10 clay slurry with 1 M $NaNO_3$									
blank	-	46.6 10^3	49.5 10^3	-	< 10	< 20	-	< 0.5	< 2
0.1% $HgCl_2$	-	49.6 10^3	52.2 10^3	-	< 0.5	< 10	-	< 0.5	< 2

Continuation Table A5.2:

Inhibitor	*[N_3^-] (mg L^{-1})*			*[Hg] (mg L^{-1})*			*[Cl^-] (mg L^{-1})*		
	3	*7*	*17*	*3*	*7*	*17*	*3*	*7*	*17*
1/10 clay slurry with 100 mM $NaNO_3$									
blank_a	-	-	-	-	-	-	-	-	-
0.1% $HgCl_2$	-	-	-	0.017	< 0.1	0.07	-	-	-
0.5% $HgCl_2$	-	-	-	0.55	0.74	0.11	-	-	-
0.1% NaN_3	0.66 10^3	0.64 10^3	0.62 10^3	-	-	-	-	-	-
1% NaN_3	6.0 10^3	6.1 10^3	6.0 10^3	-	-	-	-	-	-
0.1% CH_2O	-	-	-	-	-	-	-	-	-
1% CH_2O	-	-	-	-	-	-	-	-	-
blank_b	-	-	-	-	-	-	25.5	26.3	26.1
10 µM Tricl.	-	-	-	-	-	-	23.8	24.7	24.9
100 µM Tricl.	-	-	-	-	-	-	25.0	24.9	25.4
1000 µM Tricl.	-	-	-	-	-	-	24.7	24.7	25.1
20 mg L^{-1} Chlor.	-	-	-	-	-	-	24.7	25.0	25.2
200 mg L^{-1} Chlor.	-	-	-	-	-	-	25.4	25.1	26.6
1000 mg L^{-1} Chlor.	-	-	-	-	-	-	27.8	28.3	28.8
1/10 clay slurry with 1 M $NaNO_3$									
blank	-	-	-	-	-	-	-	-	-
0.1% $HgCl_2$	-	-	-	-	0.1	< 0.05	-	-	-

Continuation Table A5.2:

Inhibitor	*$[NO_3^-]$ (mg L^{-1})*			*$[NO_2^-]$ (mg L^{-1})*			*$[SO_4^{2-}]$ (mg L^{-1})*		
	3	*7*	*17*	*3*	*7*	*17*	*3*	*7*	*17*
1/100 clay slurry with 100 mM $NaNO_3$									
blank_a	5.60 10^3	5.62 10^3	5.91 10^3	13.6	15.1	16.6	< 0.25	< 0.25	0.74
0.1% $HgCl_2$	5.64 10^3	5.67 10^3	5.92 10^3	< 0.5	< 0.5	< 1	0.34	0.54	3.63
0.5% $HgCl_2$	5.41 10^3	5.29 10^3	5.71 10^3	< 0.5	< 0.5	< 2.5	0.45	0.91	1.98
0.1% NaN_3	5.53 10^3	5.79 10^3	5.75 10^3	< 0.25	< 0.25	0.25	0.27	< 0.25	< 0.25
1% NaN_3	5.38 10^3	6.05 10^3	5.85 10^3	< 0.25	< 0.25	< 0.25	< 0.25	< 0.25	< 0.25
0.1% CH_2O	5.65 10^3	5.39 10^3	6.06 10^3	< 0.25	< 0.25	< 0.25	< 0.25	< 0.25	< 0.25
1% CH_2O	5.63 10^3	5.69 10^3	5.98 10^3	< 0.25	< 0.25	< 0.25	< 0.25	< 0.25	< 0.25
blank_b	3.40 10^3	3.29 10^3	3.35 10^3	31.5	33.4	40.4	< 0.25	< 0.25	1.88
10 µM Tricl.	2.80 10^3	1.82 10^3	345	350	0.98 10^3	2.00 10^3	< 0.25	< 0.25	< 0.25
100 µM Tricl.	3.26 10^3	3.15 10^3	2.66 10^3	3.99	53.7	412	< 0.25	< 0.25	< 0.25
1000 µM Tricl.	3.19 10^3	3.17 10^3	3.21 10^3	< 0.25	< 0.25	< 0.25	< 0.25	< 0.25	< 0.25
20 mg L^{-1} Chlor.	2.44 10^3	1.26 10^3	215	0.64 10^3	1.37 10^3	2.11 10^3	< 0.25	< 0.25	< 0.25
200 mg L^{-1} Chlor.	3.14 10^3	2.04 10^3	441	154	0.84 10^3	1.97 10^3	< 0.25	< 0.25	< 0.25
1000 mg L^{-1} Chlor.	3.05 10^3	2.79 10^3	1.32 10^3	135	332	1.00 10^3	< 0.25	< 0.25	< 0.25

Continuation Table A5.2:

Inhibitor	*[N_3^-] (mg L^{-1})*			*[Hg] (mg L^{-1})*			*[Cl^-] (mg L^{-1})*		
	3	*7*	*17*	*3*	*7*	*17*	*3*	*7*	*17*
1/100 clay slurry with 100 mM $NaNO_3$									
blank_a	-	-	-	-	-	-	-	-	-
0.1% $HgCl_2$	-	-	-	80	72	130	-	-	-
0.5% $HgCl_2$	-	-	-	1.56 10^3	0.89 10^3	1.07 10^3	-	-	-
0.1% NaN_3	0.69 10^3	0.69 10^3	0.67 10^3	-	-	-	-	-	-
1% NaN_3	6.1 10^3	6.2 10^3	6.1 10^3	-	-	-	-	-	-
0.1% CH_2O	-	-	-	-	-	-	-	-	-
1% CH_2O	-	-	-	-	-	-	-	-	-
blank_b	-	-	-	-	-	-	25.3	25.0	26.1
10 µM Tricl.	-	-	-	-	-	-	24.6	24.8	25.0
100 µM Tricl.	-	-	-	-	-	-	25.0	25.0	25.1
1000 µM Tricl.	-	-	-	-	-	-	24.0	24.3	24.4
20 mg L^{-1} Chlor.	-	-	-	-	-	-	24.6	25.0	25.1
200 mg L^{-1} Chlor.	-	-	-	-	-	-	25.2	25.6	25.4
1000 mg L^{-1} Chlor.	-	-	-	-	-	-	25.7	26.4	26.8

Table A5.3: Chemical analysis of the supernatant of Boom Clay slurries (1/3 g Boom Clay per g RBCW) with and without 1 M $NaNO_3$ after 1 year of incubation in an anaerobic glove box. No microbial inhibitor was added to the blank samples. The composition of the slurries is given in Table 5. All values are given in mg L^{-1}.

	Blank	***Blank + 1M $NaNO_3$***	***CH_2O***	***CH_2O + 1M $NaNO_3$***
Ca	8.2	226	17.6	358
Fe	0.43	0.053	0.38	0.231
K	13	197	23.6	204
Mg	4.0	96	12.2	199
Na	440	$22.4\ 10^3$	570	$22.3\ 10^3$
Si	29.3	33	17.4	34
Mo	-	-	-	-
F^-	2.7	0,26	2.3	1.46
Cl^-	28	24	27	24
Br^-	0.46	-	0.45	-
NO_3^-	< 0.25	$63\ 10^3$	< 0.25	$63\ 10^3$
SO_4^{2-}	3.3	5.1	2.2	3.3
$S_2O_3^{2-}$	2.5	<1	<1	<1

Annex 6: Batch tests with RBCW: complete set of results of chemical analysis

First series of batch tests with RBCW and nitrate

Table A6.1: Chemical analyses of samples '0 M $NaNO_3$_0% bact' from the first series of batch tests with RBCW and nitrate (see Table 12). After each reaction period (first column), two duplicate samples (indicated by a and b) were analysed. TOC, TIC and pH measurements were performed on only one sample. The uncertainties on the concentrations are 10% ([Na^+], [Ca^{2+}], TIC) and 30-35% (TOC). The uncertainty on the pH is 0.1 units (95% confidence).

Time (days)	*[Na^+] (mg L^{-1}) a*	*[Na^+] (mg L^{-1}) b*	*[Ca^{2+}] (mg L^{-1}) a*	*[Ca^{2+}] (mg L^{-1}) b*	*pH b*	*TIC (mg C L^{-1}) a*	*TOC (mg C L^{-1}) a*
0	390	390	3.76	3.76	9.1	(*)	(*)
2	393	395	3.81	3.83	8.9	(*)	(*)
7	388	385	3.82	3.81	8.7	(*)	(*)
35	386	394	4	4	9.0	184	92
65	420	430	3.9	4.2	9.1	178	91
105	384	380	4.1	4.2	9.1	183	98
181	383	385	4.3	4.4	8.7	176	107
392	389	(*)	4.2	(*)	9.0	190	104
700	392	390	4.1	4.6	9.3	172	98

(*) Not measured

Table A6.2: Chemical analyses of samples '0.2 M $NaNO_3$_0% bact' from the first series of batch tests with RBCW and nitrate (see Table 12). After each reaction period (first column), two duplicate samples (indicated by a and b) were analysed. TOC, TIC and pH measurements were performed on only one sample. The uncertainties on the concentrations are 10% ([Na^+], [Ca^{2+}], TIC), 30-35% (TOC) and 5-6% ([NO_2^-], [NO_3^-]). The uncertainty on the pH is 0.1 units (95% confidence).

Time (days)	*[Na^+] (mg L^{-1}) a*	*[Na^+] (mg L^{-1}) b*	*[Ca^{2+}] (mg L^{-1}) a*	*[Ca^{2+}] (mg L^{-1}) b*	*[NO_3^-] (M) a*	*[NO_3^-] (M) b*	*[NO_2^-] (mM) a*	*[NO_2^-] (mM) b*	*pH b*	*TIC (mg C L^{-1}) a*	*TOC (mg C L^{-1}) a*
0	5000	5000	3.75	3.75	0.19	0.19	0.00	0.00	8.9	(*)	(*)
2	5000	5000	3.85	3.85	0.19	0.19	0.03	0.00	8.6	(*)	(*)
7	4800	4900	3.85	3.89	0.20	0.20	0.04	0.07	8.3	(*)	(*)
35	5000	5000	3.82	3.9	0.19	0.19	0.10	0.09	8.7	182	90
65	5400	5500	4.4	4.7	0.19	0.19	0.13	0.14	8.8	173	90
105	4900	4900	4.3	4.4	0.20	0.19	0.11	0.11	8.7	178	93
181	4900	4900	4.7	5.2	0.19	0.19	0.12	0.33	9.2	178	107
392	4900	(*)	6	(*)	0.19	0.19	0.18	0.11	8.8	190	106
700	4900	5000	7.2	8.2	0.19	0.19	0.23	0.33	9.1	172	92

(*) Not measured

Table A6.3: Chemical analyses of samples '0 M $NaNO_3$_1% bact' from the first series of batch tests with RBCW and nitrate (see Table 12). After each reaction period (first column), two duplicate samples (indicated by a and b) from this series have been analysed. TOC, TIC and pH measurements were performed on only one sample. The uncertainties on the concentrations are 10% ([Na^+], [Ca^{2+}], TIC, [N_3^-]) and 30-35% (TOC). The uncertainty on the pH is 0.1 units (95% confidence).

Time (days)	*[Na^+] (mg L^{-1}) a*	*[Na^+] (mg L^{-1}) b*	*[Ca^{2+}] (mg L^{-1}) a*	*[Ca^{2+}] (mg L^{-1}) b*	*[N_3^-] (mg L^{-1}) a*	*[N_3^-] (mg L^{-1}) b*	*pH b*	*TIC (mg C L^{-1}) a*	*TOC (mg C L^{-1}) a*
0	3910	3910	3.79	3.79	6400	6400	8.9	(*)	(*)
2	3940	3940	3.87	3.89	6700	6600	8.7	(*)	(*)
7	3840	3860	3.96	3.95	6500	6600	8.2	(*)	(*)
35	3870	3890	3.9	3.9	6100	6200	8.8	189	86
65	4400	4300	4.3	4.4	6600	6600	8.9	180	83
105	3800	3810	4.2	4.4	6500	6600	8.8	182	88
181	3850	3820	4.5	4.7	5900	5800	8.9	190	108
392	3780	(*)	5.2	(*)	6300	6400	8.6	195	117
700	3850	3850	6.4	7.6	6200	6300	9.1	172	97

(*) Not measured

Table A6.4: Chemical analyses of samples '0.05 M $NaNO_3$_1% bact' from the first series of batch tests with RBCW and nitrate (see Table 12). After each reaction period (first column), two duplicate samples (indicated by a and b) from this series have been analysed. TOC, TIC and pH measurements were performed on only one sample. The uncertainties on the concentrations are 10% ([Na^+], [Ca^{2+}], TIC, [N_3^-]), 30-35% (TOC), 10-20% ([NO_3^-], the presence of N_3^- increases the uncertainty from ~6 % to 10-20 %) and 5-6% ([NO_2^-]). The uncertainty on the pH is 0.1 units (95% confidence).

Time (days)	*[Na^+] (mg L^{-1}) a*	*[Na^+] (mg L^{-1}) b*	*[Ca^{2+}] (mg L^{-1}) a*	*[Ca^{2+}] (mg L^{-1}) b*	*[NO_3^-] (M) a*	*[NO_3^-] (M) b*	*[NO_2^-] (mM) a*	*[NO_2^-] (mM) b*	*[N_3^-] (mg L^{-1}) a*	*[N_3^-] (mg L^{-1}) b*	*pH b*	*TIC (mg C L^{-1}) a*	*TOC (mg C L^{-1}) a*
0	5000	5000	3.77	3.77	0.048	0.048	<0.01	<0.01	6300	6300	8.9	(*)	(*)
2	5100	5100	3.88	3.89	0.049	0.048	<0.01	<0.01	6400	6400	8.7	(*)	(*)
7	4800	4800	3.88	3.88	0.049	0.049	<0.01	<0.01	6600	6600	8.3	(*)	(*)
35	5000	5000	3.9	3.9	0.049	0.048	<0.01	<0.01	6300	6200	8.8	180	90
65	5600	5600	4.3	4.4	0.048	0.049	<0.01	<0.01	6600	6600	8.9	176	100
105	4900	4900	4.2	4.2	0.046	0.046	<0.01	<0.01	6700	6600	8.8	180	95
181	4900	4900	4.4	4.6	0.048	0.048	<0.01	<0.01	6000	6000	8.8	184	103
392	5200	(*)	5.5	(*)	0.048	0.047	<0.01	<0.01	6400	6200	8.7	193	110
700	5000	5000	7.6	9.9	0.048	0.049	<0.01	<0.01	6200	6400	9.1	178	88

(*) Not measured

Table A6.5: Chemical analyses of samples '0.2 M $NaNO_3$_1% bact' from the first series of batch tests with RBCW and nitrate (see Table 12). After each reaction period (first column), two duplicate samples (indicated by a and b) from this series have been analysed. TOC, TIC and pH measurements were performed on only one sample. The uncertainties on the concentrations are 10% ([Na^+], [Ca^{2+}], TIC, [N_3^-]), 30-35% (TOC), 10-20% ([NO_3^-], the presence of N_3^- increases the uncertainty from ~6 % to 10-20 %) and 5-6% ([NO_2^-]). The uncertainty on the pH is 0.1 units (95% confidence).

Time (days)	*[Na^+] (mg L^{-1}) a*	*[Na^+] (mg L^{-1}) b*	*[Ca^{2+}] (mg L^{-1}) a*	*[Ca^{2+}] (mg L^{-1}) b*	*[NO_3^-] (M) a*	*[NO_3^-] (M) b*	*[NO_2^-] (mM) a*	*[NO_2^-] (mM) b*	*[N_3^-] (mg L^{-1}) a*	*[N_3^-] (mg L^{-1}) b*	*pH b*	*TIC (mg C L^{-1}) a*	*TOC (mg C L^{-1}) a*
0	8500	8500	3.71	3.71	0.19	0.19	<0.01	<0.01	6200	6200	8.8	(*)	(*)
2	8600	8600	3.87	3.88	0.19	0.20	<0.01	<0.01	6400	6500	8.6	(*)	(*)
7	8400	8400	3.85	3.95	0.20	0.20	<0.01	<0.01	6500	6600	8.3	(*)	(*)
35	8400	8200	3.85	3.9	0.19	0.19	<0.01	<0.01	6100	6200	8.7	177	90
65	9200	9300	4.3	4.3	0.19	0.19	<0.01	<0.01	6300	6500	8.8	176	81
105	8400	8300	4.1	4.2	0.19	0.19	<0.01	<0.01	6900	6900	8.7	179	95
181	8400	8300	4.6	4.8	0.19	0.19	<0.01	<0.01	5800	5800	8.8	187	102
392	8300	(*)	5.6	(*)	0.19	0.19	<0.01	<0.01	6300	6300	8.7	191	105
700	8300	8300	6.9	8	0.19	0.19	<0.01	<0.01	(*)	6200	9.0	172	87

(*) Not measured

Second series of batch tests with RBCW and nitrate

Table A6.6: Chemical analyses of samples '0 M $NaNO_3$_0% bact' from the second series of batch tests with RBCW and nitrate (see Table 14). After each reaction period (first column), two duplicate samples (indicated by a and b) from this series have been analysed. TOC and pH measurements were performed on only one sample. The nitrate and nitrite concentrations were measured regularly and were always found to be below detection limit. The uncertainties on the concentrations are 10% ([Na^+], [Ca^{2+}]) and 4% (TOC) (95% confidence). The uncertainty on the pH is 0.1 units (95% confidence).

Time	*[Na^+] (mg L^{-1})*		*[Ca^{2+}] (mg L^{-1})*		*pH*	*TOC*
(days)	*a*	*b*	*a*	*b*		*(mg C L^{-1})*
0	394	n.a.	3.4	n.a.	9.3	108*
7	387	387	3.4	3.5	9.3	111*
36	410	410	3.7	3.7	9.5	112
98	400	400	3.9	3.8	9.2	116
189	389	n.a.	4.0	n.a.	9.6	116
554	420	n.a.	4.7	n.a.	9.2	111

n.a. : not analysed

*The TOC was analysed with a different TOC/TIC analyser, resulting in an uncertainty on the measurement of ~30-35%.

Table A6.7: Chemical analyses of samples '0 M $NaNO_3$_0.2% bact' from the second series of batch tests with RBCW and nitrate (see Table 14). After each reaction period (first column), two duplicate samples (indicated by a and b) from this series have been analysed. TOC, azide and pH measurements were performed on only one sample. The nitrate and nitrite concentrations were measured regularly and were always found to be below detection limit. The uncertainties on the concentrations are 4% (TOC) and 10% ([Na^+], [Ca^{2+}], [N_3^-]). The uncertainty on the pH is 0.1 units (95% confidence).

Time	*[Na^+] (mg L^{-1})*		*[Ca^{2+}] (mg L^{-1})*		*[N_3^-]*	*pH*	*TOC*
(days)	*a*	*b*	*a*	*b*	*(mM)*		*(mg C L^{-1})*
0	1080	1080	3.6	n.a.	31.17	9.2	106*
7	1060	1060	3.4	3.6	30.45	9.2	99*
36	1100	1090	3.8	3.7	31.64	9.4	108
96	1090	1090	3.9	3.9	31.17	9.1	118
189	1040	n.a.	4.3	n.a.	31.17	9.4	106
554	1140	n.a.	4.4	n.a.	n.a.	9.2	112

n.a. : not analysed

*The TOC was analysed with the standard TOC/TIC analyser, resulting in an expanded error on the measurement of ~30-35%.

Table A6.8: Chemical analyses of samples '0.1 M $NaNO_3$_0% bact' from the second series of batch tests with RBCW and nitrate (see Table 14). After each reaction period (first column), two duplicate samples (indicated by a and b) from this series have been analysed. TOC, azide and pH measurements were performed on only one sample. The uncertainties on the concentrations are 4% (TOC), 5-6% ($[NO_2^-]$, $[NO_3^-]$) and 10% ($[Na^+]$, $[Ca^{2+}]$, $[N_3^-]$). The uncertainty on the pH is 0.1 units (95% confidence).

Time	*$[Na^+]$ (mg L^{-1})*		*$[Ca^{2+}]$ (mg L^{-1})*		*$[NO_3^-]$ (mM)*		*$[NO_2^-]$ (mM)*		*$[N_3^-]$*	*pH*	*TOC*
(days)	*a*	*b*	*a*	*b*	*a*	*b*	*a*	*b*	*(mM)*		*(mg C L^{-1})*
0	2640	2640	3.7	n.a.	94	n.a.	<0.011	n.a.	<0.005	9.0	110*
7	2640	2640	3.5	3.7	95	96	0.022	0.021	n.a.	9.0	108*
36	2720	2700	3.8	3.8	98	98	0.041	0.036	<0.005	9.2	112
96	2750	2730	4.1	4.1	103	101	0.065	0.074	<0.005	9.0	118
189	2570	n.a.	4.4	n.a.	102	109	0.082	0.059	n.a.	9.3	113
554	2770	n.a.	6.1	n.a.	102	106	0.092	0.098	n.a.	9.1	111

n.a. : not analysed

*The TOC was analysed with the standard TOC/TIC analyser, resulting in an expanded error on the measurement of ~30-35%.

Table A6.9: Chemical analyses of samples '0.005 M $NaNO_3$_0.2% bact' from the second series of batch tests with RBCW and nitrate (see Table 14). After each reaction period (first column), two duplicate samples (indicated by a and b) from this series have been analysed. TOC, azide and pH measurements were performed on only one sample. The uncertainties on the concentrations are 4% (TOC), 5-6% ($[NO_2^-]$, $[NO_3^-]$) and 10% ($[Na^+]$, $[Ca^{2+}]$, $[N_3^-]$). The uncertainty on the pH is 0.1 units (95% confidence).

Time	*$[Na^+]$ (mg L^{-1})*		*$[Ca^{2+}]$ (mg L^{-1})*		*$[NO_3^-]$ (mM)*		*$[NO_2^-]$ (mM)*		*$[N_3^-]$*	*pH*	*TOC*
(days)	*a*	*b*	*a*	*b*	*a*	*b*	*a*	*b*	*(mM)*		*(mg C L^{-1})*
0	1190	1190	3.6	n.a.	5.3	n.a.	<0.011	n.a.	31.88	9.1	106*
7	1180	1180	3.6	3.6	5.6	5.1	<0.011	<0.011	31.88	8.9	103*
36	1200	1210	3.7	3.8	5.2	5.2	<0.011	<0.011	32.12	9.4	109
96	1210	1210	3.9	3.9	5.4	5.3	<0.011	<0.011	31.88	9.1	119
189	1170	n.a.	4.4	n.a.	5.2	5.2	<0.011	<0.011	30.45	9.4	106
554	1260	n.a.	4.6	n.a.	5.2	5.2	<0.005	<0.005	n.a.	9.2	110

n.a. : not analysed

*The TOC was analysed with the standard TOC/TIC analyser, resulting in an expanded error on the measurement of ~30-35%.

Table A6.10: Chemical analyses of samples '0.1 M $NaNO_3$_0.2% bact' from the second series of batch tests with RBCW and nitrate (see Table 14). After each reaction period (first column), two samples (indicated by a and b) from this series have been analysed. TOC, azide and pH measurements were performed on only one sample. The uncertainties on the concentrations are 4% (TOC), 5-6% ([NO_2^-], [NO_3^-]) and 10% ([Na^+], [Ca^{2+}], [N_3^-]). The uncertainty on the pH is 0.1 units (95% confidence).

Time	*[Na^+] (mg L^{-1})*		*[Ca^{2+}] (mg L^{-1})*		*[NO_3^-] (mM)*		*[NO_2^-] (mM)*		*[N_3^-]*	*pH*	*TOC*
(days)	*a*	*b*	*a*	*b*	*a*	*b*	*a*	*b*	*(mM)*		*(mg C L^{-1})*
0	3340	3340	3.7	3.7	83	n.a.	<0.011	n.a.	28.79	9.0	106*
7	3380	3370	3.7	3.7	91	96	<0.011	<0.011	28.79	9.2	120*
36	3410	3350	3.8	3.7	93	104	<0.011	<0.011	30.45	9.2	113
96	3510	3390	4.0	4.1	102	105	<0.011	<0.011	30.93	9.0	118
189	3330	n.a.	5.1	n.a.	98	99	<0.011	<0.011	30.45	9.2	112
554	3470	n.a.	5.4	n.a.	104	104	<0.005	<0.005	n.a.	9.0	111

n.a. : not analysed

*The TOC was analysed with the standard TOC/TIC analyser, resulting in an expanded error on the measurement of ~30-35%.

First series of batch tests with RBCW and nitrite

Table A6.11: Chemical analyses of samples '0 M $NaNO_2$_0% bact' from the first series of batch tests with RBCW and nitrite (see Table 16). After each reaction period (first column), two duplicate samples (indicated by a and b) from this series have been analysed. TOC, nitrate, nitrite, ammonium, azide and pH measurements were performed on only one sample. The uncertainties on the concentrations are 4% (TOC), 5-6% ($[NO_2^-]$, $[NO_3^-]$) and 10% ($[Na^+]$, $[Ca^{2+}]$, $[NH_4^+]$, $[N_3^-]$). The uncertainty on the pH is 0.1 units (95% confidence).

Time	***$[Na^+]$ (mg L^{-1})***		***$[Ca^{2+}]$ (mg L^{-1})***		***$[NO_3^-]$***	***$[NO_2^-]$***	***$[NH_4^+]$***	***$[N_3^-]$***	***pH***	***TOC***
(days)	***a***	***b***	***a***	***b***	***(mM)***	***(mM)***	***(mM)***	***(mM)***		***(mg C L^{-1})***
0	400	n.a.	3.41	n.a.	<0.008	<0.011	n.a.	<0.005	9.2	100*
2	400	410	3.50	3.60	<0.008	<0.011	n.a.	0.028	9.2	114*
7	400	400	3.60	3.60	<0.008	n.a.	n.a.	0.016	9.2	108
36	395	395	3.70	3.50	<0.008	<0.011	n.a.	<0.005	9.4	108
63	410	410	3.50	3.60	<0.008	<0.011	n.a.	<0.005	9.3	108
92	400	400	3.60	3.70	<0.008	n.a.	n.a.	n.a.	9.2	108
189	384	n.a.	4.20	n.a.	n.a.	<0.011	<0.008	n.a.	9.6	106
554	420	n.a.	4.30	n.a.	n.a.	<0.011	0.011	n.a.	9.2	113

n.a. : not analysed

*The TOC was analysed with the standard TOC/TIC analyser, resulting in an expanded error on the measurement of ~30-35%.

Table A6.12: Chemical analyses of samples '0.05 M $NaNO_2$_0% bact' from the second series of batch tests with RBCW and nitrite (see Table 16). After each reaction period (first column), two samples (indicated by a and b) from this series have been analysed. TOC, ammonium, azide and pH measurements were performed on only one sample. The uncertainties on the concentrations are 4% (TOC), 5-6% ($[NO_2^-]$, $[NO_3^-]$) and 10% ($[Na^+]$, $[Ca^{2+}]$, $[NH_4^+]$, $[N_3^-]$). The uncertainty on the pH is 0.1 units (95% confidence).

Time	*$[Na^+]$ (mg L^{-1})*		*$[Ca^{2+}]$ (mg L^{-1})*		*$[NO_3^-]$ (mM)*		*$[NO_2^-]$ (mM)*		*$[NH_4^+]$*	*$[N_3^-]$*	*pH*	*TOC*
(days)	*a*	*b*	*a*	*b*	*a*	*b*	*a*	*b*	*(mM)*	*(mM)*		*(mg C L^{-1})*
0	1540	n.a.	3.52	n.a.	0.17	0.17	5.0	5.0	n.a.	<0.005	9.0	103*
2	1550	1590	3.60	3.60	0.17	0.18	5.0	5.1	n.a.	<0.005	9.1	101*
7	1540	1560	3.50	3.60	n.a.	n.a.	5.0	5.0	n.a.	n.a.	9.1	107
36	1530	1530	3.60	3.80	n.a.	n.a.	5.2	5.1	n.a.	<0.005	9.3	106
63	1560	1560	3.70	3.70	0.18	0.18	5.0	5.0	n.a.	<0.005	9.2	106
92	1570	1530	3.80	3.80	0.18	0.18	5.0	5.0	n.a.	n.a.	9.0	106
189	1480	n.a.	4.30	n.a.	n.a.	n.a.	4.9	4.9	<0.008	n.a.	9.4	105
554	1590	n.a.	4.90	n.a.	0.18	n.a.	4.9	5.0	0.018	n.a.	9.1	114

n.a. : not analysed

*The TOC was analysed with the standard TOC/TIC analyser, resulting in an expanded error on the measurement of ~30-35%.

Table A6.13: Chemical analyses of samples '0 M $NaNO_2$_0.2% bact' from the second series of batch tests with RBCW and nitrite (see Table 16). After each reaction period (first column), two duplicate samples (indicated by a and b) from this series have been analysed. TOC, ammonium and pH measurements were performed on only one sample. The uncertainties on the concentrations are 4% (TOC), 5-6% ($[NO_2^-]$, $[NO_3^-]$) and 10% ($[Na^+]$, $[Ca^{2+}]$, $[NH_4^+]$, $[N_3^-]$). The uncertainty on the pH is 0.1 units (95% confidence).

Time	*$[Na^+]$ (mg L^{-1})*		*$[Ca^{2+}]$ (mg L^{-1})*		*$[NO_3^-]$ (mM)*		*$[NO_2^-]$ (mM)*		*$[NH_4^+]$*	*$[N_3^-]$ (mM)*		*pH*	*TOC*
(days)	*a*	*b*	*a*	*b*	*a*	*b*	*a*	*b*	*(mM)*	*a*	*b*		*(mg C L^{-1})*
0	1090	n.a.	3.51	n.a.	<0.008	n.a.	<0.011	n.a.	n.a.	31.64	n.a.	9.10	110*
2	1110	1120	3.60	3.60	<0.008	<0.008	0.011	<0.011	n.a.	32.36	32.60	9.17	96*
7	1110	1110	3.60	3.70	n.a.	n.a.	n.a.	n.a.	n.a.	31.64	31.41	9.17	104
36	1080	1090	3.70	3.70	n.a.	n.a.	0.014	<0.011	n.a.	31.88	31.88	9.33	106
63	1100	1120	3.60	3.70	<0.008	<0.008	0.022	<0.011	n.a.	31.17	31.64	9.20	106
92	1100	1110	3.70	3.80	<0.008	<0.008	n.a.	n.a.	n.a.	31.64	31.64	9.05	106
189	1060	n.a.	4.20	n.a.	n.a.	n.a.	<0.011	<0.011	<0.008	30.64	n.a.	9.42	104
554	1150	n.a.	4.30	n.a.	n.a.	n.a.	n.a.	n.a.	0.0061	n.a.	n.a.	9.13	114

n.a. : not analysed

*The TOC was analysed with the standard TOC/TIC analyser, resulting in an expanded error on the measurement of ~30-35%.

Table A6.14: Chemical analyses of samples '0.005 M $NaNO_2$_0.2% bact' from the second series of batch tests with RBCW and nitrite (see Table 16). After each reaction period (first column), two duplicate samples (indicated by a and b) from this series have been analysed. TOC, ammonium, azide and pH measurements were performed on only one sample. The uncertainties on the concentrations are 4% (TOC), 5-6% ($[NO_2^-]$, $[NO_3^-]$) and 10% ($[Na^+]$, $[Ca^{2+}]$, $[NH_4^+]$, $[N_3^-]$). The uncertainty on the pH is 0.1 units (95% confidence).

Time	*$[Na^+]$ (mg L^{-1})*		*$[Ca^{2+}]$ (mg L^{-1})*		*$[NO_3^-]$ (mM)*		*$[NO_2^-]$ (mM)*		*$[NH_4^+]$*	*$[N_3^-]$ (mM)*		*pH*	*TOC*
(days)	*a*	*b*	*a*	*b*	*a*	*b*	*a*	*b*	*(mM)*	*a*	*b*		*(mg C L^{-1})*
0	1220	n.a.	3.66	n.a.	<0.008	n.a.	5.1	n.a.	n.a.	31.88	n.a.	9.0	120*
2	1240	1250	3.70	3.70	<0.008	<0.008	5.2	5.2	n.a.	31.41	32.12	9.1	110*
7	1230	1230	3.70	3.70	n.a.	n.a.	5.0	4.9	n.a.	29.74	31.64	9.1	109
36	1210	1210	3.70	3.70	n.a.	n.a.	5.2	5.1	n.a.	29.74	31.88	9.3	112
63	1220	1230	3.80	3.80	<0.008	<0.008	5.1	5.0	n.a.	31.17	31.88	9.3	112
92	1230	1220	3.80	3.80	<0.008	<0.008	5.0	5.0	n.a.	31.88	31.64	9.1	112
189	1170	n.a.	4.30	n.a.	n.a.	n.a.	4.8	4.7	0.03	30.22	n.a.	9.5	107
554	1260	n.a.	4.80	n.a.	n.a.	n.a.	4.7	4.8	0.015	n.a.	n.a.	9.3	116

n.a. : not analysed

*The TOC was analysed with the standard TOC/TIC analyser, resulting in an expanded error on the measurement of ~30-35%.

Table A6.15: Chemical analyses of samples '0.05 M $NaNO_2$_0.2% bact' from the second series of batch tests with RBCW and nitrite (see Table 16). After each reaction period (first column), two duplicate samples (indicated by a and b) from this series have been analysed. TOC, ammonium, azide and pH measurements were performed on only one sample. The uncertainties on the concentrations are 4% (TOC), 5-6% ($[NO_2^-]$, $[NO_3^-]$) and 10% ($[Na^+]$, $[Ca^{2+}]$, $[NH_4^+]$, $[N_3^-]$). The uncertainty on the pH is 0.1 units (95% confidence).

Time	*$[Na^+]$ (mg L^{-1})*		*$[Ca^{2+}]$ (mg L^{-1})*		*$[NO_3^-]$ (mM)*		*$[NO_2^-]$ (mM)*		*$[NH_4^+]$*	*$[N_3^-]$ (mM)*		*pH*	*TOC*
(days)	*a*	*b*	*a*	*b*	*a*	*b*	*a*	*b*	*(mM)*	*a*	*b*		*(mg C L^{-1})*
0	2250	n.a.	3.7	n.a.	<0.008	n.a.	0.050	n.a.	n.a.	31.88	n.a.	9.1	110*
2	2290	2300	3.7	3.7	<0.008	<0.008	0.050	0.050	n.a.	31.88	31.88	9.2	98*
7	2300	2300	3.7	3.7	n.a.	n.a.	0.049	0.050	n.a.	30.93	32.12	9.1	107
36	2260	2200	3.8	3.8	n.a.	n.a.	0.048	0.051	n.a.	32.36	31.88	9.4	107
63	2240	2270	3.8	3.9	<0.008	<0.008	0.050	0.050	n.a.	30.93	30.93	9.2	107
92	2240	2260	3.8	3.9	<0.008	<0.008	0.050	0.051	n.a.	31.41	31.41	9.2	107
189	2140	n.a.	4.4	n.a.	n.a.	n.a.	0.048	0.048	0.020	29.74	n.a.	9.6	105
554	2320	n.a.	4.7	n.a.	n.a.	n.a.	0.048	0.049	0.011	n.a.	n.a.	9.6	114

n.a. : not analysed

*The TOC was analysed with the standard TOC/TIC analyser, resulting in an expanded error on the measurement of ~30-35%.

Annex 7: Batch tests with pyrite: complete set of results of chemical analysis

Batch tests with pyrite without nitrate/nitrite

Table A7.1: Chemical analyses of sample 'Pyr_0.1% bact_bicarb' from the batch tests with pyrite (see Table 18). After each reaction period (first column), a sample of the solution has been analysed. The specific surface area of the pyrite added to the solution is 1.53 ± 0.18 m^2 g^{-1}. The uncertainties on the concentrations are 2% (pyrite concentration), 4-5% ([$S_2O_3^{2-}$]), 5-6% ([NO_3^-], [NO_2^-]) and 10% ([SO_4^{2-}], [N_3^-]). The uncertainty on the pH is 0.1 units (95% confidence).

Time (days)	*Pyrite (g L^{-1})*	*[NO_3^-] (mM)*	*[NO_2^-] (mM)*	*[SO_4^{2-}] (mM)*	*[$S_2O_3^{2-}$] (mM)*	*[N_3^-] (mM)*	*[NH_4^+] (mM)*	*pH*
0	4.94	<0.004	<0.005	0.016	0.011	15.7	n.a.	9.2
29	4.65	<0.004	<0.005	0.018	0.072	n.a.	n.a.	9.2
91	4.79	<0.004	<0.005	0.013	0.15	n.a.	n.a.	9.3
182	5.34	n.a.	n.a.	0.014	0.20	n.a.	1.71	9.3
351	4.78	n.a.	n.a.	0.018	0.35	14.3	n.a.	9.4

n.a. : not analysed

Table A7.2: Chemical analyses of samples 'Pyr_0.1% bact_water' from the batch tests with pyrite (see Table 18). After each reaction period (first column), a sample of the solution has been analysed. The specific surface area of the pyrite added to the solution is 1.53 ± 0.18 m^2 g^{-1}. The uncertainties on the concentrations are 2% (pyrite concentration), 4-5% ([$S_2O_3^{2-}$]), 5-6% ([NO_3^-], [NO_2^-]) and 10% ([SO_4^{2-}], [N_3^-]). The uncertainty on the pH is 0.1 units (95% confidence).

Time (days)	*Pyrite (g L^{-1})*	*[NO_3^-] (mM)*	*[NO_2^-] (mM)*	*[SO_4^{2-}] (mM)*	*[$S_2O_3^{2-}$] (mM)*	*[N_3^-] (mM)*	*pH*
0	4.69	<0.004	<0.005	0.013	0.0056	15.2	6.8
182	4.90	n.a.	n.a.	0.012	0.14	n.a.	10.3

n.a. : not analysed

Table A7.3: Chemical analyses of samples 'Pyr_0% bact_bicarb' from the batch tests with pyrite (see Table 18). After each reaction period (first column), one sample of the solution has been analysed. The uncertainties on the concentrations are 2% (pyrite concentration), 4-5% ([$S_2O_3^{2-}$]), 5-6% ([NO_3^-], [NO_2^-]) and 10% ([SO_4^{2-}], [N_3^-]). The uncertainty on the pH is 0.1 units (95% confidence).

Time (days)	*Pyrite (g L^{-1})*	*[NO_3^-] (mM)*	*[NO_2^-] (mM)*	*[SO_4^{2-}] (mM)*	*[$S_2O_3^{2-}$] (mM)*	*[N_3^-] (mM)*	*[NH_4^+] (mM)*	*pH*
0	4.89	0.007	<0.005	0.017	0.024	0.015	n.a.	8.6
29	5.09	<0.004	n.a.	0.016	n.a.	n.a.	n.a.	8.6
91	4.79	<0.004	<0.005	0.016	0.007	n.a.	n.a.	8.7
351	4.33	n.a.	n.a.	0.016	<0.009	n.a.	0.56	8.5

n.a. : not analysed

Batch tests with pyrite and nitrate

Table A7.4: Chemical analyses of sample 'Pyr_0.005M $NaNO_3$_0.1% bact_bicarb' from the batch tests with pyrite (see Table 18Table 18). After each reaction period (first column), a sample of the solution has been analysed. The specific surface area of the pyrite added to the solution is 1.53 ± 0.18 m^2 g^{-1}. pH measurements were performed on only one sample. The uncertainties on the concentrations are 2% (pyrite concentration), 4-5% ([$S_2O_3^{2-}$]), 5-6% ([NO_3^-], [NO_2^-]) and 10% ([SO_4^{2-}], [N_3^-]) (95% confidence). The uncertainty on the pH is 0.1 units (95% confidence). The azide concentration and pH were measured in only one sample.

Time	*Pyrite (g L^{-1})*		*[NO_3^-] (mM)*		*[NO_2^-] (mM)*		*[SO_4^{2-}] (mM)*		*[$S_2O_3^{2-}$] (mM)*		*[N_3^-]*	*pH*
(days)	*a*	*b*	*a*	*b*	*a*	*b*	*a*	*b*	*a*	*b*	*(mM)*	
0	4.81	4.76	5.0	5.0	<0.005	<0.005	0.012	0.013	0.0043	n.a.	15.2	8.8
29	5.08	4.80	5.0	4.9	<0.005	<0.005	0.018	0.014	0.088	0.086	n.a.	8.9
91	5.06	4.86	4.9	4.9	<0.005	n.a.	0.014	0.014	0.18	n.a.	n.a.	9.0
182	4.77	5.04	5.0	5.0	<0.005	n.a.	0.013	0.014	0.26	n.a.	n.a.	9.1
351	4.80	4.95	4.7	4.7	<0.005	n.a.	0.016	0.017	0.39	n.a.	n.a.	9.3

n.a. : not analysed

Table A7.5: Chemical analyses of sample 'Pyr_0.005M $NaNO_3$_0.1% bact_water' from the batch tests with pyrite (see Table 18). After each reaction period (first column), a sample of the solution has been analysed. The specific surface area of the pyrite added to the solution is 1.53 ± 0.18 m^2 g^{-1}. pH measurements were performed on only one sample. The uncertainties on the concentrations are 2% (pyrite concentration), 4-5% ([$S_2O_3^{2-}$]), 5-6% ([NO_3^-], [NO_2^-]) and 10% ([SO_4^{2-}], [N_3^-]) (95% confidence). The uncertainty on the pH is 0.1 units (95% confidence). The azide and thiosulphate concentrations and pH were measured in only one sample.

Time	*Pyrite (g L^{-1})*		*[NO_3^-] (mM)*		*[NO_2^-] (mM)*		*[SO_4^{2-}] (mM)*		*[$S_2O_3^{2-}$]*	*[N_3^-]*	*pH*
(days)	*a*	*b*	*a*	*b*	*a*	*b*	*a*	*b*	*(mM)*	*(mM)*	
0	5.19	4.47	4.8	4.8	<0.005	<0.005	0.014	0.015	0.0088	15.5	6.8
182	4.76	4.77	4.8	4.8	<0.005	<0.005	0.013	0.015	0.16	n.a.	10.2

n.a. : not analysed

Table A7.6: Chemical analyses of sample 'Pyr_0.1M $NaNO_3$_0.1% bact_bicarb' from the batch tests with pyrite (see Table 18). After each reaction period (first column), a sample of the solution has been analysed. The specific surface area of the pyrite added to the solution is 1.53 ± 0.18 m^2 g^{-1}. pH measurements were performed on only one sample. The uncertainties on the concentrations are 2% (pyrite concentration), 4-5% ($[S_2O_3^{2-}]$), 5-6% ($[NO_3^-]$, $[NO_2^-]$) and 10% ($[SO_4^{2-}]$, $[N_3^-]$) (95% confidence). The uncertainty on the pH is 0.1 units (95% confidence). The azide concentration and pH were measured in only one sample.

Time	*Pyrite (g L^{-1})*		*$[NO_3^-]$ (mM)*		*$[NO_2^-]$ (mM)*		*$[SO_4^{2-}]$ (mM)*		*$[S_2O_3^{2-}]$ (mM)*		*$[N_3^-]$*	*pH*
(days)	*a*	*b*	*a*	*b*	*a*	*b*	*a*	*b*	*a*	*b*	*(mM)*	
0	4.81	5.08	101.6	102.7	<0.005	<0.005	0.015	0.013	0.027	n.a.	15.7	8.5
29	5.58	5.67	101.0	101.8	n.a.	<0.005	0.022	0.016	n.a.	0.11	n.a.	8.8
91	5.13	5.07	102.3	102.4	<0.005	n.a.	0.012	0.013	0.20	n.a.	n.a.	8.9
182	4.9	5.13	103.7	102.9	<0.005	n.a.	0.012	0.012	0.26	n.a.	n.a.	9
351	5.00	5.00	102.1	102.4	<0.005	n.a.	0.018	0.018	0.44	n.a.	n.a.	9.2

n.a. : not analysed

Table A7.7: Chemical analyses of sample 'Pyr_0.005M $NaNO_3$_0% bact_bicarb' from the batch tests with pyrite (see Table 18). After each reaction period (first column), a sample of the solution has been analysed. The specific surface area of the pyrite added to the solution is 1.53 ± 0.18 m^2 g^{-1}. pH measurements were performed on only one sample. The uncertainties on the concentrations are 2% (pyrite concentration), 4-5% ($[S_2O_3^{2-}]$), 5-6% ($[NO_3^-]$, $[NO_2^-]$) and 10% ($[SO_4^{2-}]$, $[N_3^-]$) (95% confidence). The uncertainty on the pH is 0.1 units (95% confidence). The azide concentration and pH were measured in only one sample.

Time	*Pyrite (g L^{-1})*		*$[NO_3^-]$ (mM)*		*$[NO_2^-]$ (mM)*		*$[SO_4^{2-}]$ (mM)*		*$[S_2O_3^{2-}]$ (mM)*		*$[N_3^-]$*	*pH*
(days)	*a*	*b*	*a*	*b*	*a*	*b*	*a*	*b*	*a*	*b*	*(mM)*	
0	4.97	4.86	5.2	5.2	<0.005	<0.005	0.014	0.012	<0.002	n.a.	<0.012	8.4
182	5.00	4.47	5.2	5.1	<0.005	0.020	0.016	0.24	<0.009	<0.009	n.a.	8.5

n.a. : not analysed

Note the increase in both nitrite and sulphate concentration after 182 days in the b series, which would suggest pyrite oxidation. However, as only 2 values are currently at hand for these test conditions, the results of this series will only be interpreted when more data is available.

Table A7.8: Chemical analyses of sample 'Pyr_0.1M $NaNO_3$_0% bact_bicarb' from the batch tests with pyrite (see Table 18). After each reaction period (first column), a sample of the solution has been analysed. The specific surface area of the pyrite added to the solution is 1.53 ± 0.18 m^2 g^{-1}. pH measurements were performed on only one sample. The uncertainties on the concentrations are 2% (pyrite concentration), 4-5% ($[S_2O_3^{2-}]$), 5-6% ($[NO_3^-]$, $[NO_2^-]$) and 10% ($[SO_4^{2-}]$, $[N_3^-]$) (95% confidence). The uncertainty on the pH is 0.1 units (95% confidence). The azide and thiosulphate concentrations and pH were measured in only one sample.

Time	***Pyrite (g L^{-1})***		***$[NO_3^-]$ (mM)***		***$[NO_2^-]$ (mM)***		***$[SO_4^{2-}]$ (mM)***		***$[S_2O_3^{2-}]$***	***$[N_3^-]$***	***pH***
(days)	***a***	***b***	***a***	***b***	***a***	***b***	***a***	***b***	***(mM)***	***(mM)***	
0	5.24	4.94	102.6	102.5	<0.005	<0.005	0.014	0.015	0.0069	<0.24	8.5
29	4.94	4.83	103.5	102.3	<0.005	n.a.	0.015	0.016	0.0058	n.a.	8.5
91	4.71	5.46	101.5	101.1	<0.005	<0.005	0.013	0.013	0.0049	n.a.	8.4
182	5.10	5.19	100.8	102.7	<0.005	<0.005	0.012	0.015	<0.009	n.a.	8.3
351	5.14	4.95	101.6	101.6	<0.005	<0.005	0.013	0.014	<0.009	n.a.	8.5

n.a.: not analysed

Batch tests with pyrite and nitrite

Table A7.9: Chemical analyses of sample 'Pyr_0.005M $NaNO_2$_0.1% bact_bicarb' from the batch tests with pyrite (see Table 18). After each reaction period (first column), a sample of the solution has been analysed. The specific surface area of the pyrite added to the solution is 1.53 ± 0.18 m^2 g^{-1}. pH measurements were performed on only one sample. The uncertainties on the concentrations are 2% (pyrite concentration), 4-5% ($[S_2O_3^{2-}]$), 5-6% ($[NO_3^-]$, $[NO_2^-]$), 5-10% ($[SO_4^{2-}]$) and 10% ($[N_3^-]$) (95% confidence). The uncertainty on the pH is 0.1 units (95% confidence). The azide and nitrate concentrations and pH were measured in only one sample.

Time	*Pyrite (g L^{-1})*		*$[NO_3^-]$*	*$[NO_2^-]$ (mM)*		*$[SO_4^{2-}]$ (mM)*		*$[S_2O_3^{2-}]$ (mM)*		*$[N_3^-]$*	*pH*
(days)	*a*	*b*	*(mM)*	*a*	*b*	*a*	*b*	*a*	*b*	*(mM)*	
0	4.65	4.65	<0.004	4.7	4.7	0.018	0.016	0.0063	n.a.	15.5	8.6
29	4.75	4.71	0.018	4.6	4.6	0.020	0.020	0.032	0.035	n.a.	8.7
85	4.70	4.71	<0.004	4.3	4.3	0.024	0.021	0.072	0.065	n.a.	8.9
182	4.75	4.77	<0.004	4.2	4.2	0.030	0.029	0.093	0.085	n.a.	8.9
344	4.81	4.76	n.a.	4.0	3.9	0.044	0.050	0.13	0.14	n.a.	9.0

n.a. : not analysed

Table A7.10: Chemical analyses of sample 'Pyr_0.05M $NaNO_2$_0.1% bact_bicarb' from the batch tests with pyrite (see Table 18). After each reaction period (first column), a sample of the solution has been analysed. The specific surface area of the pyrite added to the solution is 1.53 ± 0.18 m^2 g^{-1}. pH measurements were performed on only one sample. The uncertainties on the concentrations are 2% (pyrite concentration), 4-5% ($[S_2O_3^{2-}]$), 5-6% ($[NO_3^-]$, $[NO_2^-]$), 5-10% ($[SO_4^{2-}]$) and 10% ($[N_3^-]$) (95% confidence). The uncertainty on the pH is 0.1 units (95% confidence). The azide and nitrate concentrations and pH were measured in only one sample.

Time	*Pyrite (g L^{-1})*		*$[NO_3^-]$*	*$[NO_2^-]$ (mM)*		*$[SO_4^{2-}]$ (mM)*		*$[S_2O_3^{2-}]$ (mM)*		*$[N_3^-]$*	*pH*
(days)	*a*	*b*	*(mM)*	*a*	*b*	*a*	*b*	*a*	*b*	*(mM)*	
0	4.72	4.82	<0.08	49.1	49.8	0.021	0.018	<0.002	n.a.	15.5	8.8
182	4.68	4.71	n.a.	48.0	48.3	0.053	0.050	0.11	0.10	n.a.	9.2

n.a. : not analysed

Table A7.11: Chemical analyses of sample 'Pyr_0.005M $NaNO_2$_0.1% bact_water' from the batch tests with pyrite (see Table 18). After each reaction period (first column), a sample of the solution has been analysed. The specific surface area of the pyrite added to the solution is 1.53 ± 0.18 m^2 g^{-1}. pH measurements were performed on only one sample. The uncertainties on the concentrations are 2% (pyrite concentration), 4-5% ($[S_2O_3^{2-}]$), 5-6% ($[NO_3^-]$, $[NO_2^-]$), 5-10% ($[SO_4^{2-}]$) and 10% ($[N_3^-]$) (95% confidence). The uncertainty on the pH is 0.1 units (95% confidence). The azide and nitrate concentrations and pH were measured in only one sample.

Time	*Pyrite (g L^{-1})*		*$[NO_3^-]$*	*$[NO_2^-]$ (mM)*		*$[SO_4^{2-}]$ (mM)*		*$[S_2O_3^{2-}]$ (mM)*		*$[N_3^-]$*	*pH*
(days)	*a*	*b*	*(mM)*	*a*	*b*	*a*	*b*	*a*	*b*	*(mM)*	
0	4.86	4.90	<0.004	4.4	4.4	0.022	0.018	0.0063	n.a.	15.7	7.9
182	4.93	4.82	<0.004	4.2	4.0	0.019	0.018	0.065	0.059	n.a.	9.7

n.a. : not analysed

Table A7.12: Chemical analyses of sample 'Pyr_0.005M $NaNO_2$_0% bact_bicarb' from the batch tests with pyrite (see Table 18). After each reaction period (first column), a sample of the solution has been analysed. The specific surface area of the pyrite added to the solution is 1.53 ± 0.18 m^2 g^{-1}. pH measurements were performed on only one sample. The uncertainties on the concentrations are 2% (pyrite concentration), 4-5% ($[S_2O_3^{2-}]$), 5-6% ($[NO_3^-]$, $[NO_2^-]$), 5-10% ($[SO_4^{2-}]$) and 10% ($[N_3^-]$) (95% confidence). The uncertainty on the pH is 0.1 units (95% confidence). The azide and nitrate concentrations and pH were measured in only one sample.

Time	*Pyrite (g L^{-1})*		*$[NO_3^-]$*	*$[NO_2^-]$ (mM)*		*$[SO_4^{2-}]$ (mM)*		*$[S_2O_3^{2-}]$ (mM)*		*$[N_3^-]$*	*pH*
(days)	*a*	*b*	*(mM)*	*a*	*b*	*a*	*b*	*a*	*b*	*(mM)*	
0	4.71	4.79	0.020	4.8	4.7	0.014	0.017	0.009	n.a.	<0.01	8.6
29	4.76	4.66	0.019	4.6	4.7	0.023	0.02	0.045	0.040	n.a.	8.7
85	4.84	4.80	0.018	4.4	4.2	0.026	0.026	0.084	0.081	n.a.	8.8
182	4.72	4.75	0.014	4.2	4.2	0.042	0.039	0.10	0.10	n.a.	8.7
344	4.85	4.84	n.a.	4.1	4.0	0.076	0.080	0.16	0.17	n.a.	8.8

n.a. : not analysed

Biotic batch tests with pyrite and Thiobacillus denitrificans

Table A7.13: Chemical analyses of sample 'Pyr_BNS' from the batch tests with pyrite and *Thiobacillus denitrificans* (see Table 19). After each reaction period (first column), the pyrite and homogenised and a sample of the solution has been taken and analysed. The specific surface area of the pyrite added to the solution is 1.53 ± 0.18 m^2 g^{-1}. TIC and pH measurements were performed on only one sample. The uncertainties on the concentrations are 2% (pyrite concentration and TIC), 4-5% ($[S_2O_3^{2-}]$), 5-6% ($[NO_3^-]$, $[NO_2^-]$), 5-10% ($[SO_4^{2-}]$) and 10% ($[NH_4^+]$). The uncertainty on the pH is 0.1 units (95% confidence).

Time (days)	*$[NO_3^-]$ (mM)*	*$[NO_2^-]$ (mM)*	*$[SO_4^{2-}]$ (mM)*	*$[S_2O_3^{2-}]$ (mM)*	*$[NH_4^+]$ (mM)*	*pH*	*TIC (mg C L^{-1})*
0	0.0065	<0.005	1.65	<0.009	0.10	8.4	175
68	<0.004	<0.005	1.69	0.021	n.a.	8.6	n.a.
132	<0.004	<0.005	1.69	0.012	0.077	8.5	n.a.
195	<0.004	<0.005	1.68	0.024	0.16	8.4	n.a.

n.a. : not analysed

Table A7.14: Chemical analyses of sample 'Pyr_0.005M $NaNO_3$_BNS' from the batch tests with pyrite and *Thiobacillus denitrificans* (see Table 19). After each reaction period (first column), the pyrite and homogenised and a sample of each duplicate solution has been taken and analysed. The specific surface area of the pyrite added to the solution is 1.53 ± 0.18 m^2 g^{-1}. pH measurements were performed on only one sample. The uncertainties on the concentrations are 2% (pyrite concentration and TIC), 4-5% ($[S_2O_3^{2-}]$), 5-6% ($[NO_3^-]$, $[NO_2^-]$), 5-10% ($[SO_4^{2-}]$), 10% ($[NH_4^+]$ and 0.1 pH units (95% confidence).

Time	*$[NO_3^-]$ (mM)*		*$[NO_2^-]$ (mM)*		*$[SO_4^{2-}]$ (mM)*		*$[S_2O_3^{2-}]$ (mM)*		*$[NH_4^+]$ (mM)*		*pH*	*TIC*
(days)	*a*	*b*	*a*	*b*	*a*	*b*	*a*	*b*	*a*	*b*		*(mg C L^{-1})*
0	4.8	5.0	<0.005	<0.005	1.65	1.66	0.010	<0.009	0.1	0.1	8.6	170
68	4.8	4.8	0.020	0.049	1.72	1.71	0.023	<0.009	n.a.	n.a.	9.1	n.a.
132	4.6	4.7	0.056	0.051	1.74	1.74	<0.002	<0.009	0.067	0.067	8.8	n.a.
195	4.7	4.7	0.046	0.043	1.76	1.72	<0.009	<0.009	0.17	n.a.	8.7	151

n.a. : not analysed

Table A7.15: Chemical analyses of sample 'Pyr_0.005M $NaNO_2$_BNS' from the batch tests with pyrite and *Thiobacillus denitrificans* (see Table 19). After each reaction period (first column), the pyrite and homogenised and a sample of each duplicate solution has been taken and analysed. The specific surface area of the pyrite added to the solution is 1.53 ± 0.18 $m^2\ g^{-1}$. pH measurements were performed on only one sample. The uncertainties on the concentrations are 2% (pyrite concentration and TIC), 4-5% ($[S_2O_3^{2-}]$), 5-6% ($[NO_3^-]$, $[NO_2^-]$), 5-10% ($[SO_4^{2-}]$), 10% ($[NH_4^+]$) and 0.1 pH units (95% confidence).

Time	*$[NO_3^-]$ (mM)*		*$[NO_2^-]$ (mM)*		*$[SO_4^{2-}]$ (mM)*		*$[S_2O_3^{2-}]$ (mM)*		*$[NH_4^+]$ (mM)*		*pH*	*TIC*
(days)	*a*	*b*	*a*	*b*	*a*	*b*	*a*	*b*	*a*	*b*		*(mg C L^{-1})*
0	0.026	0.022	4.7	4.9	1.65	1.67	<0.009	<0.009	0.1	0.1	8.5	174
68	0.026	0.022	4.7	4.8	1.68	1.71	0.054	0.034	n.a.	n.a.	9.2	n.a.
132	0.027	0.022	4.5	4.4	1.68	1.82	0.071	<0.002	0.076	0.073	9.3	n.a.
195	0.028	0.022	4.4	4.2	1.70	1.88	0.085	<0.009	0.13	n.a.	9.4	126

n.a. : not analysed